National Library of Canada
Acquisitions and Bibliographic Services Branch
395 Wellington Street
Ottawa, Ontario
K1A 0N4

Bibliothèque nationale du Canada
Direction des acquisitions et des services bibliographiques
395, rue Wellington
Ottawa (Ontario)
K1A 0N4

Your file *Votre référence*

Our file *Notre référence*

NOTICE

The quality of this microform is heavily dependent upon the quality of the original thesis submitted for microfilming. Every effort has been made to ensure the highest quality of reproduction possible.

If pages are missing, contact the university which granted the degree.

Some pages may have indistinct print especially if the original pages were typed with a poor typewriter ribbon or if the university sent us an inferior photocopy.

Reproduction in full or in part of this microform is governed by the Canadian Copyright Act, R.S.C. 1970, c. C-30, and subsequent amendments.

AVIS

La qualité de cette microforme dépend grandement de la qualité de la thèse soumise au microfilmage. Nous avons tout fait pour assurer une qualité supérieure de reproduction.

S'il manque des pages, veuillez communiquer avec l'université qui a conféré le grade.

La qualité d'impression de certaines pages peut laisser à désirer, surtout si les pages originales ont été dactylographiées à l'aide d'un ruban usé ou si l'université nous a fait parvenir une photocopie de qualité inférieure.

La reproduction, même partielle, de cette microforme est soumise à la Loi canadienne sur le droit d'auteur, SRC 1970, c. C-30, et ses amendements subséquents.

Canada

UNIVERSITY OF ALBERTA

SCALED EXPERIMENTS OF HEAVY OIL RECOVERY STRATEGIES IN A LOW PRESSURE PHYSICAL MODEL

BY

REX C.M. MATTHIAS

A THESIS

SUBMITTED TO THE FACULTY OF GRADUATE STUDIES AND RESEARCH

IN PARTIAL FULFILLMENT OF THE REQUIREMENTS FOR THE DEGREE

OF MASTER OF SCIENCE

IN

PETROLEUM ENGINEERING

DEPARTMENT OF MINING, METALLURGICAL AND PETROLEUM ENGINEERING

EDMONTON, ALBERTA

SPRING, 1993

National Library
of Canada

Acquisitions and
Bibliographic Services Branch

395 Wellington Street
Ottawa, Ontario
K1A 0N4

Bibliothèque nationale
du Canada

Direction des acquisitions et
des services bibliographiques

395, rue Wellington
Ottawa (Ontario)
K1A 0N4

Your file Votre référence

Our file Notre référence

The author has granted an irrevocable non-exclusive licence allowing the National Library of Canada to reproduce, loan, distribute or sell copies of his/her thesis by any means and in any form or format, making this thesis available to interested persons.

L'auteur a accordé une licence irrévocable et non exclusive permettant à la Bibliothèque nationale du Canada de reproduire, prêter, distribuer ou vendre des copies de sa thèse de quelque manière et sous quelque forme que ce soit pour mettre des exemplaires de cette thèse à la disposition des personnes intéressées.

The author retains ownership of the copyright in his/her thesis. Neither the thesis nor substantial extracts from it may be printed or otherwise reproduced without his/her permission.

L'auteur conserve la propriété du droit d'auteur qui protège sa thèse. Ni la thèse ni des extraits substantiels de celle-ci ne doivent être imprimés ou autrement reproduits sans son autorisation.

ISBN 0-315-82251-1

Canada

UNIVERSITY OF ALBERTA

RELEASE FORM

NAME OF AUTHOR: Rex C.M. Matthias

TITLE OF THESIS: Scaled Experiments of Heavy Oil Recovery Strategies in a Low Pressure Physical Model

DEGREE FOR WHICH THESIS WAS PRESENTED: MASTER OF SCIENCE

YEAR THE DEGREE WAS GRANTED : SPRING, 1993

Permission is hereby granted to the UNIVERSITY OF ALBERTA LIBRARY to reproduce single copies of this thesis and to lend or sell such copies for private, scholarly or scientific research purposes only.

The author reserves other publication rights, and neither the thesis nor extensive extracts from it may be printed or otherwise reproduced without the author's written permission.

(SIGNED) Rex Matthias

PERMANENT ADDRESS:

10 Watson Street

Red Deer, Alberta

Canada

DATED : April 20/93

UNIVERSITY OF ALBERTA

FACULTY OF GRADUATE STUDIES AND RESEARCH

The undersigned certify that they have read and recommend to the Faculty of Graduate Studies and Research, for acceptance, a thesis entitled SCALED EXPERIMENTS OF HEAVY OIL RECOVERY STRATEGIES IN A LOW PRESSURE PHYSICAL MODEL submitted by REX C.M. MATTHIAS in partial fulfillment of the requirements for the degree of MASTER OF SCIENCE in PETROLEUM ENGINEERING.

.....

Professor S.M. Farouq Ali (Supervisor)

.....

Professor A.K. Ambastha

.....

Professor W.S. Tortike

.....

Professor J.M. Whiting

.....

Professor J.D. Scott (External Examiner)

Date April 6, 1993

To My Wife Bonnie, and To My Children
Curtis, Ami, and Stephanie
for their Unconditional Love, Support, and Faith in Me.

Abstract

This research involved the use of a physical model to study steamflooding recovery strategies that could be employed in marginal heavy oil reservoirs. Base case steamfloods were established for reference. Three different types of models were used in this study: homogeneous, 50% bottom water, and multi-layered.

The thermal nature of the experiments warranted investigating the dissipation of the heat after it was injected. It was found that the thermal properties of the model did not match the prototype reservoir and only about 10 % of the heat was lost to the cap and base rocks.

Scaled horizontal wells were employed in homogeneous and 50% bottom water models. The effect of horizontal well length and the position of the well was examined. It was found that horizontal wells recovered oil earlier than conventional vertical wells. It was also found that the lower the completion interval in the reservoir the greater the oil recovery.

Stratified reservoirs were successfully modelled and no mechanical methods of overcoming steam override were found .

Many thermal projects are near or at their economic limits. There is a great amount of energy in these reservoirs. It was attempted in this study to scavenge such energy to gain some incremental oil recovery. It was found that injecting water into a steam zone collapsed the steam zone and reduced the oil recovery rate.

Acknowledgements

The author wishes to express his gratitude to Dr. S.M. Farouq Ali for his very generous supervision and support throughout the course of this study.

The author wishes to extend special thanks to his friend Mr. Quang T. Doan for his invaluable guidance and advice in conducting this study, and in the preparation of this thesis.

The author wishes to acknowledge the technical assistance provided by Mr. Robert Smith in the design, modification and fabrication of equipment used in this study. Thanks are also extended to Mr. John Czuroski, Mr. Jacques Gibeau, Mr. Doug Booth, and Mr. Rob Stefaniuk.

The financial assistance of CANMET/Energy, Mines and Resources and the encouragement and technical assistance of Dr. Albert E. George is gratefully acknowledged.

Table of Contents

Chapter **Page**

1. Introduction 1
2. Statement of the Problem 2
    2.1 Experimental Objectives 2
    2.2 Theoretical Objectives 2
3. Literature Review 3
    3.1 Scaling Physical Models 3
    3.2 High Pressure and Low Pressure Physical Models 4
        3.2.1 Steamflooding in the Presence of Bottom Water 6
        3.2.2 Layered Reservoir Models 8
    3.3 Horizontal Well Applications 9
        3.3.1 Horizontal Wells in Enhanced Oil Recovery 9
            3.3.1.1 Productivity Index 10
            3.3.1.2 Suppression of Coning Problems 11
            3.3.1.3 Steam-Assisted Gravity Drainage 12
4. Scaling Parameters and Calculations 15
    4.1 Development of Scaling Parameters for the Low Pressure Model 15
        4.1.1 Unscaled Parameters 15
        4.1.2 Scaling Procedures 16
    4.2 Example Scaling Prototype to Model 20
        4.2.1 Length Scaling 20
        4.2.2 Model Production Pressure Scaling 22
        4.2.3 Model Temperature Scaling 23
        4.2.4 Scaled Steam Quality Requirement 25
        4.2.5 Calculation of Model Oil Viscosity 26

4.2.6 Calculation of the Time Scale Factor 27
4.2.7 Scaling of Model Permeability 27
4.2.8 Scaling Down of the Vertical Wells 28
4.2.9 Scaling Down the Horizontal Well 29
4.2.10 Steam Injection Rate Scaling 30
5. Experimental Apparatus and Procedure 31
5.1 Experimental Apparatus 31
5.1.1 Physical Model 31
5.1.2 Porous Media 34
5.1.3 Vertical and Horizontal Wells 34
5.1.4 Injection System 34
5.1.5 Production System 36
5.1.6 Data Acquisition System 36
5.1.7 Model Fluids 36
5.2 Preparation of the Experimental Model 38
5.2.1 Model Packing Procedure 38
5.2.2 Saturation Process 38
5.2.3 Preparation of a Bottom Water Model 38
5.2.4 Multi-layered Models 39
5.3 Conducting Experiments in the Model 39
5.4 Data Analysis 40
6. Discussion of Experimental Results 42
6.1 Presentation of Results 42
6.2 Heat Balance 46
6.3 Production History of a Typical Run 48
6.4 Production History of a 50% Bottom Water Run 56
6.5 Horizontal Wells 62

6.5.1 Horizontal Production Well Length 62
6.5.1.1 Effect of Horizontal Production Well Length in a Bottom Water Model 64
6.5.1.2 Effect of Horizontal Production Well Length in a Homogeneous Model 75
6.5.2 Completion Interval Sensitivity For Horizontal Wells 82
6.5.2.1 Vertical Position of the Horizontal Producer 82
6.5.2.2 Vertical Position of the Horizontal Injector 85
6.6 Multi-layered Models 92
6.6.1 Effect of Reservoir Heterogeneity 93
6.6.2 Unfavourable Stratification 99
6.6.2.1 Fractured Multi-layered Model 99
6.6.2.2 Horizontal Injection Well in a Multi-layered Model 103
6.7 Waterflooding, then Steamflooding Heavy Oil Reservoirs 110
6.7.1 Warm and Cold Waterfloods 110
6.7.2 Optimal Waterflood Period Prior to Steamflooding 114
6.8 Heat Scavenging 119
6.8.1 Gas Injection After a Steamflood 119
6.8.2 Waterflooding a Steamflooded Reservoir 119
6.9 Reproducibility of Result 122
7. Conclusions 128
8. Recommendations for Further Studies 129
References 131
Appendix A 137
Appendix B 144
Appendix C 166
Appendix D 174

List of Tables

Table		Page
Table 4.1	Scaling Parameters for Steam Injection/Steamflooding Processes	17
Table 4.2	Scaling Parameters for the Prototype and Model Reservoir	21
Table 4.3	Prototype and Model Scaling Values	24
Table 6.1	Summary of Experiments	44
Table 6.2	Run 136, Base Case Steamflood of a Homogeneous Model	50
Table 6.3	Run 149, Base Case Steamflood of a 50% Bottom Water Model	58
Table 6.4	Laboratory Oil Production Rate and Scaled-up Field Oil Production Rate, Vertical Producer Pattern vs. Horizontal Producer Pattern, Marginal Heavy Oil Reservoir with 50% Gross Thickness Bottom Water	73
Table B1	Total Heat Produced After the Injection of 1.00 PV of Steam, Run 136	147
Table B2	Total Heat Accumulated in the Model After the Injection of 1.00 PV of Steam, Run 136	150
Table B3	Heat Loss to Over/Underburden Using an Integrated Heat-flow Equation	153
Table B4	Sensitivity of the Analytical Solution	158
Table B5	Sensitivity of the Numerical Solution.	163
Table B6	Heat Distribution in the Overburden Using both the Analytical and Numerical Solution Methods.	164
Table D1	Experimental results of Run 108	174
Table D1	Experimental results of Run 109	175
Table D3	Experimental results of Run 110	176
Table D4	Experimental results of Run 111	177
Table D5	Experimental results of Run 114	178
Table D6	Experimental results of Run 115	179

Table D7 Experimental results of Run 120 180
Table D8 Experimental results of Run 121 181
Table D9 Experimental results of Run 124 182
Table D10 Experimental results of Run 125 183
Table D11 Experimental results of Run 126 184
Table D12 Experimental results of Run 127 185
Table D13 Experimental results of Run 132 186
Table D14 Experimental results of Run 133 187
Table D15 Experimental results of Run 136 188
Table D16 Experimental results of Run 138 189
Table D17 Experimental results of Run 140 190
Table D18 Experimental results of Run 142 191
Table D19 Experimental results of Run 149 192
Table D20 Experimental results of Run 151 193
Table D21 Experimental results of Run 152 194
Table D22 Experimental results of Run 156 195
Table D23 Experimental results of Run 157 197
Table D24 Experimental results of Run 158 199
Table D25 Experimental results of Run 159 201
Table D26 Experimental results of Run 160 203
Table D27 Experimental results of Run 161 205
Table D28 Experimental results of Run 163 207

List of Figures

Figure		Page
Figure 5.1	Schematic diagram of the experimental apparatus	32
Figure 5.2	Schematic diagram of the physical model	33
Figure 5.3	Steam quality vs. boiler temperature for mixing and non-mixing injection systems	35
Figure 5.4	Viscosity vs. temperature for the prototype and model oils	37
Figure 6.1	Overview of low pressure model experiments reported	43
Figure 6.2	Production history of a typical experiment (Run 136): base case steamflood in a homogeneous model.	49
Figure 6.3	Temperature and pressure history for Run 136, base case steamflood in a homogeneous model	52
Figure 6.4	Plan view, of the temperature distribution inside the model reservoir after the injection of: a) 0.25, b) 0.50, c) 1.00, and d) 1.50 PV CWE of steam, for Run 136: homogeneous model, vertical injection and production wells.	54
Figure 6.5	Cross-section of the temperature distribution inside the model reservoir after the injection of: a) 0.25, b) 0.50, c) 1.00, and d) 1.50 PV CWE of steam, for Run 136 homogeneous model, vertical injection and production wells	55
Figure 6.6	Production History for Run 149, Base Case Steamflood in a 50% Bottom Water Model	57
Figure 6.7	Temperature and pressure history for Run 149, base case steamflood in a 50% bottom water model	60
Figure 6.8	Plan view, of the temperature distribution inside the model reservoir after the injection of: a) 0.25, b) 0.50, c) 1.00, and d) 1.50 PV CWE of steam, for Run 149: 50% bottom water model, vertical injection, and production wells.	61
Figure 6.9	Cross-section of the temperature distribution inside the model reservoir after the injection of: a) 0.25, b) 0.50, c) 1.00, and d) 1.50 PV CWE of steam, for Run 149: 50% bottom water model, vertical injection and production wells.	63

Figure 6.10 Effect of production well length on recovery performance in a 50% bottom water model. Cumulative oil recovery vs. PV injected, for a long horizontal producer (Run 152), and a short horizontal producer (Run 151) vs. a vertical producer (Run 149) 65

Figure 6.11 Effect of production well length on recovery performance in a 50% bottom water model. Cumulative OSR and instantaneous WOR vs. PV injected, for a long horizontal producer (Run 152), and a short horizontal producer (Run 151) vs. vertical producer (Run 149). 66

Figure 6.12 Plan view,of the temperature distribution inside the model reservoir after the injection of: a) 0.40, b) 0.50, c) 0.60, and d) 1.00 PV CWE of steam, for Run 149: 50% bottom water model, vertical injection and production wells. 67

Figure 6.13 Plan view,of the temperature distribution inside the model reservoir after the injection of: a) 0.40, b) 0.50, c) 0.60, and d) 1.00 PV CWE of steam, for Run 151: 50% bottom water model, short horizontal producer (20.3-cm) and a vertical injection well 68

Figure 6.14 Plan view, of the temperature distribution inside the model reservoir after the injection of: a) 0.40, b) 0.50, c) 0.60, and d) 1.00 PV CWE of steam, for Run 152: 50% bottom water model, long horizontal producer (40.6-cm) and a vertical injection well 69

Figure 6.15 Cumulative oil recovery vs. production well type, increasing PV injected in a bottom water model 70

Figure 6.16 Schematic of reservoir development using five-spot patterns with short, small wellbore-radius horizontal wells in place of vertical producers 72

Figure 6.17 Scaled-up oil production rate per five-spot pattern, horizontal producer vs. vertical producer, marginal heavy oil reservoir with 50% gross thickness bottom water, vertical steam injector. 74

Figure 6.18 Effect of production well length on recovery performance in a homogeneous model, cumulative oil recovery vs. PV injected, for a short horizontal producer (Run 156), a medium horizontal producer (Run 158), and a long horizontal producer (Run 157) vs. vertical producer (Run 136) 76

Figure 6.19 Effect of production well length on recovery performance in a homogeneous model, cumulative OSR vs. PV injected for a short horizontal producer (Run 156), a medium horizontal producer (Run 158), and a long horizontal producer (Run 157) vs. vertical producer (Run 136) 77

Figure 6.20 Plan view, of the temperature distribution inside the model reservoir after the injection of: a) 0.25, b) 0.50, c) 1.00, and d) 1.50 PV CWE of steam, for Run 136: homogeneous model, vertical injection and production wells 78

Figure 6.21 Plan view, of the temperature distribution inside the model reservoir after the injection of: a) 0.25, b) 0.50, c) 1.00, and d) 1.50 PV CWE of steam, for Run 156: homogeneous model, short horizontal producer (20.3-cm) and a vertical injection well 79

Figure 6.22 Plan view, of the temperature distribution inside the model reservoir after the injection of: a) 0.25, b) 0.50, c) 1.00, and d) 1.50 PV CWE of steam, for Run 158: homogeneous model, medium length horizontal producer (30.5-cm), and a vertical injection well 80

Figure 6.23 Plan view, of the temperature distribution inside the model reservoir after the injection of: a) 0.25, b) 0.50, c) 1.00, and d) 1.50 PV CWE of steam, for Run 157: homogeneous model, long horizontal producer (40.6-cm) and a vertical injection well 81

Figure 6.24 Cumulative oil recovery vs. production well type with increasing PV injected in a homogeneous model 83

Figure 6.25 Effect of the vertical position of a medium length horizontal producer on recovery performance in a 50% bottom water model cumulative oil recovery vs. PV injected 84

Figure 6.26 Plan view, of the temperature distribution inside the model reservoir after the injection of: a) 0.25, b) 0.50, c) 1.00, and d) 1.50 PV CWE of steam, for Run 159: 50% bottom water model, medium length horizontal producer, (30.5-cm) placed in the middle of the oil zone, and a vertical injection well. 86

Figure 6.27 Plan view, of the temperature distribution inside the model reservoir after the injection of: a) 0.25, b) 0.50, c) 1.00, and d) 1.50 PV CWE of steam, for Run 160: 50% bottom water model, medium length horizontal producer, (30.5-cm) placed at the top of the oil zone, and a vertical injection well 87

Figure 6.28 Plan view, of the temperature distribution inside the model reservoir after the injection of: a) 0.25, b) 0.50, c) 1.00, and d) 1.50 PV CWE of steam. Run 161: 50% bottom water model, medium length horizontal producer, (30.5-cm) placed at the oil-water contact, and a vertical injection well 88

Figure 6.29 Effective of the vertical position of a long horizontal injector on recovery performance in a homogeneous model cumulative oil recovery vs. PV injected injector placed in the middle of the oil zone (Run 121) vs. injector placed at the bottom of the oil zone (Run 125) 89

Figure 6.30 Plan view, of the temperature distribution inside the model reservoir after the injection of: a) 0.25, b) 0.50, c) 1.00, and d) 1.50 PV CWE of steam, for Run 121: homogeneous model, long horizontal injector, (40.6-cm) placed in the middle of the oil zone, and a vertical production well 90

Figure 6.31 Plan view, of the temperature distribution inside the model reservoir after the injection of: a) 0.25, b) 0.50, c) 1.00, and d) 1.50 PV CWE of steam, for Run 125: homogeneous model, long horizontal injector, (40.6-cm) placed at the bottom of the oil zone, and a vertical production well 91

Figure 6.32 Effect of reservoir heterogeneity on recovery performance in multi-layered models. 94

Figure 6.33 Effect of reservoir heterogeneity on recovery performance in multi-layered models 95

Figure 6.34 Plan view, of the temperature distribution inside the model reservoir after the injection of: a) 0.25, b) 0.50, c) 1.00, and d) 1.50 PV CWE of steam, for Run 115: homogeneous model, vertical injection and production wells 96

Figure 6.35 Plan view, of the temperature distribution inside the model reservoir after the injection of: a) 0.25, b) 0.50, c) 1.00, and d) 1.50 PV CWE of steam, for Run 120: unfavourably layered model, vertical injection and production wells 97

Figure 6.36 Plan view, of the temperature distribution inside the model reservoir after the injection of: a) 0.25, b) 0.50, c) 1.00, and d) 1.50 PV CWE of steam, for Run 163: favourably layered model, vertical injection and production wells 98

Figure 6.37 Cross-section of the temperature distribution inside the model reservoir after the injection of: a) 0.25, b) 0.50, c) 1.00, and d) 1.50 PV CWE of steam, for Run 115: homogeneous model, vertical injection and production wells 100

Figure 6.38 Cross-section of the temperature distribution inside the model reservoir after the injection of: a) 0.25, b) 0.50, c) 1.00, and d) 1.50 PV CWE of steam, for Run 120: favourably layered model, vertical injection and production wells 101

Figure 6.39 Cross-section of the temperature distribution inside the model reservoir after the injection of: a) 0.25, b) 0.50, c) 1.00, and d) 1.50 PV CWE of steam, for Run 163: unfavourably layered model, vertical injection and production wells 102

Figure 6.40 Effect of a fracture in the unfavourable permeable layer in an unfavourably layered model 104

Figure 6.41 Effect of a fracture in the unfavourable permeable layer in an unfavourably layered model 105

Figure 6.42 Plan view, of the temperature distribution inside the model reservoir after the injection of: a) 0.25, b) 0.50, c) 1.00, and d) 1.50 PV CWE of steam, for Run 138: unfavourably layered model with a fracture running from the injector to the producer in the bottom layer,vertical injection and production wells 106

Figure 6.43 Plan view, of the temperature distribution inside the model reservoir after the injection of: a) 0.25, b) 0.50, c) 1.00, and d) 1.50 PV CWE of steam, for Run 142: unfavourably layered model, vertical injection and production wells 107

Figure 6.44 Effect of a horizontal injector in an unfavourably layered model 108

Figure 6.45 Effect of a horizontal injector in an unfavourably layered model, cumulative OSR and instantaneous WOR vs. PV injected, unfavourably layered with a horizontal injector and/or a solvent per-flush (Runs 126 and 124 Respectively) vs. unfavourably layered model (Run 120) 109

Figure 6.46 Plan view, of the temperature distribution inside the model reservoir after the injection of: a) 0.25, b) 0.50, c) 1.00, and d) 1.50 PV CWE of steam, for Run 120: unfavourably layered model, vertical injection and production wells 111

Figure 6.47 Plan view, of the temperature distribution inside the model reservoir after the injection of: a) 0.25, b) 0.50, c) 1.00, and d) 1.50 PV CWE of steam, for Run 124: unfavourably layered model, horizontal injector and a vertical producer, 0.10 PV solvent pre-flush prior to start of the steamflood 112

Figure 6.48 Plan view, of the temperature distribution inside the model reservoir after the injection of: a) 0.25, b) 0.50, c) 1.00, and d) 1.50 PV CWE of steam, for Run 126: unfavourably layered model, horizontal injector and a vertical producer....113

Figure 6.49 Effect of injected water temperature prior to steamflood on recovery performance....115

Figure 6.50 Plan view, of the temperature distribution inside the model reservoir after the injection of: a) 1.00, b) 1.25, c) 1.50, and d) 2.00 PV CWE of steam, for Run 114: homogeneous model, warm waterflood prior to steamflooding, vertical injection and production wells....116

Figure 6.51 Plan view, of the temperature distribution inside the model reservoir after the injection of: a) 1.00, b) 1.25, c) 1.50, and d) 2.00 PV CWE of steam, for Run 127: homogeneous model, warm waterflood prior to steamflooding, vertical injection and production wells....117

Figure 6.52 Effect of waterflood length prior to steamflood on recovery performance....118

Figure 6.53 Plan view, of the temperature distribution inside the model reservoir after the injection of: a) 1.00, b) 1.50, c) 2.00, and d) 2.20 PV CWE of steam, for Run 140: homogeneous model, gasflood subsequent to 2.00 PV steamflood, vertical injection, and production wells....120

Figure 6.54 Production history for Run 140, gasflood subsequent to a steamflood in a homogeneous model....121

Figure 6.55 Effect of heat scavenging after a steamflood, cumulative oil recovery vs. PV injected, steamflood 0.6 PV then waterflood (Run 109), steamflood 0.6 PV, inject 0.1 PV gas then waterflood (Run 110), steamflood 1.00 PV then waterflood (Run 111)....123

Figure 6.56 Plan view, of the temperature distribution inside the model reservoir after the injection of: a) 0.25, b) 0.50, c) 1.00, and d) 1.50 PV CWE of steam, for Run 109: homogeneous model, steamflood to 0.60 PV then waterflood, vertical injection, and production wells....124

Figure 6.57 Plan view, of the temperature distribution inside the model reservoir after the injection of: a) 0.25, b) 0.50, c) 1.00, and d) 1.50 PV CWE of steam, for Run 110: homogeneous model, steamflood to 0.60 PV, inject a 0.10 PV gascap then waterflood, vertical injection and production wells....125

Figure 6.58 Plan view, of the temperature distribution inside the model reservoir after the injection of: a) 0.25, b) 0.50, c) 1.00, and d) 1.50 PV CWE of steam, for Run 111: homogeneous model, steamflood to 1.00 PV then waterflood, vertical injection, and production wells 126

Figure 6.59 Reproducibility of results 127

Figure A1 Effect of steam quality on recovery performance 138

Figure A2 Effect of steam quality on CP/CI 138

Figure A3 Schematic of enthalpy balance apparatus 140

Figure A4 Schematic of enthalpy balance 141

Figure A5 Schematic of mass balance 143

Figure B1 Schematic of the heat loss problem 145

Figure B2 Temperature on either side of the sealing 1/8 inch thick neoprene sheet. Thermocouples placed 4 inches diagonally out from the injection point 151

Figure B3 Schematic illustration of the heat loss to the cap and base rocks 154

Figure B4 Temperature distribution in the cap rock vs. distance from the heat Source. Two solutions: numerical discretization of Fourier' s Equations vs. analytical solution from Carslaw and Jaeger (Ref. 45). 165

NOMENCLATURE

a	length, [L]
C	specific heat, $[L^2t^{-2}T^{-1}]$
f_{st}	steam quality, dimensionless
g	acceleration due to gravity, $[Lt^{-2}]$
h	enthalpy per unit mass, $[L^2t^{-2}]$
J	mechanical equivalence of heat energy, dimensionless
k	permeability, $[L^2]$
k_h	thermal conductivity, $[MLt^{-3}T^{-1}]$
k_r	relative permeability, dimensionless
L	length or distance, [L]
L_v	latent enthalpy per unit mass, $[L^2t^{-2}]$
l	thickness of neoprene or fiberglass layer, [L]
m	arbitrary variable, or mass [M]
P	Laplace parameter, dimensionless
p	pressure, $[ML^{-1}t^{-2}]$
Q	heat, [kJ]
q	Laplace parameter divided by α
r_w	effective wellbore radius, [L]
S	saturation, mass fraction
T	temperature, [T]
$\overline{T}$	temperature in Laplace space
t	time, [t]
v	velocity of the fluid flowing inside the horizontal well, $[Lt^{-1}]$
w	mass flow rate, $[Mt^{-1}]$
z	coordinate, [L]

Greek Symbols

α	thermal diffusivity, $[L^2t^{-1}]$
Δp	pressure drop, $[ML^{-1}t^{-2}]$
ϕ	porosity, dimensionless
μ	fluid viscosity, $[ML^{-1}t^{-1}]$
ρ	density, $[ML^{-3}]$
ω	slit width, [L]

Subscripts

form	formation
inj.	injected
j	phase (oil, water or steam)
loss	loss to the cap and base rock
o	oil or oleic phase
ob	overburden
P	prototype
prod	production
R	reference variable used to obtain a dimensionless quantity
s	steam
w	water (unless otherwise specified)

1. Introduction

In Alberta and Saskatchewan, a large number of the heavy oil deposits are considered to be marginal or uneconomical. Such reservoirs are characterized by a relatively thin pay (5 m) and the presence of an underlying communicating bottom water layer. The small thickness of the oil zone leads to prohibitive heat losses to the cap and base rocks in a steam based recovery method. In addition, a communicating bottom water layer can scavenge most of the injected energy, making the project uneconomical.

Horizontal wells are fast becoming the method of choice in exploiting these marginal reservoirs. Horizontal wells, in general, have a higher productivity index and yield better recovery than vertical wells. Horizontal well drilling technology has advanced at a greater rate than the technology to implement it, in both production and reservoir engineering. Therefore, there is a need to understand better the effects of a horizontal well in a reservoir, especially when steam is injected.

Many thermal projects are currently shut-in due to the high costs of continued steam injection and the low oil prices for heavy oil. Heat scavenging techniques could offer a means of recovering additional oil beyond the current economic limit. An investigation into the viability of scavenging the in-situ energy to mobilize and recover more oil needs to be performed.

This research included horizontal well scaling criteria for the low pressure model, and the experimental study of the effect of a horizontal well. Other areas examined included: a heat balance for the model, stratified reservoirs, heat scavenging previously steamflooded reservoirs, and waterflooding/steamflooding combinations.

2. Statement of the Problem

The objectives of this research were to examine the use of scaled horizontal wells in physical modelling of steamflooding heavy oil formations, to investigate the effects of steam override using a multi-layered reservoir, to attempt to scavenge injected heat energy to recover more oil incrementally after a steamflood is terminated, and to perform a heat balance on a steamflood. These objectives were attained using experimental and theoretical methods, which are outlined as follows:

2.1 Experimental Objectives

1. Experimental apparatus development:
   a) Development of injected steam quality testing equipment.
   b) Modification of the steam injection system to exercise more control of the injected steam quality.
   c) Utilization of a new temperature contouring program for interpretation of the experiments and for doing the heat balance.
2. Experimental strategies:
   a) Investigate horizontal well recovery schemes.
   b) Use multi-layered models to investigate the effects of steam override.
   c) Examine the effectiveness of waterflooding prior to steamflooding.
   d) Investigate the possibility of gaining incremental oil recovery by scavenging heat from a steamflooded reservoir.

2.2 Theoretical Objectives

1. Calculation/determination of the model heat balance.
2. Interpretation of selected runs.

3. Literature Review

Physical models are widely used to study hydrodynamic phenomena. The models can be classified into three groups: unscaled, partially scaled, and fully scaled. Unscaled models are the least difficult to construct and operate. They are used to detect and observe a specific flow phenomenon. Because they are unscaled these models cannot be used to directly and quantitatively predict field responses.

Partially scaled models are more difficult to construct and operate. In these models specific aspects of the flow phenomena under investigation are scaled while others are not. The specific aspects of the flow phenomena must be understood to scale and construct a partially scaled model. The results of partially scaled model experiments can provide certain quantitative field predictions, especially with respect to the aspects of the process that are scaled.

Fully scaled models are complex and difficult to build and operate; however, they are highly desirable as the results may be used directly in field predictions. Complete knowledge of the flow process under investigation is required. Limitations on a fully scaled physical model may arise due to the unavailability of materials and fluids having the physical properties that will satisfy all the scaling requirements. Scaled physical models require the derivation of scaling groups, and the use of these groups in the construction and operation of the models.

3.1 Scaling Physical Models

Early scaled physical model studies used dimensional analysis to scale prototype properties to the laboratory. Leverett, Lewis and True[1] were among the first investigators to apply scaling laws to physical models in the study of isothermal fluid flow in petroleum reservoirs. They derived, using dimensional analysis, the dimensionless scaling groups governing the water drive process for both radial and linear fluid flow. They also described the construction and operation of various physical models using their theory.

Rapoport and Leas[2], and Croes and Schwarz[3] extended the above work to investigate the effects of various parameters influencing the displacement of light oils by waterflooding.

Geertsma, Croes and Schwarz[4] derived the dimensionless similarity groups using inspectional analysis which was complemented by dimensional analysis for three processes of oil displacement: cold-water drive, hot-water drive and solvent injection. It was concluded that using both dimensional and inspectional analyses had advantages over using only one of the methods.

Pujol and Boberg[5] examined the scaling accuracy of laboratory steamflooding models, specifically with regard to capillary pressure effects. They found that for highly viscous oils (μ >100,000 mPa.s) accurate scaling of the capillary pressure was not crucial. For such oils, the ratio of capillary to viscous forces was so small that unscaled capillary pressures would have negligible effect on the measured oil recovery values. For oil with medium viscosity (μ < 10,000 mPa.s) the results of not scaling the capillary pressure generally led to optimistic predictions of oil recovery. It was also found that the oil recovery depended mainly on the energy injected and not on the injection rate.

3.2 High Pressure and Low Pressure Physical Models

Physical modelling of steamflooding processes can be further divided into two general classes: 1) those that operate at high pressures and temperatures, and 2) those that operate at low pressure (subatmospheric) conditions.

The earliest steam injection model experiments were performed at pressures and temperatures approaching the high temperature and pressure seen in the field. Because the model pressures and temperatures closely matched the field pressures and temperatures, similar rock-fluids interactions could be modelled.

Willman, Valleroy, Runberg, Cornelius and Powers[6] performed steamfloods in linear cores to investigate the use of steam as a recovery agent. They found as much as 100% greater oil recovery by steamflooding than by waterflooding. It was determined that the principal mechanisms responsible for the additional oil recovery were thermal expansion of the oil, viscosity reduction, and steam distillation. It was also found that the residual oil saturation was independent of initial oil saturation, and the steamflood recovery of lighter oils was greater because the lighter oil contained a greater fraction of steam-distillable components than the heavier oils.

Farouq Ali and Redford[7] provided a review of various scaling groups for steam injection and in-situ combustion processes. Kimber, Farouq Ali, and Puttagunta[8-10]

obtained new scaling criteria for steam and steam-additive injection experiments using an innovative and comprehensive analysis. In the above studies both inspectional and dimensional analyses were used to obtain the similarity groups. Because of the difficulty in satisfying all of the scaling criteria at the same time physically, some of the scaling groups had to be relaxed. Four different approaches were used, with each approach scaling a specific mechanism of the recovery process exactly while partially relaxing the remaining mechanisms. High pressure models were constructed and operated according to the four resulting sets of scaling criteria. The experimental results were then compared to determine the effects of the relaxation of some of the scaling groups.

Pursley[11] used Pujol and Boberg's[5] scaling criteria to model the Cold Lake reservoir using a number of three-dimensional models. He investigated the effects on oil recovery of a gas cap, a bottom water zone, and impermeable streaks. He also studied controllable variables, such as steam quality, pattern size, and the use of steam additives.

Huygen[12] used a high pressure model representing one half of a five-spot pattern to study the effects of oil viscosity, initial oil saturation, and distillation residue on oil recovery. The model used crushed Berea sandstone, and only heat flow was considered in the scaling calculations.

Low pressure models operate at pressures below field pressures and therefore the steam saturation temperatures are lower than field saturations temperatures. At saturated conditions, the pressure and temperature are interdependent and are related by the Clausius-Clapeyron relationship, which in the basic form is:

$$p_{sat} = p_{sat}\,(T_{sat}) \tag{3.1}$$

Stegemeier, Laumbach and Volek[13] suggested that to obtain a good match of the Clausius-Clapeyron equation the pressure must be reduced to vacuum pressure levels. To best satisfy all the relevant scaling criteria, the fluids used in the low pressure model must have different properties than the fluids present in the prototype, due to the lower temperature and pressure range.

Stegemeier et al.[13] performed the earliest low pressure scaled model study of steamflooding heavy oil reservoirs. They described the low pressure scaling criteria which have been the basis of several studies[14-17,19,20]. They carried out numerous steam injection experiments in two dipping reservoirs that simulated the Mt. Poso and the Midway Sunset fields.

B.J. Kristoff[14] carried out experimental studies of the Tangleflags steamflood in a low pressure model. The steamflood was also numerically simulated. The experimental results were in close agreement with the field observations, whereas the numerical simulations were still not close despite many adjustments of the data.

Previously an investigation was carried out in a model similar to the one used in this investigation. Proctor[15] applied the low pressure scaling criteria presented by Stegemeier et al.[13] and built the model and tested the flexibility of it. His three-dimensional physical model represented one-quarter of a five-spot in the Aberfeldy reservoir. This work was followed by Oracheski[16] who examined injecting a small solvent slug prior to steam injection in bottom water reservoirs.

The above section provides an overview of the historical development of scaling of physical models. In this study the model built by Proctor[15] following the work performed by Stegemeier et al.[13] was the building block for this study.

3.2.1 Steamflooding in the Presence of Bottom Water

Because of the high specific heat capacity of water, it is an ideal energy carrier. The specific heat capacity of water is advantageous when injecting energy, but it can be detrimental when there is a pre-existing water zone in communication with the pay zone. The connate water can scavenge large amounts of energy from the targeted area.

Hall and Bowman[17] reported one of the earliest cases of injecting steam into an underlying water zone. Because of the very large amounts of steam injected, the economics of the project were greatly reduced in spite of the relatively high oil saturation (65%).

Prats[18] models of the Peace River oil sand were constructed based on the low pressure modeling approach of Stegemeier et al[13]. He used five different models which covered variations in the thickness, permeability, and saturations in the oil and underlying water zones likely to be encountered in the prime portions of the reservoir. One of the operating strategies used to overcome low oil recovery after steam breakthrough was to pressurize the zone while producing oil, then to blow down the pressure.

Ehrlich[19] performed steamfloods in cores, and then used the experience to design scaled physical model experiments. The high pressure physical model experiments

simulated a thin heavy oil reservoir with a communicating bottom water zone. The experiments incorporated horizontal barriers and wells with dual completions designed for fluid injection separately into the bottom water zone and the oil zone. Initially, steam was injected into the bottom zone to preheat the oil. Following the preheating stage, the bottom completions were shut off, and the steam was injected into the oil sand. From the experimental results, it was concluded that a significant part of the OOIP could be recovered prior to steam breakthrough when the steam drive was initiated through the water zone.

Huygen and Lowery[20] performed steamflood experiments in a high pressure model that simulated a heavy oil formation with a communicating bottom water zone. They concluded that the bottom water zone provided the initial injectivity needed, but heating the tar sand was slow and the water zone scavenged much of the heat from the tar sand.

Huygen and Black[21] conducted scaled model experiments to investigate the effectiveness of different horizontal and vertical wells combinations in steamflooding Athabasca oil sand. The authors noted that for accurate physical modelling of steaming through horizontal wells, both the heat flow (conduction and convection) and mass transport (due to gravity drainage and phase changes) must be scaled properly. Performance of the floods depended significantly on the geometry and communication between the injector and the producer. In comparing the various geometries, it was determined that communication must be established mechanically (i.e. fracturing or use of horizontal wells). Also, steamflooding through a single horizontal well was a viable and productive strategy for mobilizing bitumen.

Ahner and Sufi[22] used a scaled rectangular low pressure physical model to study the steamflood drainage areas by parallel horizontal wells. In many of the experiments, the horizontal wells (placed between pairs of line drive vertical injectors and producers) were used to heat the surrounding formation by conduction and thus provide initial fluid mobility prior to steam injection through the conventional vertical injectors. In spite of the high permeability communication path between the vertical injector and producer provided by the horizontal well at the base of the model, it was found that the steam zone still rose to the top of the model and swept it from the top down instead of from the base up. The authors concluded that a higher sweep efficiency could be achieved for smaller well spacings and that an increase in the steam injection rate led to a higher oil production rate and water-oil ratio.

Chang, Farouq Ali and George[23] reported results of low pressure, scaled-model experiments utilizing different combinations of vertical and horizontal wells for steamflooding heavy oil formations underlain by a bottom water zone of different thicknesses. The well combinations were: vertical injector-producer, horizontal injector-producer, vertical injector-horizontal producer, and horizontal injector-vertical producer. Horizontal wells were found to have better performance in thin bottom water situations than in homogeneous reservoirs having no bottom water. In addition, solvent injection ahead of the steam only marginally improved the recovery performance in thin (10% gross thickness) bottom water cases.

Nasr and Pierce[24] examined the potential of steamflooding heavy oil reservoirs through a bottom water zone in Cold Lake, Alberta. They performed a series of experiments in a scaled high pressure model. The prototype reservoir had 13 m of pay with a 2 m thick bottom water zone. They concluded that the primary advantage of a bottom water zone was the initial injectivity. It was also concluded that: steamflooding was gravity dominated, recovery and the OSR were sensitive to the injection rate, there could be a delay in oil production for up to one year, and after three pore volumes injected, 60% of the energy was lost in the produced fluids.

3.2.2 Layered Reservoir Models

Gümrah, Palmgren, Bruining, and Godderij[25] studied the steam drive process in layered reservoirs using a low pressure scaled physical model. The model used was a two-layered reservoir with the high permeability layer located at the top. The laboratory displacements were performed in a dipping reservoir. The results were compared with a theoretical interface model which combined the heat loss with the adjacent rock and fluid flow. The authors reported satisfactory agreement between the theory and experiments.

Yang and Butler[26] performed steamflood experiments in a physical model which simulated heterogeneous reservoirs. The types of reservoirs included reservoirs containing horizontal layers of different permeabilities and reservoirs with thin shale layers. The results for the horizontal layered reservoir indicated that the initial production was dominated by the top layer and the early performance was the same as if the reservoir was completely filled with the top layer porous medium. In the case of a low permeability layer overlaying a high permeability layer, the gravity drainage of bitumen above the permeability interface was enhanced by the steam sweeping under the low

permeability layer. For reservoirs with thin shale layers it was concluded that the short barrier did not greatly affect performance. In reservoirs with long horizontal barriers the production rate was dependent on the well configuration, with steam injection in the upper portion of the zone resulting in the highest oil recovery.

3.3 Horizontal Well Applications

3.3.1 Horizontal Wells in Enhanced Oil Recovery

Dietrich[27] described the Kern River horizontal well steam pilot which involved the drilling and completion of eight horizontal wells of varying lengths from a vertical shaft. The horizontal wells were arranged in a spoke-like fashion (rotating pattern), 45° apart from each other, and used for production. Poor oil response in initial periods was believed to have been caused by the placement of the horizontal wells in a highly unfavourable reservoir environment of low vertical permeability and depleted oil saturation and pressure at the pilot site. The termination of the pilot was followed by numerical studies aimed to develop better operating strategies and to predict future potential. The main conclusion derived from the simulation studies was that horizontal wells can be effective at reducing steam override.

Buller[28] described a unique pilot steamflood that incorporated one horizontal, one radial, and three vertical steam injection wells. The intent of the horizontal and radial wells was to reduce the steam override problem and improve sweep efficiency. The horizontal injector was a medium radius well that had 122 m (400 ft) completed in the pay zone. The radial well had four completed, near-horizontal, ultra-short radius laterals drilled within a short vertical section. Production data from offset producers, injection profile data, temperature data, log data, and observation data were used to compare the three different injection strategies. It was concluded that the horizontal wells had twice as high an OSR than the vertical wells, indicating that the horizontal wells were more efficient. The radial wells appear to effectively concentrate the steam in distinct vertical intervals. Due to the short period of the pilot no pattern-wide production increases had been seen yet.

Best, Lesage and Arthur[29] investigated steam circulation in horizontal wellbores. The need for this practice has come from limited thickness reservoirs in combination with low injectivity, thus requiring fracturing to establish sufficient steam injectivity. As a consequence of these high injection pressures, fractures communicating with

underlying water zones cause high water production at the start of the project. Theoretical studies which were carried out indicated that horizontal wells could allow sufficient sub-fracture steam injectivity and subsequent oil production. The authors developed a model to describe the heat transfer and fluid flow in a horizontal well. The model determined that low flow rates were the most effective in heating a reservoir during steam circulation in horizontal wells.

3.3.1.1 Productivity Index

Horizontal wells offer several advantages over conventional vertical wells. The most significant include better control of coning, higher productivity index, and a greater probability of intersecting fracture systems.

Vertical wells act as a point sink and as fluids flow to the vertical production well the area for flow decreases, the flow velocity increases, and the pressure gradient rises rapidly near the vertical well. Horizontal wells can improve the fluid production rate and the efficiency of a recovery process by providing a larger and more effective contact area between the well and the reservoir. Because of the larger contact area the pressure gradient near the production well is not as large. This results in higher drainage or production rates. In addition, the velocity is lower near a horizontal well than a vertical well thus resulting in a more uniform flow distribution.

Joshi[30] developed an equation to calculate the steady-state oil production rate that considered the elliptical drainage area created by a horizontal production well. Included in the investigation were the considerations of reservoir anisotropy, formation thickness, well drainage area, gas and water coning to a horizontal well, and well location (well not in the center of the reservoir). In comparing the productivity index of a horizontal well with that of a vertical well one important assumption was that the drainage areas were box-shaped and of equal size for both types of wells. From the study, it was concluded that the improvement in the productivity of a horizontal well over the productivity of a vertical well was dependent on the reservoir thickness, the length of the horizontal well, and reservoir anisotropy (coning of gas or water).

Giger[31] used the theory of complex functions to develop equations for the steady-state flow into horizontal wells and the pressure distribution along a horizontal well. Using these equations the author compared vertical and horizontal well performance in low permeability reservoirs, examined the effect of permeability anisotropy, and

compared the economics of horizontal wells with vertical wells. The criteria for the equations were based on the concepts of equivalent wellbore radius and equivalent drainage area. The author calculated how many vertical wells were required to match the performance of a single horizontal well draining the same area. From the above study it was concluded that horizontal wells are well-suited for thin reservoirs with good vertical permeability. A method to determine optimal well spacing was also presented.

Dikken[32] studied the effect of pressure drop in horizontal wells on production performance. He noted that often the flow in a horizontal well has been considered to be laminar which results in significantly lower flow resistance than for turbulent flow. This was supported with calculated examples. The author presented an analytical method that links single-phase turbulent well flow with stabilized reservoir flow. The second-order differential equation was solved numerically for various boundary conditions. The following conclusions were drawn: the flow inside a horizontal well is not laminar, turbulent flow inside a horizontal well could result in a large pressure drop along the length of the wellbore, and at a critical horizontal well length the accumulated drawdown loss can reach the drawdown applied at the beginning of the horizontal section.

3.3.1.2 Suppression of Coning Problems

Horizontal wells have the potential to improve recovery performance for reservoirs that experience water or gas coning problems. Independent of the type of production well, there is always a "critical velocity" that once exceeded can lead to the production of undesirable fluids. As stated previously, a horizontal well has a larger contact area with the reservoir and can reduce significantly the pressure gradient near the well. As a result of the reduction in pressure gradient, the horizontal well is able to produce at a comparable rate to a vertical well at a lower pressure drawdown. Conversely, with the same pressure drawdown the horizontal well would provide a higher fluid production rate than a vertical well. This higher fluid production rate could make or break a marginal development.

Chaperon[33] reported results of a study aimed at estimating the critical production rate of a horizontal well in anisotropic formations. The author used Muskat's approach with the following assumptions: steady-state or pseudo-steady state flow conditions, only stable cones were considered, and only flow in the plane orthogonal to the horizontal was examined. A simple equation to calculate the critical fluid production rate per unit length of horizontal well in an isotropic and an anisotropic reservoir was derived. The critical

production rate for a horizontal well was compared with that for a vertical well. It was determined that the critical cones usually came closer to the horizontal well than the vertical well. It was also concluded that the critical production rate per unit length of a horizontal well was a function of: the oil column thickness, the distance between the well and lateral boundaries, and the horizontal transmissibility of the oil layer. In addition, the horizontal well displayed less sensitivity to vertical permeability changes than a vertical well.

Joshi[34] applied the above work to bottom water drive reservoir and proposed a modification to a convectional equation used to determine water cone height for vertical wells so water breakthrough and water cut could be calculated for horizontal wells. From the work performed it was concluded that the critical production rate for a horizontal well was substantially higher than that for a vertical well, and gains in the critical rate for horizontal wells depended mainly on the well length and drainage area.

3.3.1.3 Steam-Assisted Gravity Drainage

Steam-assisted gravity drainage involves the continuous injection of steam into a constant-pressure steam zone which expands slowly in different directions and mobilizes (by conductive heat transfer) the surrounding heavy oils. The vertical growth of the steam zone would appear to be larger than lateral growth, but eventually the vertical growth is limited by the top of the reservoir and the lateral growth would then become critical. The mobilized heavy oil is drained continuously by gravity downwards into a horizontal well at the base of the formation. The main advantages of steam-assisted gravity drainage over conventional steam stimulation processes (steamflooding and cyclic steam stimulation) are a slower and more uniform displacement front which results in a higher sweep efficiency, and improved mobility due to the oil and the other phases having separate flow paths, thereby not interfering with each other during displacement.

Butler, McNab, and Lo[35] presented a study on steam-assisted gravity drainage of heavy oil to horizontal wells placed at the bottom of the oil reservoir. The study included scaled physical model experiments in both high and low pressure models and theoretical analysis. An equation to predict the rate of drainage of heavy oil around an expanding steam chamber, which is above a horizontal well, was derived. Experiments were carried out to validate theoretical analysis using actual Cold Lake crude. Agreement between observed production and predicted production was fairly good. The observed

production rates were less than predicted. This was attributed to the smaller gravity head in the model.

Butler and Stephens[36] extended the above work to consider a drainage area which was a series of parallel horizontal wells. Theoretical equations were derived for the rate of drainage as a function of the main variables. Included in the modifications to the equations was the effect of using some of the available gravity head to move the oil laterally to the horizontal well. The equations differed in that they considered the time required for the steam zone to move horizontally to the no-flow plane located halfway between a horizontal well pair. Again, as in the above work, an experimental investigation was performed to validate the theoretical analysis. The modified equations gave results comparable with the experimental data.

Griffin and Trofimenkoff[37] performed laboratory studies of the steam-assisted gravity drainage process in support of the Cold Lake pilot project of Esso Resources Canada Limited. They conducted two types of experiments: those in a low pressure visual model and others in a high pressure model. The visual model showed that the theory developed by Butler et al.[35] accurately predicted oil production rates and the effect of oil viscosity. The scaled models demonstrated that the process had a long life span and that the steam override and heat loss to the overburden were not as great as was initially indicated by theory.

Butler[38] presented a method for predicting bitumen drainage from around a growing steam chamber located above a horizontal well. In this method the interface was treated as a number of segments. The oil drainage for each segment was calculated for successive time steps and these rates were used to calculate the displacement of oil from the whole interface. The change in the accumulated heat penetration from the steam zone to the surrounding bitumen was estimated using an approximate differential equation. It was concluded that the new method predicted drainage rates of the same order as those obtained from earlier methods, and that the thermal efficiency of the process for unconfined wells was highly dependent on the degree of steam override.

Joshi[39] extended work on steam-assisted gravity drainage using a physical model to investigate the effects of different well configurations, shale barriers, and limited initial steam injectivity. Two well configurations were employed: horizontal injector and producer, vertical injector and horizontal producer. Two different shale barriers were employed in the model: continuous and discontinuous. It was concluded from the

experimental results that a vertical steam injector and a horizontal producer yielded higher and more rapid oil recovery than was obtained using a horizontal well pair for reservoirs with shale barriers. The presence of shale barriers was deemed not to have a significant impact on the final oil recovery, but it did take slightly longer and require more steam injection than in a uniform permeability reservoir. The effect of limited steam entry caused by vertical fractures did not adversely affect the gravity drainage process. It did, however, result in high initial oil production.

Edmunds, Haston, and Best[40] described the steam-assisted gravity drainage project at the AOSTRA Underground Test Facility (UTF). The authors analyzed the steam zone growth rate in terms of the ceiling and slope drainage. Slope and ceiling drainage occur in the steam zone at the sides or at the top of the steam zone, respectively. Included in the study were the effects of anisotropy, heterogeneities, solution gas, and capillary pressure on the steam zone growth rate. The authors reported the design and implementation of the pilot program to evaluate the use of steam-assisted gravity drainage in oil sands. The pilot consisted of utilizing three horizontal well pairs located in the lower interval of the McMurray zone. The spacing between the well pairs was 25 m, and the vertical spacing between each of the well pairs was approximately 5 m. The wells had 60 m of completion with sand screens along this length. The test program recorded satisfactory production results and the testing program was projected to successfully meet all of the objectives.

4. Scaling Parameters and Calculations

The following chapter describes the method used in developing the low pressure physical model used in this study. The scaling criteria proposed by Stegemeier, Laumbach and Volek[13] were used to construct the low pressure physical model and determine operating parameters. In addition, a scaling criterion derived by Doan, Farouq Ali, and George[41] was used to design the model horizontal well. Parameters are presented for scaling-up the physical model to field scale. The technique to implement the scaling criteria is illustrated, including example calculations. The governing equations and the assumptions used to develop the scaling criteria are provided.

4.1 Development of Scaling Parameters for the Low Pressure Model

4.1.1 Unscaled Parameters

As stated previously, complete scaling of different aspects of the steamflooding process is not possible for two reasons - first, because several of the scaling groups are not compatible with each other and, secondly, due to the unavailability of materials and fluids having the physical properties that will satisfy all scaling requirements. These physical constraints unfortunately lead to approximations and simplifications in the final product. As a result, a reduced number of parameters known as scaling parameters were generated.

The parameters which were unscaled between the model and prototype systems in this study are as follows:

1. Steam distillation of the crude oil.
2. Capillary pressure and relative permeability.
3. Thermal expansion and compression of the reservoir fluids and matrix.
4. The extent of emulsification and its mechanism.
5. Specifications corresponding to the injection and production of a horizontal well (such as: pressure drop in the vicinity of and within the well-bore, skin factor, and the most desirable perforation intervals).
6. Effects of asphaltene flocculation.

To best scale down the field the relative permeability and capillary pressure relationship would have to be the same functions of saturation in both the model and prototype. Because of the large difference in the prototype and model matrixes they can not be scaled. Prats[17] stated that the three-phase curves for the prototype could not be determined if the relative permeabilities were not scaled. Prats[17] produced good correlations between the Peace River prototype and the physical model despite the limitations of the scaling procedure. Pujol and Boberg showed that for highly viscous oils (μ > 100,000 mPa.s) accurate scaling of the capillary pressure was not crucial.

The unscaled parameters listed above could be more readily addressed by a high pressure model where the pressures, temperatures, fluids and matrix of the prototype could be reproduced in the model. However, the success of vacuum model studies implies that the above listed parameters have only a second order effect on the processes involved. It is also noted that although the parameters are not scaled they may exist during the steam drive process.

4.1.2 Scaling Procedures

The scaling parameters in Table 4.1 were obtained using the procedure presented by Stegemeier et al.[13]. The procedure is presented below. Development of the scaling parameters started with the formulation of the governing partial differential equations of fluid flow and heat transfer. These equations were put into dimensionless form (m_D). This was done by dividing the dimensional variable (m) by a suitable reference quantity (m_R).

Thus:
$$m_D = \frac{m}{m_R} \tag{4.1}$$

Next the set of similarity parameters was identified by inspectional analysis. This was followed by combining and modifying, using engineering judgement, the similarity parameters which could be matched between the scaled model and field prototype.

Stegemeier et al.[13] made the following assumptions when deriving the scaling criteria for the low pressure model:

1. Three phases consisting of oleic, aqueous and vapour phase (no volatile hydrocarbons) may exist.

Table 4.1 — Scaling Parameters for Steam Processes (Modified from Ref. 13).

Number	Scaling Parameter	Name of Scaling Parameter
I	$\frac{p_R}{\rho_R g_R L_R}$	Poiseuille Number divided by Stokes Number.
II	$\left(\frac{f_{sR} L_{vt}}{C_R T_R} + 1\right) \times A^*$	Modified Jacob Number + 1.
III	$\frac{f_{sR} \mu_{sR} \rho_R}{\mu_R \rho_{sR}}$	Ratio of steam pressure gradient to oil pressure gradient.
IV	$\frac{k_{hR} t_R}{\phi_R S_R \rho_R C_R L_R^2} \times A^*$	Fourier Number or Peclet Number.
V	$\frac{\phi_R S_R \mu_R L_R}{k_R \rho_R g_R t_R}$	Stokes Number.
VI	$\frac{w_R t_R}{\rho_R \phi_R S_R L_R^3}$	Poiseuille Number divided by Modified Poiseuille Number.

* Subscript 'R' denotes the reference variable used to obtain a a dimensionless term.

** When $\phi\Delta S$ is not matched, A^* takes on a value between unity and $\phi_R S_R \left(\frac{\rho_R C_R}{\rho_{cR} C_{cR}}\right)$.

— If reservoir heating or heat production predominates, use unity.

— If cap and base rock heating predominates, then use $\phi_R S_R \left(\frac{\rho_R C_R}{\rho_{cR} C_{cR}}\right)$.

2. There is no partitioning into or out of the oil phase (dead oil assumption).

3. Rock compressibility and thermal expansion are negligible.

4. Darcy's and Fourier's equations are valid.

5. Capillary pressure effects are negligible.

6. The system is in local thermodynamic equilibrium.

7. Kinetic energy, and potential energy, are negligible compared with the thermal energy.

8. The enthalpy and internal energy are essentially equal for the oleic phase and for the aqueous phase and are linear functions of temperature.

9. The difference between the steam enthalpy and internal energy can be neglected.

10. The time rate of change of the specific steam enthalpy in the steam zone is negligible.

11. The internal energy of the rock is a linear function of temperature.

12. The saturated steam temperature is the maximum temperature at any location.

13. Relative permeabilities depend exclusively on the saturations.

14. S_{or} and S_{wc} are constant and uniform throughout the model.

15. Critical saturation for steam flow is assumed to be zero.

16. The changes in the density of the immobile water and residual oil are negligible.

With the above assumptions and applying the conservation of mass balance to the oil phase, denoted by the subscript 'o', yields:

$$\phi \frac{\partial(\rho_o S_o)}{\partial t} + \nabla \cdot (\rho_o \vec{u}_o) = 0 \qquad (4.2)$$

The continuity equation for water, (in both liquid and vapor phases denoted by subscript 'w' for water in the liquid phase and 's' for the vapor) is given by:

$$\phi\frac{\partial(\rho_w S_w)}{\partial t}+\nabla\cdot(\rho_w\vec{u}_w)+\phi\frac{\partial(\rho_s S_s)}{\partial t}+\nabla\cdot(\rho_s\vec{u}_s)=0 \tag{4.3}$$

From the assumption that Darcy's equation is valid, the following equation was written for any phase j, where j=o, w, or s (z-coordinate is positive downward):

$$\vec{u}_j=-\frac{kk_{rj}}{\mu_j}\left(\nabla p_j-\rho_j\vec{g}\right) \tag{4.4}$$

The conservation of energy for the reservoir can be expressed as:

$$\begin{aligned}&\left[(1-\phi)\rho_r C_r+\phi(\rho_o C_o S_o+\rho_w C_w S_w)\right]\frac{\partial T}{\partial t}+L_v\left[\phi\frac{\partial(\rho_s S_s)}{\partial t}+\nabla\cdot(\rho_s\vec{u}_s)\right]\\&+(\rho_o C_o\vec{u}_o+\rho_w C_w\vec{u}_w)\cdot\nabla T+\rho_s\vec{u}_s\cdot\nabla h_s+\nabla\cdot\vec{q}=0\end{aligned} \tag{4.5}$$

Conductive heat flux was expressed by the Fourier equation as:

$$\vec{q}=-k_h\nabla T \tag{4.6}$$

When all three phases were present, the constraint equation became:

$$S_O+S_W+S_S=1 \tag{4.7}$$

At saturation conditions the interdependence of the pressure and temperature are related by the Clausius-Clapeyron relationship which, in the functional form, is:

$$p_{sat}=p_{sat}(T_{sat}) \tag{4.8}$$

The constitutive equations, required to describe the remaining dependence of the material properties in the reservoir system on the thermodynamic state variables, were expressed in their functional forms as:

$$\phi=\phi(x, y, z) \tag{4.9}$$

$$\rho_j=\rho_j(p, T) \tag{4.10}$$

$$k = k\,(x, y, z) \tag{4.11}$$

$$k_{rj} = k_{rj}\,(S) \tag{4.12}$$

$$\mu_j = \mu_j\,(T) \tag{4.13}$$

$$h_s = h_s\,(T) \tag{4.14}$$

$$L_v = L_v\,(T) \tag{4.15}$$

$$k_h = k_h\,(x, y, z) \tag{4.16}$$

$$\phi_r = \phi_r\,(x, y, z) \tag{4.17}$$

where S denotes phase saturation dependence and j denotes the phase.

4.2 Example of Scaling Prototype to Model Conditions

The first step towards making the physical model was the selection of the values to represent the prototype. The prototype for the physical model was one quarter of an 8-ha (20-acre), five-spot pattern of a typical moderately viscous oil deposit in the Lloydminster, Saskatchewan, area. Currently, the prototype reservoir is being produced using vertical production wells only. Table 4.2 contains data for the prototype reservoir, and some of the more important data of the model reservoir.

Often a single value of a quantity must be chosen to represent the whole field. This single value may not be characteristic of the whole field or the element of symmetry to be modelled. In such a case the decision to construct the model with a similar distribution or a "constant" average value must be made. One method is to use an average, as in the case of the permeability, where the permeability will vary throughout the field but a single permeability was needed in the scaling calculations.

4.2.1 Length Scaling

The length scale for the model, although somewhat arbitrary, was determined by the physical size of the model and the pressure-temperature relationships. Stegemeier et al.[13] recommended that if the production pressure was 689 kPa (100 psia) or less, then to match the temperature-pressure relationship for saturated steam the length scale, g(L), should be made as small as possible. Thus, the model should be as large as possible

Table 4.2: Scaling Parameters for the Prototype Reservoir

Field Property	Prototype Value	Model Value
Well Spacing	1/4 of 20 acre, 5-spot	1/4 of 5-spot
Length	141.4 m	0.8128 m
Net Pay Thickness	11 m	0.0632 m
Porosity	0.31	0.34 (average value)
Permeability	4.0 darcies	4498.5 darcies (scaled value)
Thermal Conductivity	0.002077 kW/m•K	0.003266 kW/m•K
Heat Capacity	2.1803 kJ/kg•K	2.3824 kJ/kg•K
Initial Fluid Saturations	$S_o = 0.73$ $S_w = 0.25$ $S_g = 0.02$	$S_o = 0.92$ $S_w = 0.075$ $S_g = 0.005$
Steamflood Residual Oil Saturation	$S_{or} = 0.15$ (estimated)	$S_{or} = 0.25$ (estimated)
Oil Density	993 kg/m^3	879.9 kg/m^3
Oil Viscosity	1275 mPa•s at 23.9°C 865 mPa•s at 32.2°C 220 mPa•s at 65.6°C 26 mPa•s at 135.0°C 1.3 mPa•s at 301.7°C	270 mPa•s at 22.9°C 238 mPa•s at 25.0°C 137 mPa•s at 35.0°C 123 mPa•s at 37.0°C 57.1 mPa•s at 52.0°C
Water Viscosity	0.891mPa•s at 25.8°C	0.891mPa•s at 25.8°C
Initial Reservoir Temperature	23.3°C	3.0°C
Initial Reservoir Pressure	3.45 MPa	0.0267 MPa
Production Pressure	0.345 MPa (gauge)	0.01397 MPa (abs.)
Steam Injection Pressure	3.345 MPa (gauge)	0.068 MPa (abs.) (scaled value)
Steam Injection Rate	100 - 150 m^3/D	212.0 ml/min (scaled value)
Steam Quality	0.70	0.11
Horizontal Wells		
Length		
Short Medium Long	35.4 m (116 ft) 53.1 m (174 ft) 70.7 m (232 ft)	20.3 cm (8 inch) 30.5 cm (12 inch) 40.6 cm (16 inch)
Outside Diameter	8.89 cm (3.5 inch)	4.75 mm (0.187 inch)

within practical constraints of cost, time to prepare and conduct experiments, laboratory space restrictions, etc. The larger the model, the greater the possibility of leaks and the more likelihood of difficulty in detecting those leaks. Also, the larger the model the, greater the required thickness of the base and cap rocks to eliminate the heat loss boundary effects.

The prototype length, L_p, for the element of symmetry was 141.4 m (463.9 ft) which was represented in the laboratory with a length of 0.813 m (32 inches). This resulted in a length scale of 174, i.e.:

$$\frac{L_P}{L_M} = g(L) = 174, \tag{4.18}$$

where the subscripts p and m signify prototype and model, respectively. Applying the length scale factor to the three dimensions of the prototype results in a model with the following dimensions: 0.813 m x 0.813 m x 0.063 m thick.

4.2.2 Model Production Pressure Scaling

There is an appreciable pressure drop in the steam zone and thus the pressure-temperature relation for saturated steam must be scaled. For prototype pressures as low as 0.345 MPa (50 psia) and length scale factors of 100 to 200, the best match can be obtained by selecting the lowest possible production pressure. From a physical perspective the lowest pressure an available vacuum pump can maintain is approximately 33 cm of mercury; also, the vapor pressure of water must be considered. With the above limitations the value of the production pressure in the following calculations was taken as 13.79 kPa, i.e.:

$$(P_P)_M = 13.79\text{kPa}$$

From scaling parameter 1 in Table 4.1 the parametric equality is:

$$\gamma(\Delta P) = \frac{(P - P_P)_P}{(P - P_P)_M} = \frac{\rho_P g_P L_P}{\rho_M g_M L_M} \tag{4.19}$$

where:

$$\gamma(\rho_r) = \frac{\rho_P}{\rho_M} = 0.9 \tag{4.20}$$

$$g(g_r) = \frac{g_P}{g_M} = 1.0 \tag{4.21}$$

$$(P_P)_P = 0.345\text{MPa} \ (50 \text{ psia})$$

$$(P_P)_M = 13.79 \text{ kPa} \ (2 \text{ psia})$$

where P_p denotes the production well pressure. Substituting the corresponding values, the pressure scaling relationship is:

$$\frac{(P - 0.345 \text{ MPa})_P}{(P - 0.01378\text{MPa})_M} = 0.9 \times 1.0 \times 174$$

which reduces to:

$$P_M = 0.011567 + 0.006387 P_P \tag{4.22}$$

In carrying out the scaling calculations Table 4.3 was created. Several prototype pressures covering the range of scaling are tabulated along with their corresponding saturated steam temperatures T_S, the enthalpy of water at steam temperature. The table also contains the calculated model pressures with corresponding steam saturation temperatures and other quantities yet to be determined.

4.2.3 Model Temperature Scaling

To scale the model temperature it was desired to have the largest temperature range possible to obtain the best match between the model and prototype oil-viscosity curves. The lower limit was set by the freezing point of water.

Because of the dynamics of the experiments the injection pressure changes a great deal from the start of the experiment to the end. With the dynamics of the experiment considered, a single point pressure and temperature had to be chosen for scaling purposes. Stegemeier et al.[13] suggested that it is best to take a value from the middle or upper parts of the pressure range for finding the temperature difference ratio, the reason for this is that most of the oil will be produced when the temperature is high. Steady

Table 4.3: Prototype and Model Scaling Values .

Prototype Values							Model Values										
p (MPa)	Ts (C)	hw (kJ/kg)	CwΔT (kJ/kg)	Lv (kJ/kg)	ρ (kg/m3)	μs (cp)	p (MPa)	Ts (C)	Tsc (C)	hw (kJ/kg)	CwΔT (kJ/kg)	Lv (kJ/kg)	ρ (kg/m3)	μs (cp)	fs	μom/μop (cp/cp)	wa/wt
*	*	*	*	*	*	**	Eq.4.22	*	Eq.4.24	*	*	*	*	**	Eq.4.37	Eq.4.39	Eq.4.38
3.45	241.73	1045.6	949.1	1757.9	17.346	0.01729	0.0336	71.80	76.00	299.3	286.7	2325.8	0.213	0.01086	0.051	4.12	0.8827
3.00	233.90	1008.4	911.9	1795.7	15.035	0.01708	0.0307	69.60	73.38	291.3	278.7	2334.9	0.195	0.01079	0.069	5.37	0.8689
2.50	223.99	962.1	865.6	1841.0	12.508	0.01680	0.0275	67.30	70.07	285.9	273.3	2336.4	0.177	0.01072	0.077	5.47	0.8646
2.00	212.42	908.8	812.3	1890.7	10.037	0.01645	0.0243	64.40	66.20	269.5	256.9	2347.8	0.157	0.01062	0.082	5.36	0.8658
1.50	198.32	844.9	748.4	1947.3	7.589	0.01598	0.0211	61.50	61.49	257.4	244.8	2354.9	0.139	0.01053	0.091	5.21	0.8620
1.00	179.91	762.8	666.3	2015.3	5.143	0.01527	0.0180	57.80	55.34	241.9	229.3	2364.0	0.118	0.01042	0.104	4.90	0.8559
0.50	151.86	640.2	543.7	2108.5	2.667	0.01406	0.0148	53.75	45.96	224.9	212.4	2373.9	0.099	0.01029	0.132	4.13	0.8372
0.345	138.36	582.0	485.5	2149.7	1.966	0.01346	0.0138	52.20	41.45	218.5	205.9	2377.6	0.092	0.01024	0.149	3.86	0.8232

* "Fundamentals of Classical Thermodynamics", 3rd Ed., SI Version by G.J. Van Wylen and R.E. Sonntag (1985), Ref. 43

** μs=-5.46807E-4+6.8949E-6*T-3.39999E-8*T^2+8.29842E-11*T^3-9.9706E-14*T^4+4.7194E-17*T^5, Ref. 42

state injection temperatures and pressures in the model were about 74°C and 45 kPa absolute pressure, respectively.

Using the injection pressure of the prototype of 1.9 MPa, the corresponding temperature for saturated steam is 198.32°C. With the above temperatures the temperature ratio can be determined as follows:

$$\frac{(\Delta T)_P}{(\Delta T)_M} = \frac{\left(T_{inj} - T_I\right)_P}{\left(T_{inj} - T_I\right)_M} = \frac{\left(T_{sat} - T_I\right)_P}{\left(T_{sat} - T_I\right)_M} \tag{4.23}$$

Using the steady state steam saturation temperatures:

$(T_{initial})\ P = 23.3°C$

$(T_{initial})\ M = 3.0\ °C$

$(T_{sat})\ P = 198.32°C$

$(T_{sat})\ M = 74.0°C$

substitution of these values results in:
$$\frac{(\Delta T)_P}{(\Delta T)_M} = \frac{198.32°C - 23.3°C}{61.5°C - 3.0°C}$$

which yields the identity:
$$\frac{(\Delta T)_P}{(\Delta T)_M} = 2.9918 \tag{4.24}$$

The above ratio must be constant over the temperature range to have the proper proportion of energy stored as internal energy, thus:

$$\frac{\left(T_{sat} - 23.3°C\right)_P}{\left(T_{sat} - 3.0°C\right)_M} = 2.9918$$

which reduces to:
$$T_M = 0.3342T_P - 4.7879 \tag{4.25}$$

4.2.4 Scaled Steam Quality Requirement

The scaled steam quality was determined from parameter II in Table 4.2. The prototype reservoir was quite thin and thus it was assumed that cap and base rock heating predominates. The scaled model steam quality was given by:

$$f_{st,M} = \left(\frac{C_w \Delta T}{L_v}\right)_M \left\{\left(\frac{f_{st} L_v}{C_w \Delta T} + 1\right)_P \times \left[\left(\frac{\phi_P \Delta S_P}{\phi_M \Delta S_M}\right)\left(\frac{\rho_P C_P}{\rho_M C_M}\right)\left(\frac{\rho_{cM} C_{cM}}{\rho_{cP} C_{cP}}\right)\right] - 1\right\} \tag{4.26}$$

Example 1:

Unless otherwise specified all sample data was from the last row of data in Table 4.3. Substituting in values for the steam quality calculation at steady state steam injection conditions yields:

$$f_{st,M} = \left(\frac{205.9 kJ/kg}{2377.6 kJ/kg}\right)_M \left\{\left(\frac{0.7 \times 2149.7 kJ/kg}{485.48 kJ/kg} + 1\right)_P \left[\left(\frac{0.31 \times 0.62}{0.34 \times 0.85}\right)(1)(1)\right] - 1\right\} = 0.149$$

4.2.5 Calculation of Model Oil Viscosity

It is important to scale the oil viscosity at conditions after steam breakthrough which is when most of the oil is produced. To match the pressure gradient in the steam zone and the oil zone, the oil viscosity must be scaled according to Parameter III from Table 4.1:

$$\frac{\mu_{oM}}{\mu_{oP}} = \left(\frac{f_{st,M}}{f_{st,P}}\right)\left(\frac{\mu_{sM}}{\mu_{sP}}\right)\left(\frac{\rho_{sP}}{\rho_{sM}}\right)\left(\frac{\rho_{oM}}{\rho_{oP}}\right) \tag{4.27}$$

Example 2

Substituting the data at the saturation temperature into equation (4.3) yields:

$$\frac{\mu_{oM}}{\mu_{oP}} = \left(\frac{0.149}{0.70}\right)\left(\frac{0.01024}{0.01346}\right)\left(\frac{1.966}{0.092}\right)\left(\frac{1}{0.9}\right) = 3.845$$

The actual oil viscosity using physical viscosity measurements and reported field data was correlated using Andrade' s equation. This resulted in the following equations:

$$(\mu_o)_P = 0.00080869 \times \exp(4239.8/(T + 273.15)) \tag{4.28}$$

$$(\mu_o)_M = 0.000007782 \times \exp(5140.9/(T + 273.15)) \tag{4.29}$$

4.2.6 Calculation of the Time Scale Factor

Because this study involves thin formations it was assumed that cap and base rock heating predominates. Thus, the time scale ratio was determined using the dimensionless scaling parameter (IV) where A^* is given by $A^* = \phi_R S_R (\rho_R C_R / \rho_{cR} C_{cR})$, from Stegemeier et al.[13]. This results in the following dimensionless scaling group:

$$\frac{t_M}{t_P} = \left(\frac{k_{hP}}{k_{hM}}\right)\left(\frac{\rho_{cM} C_{cM}}{\rho_{cP} C_{cP}}\right)\left(\frac{L_M}{L_P}\right)^2 \tag{4.30}$$

where: $k_{hM} = k_{granite} = 0.003266$ kW/m•K (2.81 kcal/(m•hr•°C))

$k_{hP} = k_{sandstone} = 0.002077$ kW/m•K (1.79 kcal/(m•hr•°C))

$\rho_{cM} C_{cM} = 2.3824$ kJ/kg•K (granite cap block)

$\rho_{cP} C_{cP} = 2.1803$ kJ/kg•K (sandstone cap block)

Substituting those data, and the identity (4.18), into equation (4.30) yields:

$$\frac{t_M}{t_P} = \left(\frac{0.002077}{0.003266}\right)\left(\frac{2400}{2242}\right)\left(\frac{2.3824}{2.1803}\right)\left(\frac{1}{174}\right)^2 = 2.4572 \times 10^{-5}$$

For t_M in minutes (lab time units) and t_P in years (field time units), the final form of the time ratio is:

$$\frac{t_M}{t_P} = 2.4569 \times 10^{-5} \times 365\,\text{D/yr} \times 24\,\text{hr/D} \times 60\,\text{min/hr}$$

$$\frac{t_M}{t_P} = 12.92\,\text{min/yr} \tag{4.31}$$

This time ratio means that 12.92 minutes of experiment in the model are equivalent to one year in the prototype.

4.2.7 Scaling of Model Permeability

To calculate the permeability of the model porous medium Stegemeier et al.[13] used Stokes Number (Parameter Number V) in Table 4.1:

$$\frac{k_M}{k_P} = \left(\frac{\phi_M \Delta S_M}{\phi_P \Delta S_P}\right)\left(\frac{L_M}{L_P}\right)\left(\frac{\mu_M}{\mu_P}\right)\left(\frac{\rho_{oP}}{\rho_{oM}}\right)\left(\frac{t_P}{t_M}\right) \tag{4.32}$$

It can be seen that k_M/k_P is temperature dependent since μ_m/μ_p is a function of temperature. However, k_M/k_P cannot be a function of temperature in order to scale it, therefore, a single representative value of μ_M/μ_P must be selected to calculate a single value for the scaled model permeability. To select this single value it was suggested that the μ_M/μ_P ratio is significant only when steam pressures are low. This occurs only after steam breakthrough and around the vicinity of the production well. In addition this permeability value is most significant in the vicinity of the production well. For this reason the ratio was taken at the prototype steam injection temperature of 240 °C using Equations (4.28) and (4.29). Substituting in the values to the constants defined in Equations (4.18), (4.20), (4.30), (4.32) to (4.35) into Equation (4.40) yields:

$$\frac{k_M}{k_P} = \frac{0.34 \times 0.65}{0.31 \times 0.60}\frac{1}{174} \times \frac{11.38}{3.16} \times \frac{1}{.89} \times \frac{1}{2.4572 \times 10^{-5}} = 1124.48$$

Since the permeability of the prototype, k_P, is 4 darcies:

$$k_M = k_P \times 4 \text{ darcies} = 1124.48 \times 4 \text{ darcies} = 4497.9 \text{ darcies.} \tag{4.33}$$

4.2.8 Scaling Down of Vertical Wells

Direct geometric scaling of vertical wells would not work. With the length scale of 174, the scaled down size of the well would introduce a mechanical problem of constructing such a well. Of more significance was the relative size of the glass beads at the well. The bead diameter could be larger than the well diameter and this could cause flow through beads to dominate flow through the well.

Stegemeier et al.[13] introduced the 'slit' well concept for scaling of the vertical wells. In this concept the effective radius of the slit well is a function of the slit width and the bead pack directly in front of the slit. The relationship between the slit width and the effective model well radius is:

$$\omega = 2\pi r_m \tag{4.34}$$

where ω = slit width, and r_m= the effective radius of the model well.

The effective radius was determined by assuming a prototype well radius of 15.24 cm (6 inches), and substituting that into identity (4.18) yields:

$$L_M = \frac{L_P}{174} = \frac{15.24}{174} = 0.0876 \text{ cm} = d_M.$$

Thus, the model well radius was 0.0438 cm, the slit width can now be calculated from equation (4.34):

$$\omega = 2\pi(0.0438) = 0.2752 \text{ cm.} \tag{4.35}$$

4.2.9 Scaling Down the Horizontal Well

Doan et al.[41] suggested the following scaling criterion for scaling down the size of a prototype horizontal well:

$$\left[\frac{\mu_o r_w^2 v}{JLk(\Delta p)}\right]_P = \left[\frac{\mu_o r_w^2 v}{JLk(\Delta p)}\right]_M \tag{4.36}$$

Rearranging the above group and solving for the radius of the model horizontal well results in:

$$(r_w)_M = \left[(r_w)_P^2 \frac{(\mu_o)_P}{(\mu_o)_M} \frac{L_M}{L_P} \frac{v_P}{v_M} \frac{k_M}{k_P} \frac{(\Delta p)_M}{(\Delta p)_P}\right]^{0.5}.$$

Assuming that the flow velocity in the prototype was one-tenth of that in the model, and that the prototype horizontal producer had an O.D. of 8.89 cm (3.5 inch), then:

$$(r_w)_M = \left[4.445^2 \frac{3.16}{11.4} \frac{1}{1740} \frac{4497.9}{4.0} \frac{0.05459}{3.0}\right]^{0.5} = 0.254 \text{ cm} \tag{4.37}$$

For this study, a steel tubing of 4.75-mm O.D. was used for the horizontal well (either producer or injector), since 0.508-cm O.D. tubing is not a standard size. This resulted in a 6.5% difference between the actual well size and the value determined by the scaling criterion. As a consequence, this led to a 12.6% difference in the assumed velocity ratio between prototype and model conditions. Scaling of the horizontal well length was straight forward, using a length scaling factor of 174 (as in the case of the model length). In the experiments, three different lengths of the model horizontal producer were used: 20.3 cm (8 inches), 30.5 cm (12 inches), and 40.6 cm (16 inches). These values

correspond to 35.4 m, 53.1 m and 70.7 m long horizontal wells in the field, respectively. In addition, well perforations were simulated by covering the slotted tubing with duct tape. For the short horizontal well experiments half of the well length was covered by duct tape.

4.2.10 Steam Injection Rate Scaling

The following scaling criterion, parameter (VI) in Table 4.1, was used to determine the ratio between model and prototype steam injection rates:

$$\frac{W_M}{W_P} = \frac{(\rho_o)_M}{(\rho_o)_P}\left(\frac{L_M}{L_P}\right)^3 \frac{(\phi\Delta S)_M}{(\phi\Delta S)_P}\frac{t_M}{t_P} \tag{4.38}$$

Substituting appropriate values in the above led to:

$$\frac{W_M}{W_P} = \frac{0.89}{1.0}\left(\frac{1}{174}\right)^3 \frac{0.34\times 0.65}{0.31\times 0.60}\frac{1}{2.4572\times 10^{-5}} = 0.00817$$

According to this ratio, a steam injection rate of 1.0 sm^3/day in the prototype is equivalent to a steam injection rate of 5.63 ml/min in the model.

5. Experimental Apparatus and Procedure

5.1 Experimental Apparatus

As illustrated in Chapter 4, the low-pressure physical model used in this study was designed after the scaling criteria for vacuum models proposed by Stegemeier et al.[13] and Doan et al.[41]. Figure 5.1 shows the experimental apparatus used in this study. It consisted of four sub-systems: the scaled physical model (fiberglass tray), steam injection system, produced fluid collection system, and data acquisition system.

5.1.1 Physical Model

As shown the physical model was designed to represent one-quarter of an eight hectare (20 acre) five-spot pattern. The element of symmetry had dimensions of 281.55 m x 281.55 m x 11 m (thick). The length scale factor used was 174. With this factor the dimensions of the physical model were 81.28 cm (32 inch) x 81.28 cm (32 inch) x 6.35 cm (2.5 inch).

Fiberglass was the material used for the model tray because of its low thermal conductivity, it is strong and easy to machine, and it is inexpensive. Granite blocks were placed above and below the model to simulate the overburden and underburden heat sinks; granite closely modeled the thermal conductivity and heat capacity of the prototype overburden and underburden. Altogether, 36 thermocouples were placed at different positions inside the physical model to monitor the reservoir temperatures during an experiment. The thermocouples were placed in two horizontal layers, sixteen in each layer, and one thermocouple in each of the four corners of the square model. The thermocouple layers were at one-third and two-thirds of the model thickness. Pressure transducers and thermocouples were placed at the injection and production wells to measure the pressure and temperature at these two points. Pressure transducers were also used to measure the pressure drop along the horizontal well. The physical model is shown in Figure 5.2 which also displays the approximate locations of the upper layer of thermocouples.

The scaling criteria required that the initial model temperature be 3°C. To create a bottom water layer, saline bottom water had to be frozen in place prior to saturating the model with oil. For these reasons the cooler was required to work both as a cooler and a freezer. The model was supported by a cart running on tracks that went from the experimental area into the cooler/freezer. With the cart/rail system the model could easily

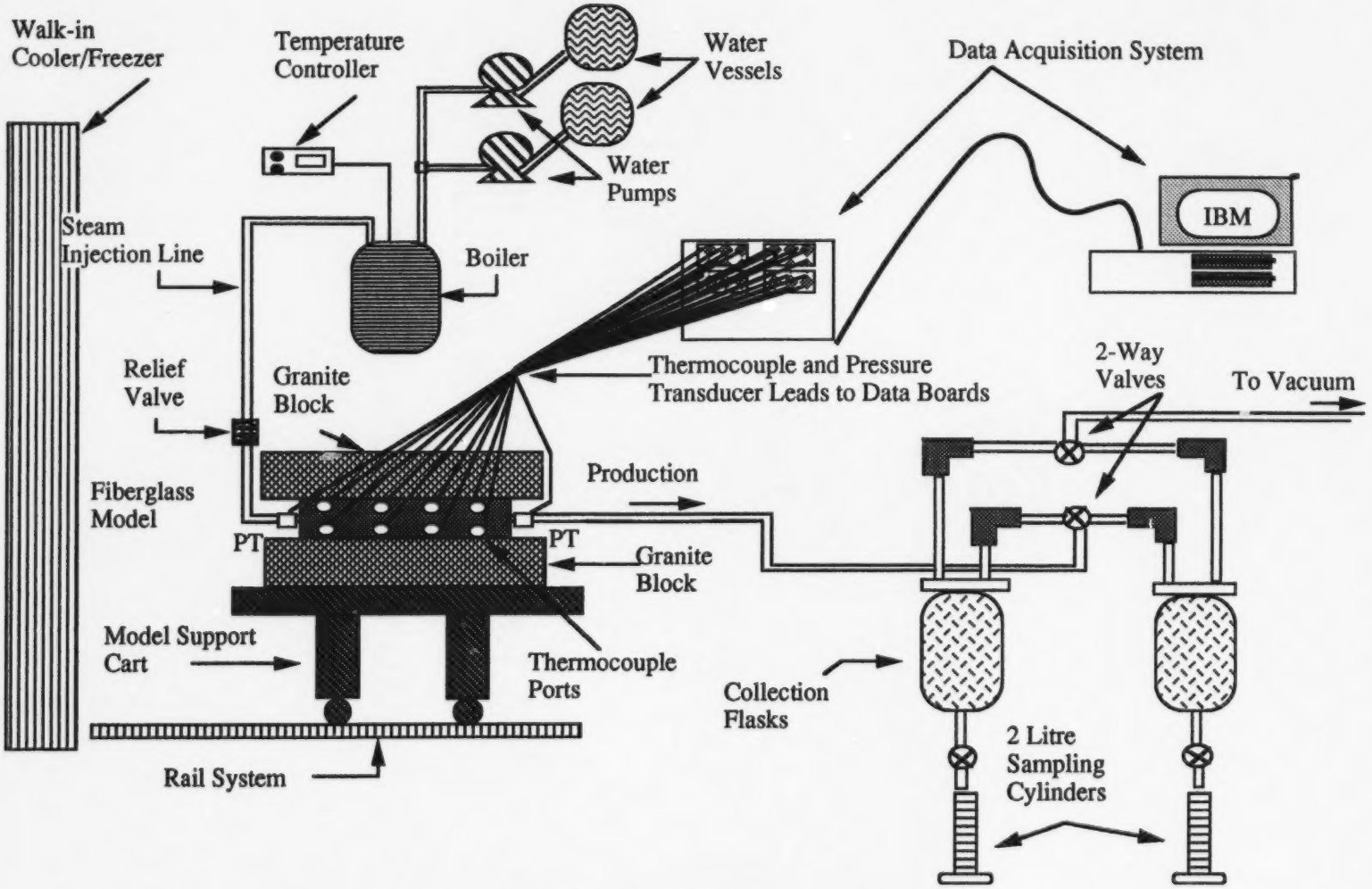

Figure 5.1 — Schematic Overview of Experimental Apparatus Setup.

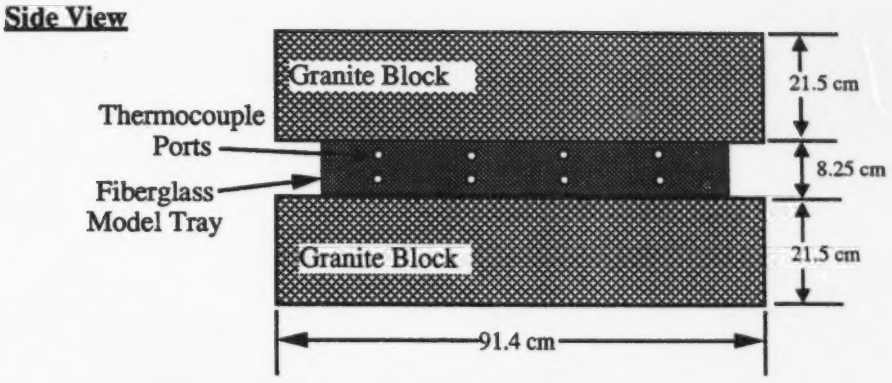

Plan View of the Model: Displays the Cap and Base Rocks and the Relative Level of the Upper and Lower Thermocouple Ports.

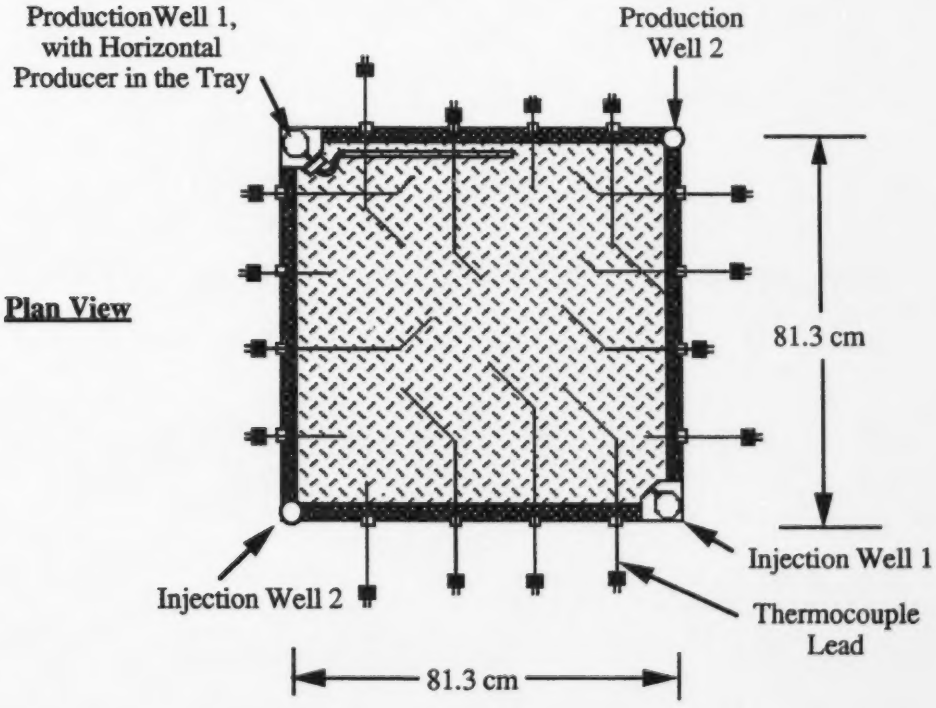

This plan view illustrates the approximate positions of the top layer of thermocouples.

Figure 5.2 — Schematic Overview of the Physical Model and One Layer of Thermocouples.

be pushed in and out of the cooling unit. The cart was designed to allow the entire model, with both granite blocks clamped in place, to be tilted to a 45° angle from the horizontal.

5.1.2 Porous Media

To achieve the high permeability required by the scaling criteria, glass beads having an average diameter of 3 mm (6-8 U.S. mesh) were used for all the homogeneous experiments. For the multi-layered experiments a large contrast in the permeability was desired. To meet this requirement, 1 mm (12-13 U.S. mesh) average diameter glass beads were used in conjunction with the 3 mm diameter glass beads.

5.1.3 Vertical and Horizontal Wells

The vertical injection and production wells were designed according to the slot well method in which the effective radius of the slit is a function of the bead pack directly in front of the well. The wells could have selectively blanked off sections to simulate different completion intervals. The scaling criterion derived by Doan et al.[41] was used to design the model horizontal well. Steel tubing of 4.75-mm O.D. was used for the horizontal well. One side of the tubing was slotted along its entire length; this allowed selected areas to be blanked off for different horizontal well strategies.

5.1.4 Injection System

Critical to any successful experiment is a good control of what is injected. The injection system consisted of two reciprocating control volume pumps. Initially one pump transported room temperature water to a mixing point. The other one pumped into a steam generator and drove superheated steam to the mixing point. From the mixing point the steam traveled a short length of the insulated tubing to the injection point. To gain more control of the injected steam quality the mixing system was changed to route all the injected fluids through the steam generator. Figure 5.3 shows the relationship between the boiler temperature and the steam quality. Clearly the non-mixing system has a smaller steam quality range over the same boiler temperature range, thus giving much better control of the steam quality. The steam quality experiments are explained in Appendix A.

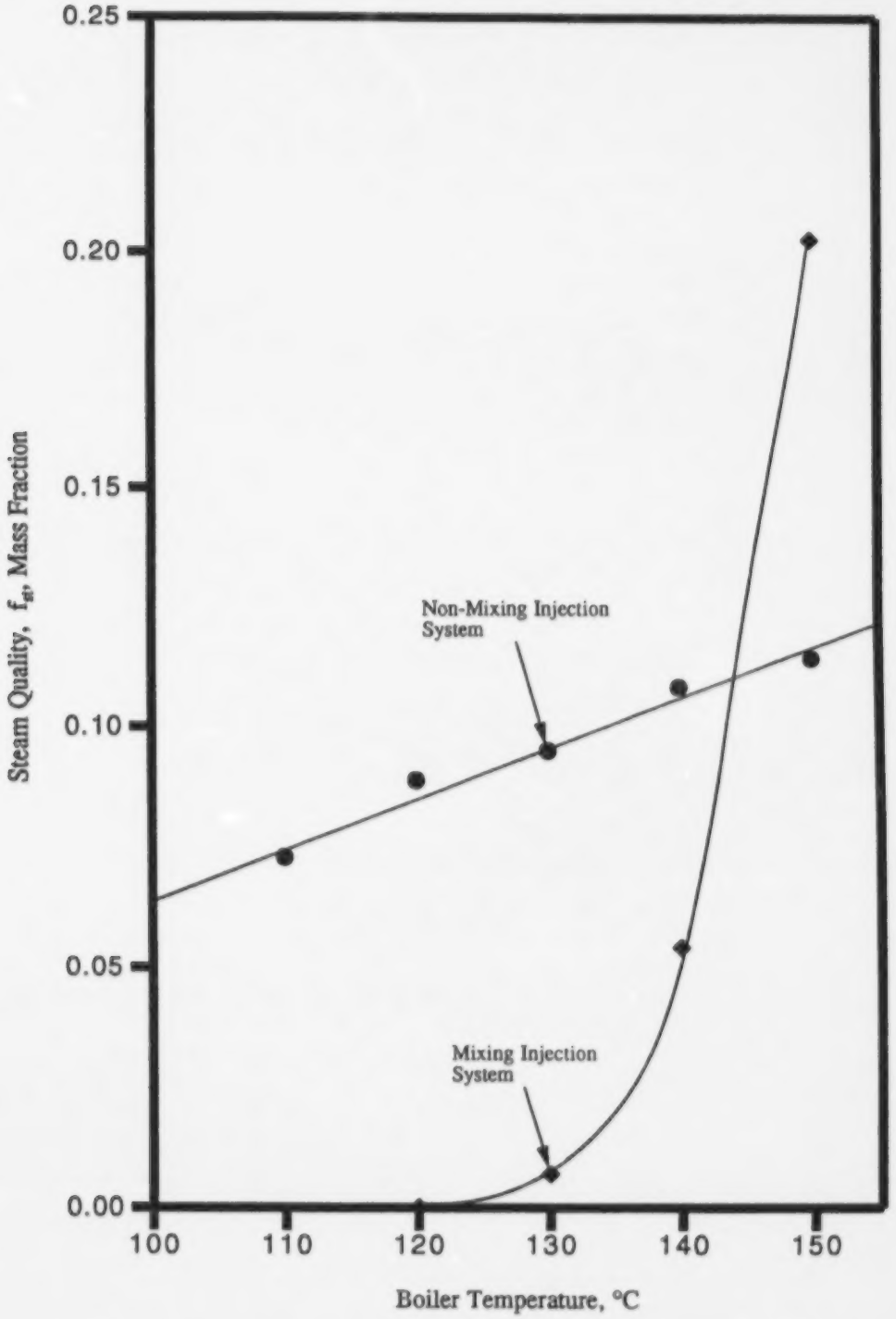

Figure 5.3 — Steam Quality vs. Boiler Temperature for Both the Mixing and Non-mixing Steam Injection Systems.

5.1.5 Production System

The collection system consisted of two traps, a vacuum pump, a pressurized discharge system and a cooling system. Under standard experimental conditions the vacuum pump maintained a constant vacuum of 78 cm of mercury. Two traps were used so that each trap could be individually isolated from the experiment during sample collection. Initially the produced fluids were cold because of the very high viscosity of the oil and they had to be forced out using the pressurized discharge system. As the experiment progressed and the production temperatures increased, the produced fluids had to be cooled to reduce the vapour lost out through the vacuum pump.

5.1.6 Data Acquisition System

The data acquisition system consisted of an IBM computer with a Das-8 card inside, eight EXP-16 multiplexers, one ten-channel Validyne board and the Labtech Notebook Software package. The software package processed all raw thermocouple and pressure transducer data in millivolts and converted them to real values of temperature (°C), pressure (kPa), and time (seconds). The pressure transducers were connected to a Validyne board which fed into an EXP-16 data board that was dedicated to pressure data acquisition. The thermocouples were connected directly into four of the EXP-16 boards each of which had sixteen input channels. The EXP-16 boards were connected to the Das-8 card in the IBM computer. The Labtech Notebook Software scanned each pressure and temperature channel every half minute. The experimental data was stored in ASCII file format which allowed it to be analyzed in Lotus 1-2-3 or Microsoft Excel.

5.1.7 Model Fluids

Figure 5.4 shows the viscosity-temperature relationship for the refined oil used in this study and the prototype oil. The smaller pressure and temperature ranges in the model require an oil with different characteristics than the prototype oil. The most important characteristics to match between the prototype oil and the model oil are the initial temperature-viscosity points. This is because most of the oil is produced in the low temperature range. Once the temperature increases sufficiently the temperature and viscosity become less of a factor in oil recovery. Faxam 100 gave the best match to the prototype oil in the low temperature range, and hence was selected to represent the prototype oil in the experiments.

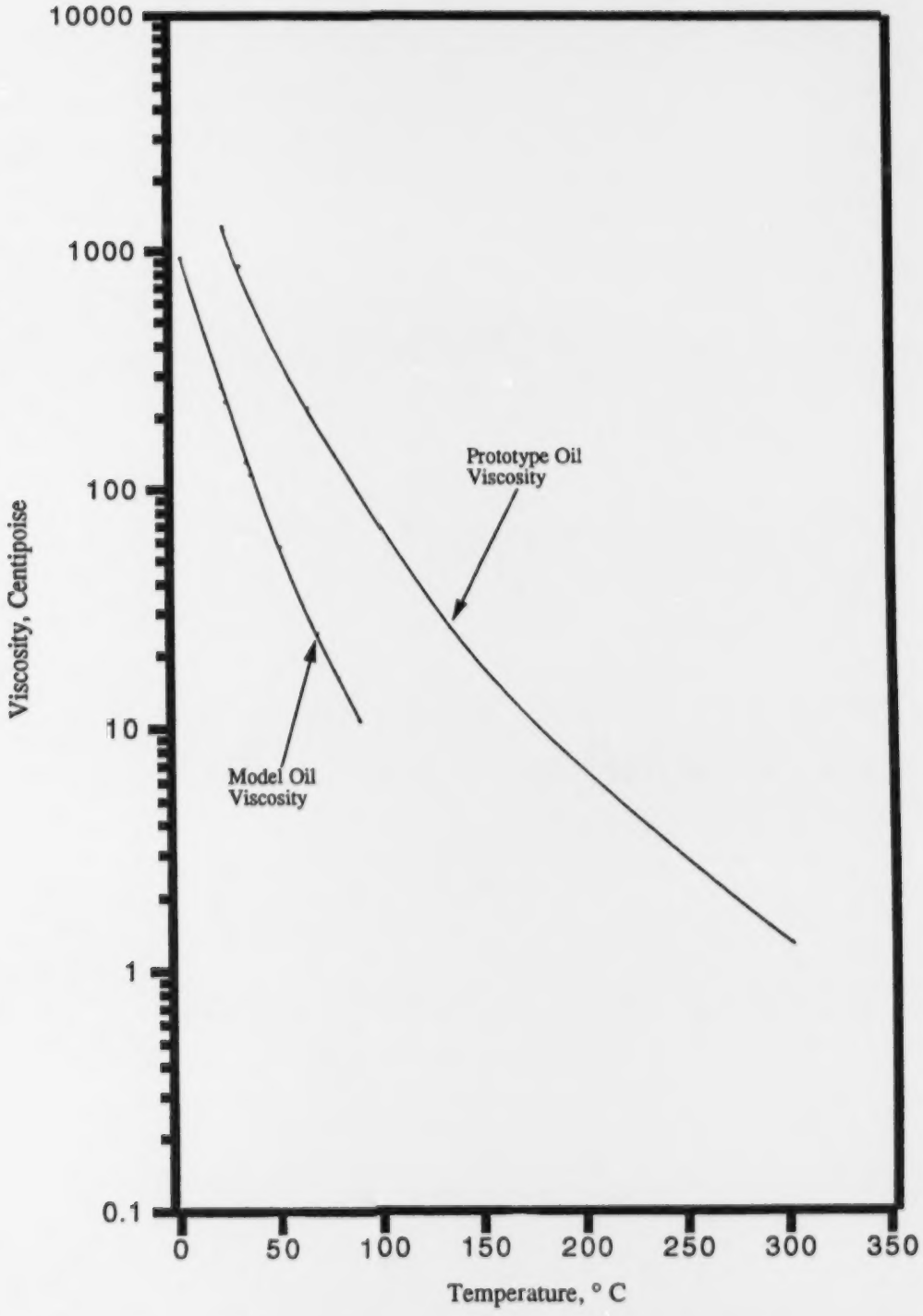

Figure 5.4 — Viscosity-Temperature Relationships for the Prototype Oil and the Model Oil.

5.2 Preparation of the Experimental Model

5.2.1 Model Packing Procedure

Due to the size and shape of the model, vibrating and tamping of the model were not practical. The need for uniform properties throughout the pack required the use of a particle distributor. The particle distributor concept was first presented by Currie and Gregory and was latter modified by Wygal[42]. According to Wygal[42] the particle distributor produced mechanically stable packs with uniform properties throughout and, these packs could be accurately reproduced. The particle distributor was placed over the fiberglass tray and approximately 70 kg of glass beads were poured through the particle distributor. Once the glass beads had passed through the distributor it was removed and the excess beads were scraped off so the bead pack was level the sides of the tray.

5.2.2 Saturation Process

After the extra beads were removed a thin layer of silicone sealant was applied to the top edge of the fiberglass tray. A 86-cm x 86-cm x 32-mm closed-cell Neoprene sheet was placed on top of the tray, thus sealing the model. The upper granite block was lowered onto the tray and clamped into place.

To saturate the model, it was tilted to about 45° from the horizontal to provide a gravity stabilized saturation front. Six saturation ports, three each at the up-dip and down-dip ends of the model, were used to saturate the model. The saturating fluids which were exposed to atmospheric pressure entered the model at the down-dip end and, were pushed to the up-dip ports because of the low pressure caused by a vacuum applied to those ports. Initially a known volume of water was placed in an open container at the down-dip end of the model. The pore volume was determined by the volume of water accumulated in the model. Once the model was water-saturated, oil was drawn into the model using the same method as for the water. Oil was drawn in until it was produced from the up-dip saturation ports. At this point the model was at the irreducible water saturation. Once the oil was produced, the production and injection fittings were disconnected and the model was leveled and pushed into the cooler. The model was cooled for approximately twenty-four hours to get it to a uniform initial temperature of 3°C.

5.2.3 Preparation of a Bottom Water Model

The most marginal reservoir models displayed the most sensitivity to changes in the recovery strategy, and it is partially for that reason that bottom water models were used in this study. To create a bottom water model 5% (by weight) sodium chloride water was used. The saline water enabled monitoring of the movement of the bottom water during saturation and recovery processes. A predetermined volume of water was put in the model tray, then glass beads were sprinkled in the model until there was a layer of glass beads above the water level. The bottom water was then frozen in place with the glass beads. Due to the salinity of the bottom water a maximum temperature of -17°C was required to freeze the water. Once the water was frozen the model was filled with glass beads and the saturation process described above was employed. After saturation the model was rolled into the cooler. With the frozen bottom water, the model reached the initial temperature of 3°C faster than a homogeneous model, usually in about 15 hours.

5.2.4 Multi-layered Models

The objective for these experiments was to study the effects of controlled steam override. During the packing process, a permeable membrane made of 100% nylon was placed between the two layers of different bead sizes. The membrane was required to stop the upper glass beads from working down into the lower zone during the saturation and experimental processes. A high permeability contrast was obtained using the 3 mm diameter glass beads in the high permeability zone and 1 mm diameter glass beads in the low permeability zone. These bead sizes gave calculated permeability contrast of about nine to one .

5.3 Conducting Experiments in the Model

After the internal temperature of the model reached 3°C an experiment could be performed. Prior to the start of an experiment some preparations had to be done. The boiler was turned on and after it reached the operating temperature the injection pumps were started. This heated the injection line and prevented heat losses to the tubing in the early stages and stabilized the steam generator output. Just prior to an experiment, the pressure transducers were zeroed and calibrated with a manometer because of the tendency of the Validyne to wander from zero after the power was turned off. The model was wheeled out of the cooler and the sensor leads were connected while the data

acquisition program was activated. This was done for two reasons; first, the data acquisition system needed to warm up and second, any bad connections could be fixed.

Once the leads were connected the experiment could be started. The production system was first evacuated. The data acquisition system was restarted and the initial model temperature and pressures were recorded. Once the data acquisition system was started the vacuum line to the model was opened, and the injection line was connected to the model.

After the start of the experiment and when the samples started to get warm the chilling system was turned on to reduce the loss of sample fluid as vapour through the vacuum pump. Samples were taken every seven minutes for consistency with the pore volumes injected, which resulted in 1450 ml samples, at steady state. Initially, the experiments lasted until the injection of 2.00 PV (approximately two hours). Some of the experiments toward the end of this study lasted up to five hours.

5.4 Data Analysis

Following each experiment the oil and water in the samples were allowed to separate for up to one week. Once they had separated the volumes of each phase in each sample were recorded. The volume information was put on a spreadsheet and the data was manipulated for graphical presentation. The following variables were then plotted as a function of the pore volumes injected: % oil in sample, % cumulative oil recovery (%OOIP), instantaneous WOR, and cumulative OSR.

The temperature data was analyzed using a commercially available contouring package (SURFER). The SURFER gridding and graphics software was used to generate the temperature contours which helped in the experimental analysis. SURFER is a powerful menu driven multi-featured program that combines a variety of different options. It allows the user to do a complete data interpolation in very few steps. SURFER has a sophisticated gridding feature that can take irregularly spaced data and create a regularly spaced grid of any density desired. Once the data is gridded it can be passed on to one of the other programs. In most cases the data was passed to "TOPO". TOPO is a contouring program that creates contour maps for output to the screen, printer, or plotter. SURFER also has a program called UTIL, which has the options of determining the volume of a contoured surface or in slicing the contour vertically. The volume feature was very useful in performing the heat balance calculation. Being able to

slice the model down the diagonal allowed a profile view of the temperature distribution in the model. SURFER gave representative contours that were corroborated by plotting the actual data on a contour plot and in all cases the contours properly represented the data.

6. Discussion of Experimental Results

The objective of this study was to seek optimal oil recovery from various types of heavy oil reservoirs using several steamflooding recovery techniques in a scaled physical model. The results of these experiments gave some insight into what occurs in the field. The following types of experiments were analyzed and discussed: horizontal well strategies, steamflooding multi-layered models, waterflooding, and heat scavenging. This chapter also looks at the results of a heat balance calculation performed on the scaled physical model.

6.1 Presentation of Results

Fifty-five experiments were conducted in the physical model. The following section discusses steam injection experiments of several types from twenty eight of these experiments. The other twenty-seven experiments include eight misruns and a preliminary look at the following areas: anisotropic reservoirs (shale barriers), reservoir bottom topography effects, steam alternating water injection, laboratory phenomena, injected steam quality, and steam quality control experiments. Figure 6.1 schematically illustrates the steamflooding experiments performed. Table 6.1 summarizes recovery results and the pertinent initial model properties, such as porosity and the initial fluid saturations. The experimental results are discussed by analyzing both the production and thermal data. Production data for each experiment was plotted against the results of a base case experiment to examine the effects of the recovery strategy under investigation. The use of temperature sensors in the model to map the temperature distribution during an experiment helped to evaluate where the injected heat went during an experiment. The temperature data was plotted using a contouring software package (SURFER) to enable visual inspection of the temperature distribution inside the model reservoir through the course of an experiment. Several base case steamfloods using a vertical injector and a vertical producer were conducted in a homogeneous model to establish a base case range. Once a base case or datum was established, other experimental results could be compared with it. Detailed experimental results are given in Appendix C.

6.1 Heat Balance

One of the critical parameters in steam injection experiments is the distribution of the heat injected into the model reservoir. The scaling of the model assumes that cap and base rock heating predominates. In the following discussion, heat balance refers to

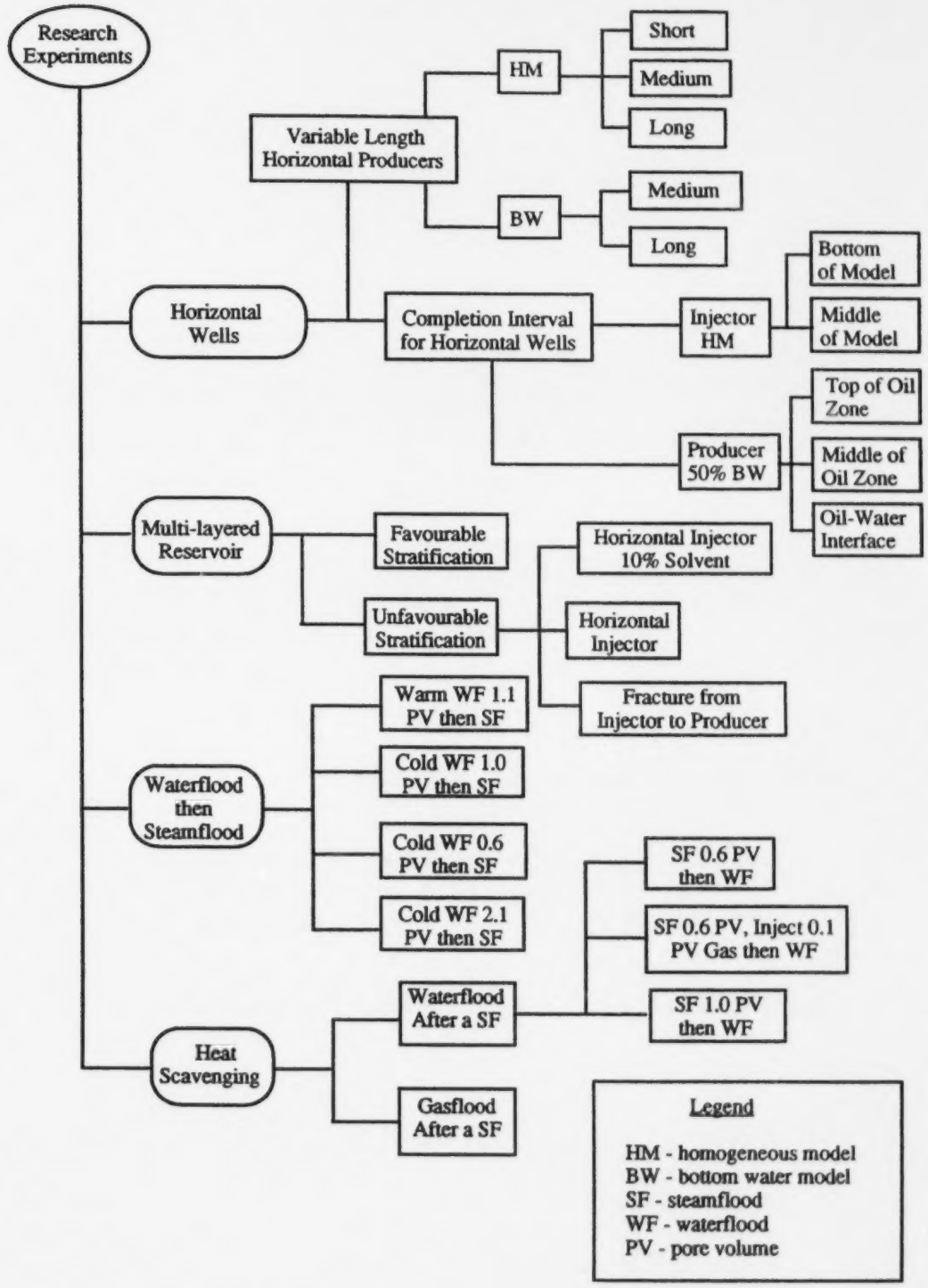

Figure 6.1 — Overview of Low Pressure Model Experiments Carried Out.

Table 6.1— Summary of Experiments Conducted

Run No.	Model Type	Type of Process	Porosity (%)	Soi (%)	Swi (%)	Bottom Water (% Gross Thickness)	Cum. Rec. (%OOIP)	Cum. PV Inj. (PV)
108	HM	SF (fst=14%)	33.8	92.0	8.0	- -	64.1	1.99
109	HM	SF to 0.6 PV proir to W/F	35.5	91.8	8.3	- -	39.2	2.04
110	HM	SF 0.6 PV Gas 0.1 PV WF	34.2	92.7	7.3	- -	41.2	2.08
111	HM	SF 1.0 PV prior to WF	35.5	92.8	7.2	- -	61.7	2.16
112	HM	*Hot WF (Boiler Trouble)	34.6	92.0	8.0	- -	51.6	2.19
113	HM	*Vacuum Lost				- -		
114	HM	WF prior to SF	33.8	92.3	7.7	- -	61.3	2.62
115	HM	SF Base Case	34.1	94.1	5.9	- -	54.9	2.13
116	HM	SF to 0.6 PV, WF 0.1 PV; SF	33.5	92.3	7.7	- -	57.1	2.04
117	BW	SF to 0.6 PV, WF 0.1 PV; SF	33.3	85.7	14.3	- -	52.0	2.01
118	M-L	SF, Low k Bottom	34.7	92.6	7.4	- -	42.3	2.12
119	M-L	SF, Low k Top	36.9	93.4	6.6	- -	54.3	2.08
120	M-L	SF, Low k Bottom	36.8	92.2	7.8	- -	50.0	2.04
121	M-L	SF: HIVP	33.0	93.6	6.5	- -	46.0	2.06
122	Misrun					- -		
123	HM	* SF: HIHP	34.4	92.7	7.3	- -	51.0	2.01
124	M-L	Low k Bottom, HIVP Solvent	36.9	92.2	7.8	- -	55.0	2.00
125	HM	HIVP, Inj. Bottom Formation	34.3	92.3	7.7	- -	53.0	2.10
126	M-L	Low k Bottom, HIVP	37.6	91.4	8.6	- -	46.0	2.03
127	HM	W/F to 10 WOR, then SF	34.3	90.2	9.8	- -	45.0	2.10

Table 6.1 (Continued)

Run No.	Model Type	Type of Process	Porosity (%)	Soi (%)	Swi (%)	Bottom Water (% gross Thickness)	Cum. Rec. (%OOIP)	Cum. PV Inj. (PV)
128	HM	W/F to 7 WOR then SF	33.9	92.6	7.4	- -	54.0	1.99
129	HM	W/F to 23 WOR then SF	34.4	90.8	9.2	- -	21.0	2.04
130	Misrun	*Boiler Trouble	34.8	93.2	6.8	- -	42.0	1.65
131	Misrun	*Boiler Thermocouple Shorted	34.4	91.9	8.1	- -	54.0	2.06
	Model bottom leveled and two liters of extra material removed, no increase in depth.							
132	HM	No Thermocouples	33.7	91.8	8.2	- -	56.0	2.05
133	HM	Thermocouples	33.4	92.5	7.5	- -	58.0	2.09
134	HM	*Boiler Trouble	33.6	93.4	6.6	- -	50.0	2.09
135	HM	*Boiler Trouble	33.6	93.6	6.5	- -	47.6	2.04
	Change Injection System to Non-mixing					- -		
136	HM	Base Case	34.1	92.6	7.4	- -	48.0	1.93
137	HM	HIVP	34.7	92.7	7.3	- -	47.3	2.03
138	M-L	Low k Bottom	35.7	92.4	7.6	- -	49.0	2.07
	Fracture Running from Injector to Producer					- -		
139	HM	Pattern Inversion	33.7	94.9	5.1	- -	44.0	2.04
140	HM	Heat Scavenging, N2 @ 2PV	34.1	94.0	6.0	- -	46.4	2.00
141	BW	*HIVP	30.6	80.1	19.9	- -	55.3	2.07
142	M-L	Low k Bottom	35.4	93.6	6.4	- -	50.7	2.09
143	HM	VIHP	33.6	93.8	6.2	- -	47.7	2.06
144	HM	HIHP	35.1	93.1	6.9	- -	44.8	2.09
145	BW	VIVP	28.0	61.8	38.2	44.7	33.0	2.01
146	BW	VIHP	26.4	62.5	37.5	45.9	26.5	2.01

Table 6.1 (Continued)

Run No.	Model Type	Type of Process	Porosity (%)	Soi (%)	Swi (%)	Bottom Water (% Gross Thickness)	Cum. Rec. (%OOIP)	Cum. PV Inj. (PV)
147	BW	VIHP, Medium Length Prod.	26.7	53.1	46.9	46.4	21.8	2.08
148	BW	VIHP, Short Producer	29.3	57.6	42.4	45.5	26.7	2.03
149	BW	VIVP, Adaptor	28.7	57.8	42.3	48.1	24.9	2.05
150	BW	VIHP, Medium Length Prod.	31.3	49.7	50.3	49.2	44.8	2.09
151	BW	VIHP, Medium Length Prod.	30.9	54.5	45.5	47.1	25.9	2.05
152	BW	VIHP, Long Producer Prod.	29.8	54.7	45.3	46.8	25.3	2.01
153	BW	VIHP, Short Producer	29.3	46.0	54.0	45.2	38.5	2.04
154	BW	VIHP, Long Producer	30.2	56.4	43.6	47.0	44.8	2.09
155	BW	* HIHP, Medium Length Prod.	26.3	96.2	3.8	38.9	36.1	2.01
156	HM	VIHP, Short Producer	34.3	92.4	7.6	- -	52.7	1.95
157	HM	VIHP, Long Producer	33.4	94.0	6.0	- -	55.5	2.00
158	HM	VIHP, Medium Length Prod.	33.8	92.1	7.9	- -	55.2	1.99
159	BW	VIHP, Medium Length Prod.	29.6	50.2	49.8	51.0	21.6	2.01
160	BW	VIHP, Medium Length Prod.	29.6	54.8	45.2	46.9	17.1	2.01
161	BW	VIHP, Medium Length Prod.	29.4	53.7	46.3	49.9	- -	- -
162	HM	*Misrun	35.1	93.1	6.9	- -	44.8	2.09
163	M-L	Low k Top	36.0	92.6	7.4	- -	67.7	1.91

Legend: HIVP — Horizontal Injector and Vertical Producer
VIHP — Vertical Injector and Horizontal Producer
HIHP — Horizontal Injector and Horizontal Producer
M-L — Multi-layered Model
BM - Bottom Water Model
HM - Homogeneous Model
SF - Steamflood
WF - Waterflood
*—Misrun

cumulative heat balance and not instantaneous heat balance. The overall heat balance equation at any time, t, is:

$$Q_{inj} = Q_{production} + Q_{loss} + Q_{form} \quad (6.1)$$

Where:

Q_{inj} = Injected energy, (kJ)

$Q_{production}$ = Produced energy, (kJ)

Q_{loss} = Energy loss to the cap and base rock, (kJ)

Q_{form} = Heat accumulated in the formation, including the matrix (glass beads), oleic phase, aqueous phase, and the vapour phase (steam), (kJ).

Run 136 was a base case experiment and it was used to answer the question of how much heat is injected in an experiment, and where this heat went once it was injected. The heat balance considered the cumulative heat injected in to the model at an instant during the experiment. The instant chosen was after the injection of 1.00 pore volume of 10% quality steam and this was just prior to steam breakthrough. At steam breakthrough the produced energy could not be easily accounted for. A detailed illustration of the heat balance calculations are presented in Appendix B. The results of the heat balance calculations for Equation 6.1 are:

Q_{inj} = 6789 kJ

$Q_{production}$ = 2021 kJ

Q_{loss} = 735 kJ

Q_{form} = 4033 kJ

These results indicate that the heat losses to the cap and base rocks are about 735 kJ in total, this is 10.8 % of the injected heat. The model was scaled for the heat loss to the cap and base rock to dominate, but this is not the case. Because of the small amount of heat loss to the cap and base rock it is surmised that the experimental results are optimistic and steam breakthrough occurs sooner than it should.

6.4 Production History of a Typical Run

Figure 6.2 illustrates graphically the production history of a typical experiment using a vertical steam injector and a vertical producer. This experiment represents one type of base case for this research, and hence it will be discussed in detail. The experiment selected was Run 136, which was one of several base case steamfloods performed during this study. The experiment was carried out in a homogeneous model with a permeability of 5390 darcies, a measured porosity of 34.1%, and an initial oil saturation of 92.6%. Ten percent quality steam was injected into the model at a constant rate of 211 ml/min CWE. Since most of the model reservoir was at the steam saturation temperature after about 2.00 PV CWE were injected, this experiment, as with most other experiments, was terminated. In addition, the production data did not show any significant changes to warrant the continuation of the experiments.

Table 6.2 presents the results which were used to generate the curves in Figure 6.2. In Figure 6.2 the instantaneous oil production per sample, cumulative oil recovery, water-oil ratio (WOR) (all three on the left vertical axis), and cumulative oil-steam ratio (OSR) (on the right vertical axis), were plotted versus cumulative PV cold water equivalent (CWE) of steam injected. An examination of the instantaneous oil production volume per sample (bar graphs) shows an expected trend with high initial production that stays above 20% for the first PV of steam injected. The oil cut in the produced samples drops off gradually as more of the reservoir is depleted. Starting with an initial value of 2.3 : 1 (ml of oil produced per ml of water produced), the instantaneous WOR curve climbs to 7.8 : 1 after the injection of 1.90 PV of steam. The cumulative OSR curve starts with a positive slope and climbs to a peak value of 0.3 ml of oil per 1 ml of steam CWE injected, then, as the reservoir becomes depleted, the OSR curve decreases steadily. The inset plot displays the cumulative fluid volume produced (CP) divided by the cumulative steam volume CWE injected (CI), versus the cumulative PV of steam injected. The CP/CI curve shows that prior to 0.50 PV of steam injected, the model reservoir allows more fluid to enter the model than is produced. The reason for this is the immobility of the fluids in the model cause the pressure at the injection point to increase to about 90 kPa absolute. This high pressure causes the Neoprene sheet to balloon up and contact the bottom of the upper granite block creating a slightly larger model volume.

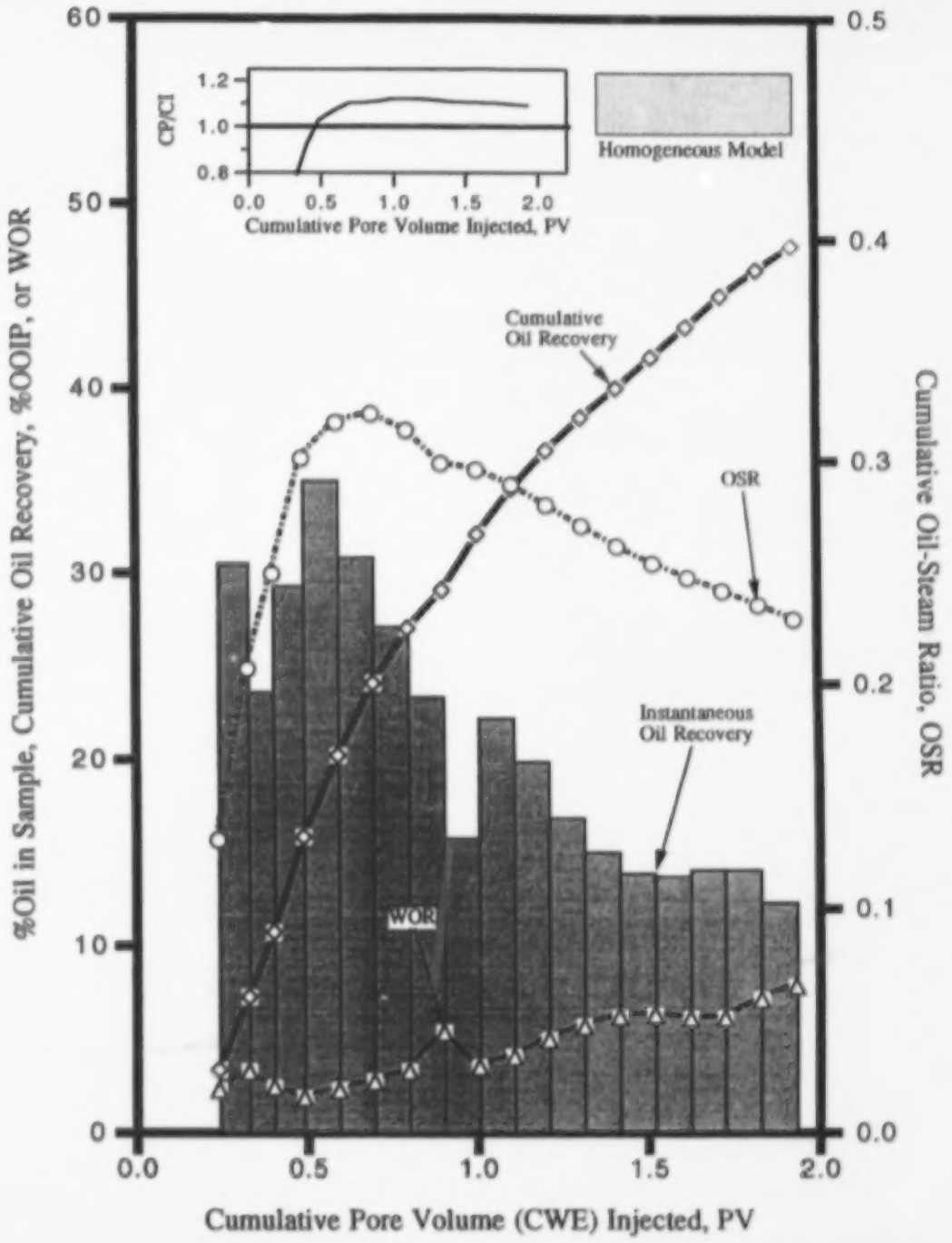

Figure 6.2 — Production History of a Typical Experiment (Run 136); Instantaneous Percent Oil in Sample, Cumulative Oil Recovery, Instantaneous WOR, and Cumulative OSR vs. PV of Steam Injected (CWE). Inset Plot is CP/CI vs. PV Injected.

Table 6.2—Run 136:Steamflood of a Homogenous Model (Base Case), Vertical Injector and a Vertical Producer

HC Pore Volume:	13250 ml	Type of Oil Used:	Faxam-100
Pore Volume:	14310 ml	Initial Model Temperature:	3.0° C
Bulk Volume:	42000 ml	Total Flow Rate of Steam:	211 ml/min.
Porosity:	34.1%	Steam Quality, fst:	0.1
Initial Oil Saturation:	92.6%	Total Steam Volume Injected:	24687
Initial Water Saturation	7.4%		
Net Oil Recovery:	**47.7%**	**Final Oil Saturation:**	**44.9%**

Cylinder No.	Total Vol. Produced (ml)	Instantaneous Oil Prod. (ml)	Cum. Oil Recovery (ml)	Cum. Oil Rec. %OOIP	Instantaneous Produced WOR	% Sample Vol. Oleic Phase	Cum. PV Injected
1	1440	440	440	3.3	2.27	30.6	0.24
2	2200	520	960	7.2	3.23	23.6	0.32
3	1570	460	1420	10.7	2.41	29.3	0.40
4	1940	680	2100	15.8	1.85	35.1	0.49
5	1880	580	2680	20.2	2.24	30.9	0.59
6	1880	510	3190	24.1	2.69	27.1	0.69
7	1670	390	3580	27.0	3.28	23.4	0.80
8	1710	270	3850	29.1	5.33	15.8	0.90
9	1800	400	4250	32.1	3.50	22.2	1.00
10	1660	330	4580	34.6	4.03	19.9	1.11
11	1600	270	4850	36.6	4.93	16.9	1.21
12	1570	236	5086	38.4	5.65	15.0	1.31
13	1510	210	5296	40.0	6.19	13.9	1.42
14	1600	220	5516	41.6	6.27	13.8	1.52
15	1560	220	5736	43.3	6.09	14.1	1.62
16	1560	220	5956	45.0	6.09	14.1	1.73
17	1540	190	6146	46.4	7.11	12.3	1.83
18	1500	170	6316	47.7	7.82	11.3	1.93

Figure 6.3 displays the temperature and pressure profiles of Run 136. The production pressure curve displays some interesting points early in the experiment. The curve starts at 13 kPa absolute which is the initial model pressure. The production pressure then drops to 5 kPa absolute for up to 0.10 PV of steam injected. At 0.10 PV injected the production pressures peak. This indicates that the pressure wave from the injector has arrived at the production well. At this point the drawdown is 35 kPa absolute. The drawdown continues to increase to a maximum of 70 kPa absolute. The reason that the drawdown continues to increase is that cold oil was blocking the production line and a higher drawdown is needed to overcome this. The many peaks and dips between 0.10 and 0.30 PV of steam injected are caused by the cold oil being produced. Slugs of cold oil temporarily block the production tubing, causing the production pressure to drop and the injection pressure to increase. The increasing drawdown then overcomes the blockage, and the production pressure peaks as the higher-pressure fluids push past the pressure sensor. After 0.40 PV of steam is injected the production pressure stabilizes because now the produced oil is warmer and more mobile.

The injection pressure and temperature curves are interdependent, and it is for this reason that they will be discussed together. It takes one minute to heat up the short injection line from the initial model temperature of 3°C. The pressure and temperature then rise very rapidly to 130 kPa absolute and 105°C, respectively. These high values persist until about 0.40 PV of steam is injected. At this time, the injection pressure decreases. The high pressure can reduce the quality of the steam injected to zero. The latent heat of steam increases the temperature, while the steam quality is reduced by an increase in pressure. Though the injected steam quality might be lower, the enthalpy injected remains approximately the same as when 10% quality steam is injected. Because of the dynamics of the experiments, some values have to be chosen at a single point for scaling and operating purposes, and for this study steam quality and the pressure and temperature associated with it were taken when the quality was 10%. There could be a slight difference in the enthalpy injected at the elevated pressure, but this short period is assumed to be negligible. After 0.40 PV of "steam" was injected, the pressure and temperature drop to 36 kPa absolute and 74°C, respectively. This drop happens as the production temperature increases and the model fluids become more mobile. At these pressures and temperatures, the right conditions then exist to inject 10% quality steam into the model. The production temperature curve indicates that with up to 0.40

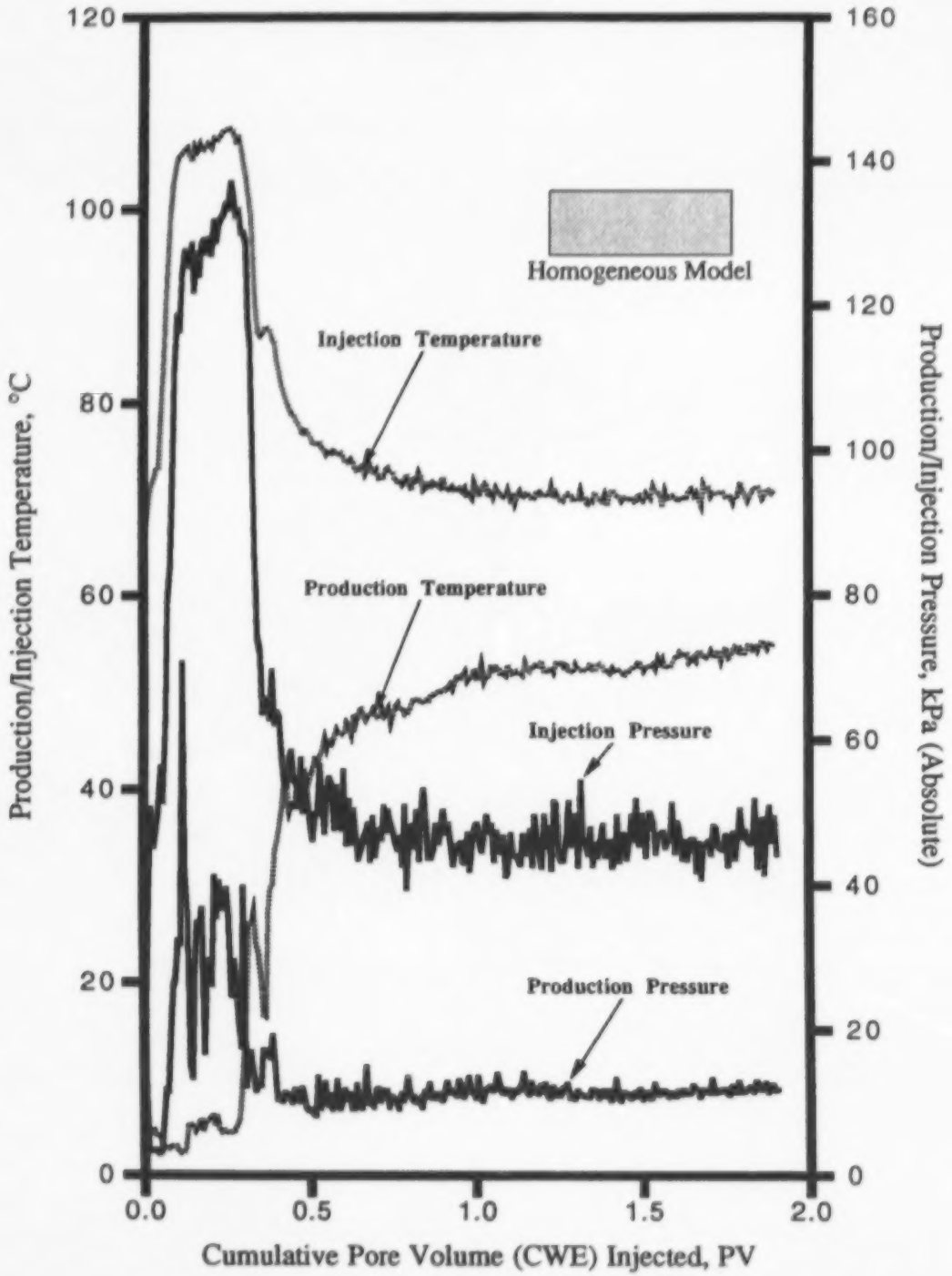

Figure 6.3 — Production History of a Typical Experiment (Run 136); Injection or Production Pressure/Temperature vs. Cumulative PV Injected; Vertical Injection and Production Wells in a Homogeneous Model.

PV of steam injected, initial reservoir temperature fluids are being produced. Once the temperature starts to increase, it does so rapidly to 40°C, and then continues to rise slowly until the termination of the experiment.

Figure 6.4 displays four temperature contour plots at different times (0.25, 0.50, 1.00, and 1.50 PV of steam injected) during the experiment. At 0.25 PV of steam injected the plot displays radial flow, and the start of a steam zone in the upper and lower portions of the pack. It also shows that hot condensate has reached further into the lower portion of the porous pack. After 0.50 PV of steam has been injected the upper 70°C contour is very much further ahead of the lower 70°C contour — indicating there is steam override. At 1.00 PV of steam injected a large part of the upper portion of the reservoir is now at the saturation temperature. There is a hot condensate channel in the lower portion of the model reaching towards the producer. At 1.50 PV of steam injected there is steam breakthrough with most of the upper portion of the model at or near the steam saturation temperature. There is a narrow channel from the injector to the producer at the saturation temperature in the lower portion.

Figure 6.5 shows the cross-section profiles of Run 136 corresponding to the top view temperature profiles of Figure 6.4. The cross-section diagonally slices the model from the vertical injector to the vertical producer. At 0.25 PV of steam injected the contours show the steam zone having a rather uniform vertical front. Hot condensate leaving the steam zone creates a vertical hot waterflood effect ahead of the steam zone. As the condensate cools down it also drops to the lower portion of the model. This gives rise to a cold waterflood in the lower portion of the model ahead of the hot waterflood and the steamflood. The start of steam override can be seen in the 0.50 PV plot. The contour at the steam saturation temperature (70°C) starts out near the injector at the bottom of the model and reaches out just past the middle of the model when it intercepts the top of the model. The lower portion of the model that was cold waterflooded by the condensate initially is now being hot waterflooded, demonstrating the three mechanisms that a steamflood consists of: cold waterflood, hot waterflood, and steamflood. In the upper portion of the model, half of the zone near the producer has not been heated. At 1.00 PV of steam injected, steam breakthrough is imminent. There is still a cool area in the upper portion near the producer that has to be heated prior to steam breakthrough. It can be seen that the lower portion has hot water going to the producer, showing how the waterflood pre-sweeps the oil zone prior to the steamflood. At 1.50 PV of steam injected the entire diagonal of the model (injector to producer) is at the saturation temperature.

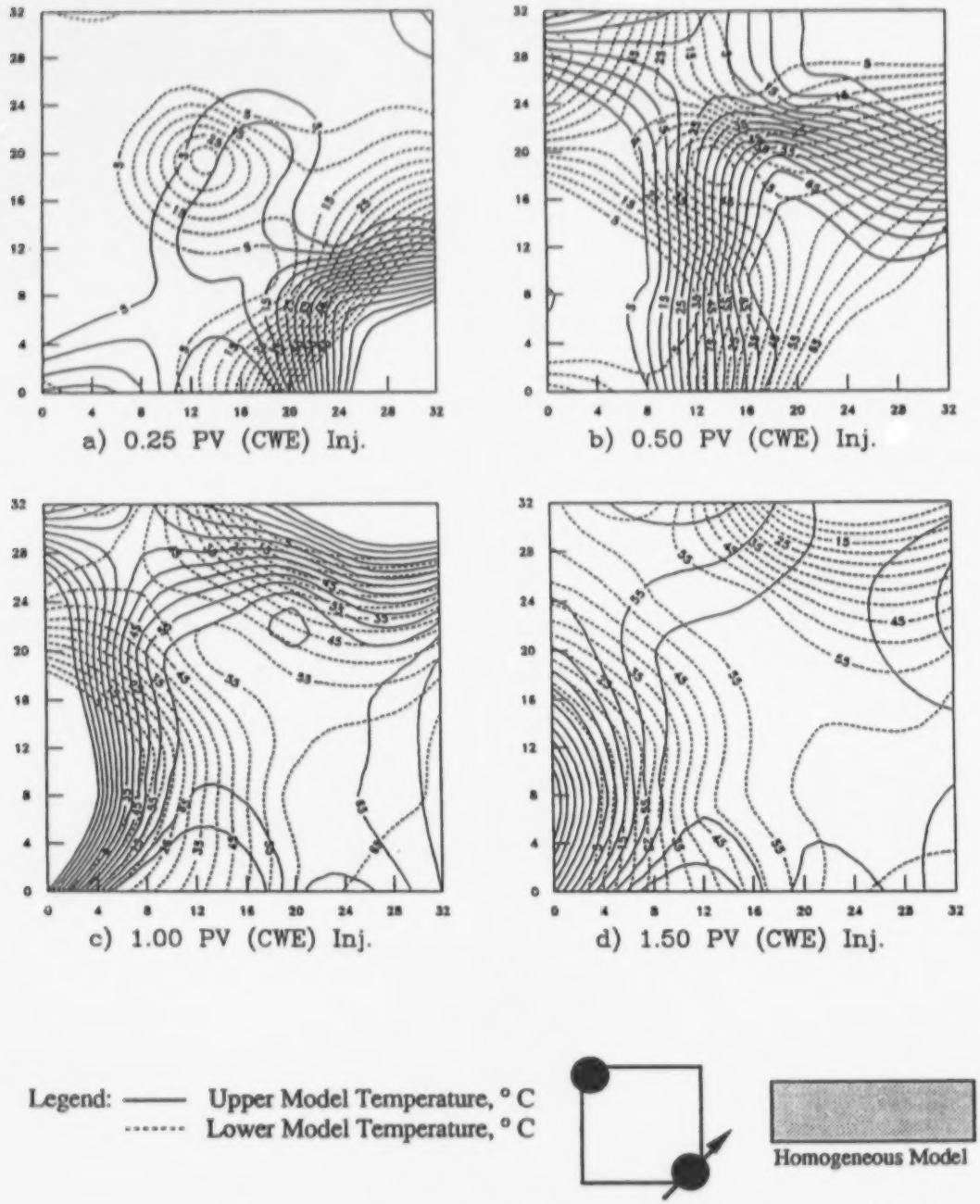
a) 0.25 PV (CWE) Inj.
b) 0.50 PV (CWE) Inj.
c) 1.00 PV (CWE) Inj.
d) 1.50 PV (CWE) Inj.
Legend: —— Upper Model Temperature, ° C
------- Lower Model Temperature, ° C
Homogeneous Model

Figure 6.4 — Plan view, of the temperature distribution inside the model reservoir after the injection of: a) 0.25, b) 0.50, c) 1.00, and d) 1.50 PV CWE of steam, for Run 136: homogeneous model, vertical injection and production wells.

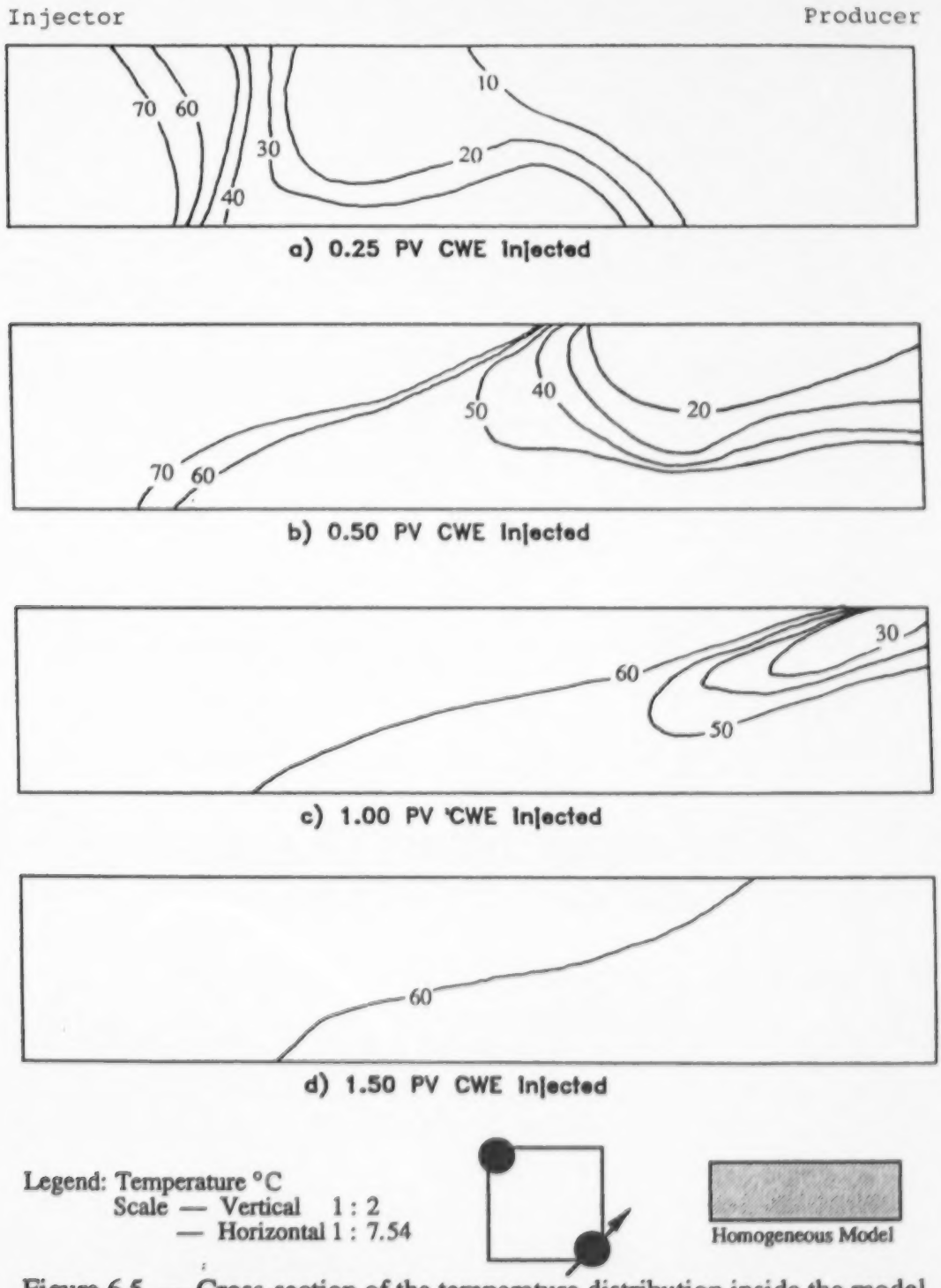

Figure 6.5 — Cross-section of the temperature distribution inside the model reservoir after the injection of: a) 0.25, b) 0.50, c) 1.00, and d) 1.50 PV CWE of steam, for Run 136 homogeneous model, vertical injection and production wells.

This run is a representative base case experiment that was compared with other experiments, and with consistent experimental procedures the error in the cumulative oil recovery was found to be ±2.5%. The reproducibility of the results is addressed later in this chapter. This experiment was compared with other experiments that were performed under the same operating conditions. The results of Run 136 demonstrate how initially the steam front is vertical and as the experiment proceeds the steam overrides and the condensate underrides, with the condensate preceding the steam front.

6.4 Production History of a 50% Bottom Water Run

Figure 6.6 illustrates graphically the production history of Run 149 which is a base case 50% bottom water experiment using a vertical steam injector and a vertical producer. The permeability was 5390 darcies, porosity 28.7%, and initial oil saturation 57.8%. This lower oil saturation is caused by the thick bottom water layer in the model. The steam was injected at a constant rate of 211 ml/min CWE. Table 6.3 presents the experimental results.

An examination of the instantaneous oil production volume per sample profile (bar graph) in Figure 6.6 reveals that there is no oil production for the first 0.70 PV of steam injected. The water in the bottom water layer has a much higher mobility than oil during this initial production period. Oil is not produced until it is warmed and its mobility increased. The first six samples had no oil in them, the next two samples had oil cuts of less than 5%, and the third sample had the largest oil cut at 17%. The samples after the third show very similar oil cuts, with the oil cut dropping off slightly as the model was depleted. The cumulative oil recovery curve shows no oil production early on, but after eight samples the slope of the recovery curve is almost linear and quite steep. The net oil recovery after the injection of 2.4 PV of steam is 31.2%; 25% lower than what is recovered in a homogeneous model. The instantaneous WOR curve is undefined until oil is produced at 0.70 PV of steam injected. Samples 7 and 8 had only traces of oil in them so the WOR is very high. Once significant oil production starts the WOR drops to a low of 5 : 1, and then it starts to rise. When the experiment was terminated, the WOR was 10 : 1 and climbing, indicating oil depletion. The cumulative OSR curve is zero until oil is produced, then the OSR curve starts to climb and peaks at 2.40 PV of steam injected.

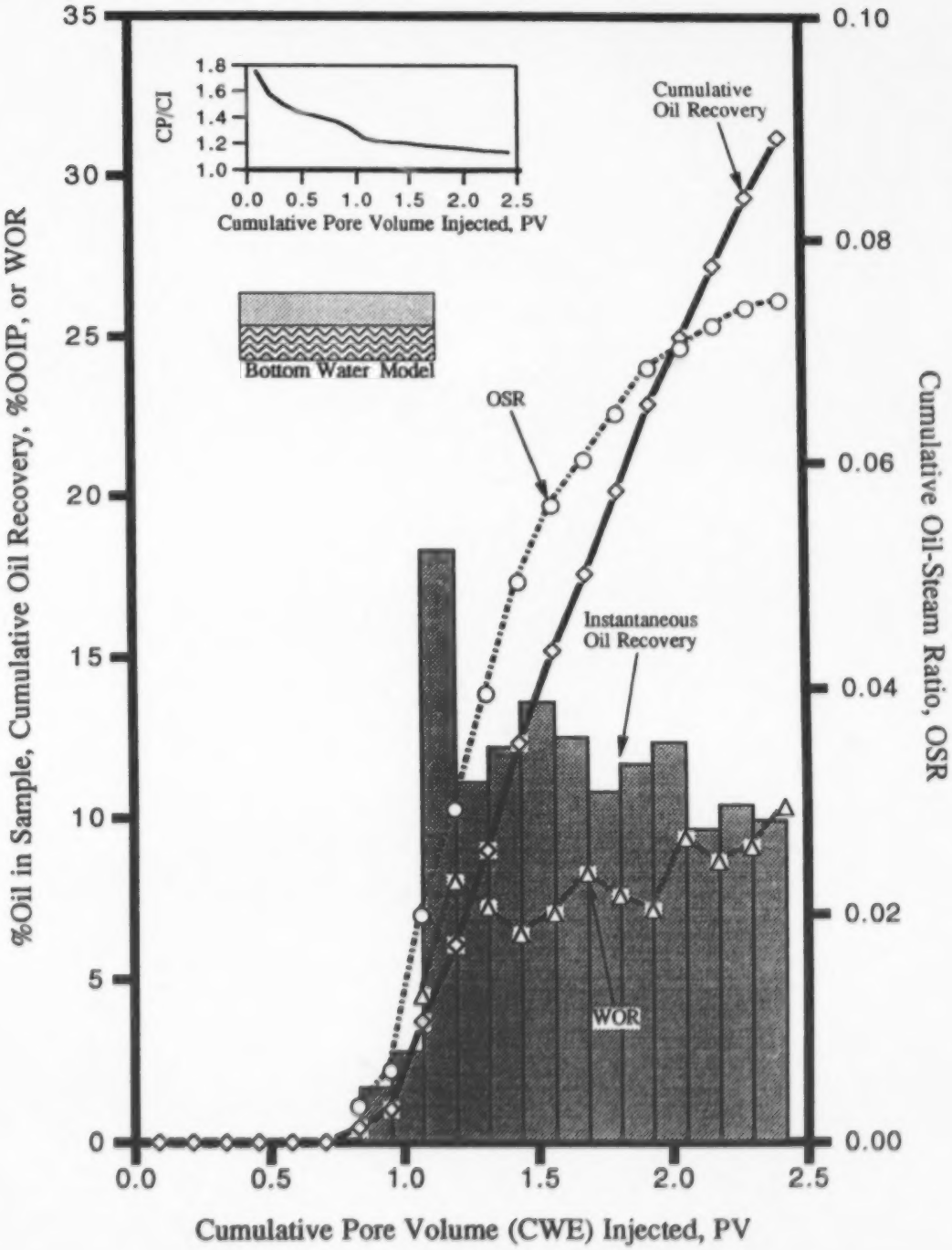

Figure 6.6 — Production History of a 50% Bottom Water Experiment (Run 149); Instantaneous Percent Oil in Sample, Cumulative Oil Recovery, Instantaneous WOR, and Cumulative OSR vs. PV Injected (CWE). Inset Plot Cumulative Produced/Cumulative Injected vs. PV Injected.

Table 6.3—Run 149: Base Case Steamflood of a 50% Bottom Water Model Using a Vertical Injector and a Vertical Producer.

HC Pore Volume:	6955 ml	Type of Oil Used:	Faxam-100
Pore Volume:	12042.5 ml	Initial Model Temperature:	3.0 °C
Bulk Volume:	42000 ml	Total Flow Rate of Steam:	211 ml/min.
Porosity:	28.7%	Steam Quality, fst:	0.1
Initial Oil Saturation:	57.8%	Total Steam Volume Injected:	27641 ml
Initial Water Saturation:	42.3%	Bottom Water Thickness:	48.2% (% Gross Thickness)
Net Oil Recovery:	**31.2%**	**Final Oil Saturation:**	**26.5%**

Cylinder No.	Total Vol. Produced (ml)	Instantaneous Oil Prod. (ml)	Cum. Oil Recovery (ml)	Cum. Oil Rec. %OOIP	Instantaneous Produced WOR	% Sample Vol. Oleic Phase	Cum. PV Injected
1	1850	0	0	0.0	0.0	0.0	0.09
2	2140	0	0	0.0	0.0	0.0	0.21
3	2020	0	0	0.0	0.0	0.0	0.33
4	1920	0	0	0.0	0.0	0.0	0.46
5	1970	0	0	0.0	0.0	0.0	0.58
6	1850	0	0	0.0	0.0	0.0	0.70
7	1790	30	30	0.4	58.7	1.7	0.82
8	1440	40	70	1.0	35.0	2.8	0.95
9	1010	185	255	3.7	4.5	18.3	1.07
10	1485	165	420	6.0	8.0	11.1	1.19
11	1680	205	625	9.0	7.2	12.2	1.31
12	1690	230	855	12.3	6.3	13.6	1.44
13	1600	200	1055	15.2	7.0	12.5	1.56
14	1525	165	1220	17.5	8.2	10.8	1.68
15	1540	180	1400	20.1	7.6	11.7	1.80
16	1540	190	1590	22.9	7.1	12.3	1.93
17	1500	145	1735	24.9	9.3	9.7	2.05
18	1490	155	1890	27.2	8.6	10.4	2.17
19	1510	150	2040	29.3	9.1	9.9	2.30
20	1470	130	2170	31.2	10.3	8.8	2.42

The inset plot of the CP/CI versus the cumulative PV of steam injected shows initially a greater volume was produced than was injected. This indicates that the steam zone was expanding from the start of the run, unlike in the homogeneous case where the high injection pressure and the very low mobility of the model fluids suppressed the initial rate of steam zone expansion.

Figure 6.7 displays the temperature and pressure profiles of Run 149. The curve representing the injection pressure fluctuates greatly as explained previously, however, the mean pressure is about 63 kPa absolute which is reached within the first 0.1 PV of steam injection. The high mobility of the bottom water allows the injected fluid to displace the connate water out of the producer, thus stabilizing the pressure inside the model at the beginning of the run. As seen in the homogeneous experiments the injection pressure exceeds 100 kPa absolute with the initial 0.40 PV of steam injected, and then drops to about 45 kPa absolute. In the bottom water case, the production pressure starts at 17 kPa absolute and has a slightly negative slope to 0.75 PV of steam injected. The pressure then slowly increases to 19 kPa absolute at the end of the experiment. The inflection point where the slope turns up coincides with the start of oil production. The reason for this is that the communication between the injector and the producer becomes more established as oil is depleted. Also the mobility of the fluids in the model increases as they are heated. The slope of the production pressure curve increases when the production temperature reaches about 35°C. The production temperature curve increases gradually from the initial model temperature. This is in contrast to the homogeneous case where the temperature jumps up suddenly when the hot condensate reaches the producer.

Figure 6.8 displays four temperature contour plots at different points (0.25, 0.50, 1.00, and 1.50 PV of steam injected) during the experiment. At 0.25 PV of steam injected there is radial flow and the start of a steam zone in the upper and lower portions of the pack. It also shows that there is steam override in the upper portion of the model. At 0.50 PV of steam injected the lower contours (bottom water layer) show a large heated channel going to the production well. The upper layer has a steam zone covering about half of the area of the model. At 1.00 PV of steam injected most of the upper portion of the model is at the steam saturation temperature. At 1.50 PV of steam injected all but the corners without wells are at the steam saturation temperature.

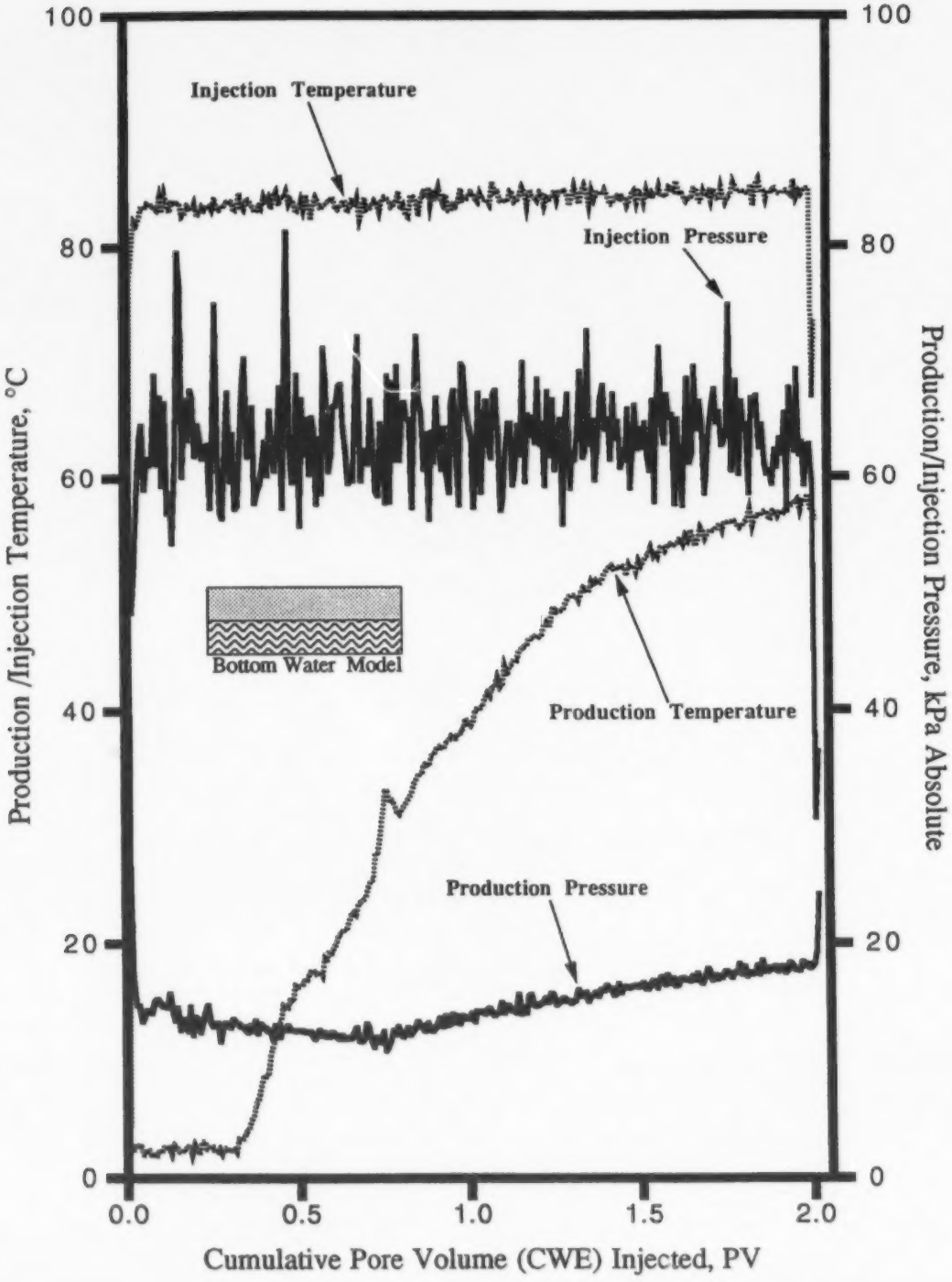

Figure 6.7 — Production History of a Typical Experiment (Run 149); Injection or Production Pressure/Temperature vs. Cumulative PV Injected, Vertical Injection and Production Wells in a 50% Bottom Water Model.

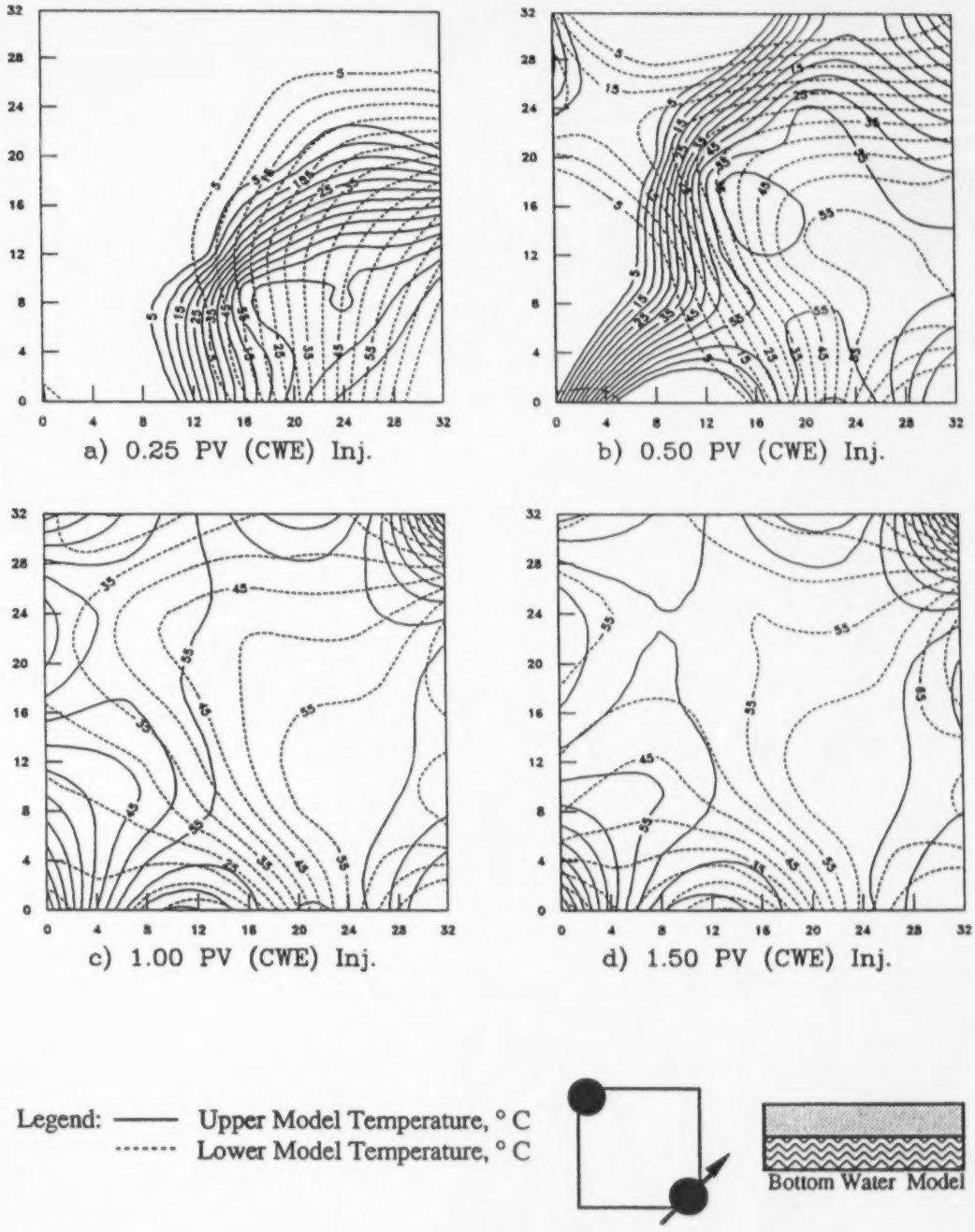
a) 0.25 PV (CWE) Inj.
b) 0.50 PV (CWE) Inj.
c) 1.00 PV (CWE) Inj.
d) 1.50 PV (CWE) Inj.
Legend: —— Upper Model Temperature, ° C
------- Lower Model Temperature, ° C
Bottom Water Model

Figure 6.8 — Plan view, of the temperature distribution inside the model reservoir after the injection of: a) 0.25, b) 0.50, c) 1.00, and d) 1.50 PV CWE of steam, for Run 149: 50% bottom water model, vertical injection, and production wells.

Figure 6.9 shows the cross-section profile of Run 149 at the same times that the top view temperature profiles were plotted (0.25, 0.50, 1.00, and 1.50 PV of steam injected). At 0.25 PV of steam injected the steam overrides almost half of the model's diagonal. The lower portion of the model does not show hot condensate underriding as seen in the homogeneous case. After 0.50 PV of steam injected the top of the steam zone has not advanced significantly. The temperature contours indicate the porous pack below the steam zone increases in temperature due to conduction heating. The 1.00 and 1.50 PV of steam injected plots show that the full thickness of the model is at the saturation temperature at the middle of the model.

This experiment was representative of a 50% bottom water experiment. It can be seen from the graphical presentation that the bottom water allows high rate low pressure initial injectivity. It can also be seen that the bottom water scavenges a great deal of the energy injected, thus reducing the thermal efficiency of the steam injection process.

6.5 Horizontal Wells

An increasing number of horizontal wells are being used to recover hydrocarbons from heavy oil and oil sand deposits. In the field, horizontal wells are becoming increasingly longer and more accurately placed. There is an increasingly greater interest in the productivity around the "toe" of a horizontal well. It is felt that the toe in many horizontal wells is nonproductive and, therefore an unwarranted expense. One of the objectives of this study was to investigate the effect of the horizontal well length and the vertical placement of a horizontal well in the horizon of interest. Four different situations were considered: 1) effect of horizontal producer length in a bottom water model, 2) effect of horizontal producer length in a homogeneous model, 3) vertical position of the horizontal producer, and 4) vertical position of the horizontal injector.

6.5.1 Horizontal Production Well Length

Three different lengths of horizontal production wells were used in this series of experiments. They were 20.3, 30.5, and 40.6-cm long. In terms of the prototype length, the three length values represent 25, 37.5, and 50% of the length of one-quarter of an 8-ha (20-acre), five-spot pattern (35.4, 53.1, and 70.7 m, respectively). In the following discussion, the 20.3-cm (8 inch) horizontal well is referred to as the short well, the 30.5-cm (12 inch) well as the medium well, and the 40.6-cm (16 inch) as the long well. All of the following experiments that used a horizontal well had a vertical well as the

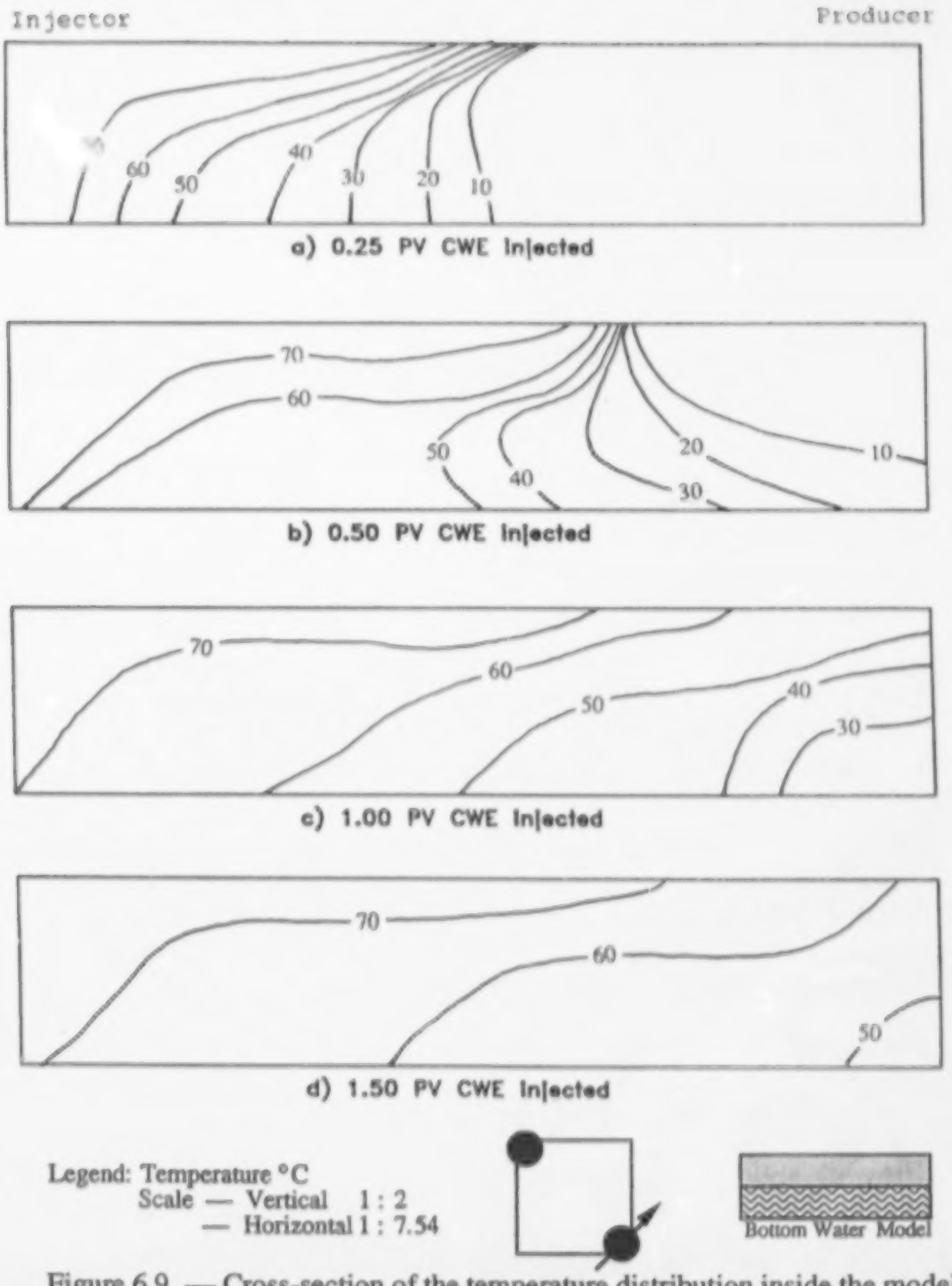

Figure 6.9 — Cross-section of the temperature distribution inside the model reservoir after the injection of: a) 0.25, b) 0.50, c) 1.00, and d) 1.50 PV CWE of steam, for Run 149: 50% bottom water model, vertical injection and production wells.

complementary well, i.e., a vertical injector and a horizontal producer or a horizontal injector and a vertical producer.

6.5.1.1 Effect of Horizontal Production Well Length in a Bottom Water Model

Steamflood recovery performances using two different lengths of horizontal production wells (long (Run 152) and short (Run 151)) were compared with a vertical production well in a 50% bottom water model. Figures 6.10 and 6.11 compare the cumulative oil recovery and cumulative OSR of the experiments with a vertical production well (Run 149). The long production well had the earliest oil production, after approximately 0.45 PV CWE of steam injected. The short horizontal well started to produce oil after approximately 0.60 PV CWE of steam injected. The vertical production well had the latest oil production, after the injection of approximately 0.80 PV. The ultimate oil recovery for all three cases was less than 35% of the original oil in place (OOIP). The runs were terminated before the oil production rate started to decline. The cumulative recovery curve for the long horizontal well started 0.55 PV sooner than that for the vertical producer, and 0.10 PV than that for the short horizontal producer. The cumulative OSR curves in Figure 6.11 show that the long horizontal well achieved a higher OSR than both the short horizontal producer and the vertical producer for up to 1.80 PV of steam injected. However, this trend was reversed with the vertical producer achieving a higher OSR after 2.00 PV of steam had been injected.

Figures 6.12, 6.13, and 6.14 display the temperature contour plots for the three runs at 0.40, 0.50, 0.60, and 1.00 PV of steam injected. Comparing the three runs at 0.40 PV of steam injected, the horizontal well cases have the sweep moving up along the right side rather than across the bottom of the reservoir. The temperature contours at 0.40 PV of steam injected for Run 149 show a more radial flow. At 1.00 PV of steam injected the left side of the model in the horizontal well experiments (Runs 151 and 152) has a cool area, while for the vertical well case all but the inactive corners are at or near the saturation temperature. Figure 6.15 displays the cumulative oil recovery versus the production well type with increasing PV volumes injected. At 1.00 PV of steam injected, the long horizontal production well recovered about 3% more oil than the short horizontal well, and 4% more oil than the vertical production well. At 1.50 PV of steam injected the relationship between well type and recovery appears linear with the long horizontal producer recovering the most oil.

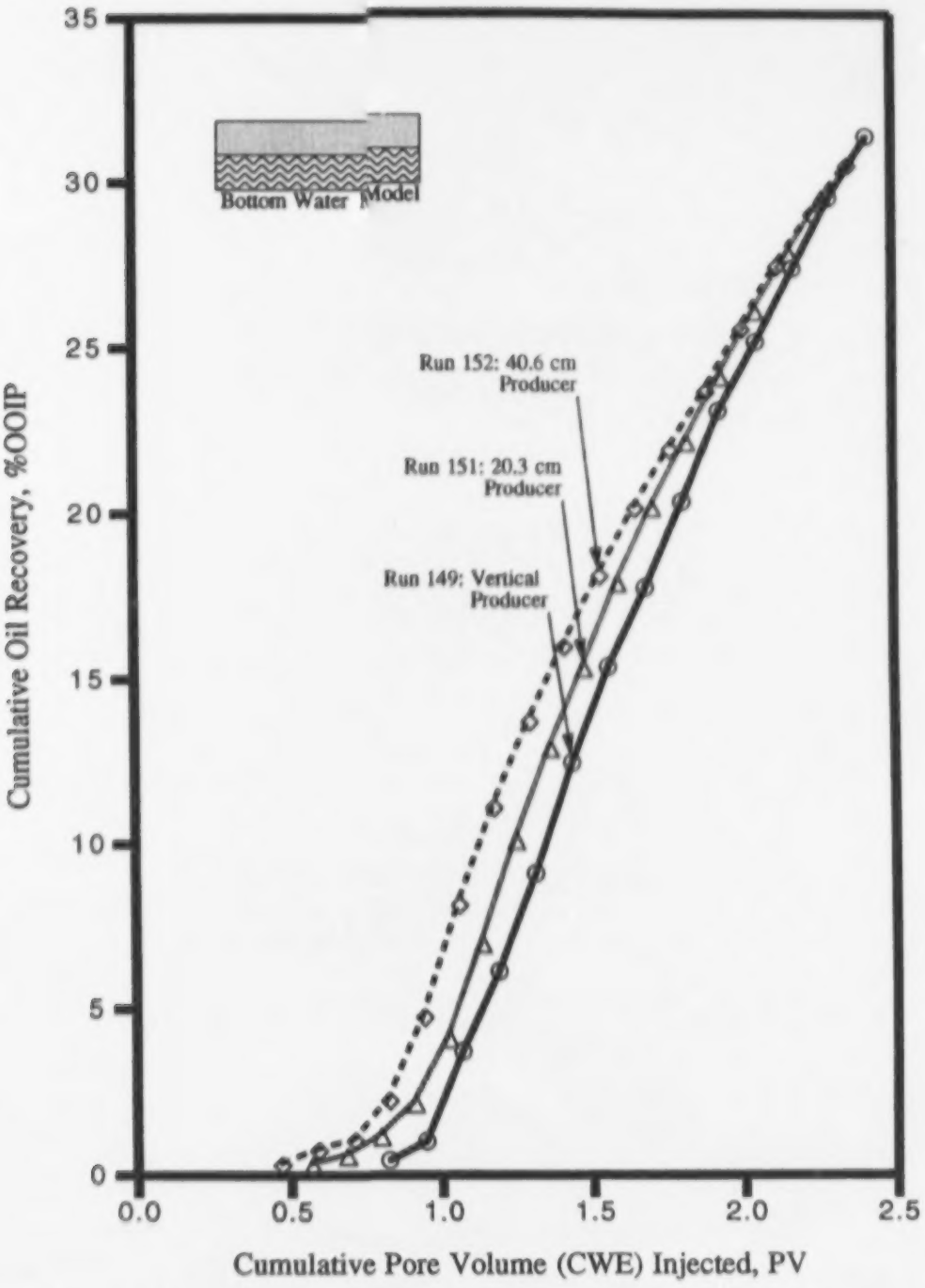

Figure 6.10 — Cumulative Oil Recovery vs. Cumulative PV Injected for Two Different Lengths of Horizontal Production Well and a Vertical Production Well in 50% Bottom Water Models, Vertical Steam Injection Well.

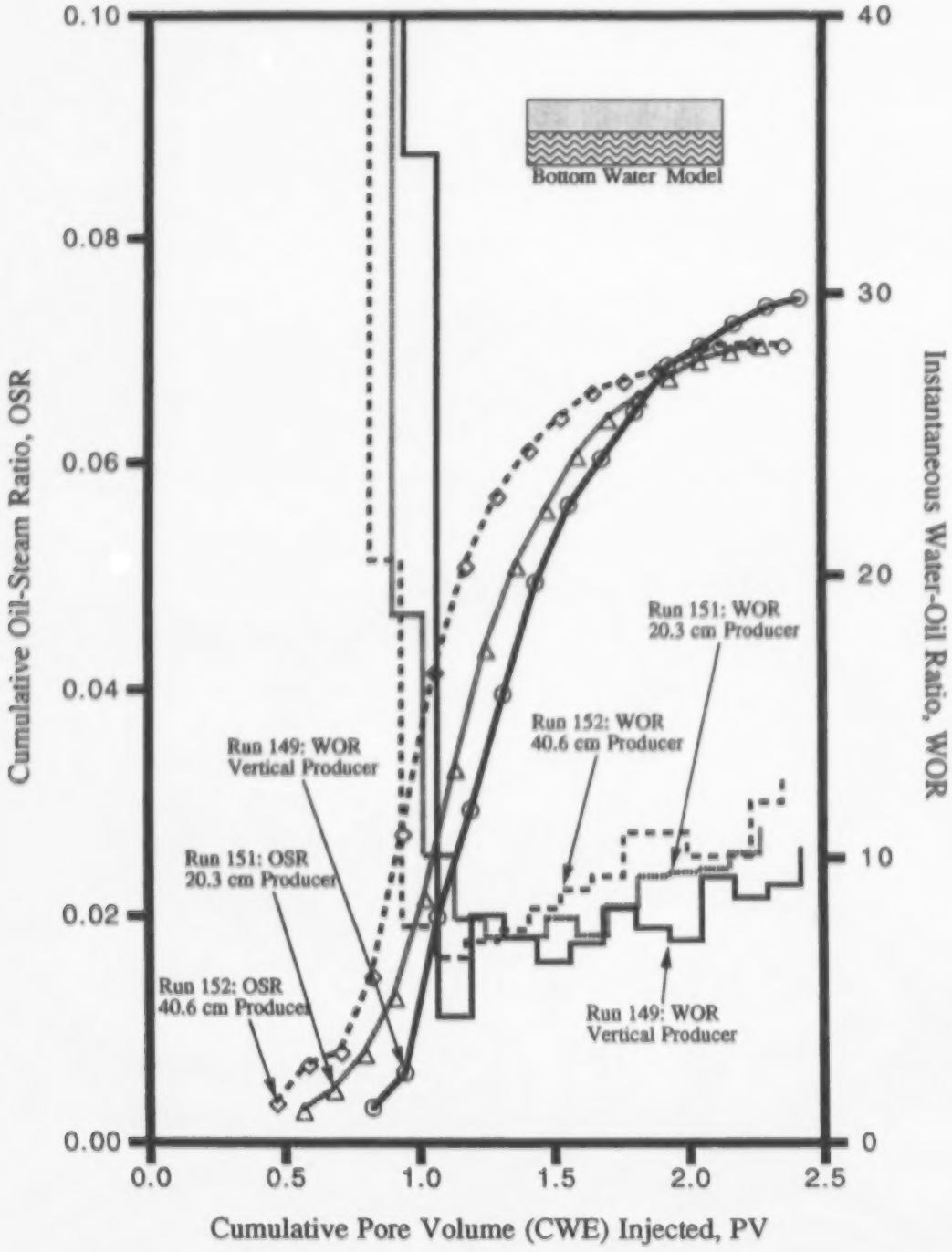

Figure 6.11 — Cumulative OSR and Instantaneous WOR vs. Cumulative PV Injected for Two Different Lengths of Horizontal Production Well and a Vertical Production Well in 50% Bottom Water Models, Vertical Steam Injection Well.

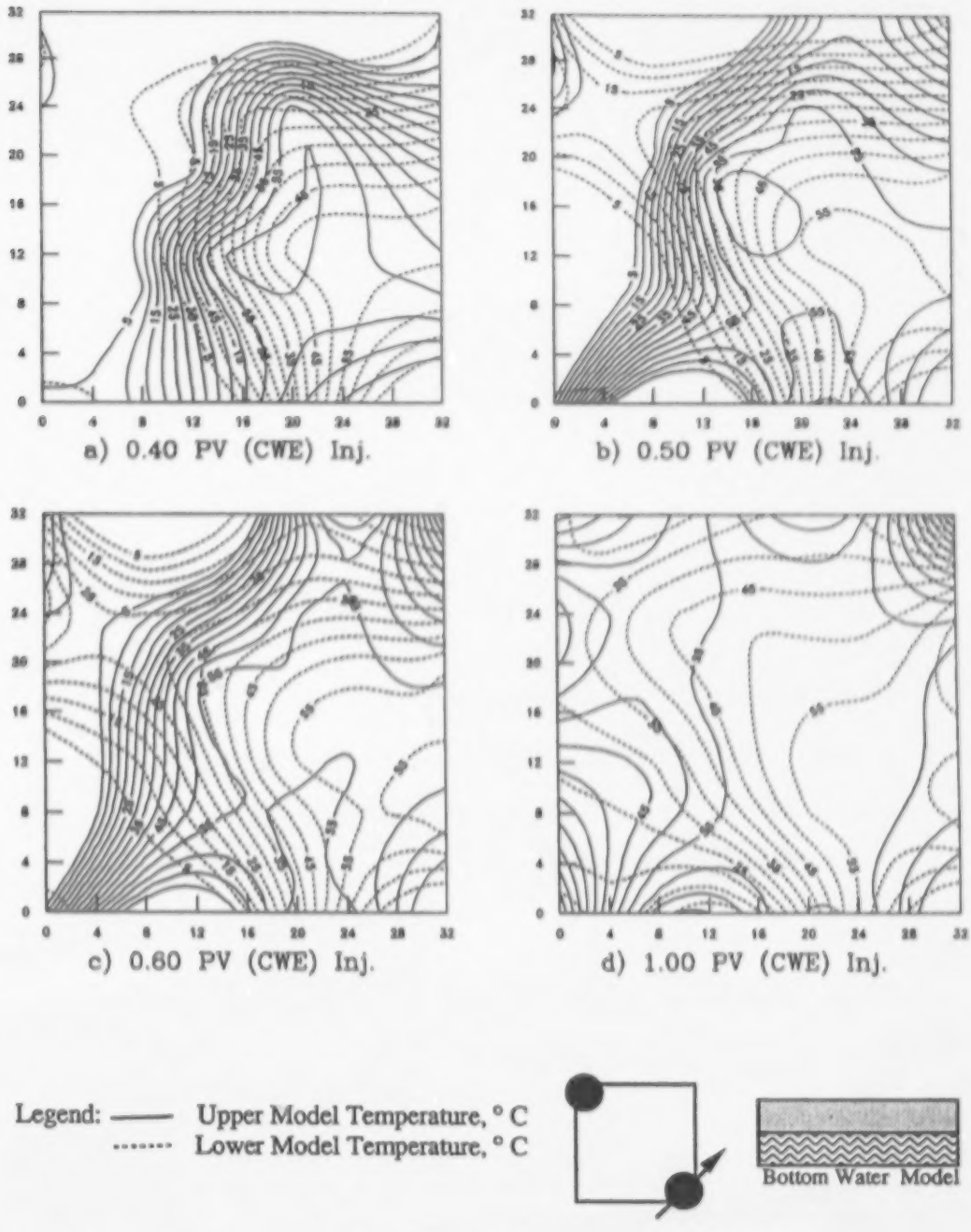
a) 0.40 PV (CWE) Inj.
b) 0.50 PV (CWE) Inj.
c) 0.60 PV (CWE) Inj.
d) 1.00 PV (CWE) Inj.
Legend: —— Upper Model Temperature, ° C
------- Lower Model Temperature, ° C
Bottom Water Model

Figure 6.12 — Plan view,of the temperature distribution inside the model reservoir after the injection of: a) 0.40, b) 0.50, c) 0.60, and d) 1.00 PV CWE of steam, for Run 149: 50% bottom water model, vertical injection and production wells.

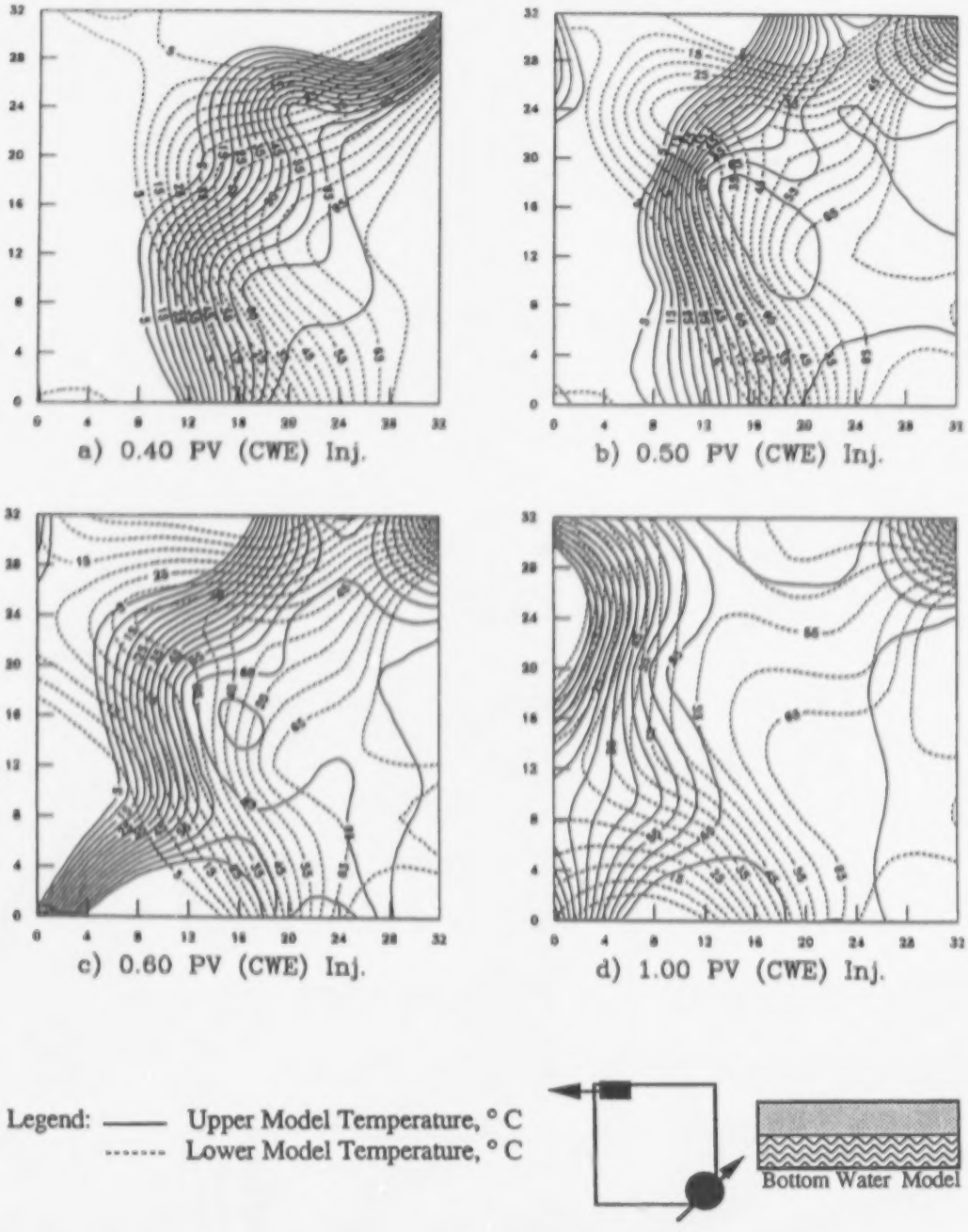
a) 0.40 PV (CWE) Inj.
b) 0.50 PV (CWE) Inj.
c) 0.60 PV (CWE) Inj.
d) 1.00 PV (CWE) Inj.
Legend: —— Upper Model Temperature, ° C
------- Lower Model Temperature, ° C
Bottom Water Model

Figure 6.13 — Plan view,of the temperature distribution inside the model reservoir after the injection of: a) 0.40, b) 0.50, c) 0.60, and d) 1.00 PV CWE of steam, for Run 151: 50% bottom water model, short horizontal producer (20.3-cm) and a vertical injection well.

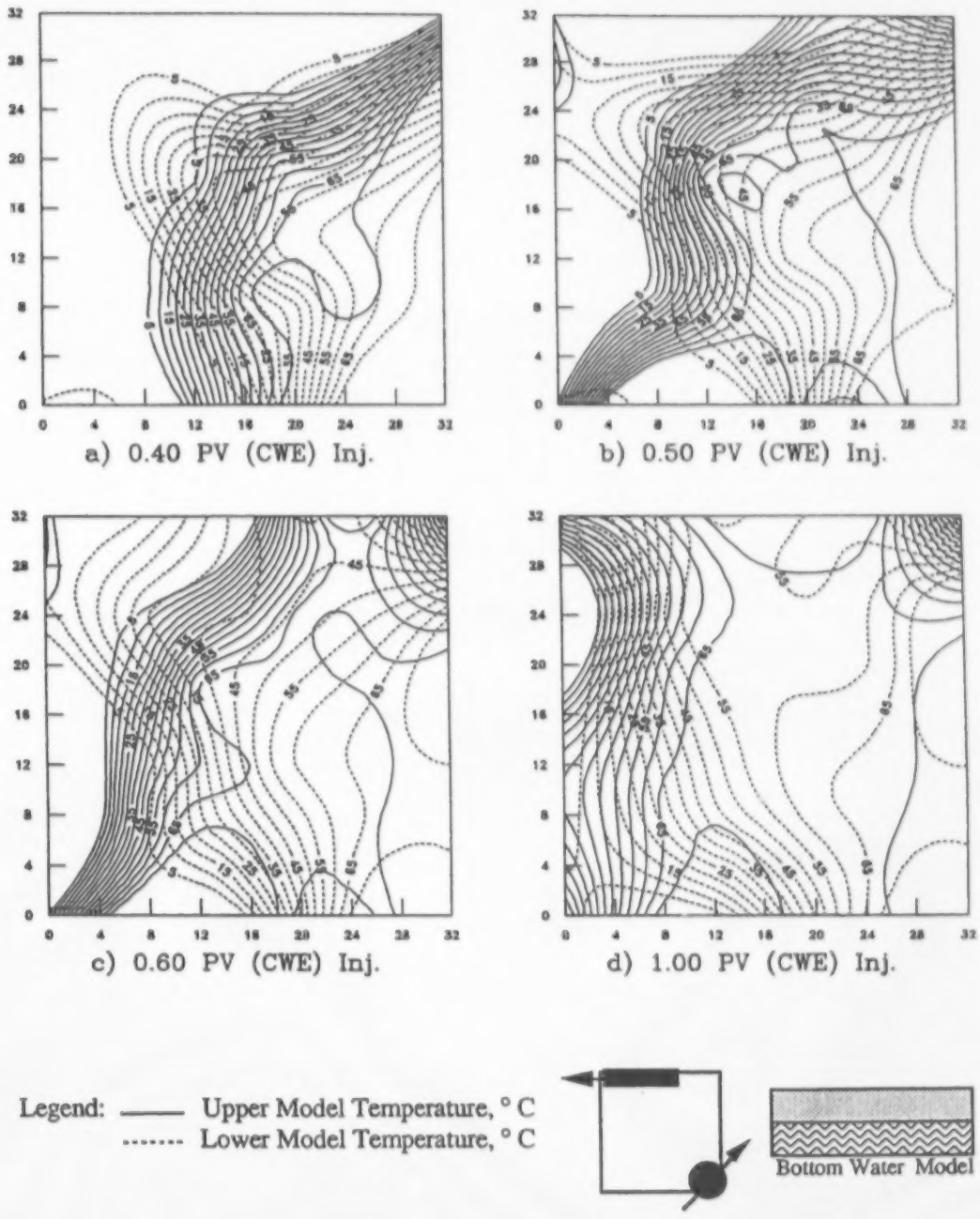
a) 0.40 PV (CWE) Inj.
b) 0.50 PV (CWE) Inj.
c) 0.60 PV (CWE) Inj.
d) 1.00 PV (CWE) Inj.
Legend: —— Upper Model Temperature, ° C
------- Lower Model Temperature, ° C
Bottom Water Model

Figure 6.14 — Plan view, of the temperature distribution inside the model reservoir after the injection of: a) 0.40, b) 0.50, c) 0.60, and d) 1.00 PV CWE of steam, for Run 152: 50% bottom water model, long horizontal producer (40.6-cm) and a vertical injection well.

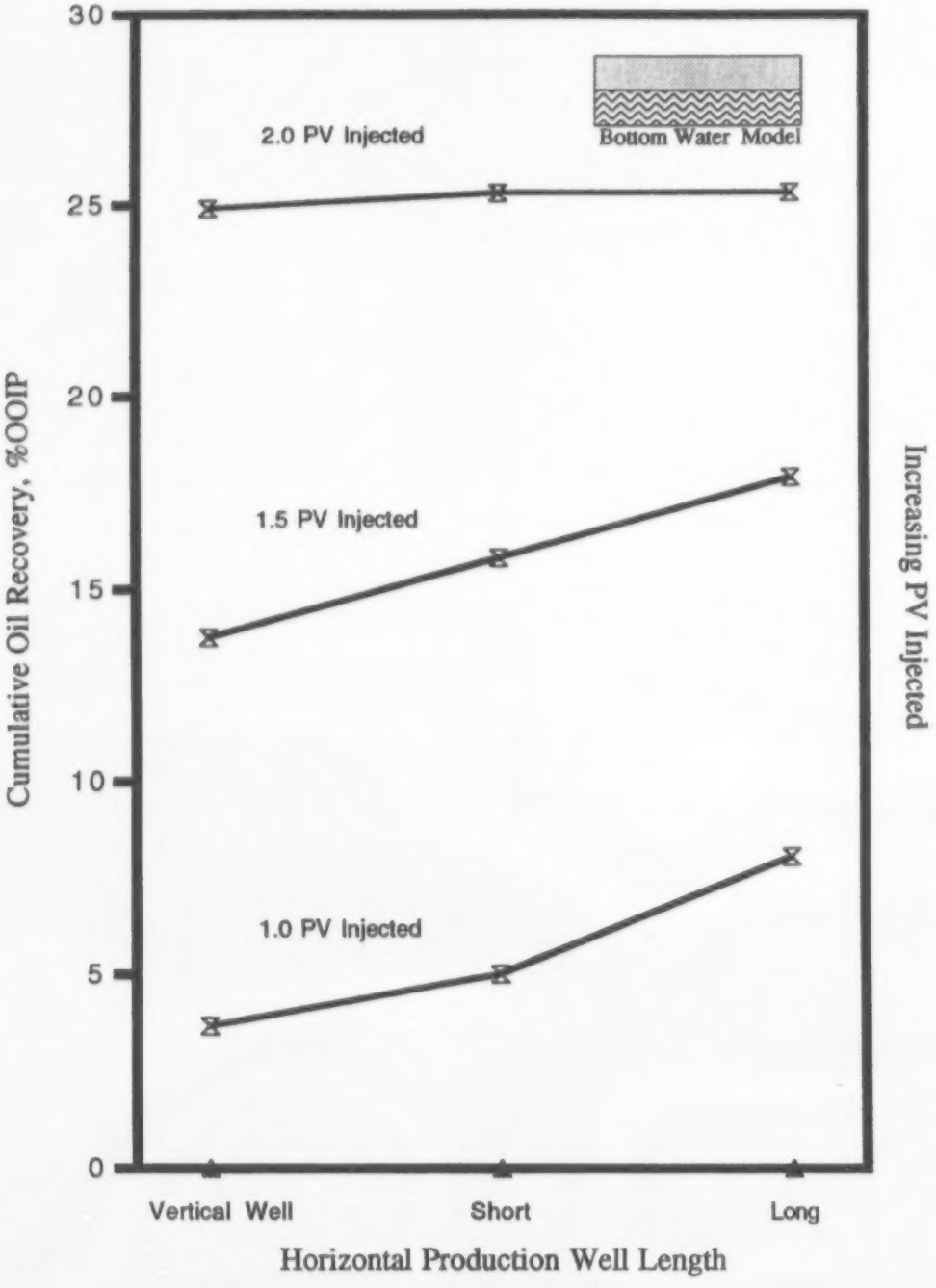

Figure 6.15 — Effect of Production Well Length on Recovery Performance; Cumulative Oil Recovery vs. Production Well Length for Increasing Steam Volumes Injected. Vertical Producer vs. Short (20.3 cm), and Long (40.6 cm) Horizontal Producers, Using Vertical Steam Injectors in 50% Bottom Water Models.

The experimental results presented above show potential for using short, small wellbore-radius horizontal wells for steamflooding viscous heavy oil reservoirs with a thick bottom water zone. The following provides a scaled up prediction of field performance for the five-spot pattern when these horizontal wells are used in place of conventional vertical producers. Figure 6.16 provides a schematic representation for such a pattern in the field. It can be seen that this scheme of reservoir development will involve the drilling of multiple, parallel rows of 141.2-m horizontal wells along the east-west of north-south boundaries of the five-spot patterns.

Laboratory oil production rates for two types of experiments (vertical injector-vertical producer and vertical injector-long horizontal producer) are listed in Table 6.4. These oil production rates can be scaled up[13], to predict the oil production rate for the prototype. For example, the oil production rate during the tenth sample (between the 61st and 68th minute) of the long horizontal well experiment was 23.6 ml/min. for the quarter of a five-spot. In field terms this rate is equivalent to

$$(q_P)_{5-spot} = \frac{q_M}{5.62987} \times 4 = \frac{23.57}{5.62987} \times 4 = 16.75 \text{ m}^3 / \text{Day}.$$

The scaled up rates for both schemes are included in Table 6.4 along with the scaled up time. Figure 6.17 shows a plot of the predicted field production rate per five-spot pattern as a function of field time for these two cases. It can be seen that the horizontal well pattern recovered oil earlier than the conventional vertical well pattern. More important, the oil production rate for the horizontal well pattern started out to be much higher than that for the vertical pattern, showing the ability of horizontal wells to accelerate production rates.

It can be concluded that both the long and the short horizontal wells recovered oil earlier than the conventional vertical producer. In addition, they achieved a higher cumulative oil recovery for comparable volumes of steam injected, and generally a higher cumulative oil-steam ratio than the vertical producer. The cumulative oil recovery varied with well length, i.e., the longer horizontal well achieved higher oil recovery and cumulative OSR for comparable volumes of steam injected than the short horizontal well.

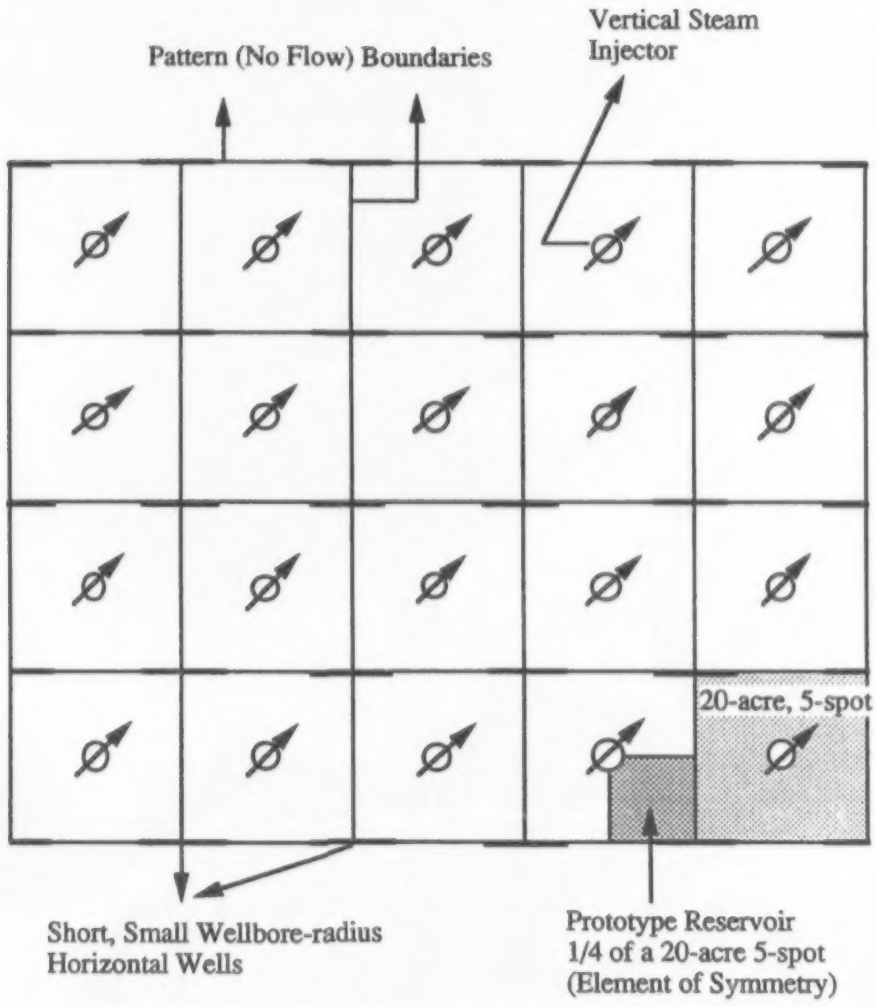
Pattern (No Flow) Boundaries
Vertical Steam Injector
20-acre, 5-spot
Short, Small Wellbore-radius Horizontal Wells
Prototype Reservoir 1/4 of a 20-acre 5-spot (Element of Symmetry)

Figure 6.16 — Schematic of Reservoir Development Using Five-spot Patterns With Short, Small Wellbore-radius Horizontal Wells In Place of Conventional Vertical Producer.

Table 6.4—Laboratory Oil Production Rate and Scaled-up Field Oil Production Rate, Vertical Producer Pattern vs. Horizontal Producer Pattern. Marginal Heavy Oil Reservoir with 50% Gross Thickness Bottom Water.

Vertical Producer				Long Horizontal Producer			
Laboratory Data		Prototype Values		Laboratory Data		Prototype Values	
Time minutes	Oil Prod. Rate ml/min.	Time Year	Oil Prod. Rate BPD/Pattern	Time minutes	Oil Prod. Rate ml/min.	Time Year	Oil Prod. Rate BPD/Pattern
5.	0.0	0.4	0.0	7.	0.0	0.5	0.0
12.	0.0	0.9	0.0	14.	0.0	1.1	0.0
19.	0.0	1.5	0.0	21.	0.0	1.6	0.0
26.	0.0	2.0	0.0	28.	2.9	2.2	12.7
33.	0.0	2.6	0.0	35.	4.3	2.7	19.0
40.	0.0	3.1	0.0	42.	2.9	3.3	12.7
47.	4.3	3.6	19.0	49.	11.4	3.8	50.7
54.	5.7	4.2	25.3	56.	24.3	4.3	107.7
61.	26.4	4.7	117.2	63.	32.9	4.9	145.7
68.	23.6	5.3	104.5	70.	28.6	5.4	126.7
75.	29.3	5.8	129.9	77.	25.0	6.0	110.9
82.	32.9	6.4	145.7	84.	22.1	6.5	98.2
89.	28.6	6.9	126.7	91.	20.7	7.0	91.9
96.	23.6	7.4	104.5	98.	20.0	7.6	88.7
103.	25.7	8.0	114.0	105.	17.1	8.1	76.0
110.	27.1	8.5	120.4	112.	17.1	8.7	76.0
117.	20.7	9.1	91.9	119.	18.6	9.2	82.4
124.	22.1	9.6	98.2	126.	18.6	9.8	82.4
131.	21.4	10.1	95.0	133.	15.7	10.3	69.7
138.	18.6	10.7	82.4	140.	14.3	10.8	63.3

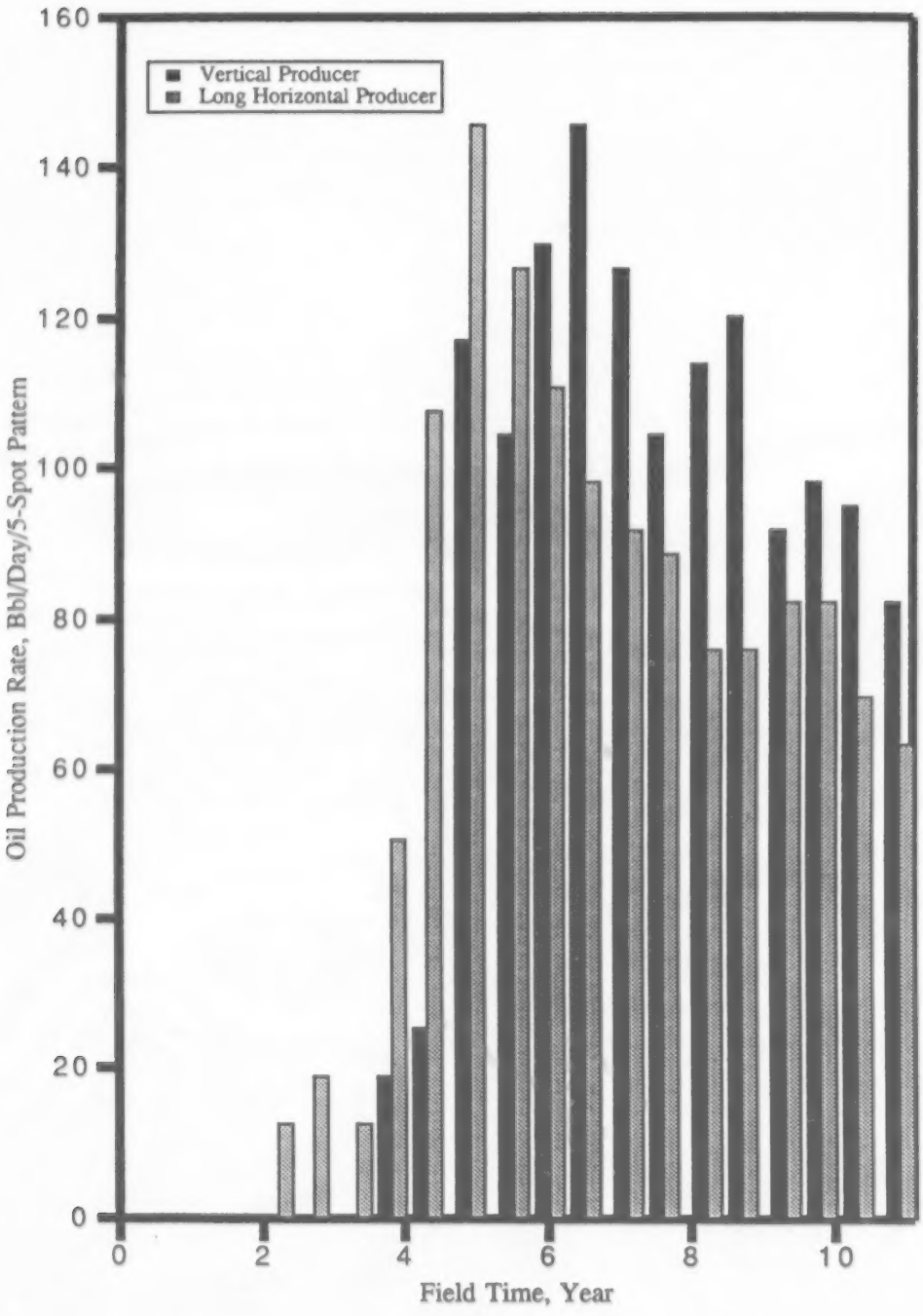

Figure 6.17 — Scaled-up Oil Production Rate per 5-Spot Pattern, Horizontal Producer vs. Vertical Producer, Marginal Heavy Oil Reservoir With 50% Gross Thickness Bottom Water, Vertical Steam Injector.

6.5.1.2 Effect of Horizontal Production Well Length in a Homogeneous Model

Steamflood recovery performances of three different lengths of horizontal production wells were compared with a vertical production well in a homogeneous model. Runs 136, 156, 158, and 157 used the following types of production wells: vertical, short horizontal (20.3-cm, 8-inch), medium horizontal (30.4-cm, 12-inch), and long horizontal (40.6-cm, 16-inch), respectively. Tables D.15, D.22, D.23, and D.24 contain the data for these runs.

Figure 6.18 compares the cumulative oil recovery of Runs 136, 156, 157, and 158. Throughout the same duration of steam injection the vertical production well achieved lower oil recovery than the three horizontal producers. At 1.50 PV of steam injected the short horizontal producer starts to have a decline in the oil production rate compared to the two longer horizontal producers. At 2.50 PV injected the medium horizontal producer has the highest oil production rate. The net oil recoveries at 4.00 PV of steam injected are: 69.8% for the short horizontal producer, 75.3% for the long, and 77.8% for the medium length horizontal producer. Run 136 (vertical producer) was terminated at 2.00 PV of steam injected because there are no significant changes after that and that is more than what would be injected in the field.

Figure 6.19 displays the cumulative OSR curves for these experiments. The long horizontal producer has the highest cumulative OSR at 0.75 PV of steam injected. After 1.50 PV of steam injected, the cumulative OSR curves for the long and medium wells are essentially similar for the duration of the experiments. It should be noted that all the OSR curves are above 0.10 ml of oil per 1 ml of steam.

Figures 6.20, 6.21, 6.22, and 6.23 display the temperature contours of these runs for up to 1.50 PV of steam injected. The contours in Figure 6.21 show warm fluids entering the entire length of the short horizontal producer at all four time intervals. In the case of the medium length horizontal well (Figure 6.23), the contours reach the "toe" of the well in the lower portion of the model after the first 0.25 PV of steam injected. At 0.50 PV of steam injected the lower contours indicate warm fluids entering the entire length of the well, and the upper contours have not. At 1.00 PV of steam injected, the upper contours indicate hot fluids entering the "toe" and lower temperature contours have reached ahead of the upper contours to the "heel" of the medium length horizontal well. The long horizontal producer gives a similar response to that of a vertical producer for the

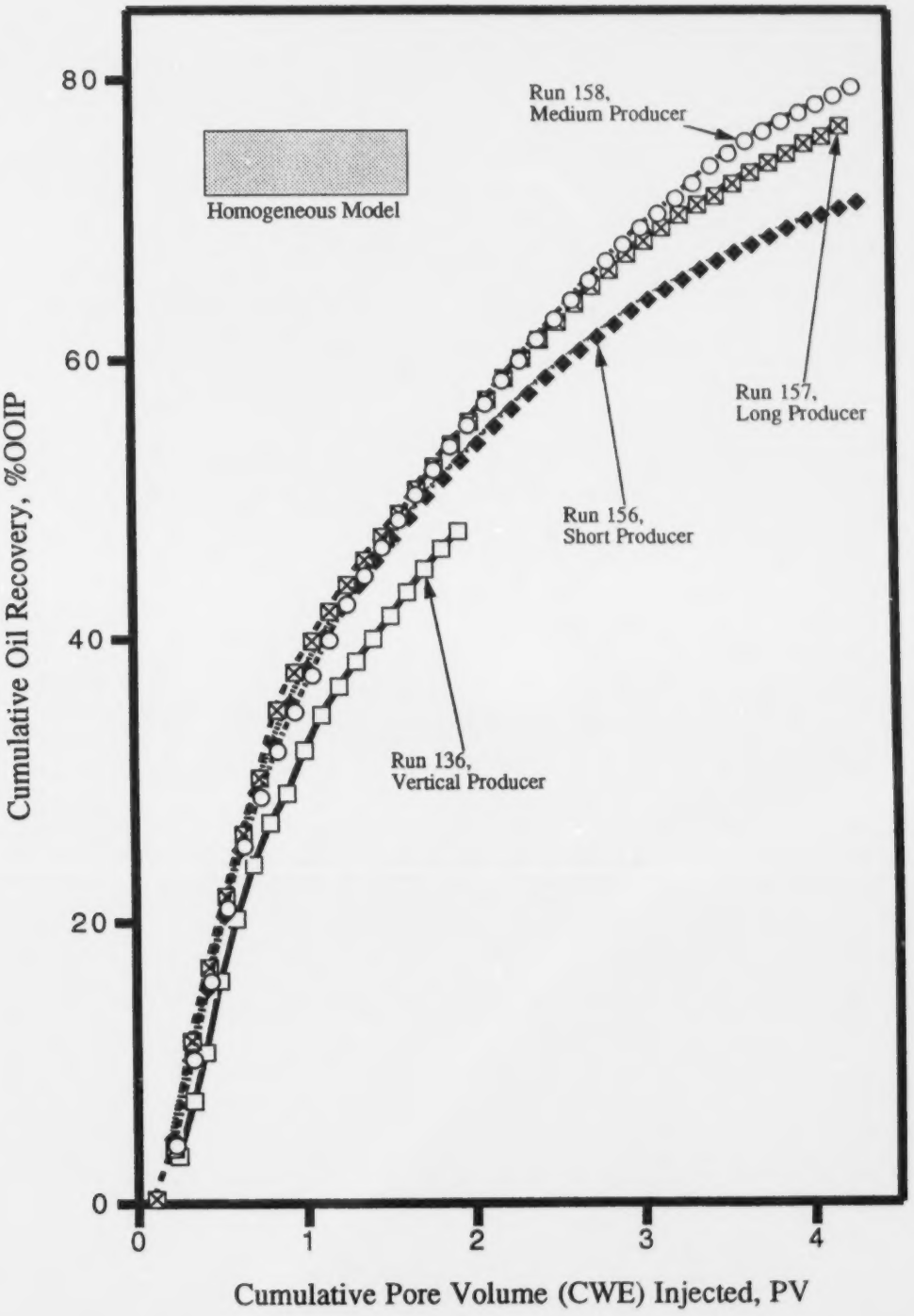

Figure 6.18 — Cumulative Oil Recovery vs. Cumulative PV Injected for Three Different Lengths of Horizontal Producers and a Vertical Producer, Vertical Steam Injection Wells in Homogeneous Models.

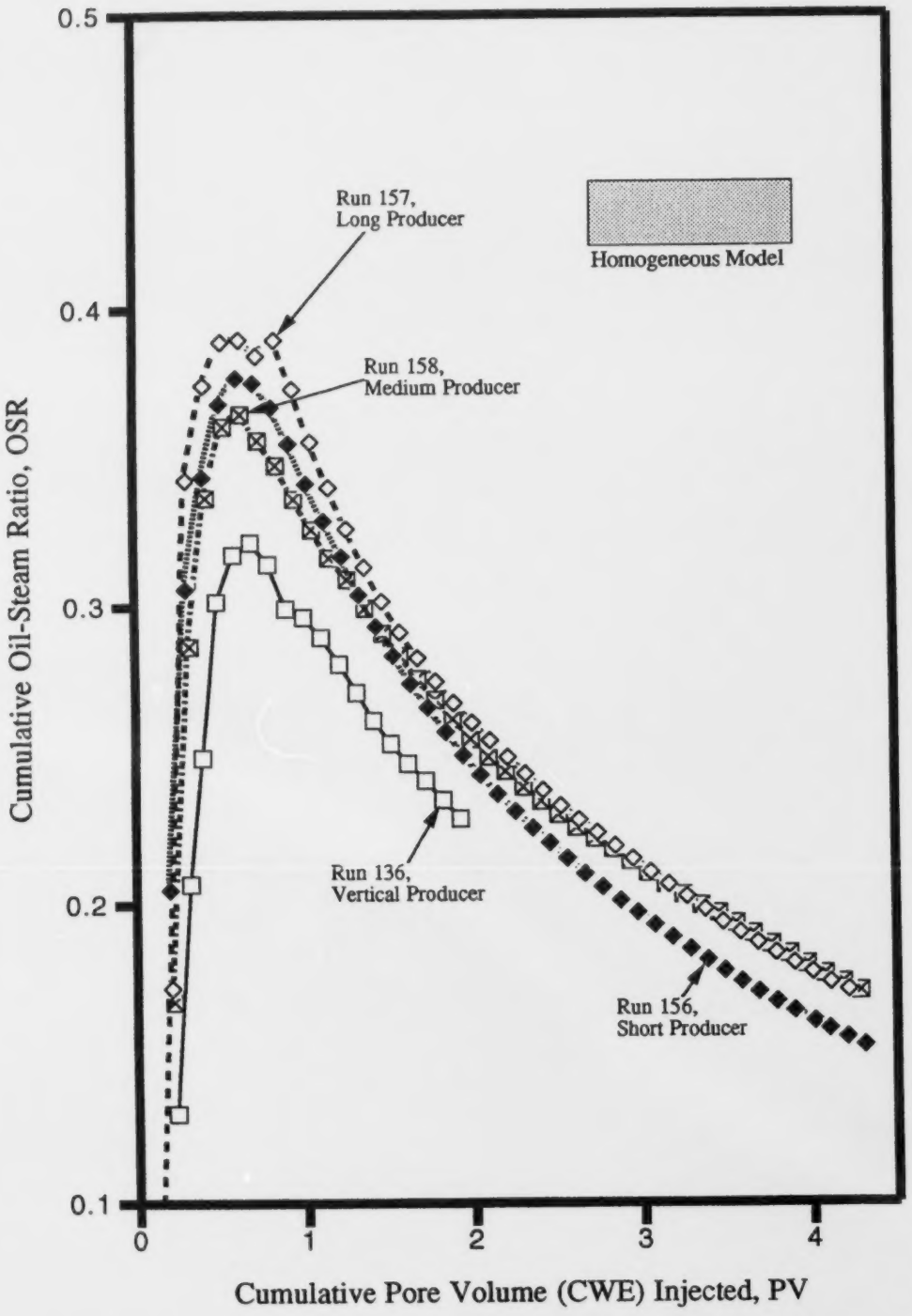

Figure 6.19 — Cumulative OSR vs. Cumulative PV Injected for Three Different Lengths of Horizontal Producers and a Vertical Producer in Homogeneous Models, Vertical Steam Injection Wells.

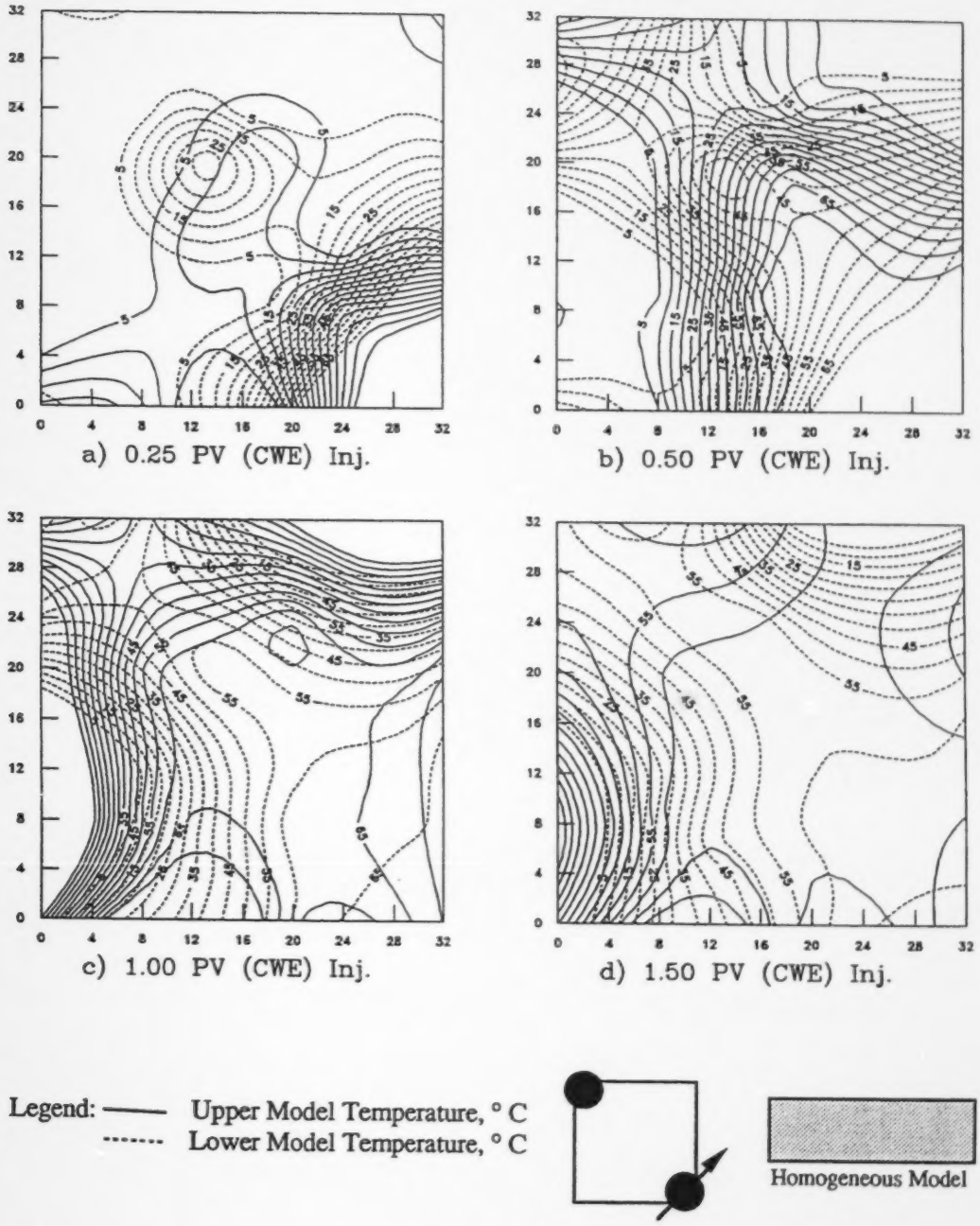
a) 0.25 PV (CWE) Inj.
b) 0.50 PV (CWE) Inj.
c) 1.00 PV (CWE) Inj.
d) 1.50 PV (CWE) Inj.
Legend: —— Upper Model Temperature, ° C
------- Lower Model Temperature, ° C
Homogeneous Model

Figure 6.20— Plan view, of the temperature distribution inside the model reservoir after the injection of: a) 0.25, b) 0.50, c) 1.00, and d) 1.50 PV CWE of steam, for Run 136: homogeneous model, vertical injection and production wells

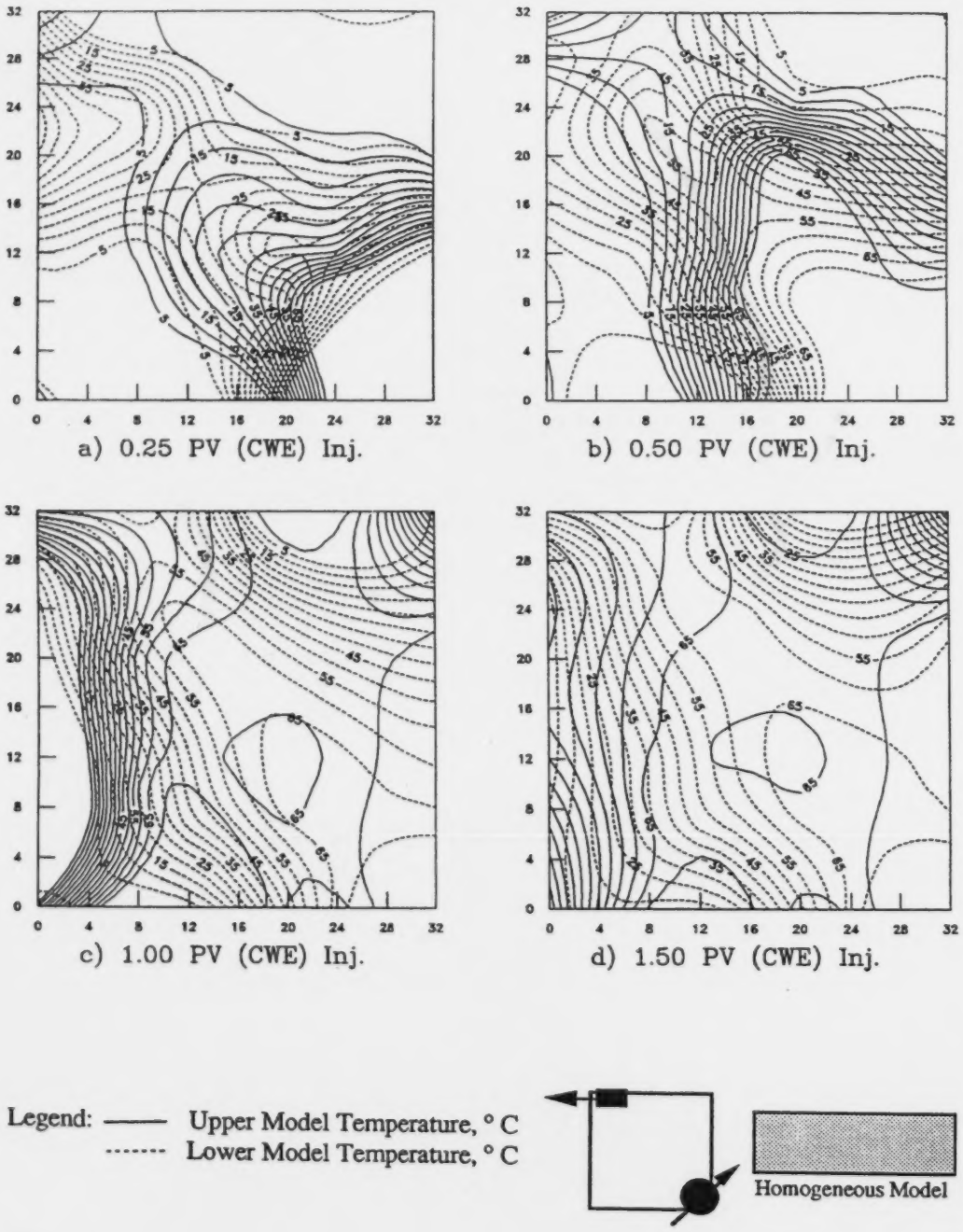
a) 0.25 PV (CWE) Inj.
b) 0.50 PV (CWE) Inj.
c) 1.00 PV (CWE) Inj.
d) 1.50 PV (CWE) Inj.
Legend: —— Upper Model Temperature, ° C
------- Lower Model Temperature, ° C
Homogeneous Model

Figure 6.21— Plan view, of the temperature distribution inside the model reservoir after the injection of: a) 0.25, b) 0.50, c) 1.00, and d) 1.50 PV CWE of steam, for Run 156: homogeneous model, short horizontal producer (20.3-cm) and a vertical injection well.

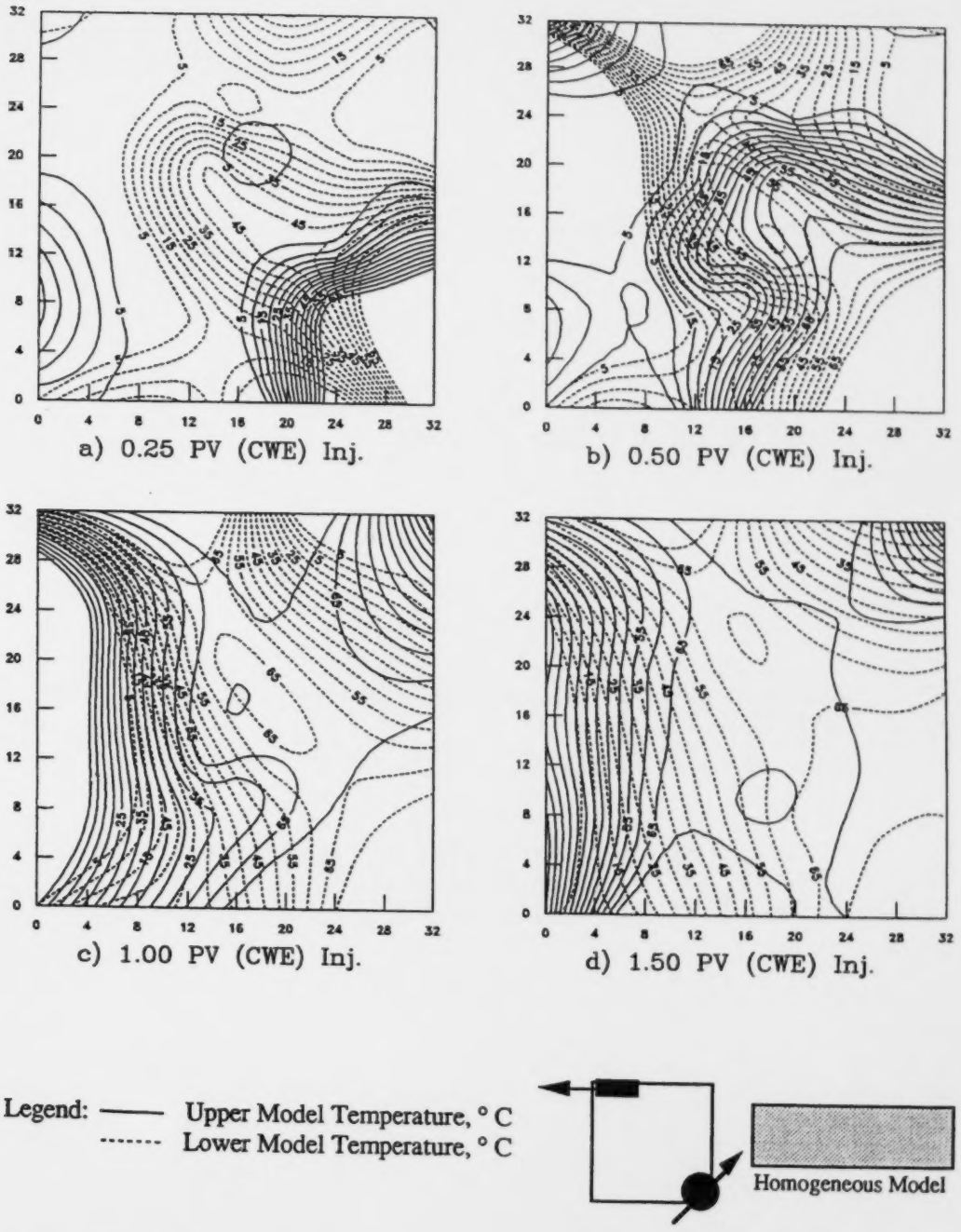
a) 0.25 PV (CWE) Inj.
b) 0.50 PV (CWE) Inj.
c) 1.00 PV (CWE) Inj.
d) 1.50 PV (CWE) Inj.
Legend: —— Upper Model Temperature, ° C
------- Lower Model Temperature, ° C
Homogeneous Model

Figure 6.22 — Plan view, of the temperature distribution inside the model reservoir after the injection of: a) 0.25, b) 0.50, c) 1.00, and d) 1.50 PV CWE of steam, for Run 158: homogeneous model, medium length horizontal producer (30.5-cm), and a vertical injection well.

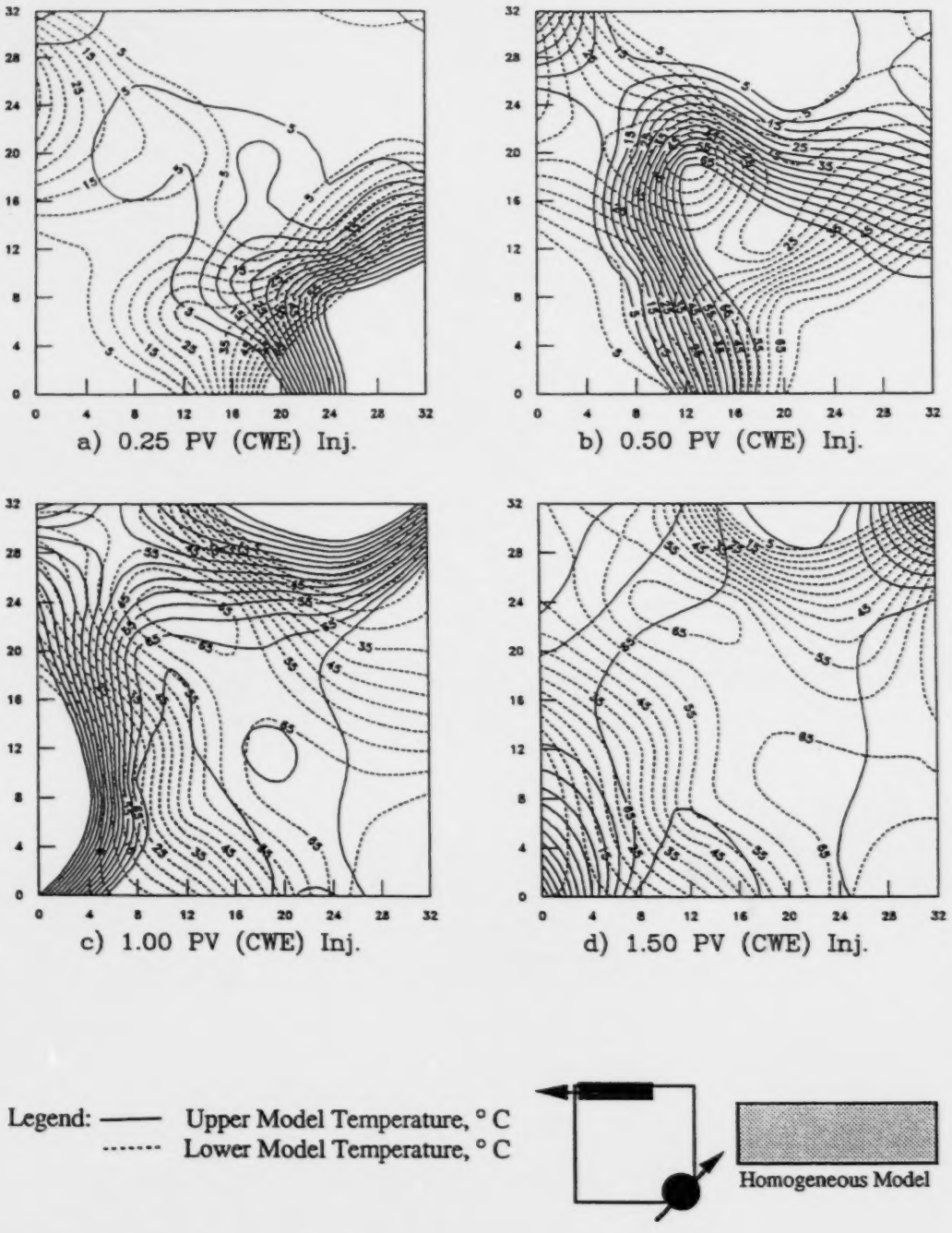
a) 0.25 PV (CWE) Inj.
b) 0.50 PV (CWE) Inj.
c) 1.00 PV (CWE) Inj.
d) 1.50 PV (CWE) Inj.
Legend: —— Upper Model Temperature, ° C
------- Lower Model Temperature, ° C
Homogeneous Model

Figure 6.23— Plan view, of the temperature distribution inside the model reservoir after the injection of: a) 0.25, b) 0.50, c) 1.00, and d) 1.50 PV CWE of steam, for Run 157: homogeneous model, long horizontal producer (40.6-cm) and a vertical injection well.

first 0.50 PV of steam injected (Figures 6.20 and 6.22). The temperature contours do not reach the "toe" of the well until after the injection of 1.00 PV of steam.

Figure 6.24 displays the cumulative oil recovery versus the type of production well at increasing PV injected. At 2.00 PV of steam injected, the horizontal producers recovered about the same amount of oil (52%), which was 10% more oil than the vertical producer. The medium length horizontal producer then starts to out-perform the other horizontal producers. Based on these experimental results, it can be seen that the sweep efficiency is affected by the horizontal well length, with the medium length being the most productive.

In summary, it can be concluded that in a homogeneous model the effect of the horizontal well length does not manifest itself until after 2.00 PV injected. A horizontal well does not recover oil earlier than a vertical well. Cumulative oil recovery varies with well length. It appears that there is an optimal well length; as the length passes a certain percentage of the model length the oil recovery does not increase correspondingly.

6.5.2 Completion Interval Sensitivity For Horizontal Wells

The following experiments examine the effect of the position of a horizontal well in the vertical plane on oil recovery and sweep efficiency. Five experiments were performed using different horizontal and vertical well combinations. Runs 159, 160, and 161 were performed in 50% bottom water models. A medium length horizontal producer, placed at three different vertical positions in the oil zone, was used with a vertical injection well. The other two experiments were carried out in homogeneous models using a long horizontal injection well, placed at two different vertical positions in the oil zone, with a vertical producer. Tables D.8, D.10, D.25, D.26, and D.27 contain the data for these runs.

6.5.2.1 Vertical Position of the Horizontal Producer

The medium length horizontal producer was placed at three different positions in the vertical plane during the packing of the model: middle of the oil zone (Run 159), top of the oil zone (Run 160), and at the oil-water contact (Run 161).

Figure 6.25 shows the cumulative oil recovery for the three cases with the same volume of steam injected. As mentioned previously, there was no significant initial oil

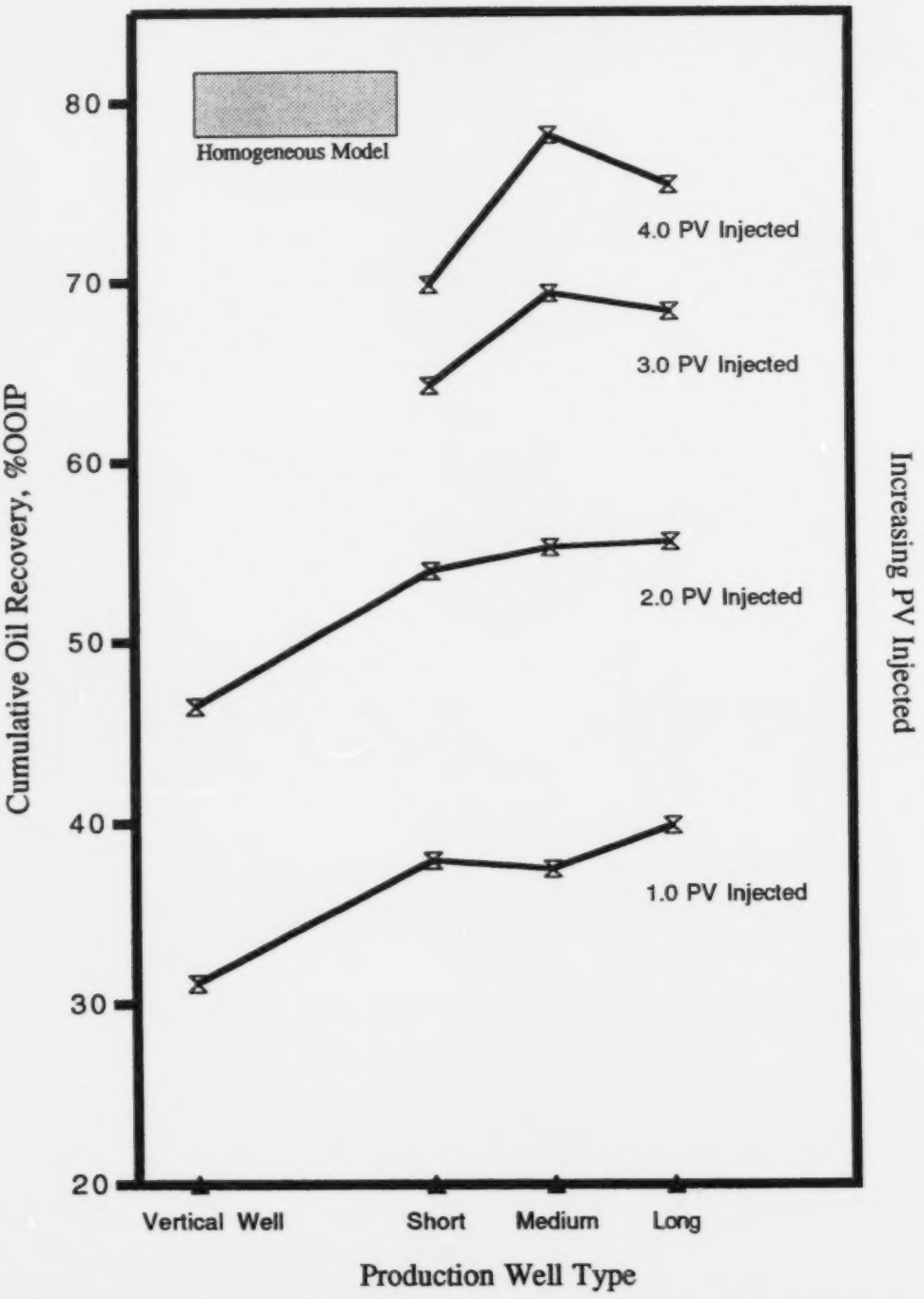

Figure 6.24 — Effect of Production Well Length on Recovery Performance; Cumulative Oil Recovery vs. Production Well Length for Increasing Steam Volumes Injected. Vertical Producer vs. Short, Medium and Long Horizontal Producers, Vertical Steam Injectors in Homogeneous Models.

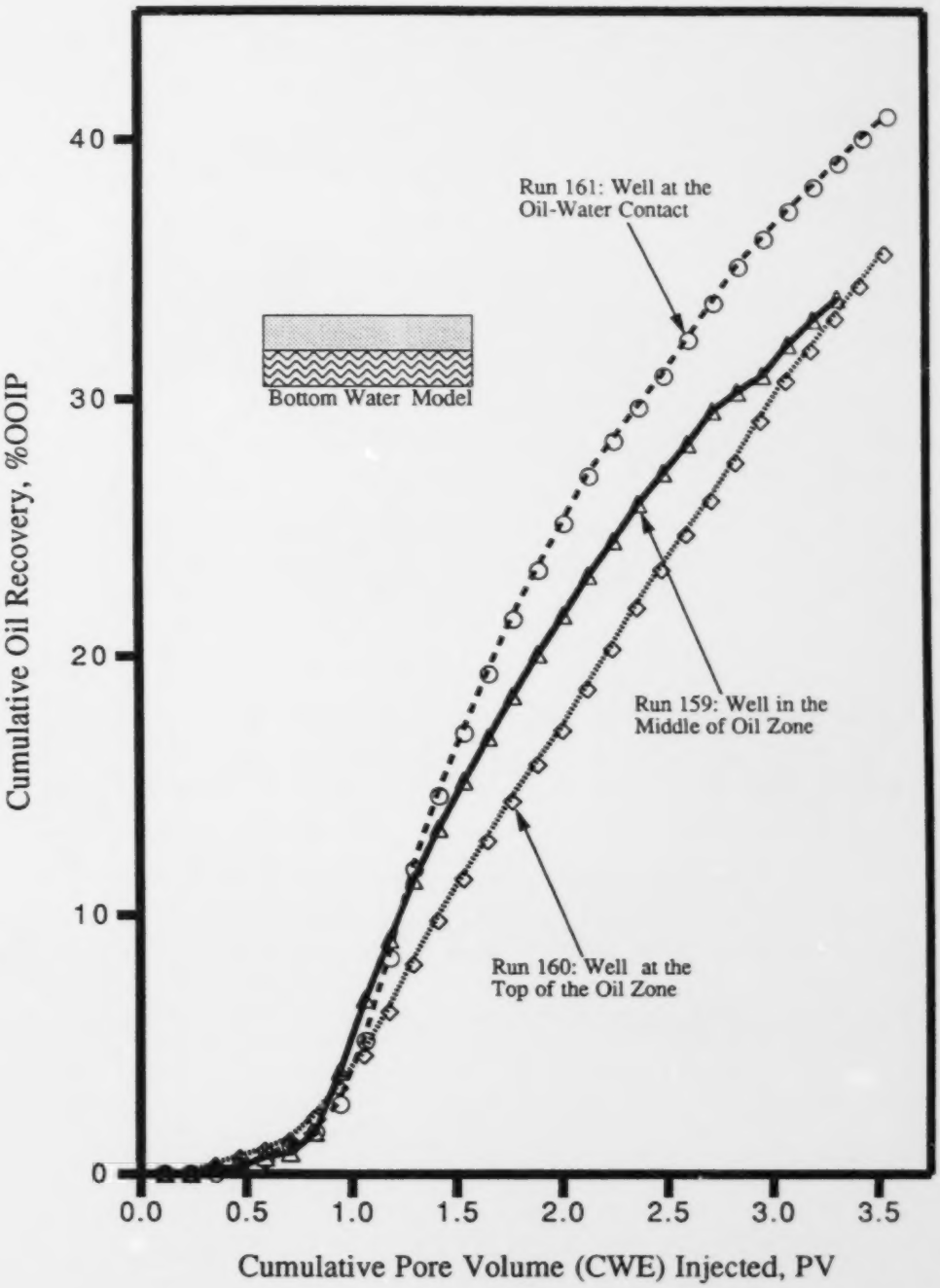

Figure 6.25 — Cumulative Oil Recovery vs. Cumulative PV Injected, for a Medium Length (30.5 cm) Horizontal Producer Placed at the Top of the Oil Zone (Run 160), the Middle of the Oil Zone (Run 159), or at the Oil-Water Contact (Run 161), Using aVertical Injector in a 50% Bottom Water Model.

production primarily because of the 50% bottom water and the very high mobility contrast between the oleic and aqueous phases. From the start to 0.75 PV of steam injected, the profiles are similar. When the production well was placed at the top of the oil zone, the bottom water coned up through the oil and was produced until the oil had been mobilized. At 1.00 PV of steam injected the curves separated. The oil recovery rate for Run 160 (well placed at the oil-water contact) drops off the most.

Figures 6.26, 6.27 and 6.28 display the temperature contour plots for these three runs. Up to 0.50 PV of steam injected the runs have similar temperature contour plots. At 1.00 PV of steam injected, Run 160 (well placed at the oil-water contact) has steam breakthrough at the "toe" of the horizontal well with a large part of the left side of the model unswept In the following plot (1.50 PV of steam injected) there is an area on the left side of the model at the initial model temperature, despite the presence of a channel at the steam saturation temperature which sweeps a wide vertical section of the reservoir from the injector to the "toe" of the producer. At 1.00 PV of steam injected, Runs 159 and 161 have steam breakthrough with more of the left side of the model heated than seen in Run 160.

6.5.2.2 Vertical Position of the Horizontal Injector

Runs 121 and 125 were conducted in a homogeneous model. Both used a long (40.6-cm, 16-inch) horizontal steam injection well and a vertical production well. Run 121 had the horizontal steam injection well placed 3.2 cm (1.25 inch) off the bottom of the model, and Run 125 had the horizontal injection well at the bottom of the model.

Figure 6.29 shows the cumulative oil recovery for these two runs. Initially, the response is the same for both experiments, but after 0.40 PV of steam injected the recovery curves start to separate. At 1.50 PV of steam injected, Run 125 has a 6% higher recovery than Run 121.

Figures 6.30 and 6.31 display the temperature contour plots for the two experiments. Because of the initial construction of the horizontal wells, the horizontal steam injector in Run 125 is placed on the adjacent side of the model to the placement of the steam injector in Run 121. Because of this there is a gross difference in the plots of Figures 6.30 and 6.31. This difference is that in one case (Run 121) the horizontal steam injector is on the bottom of the plots and in the other case (Run 125) the horizontal steam injector is on the right side of the plots. Comparing the plots at 0.25 PV of steam

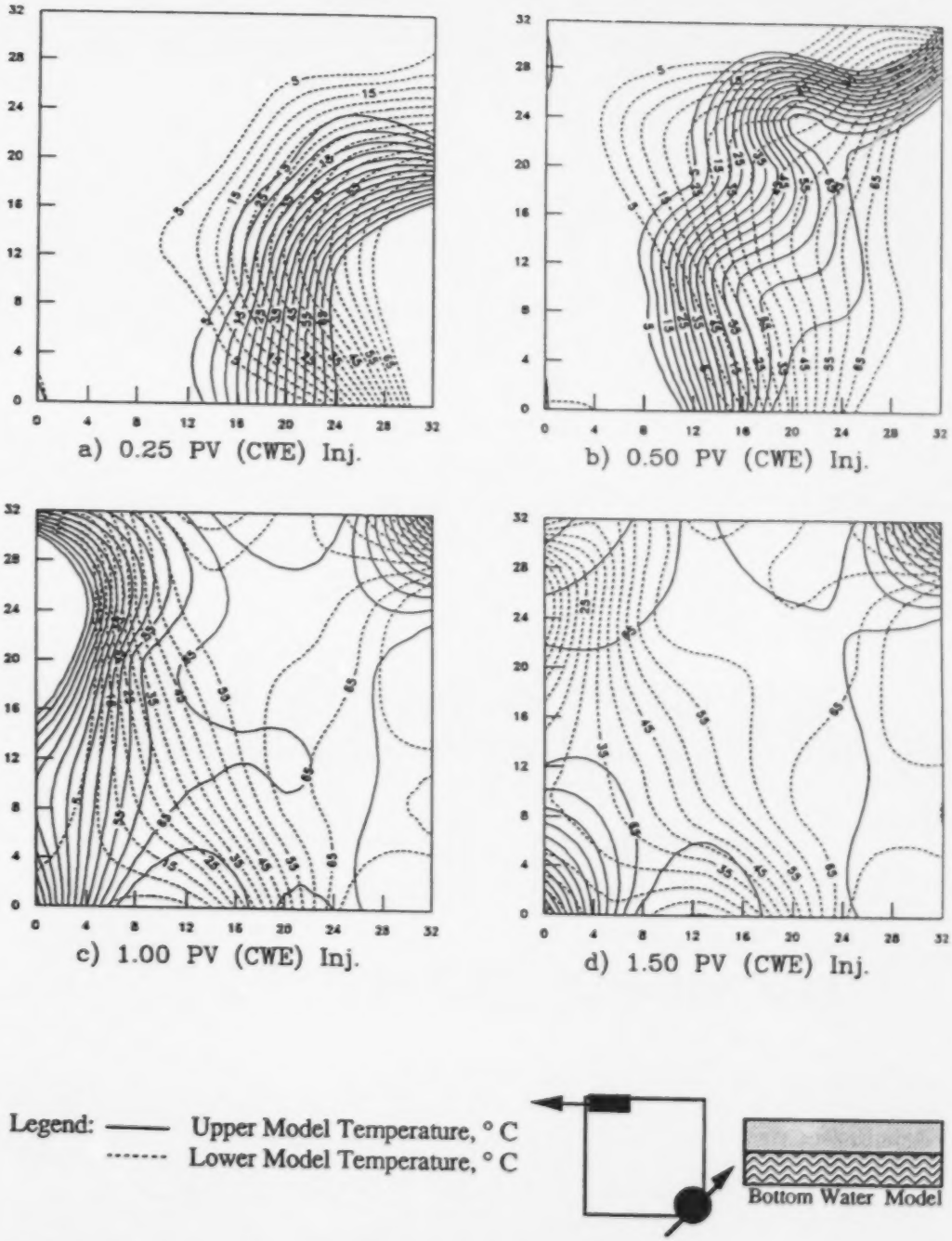
a) 0.25 PV (CWE) Inj.
b) 0.50 PV (CWE) Inj.
c) 1.00 PV (CWE) Inj.
d) 1.50 PV (CWE) Inj.
Legend: —— Upper Model Temperature, ° C
------- Lower Model Temperature, ° C
Bottom Water Model

Figure 6.26— Plan view, of the temperature distribution inside the model reservoir after the injection of: a) 0.25, b) 0.50, c) 1.00, and d) 1.50 PV CWE of steam, for Run 159: 50% bottom water model, medium length horizontal producer, (30.5-cm) placed in the middle of the oil zone, and a vertical injection well.

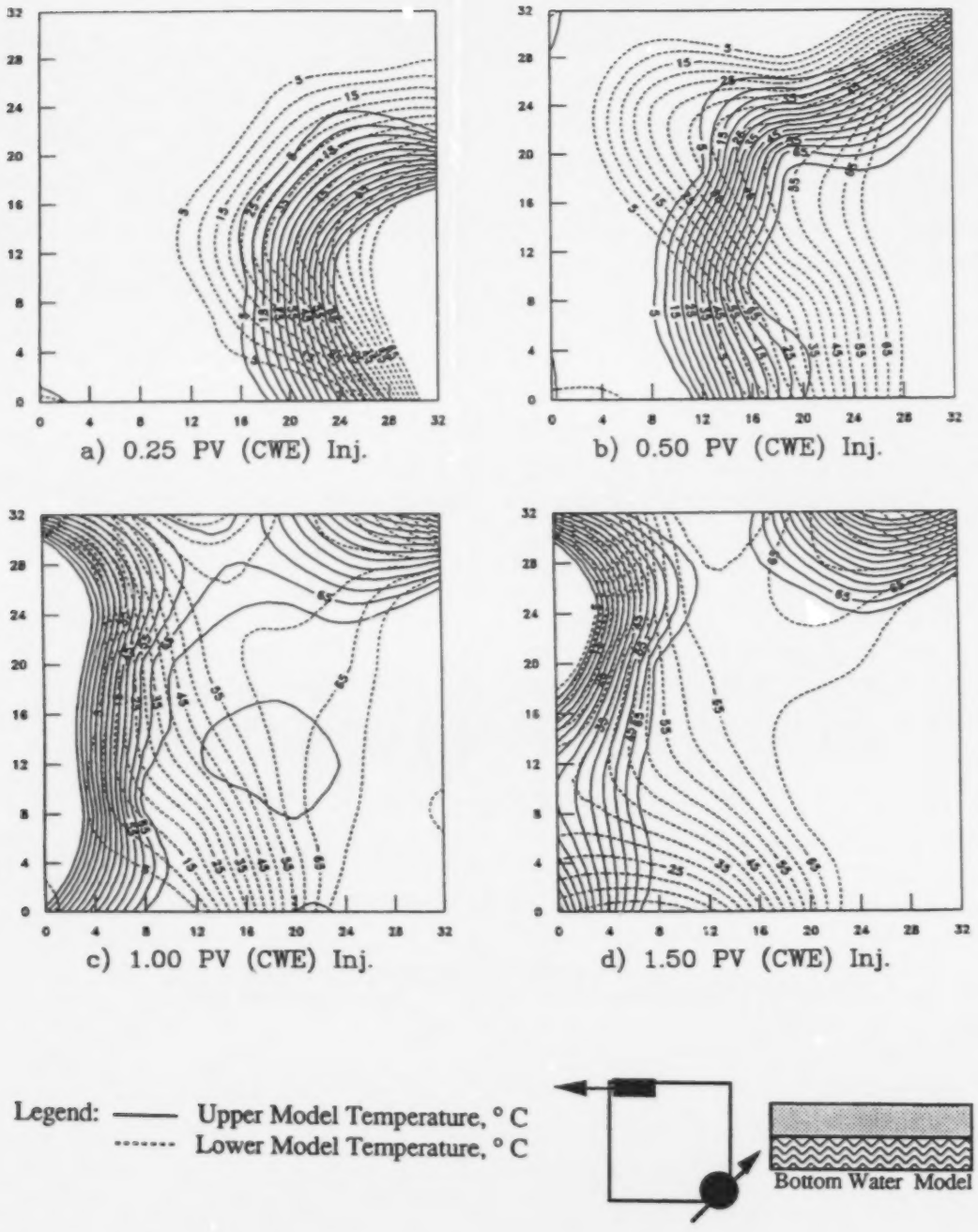
a) 0.25 PV (CWE) Inj.
b) 0.50 PV (CWE) Inj.
c) 1.00 PV (CWE) Inj.
d) 1.50 PV (CWE) Inj.
Legend: —— Upper Model Temperature, ° C
------- Lower Model Temperature, ° C
Bottom Water Model

Figure 6.27— Plan view, of the temperature distribution inside the model reservoir after the injection of: a) 0.25, b) 0.50, c) 1.00, and d) 1.50 PV CWE of steam, for Run 160: 50% bottom water model, medium length horizontal producer, (30.5-cm) placed at the top of the oil zone, and a vertical injection well.

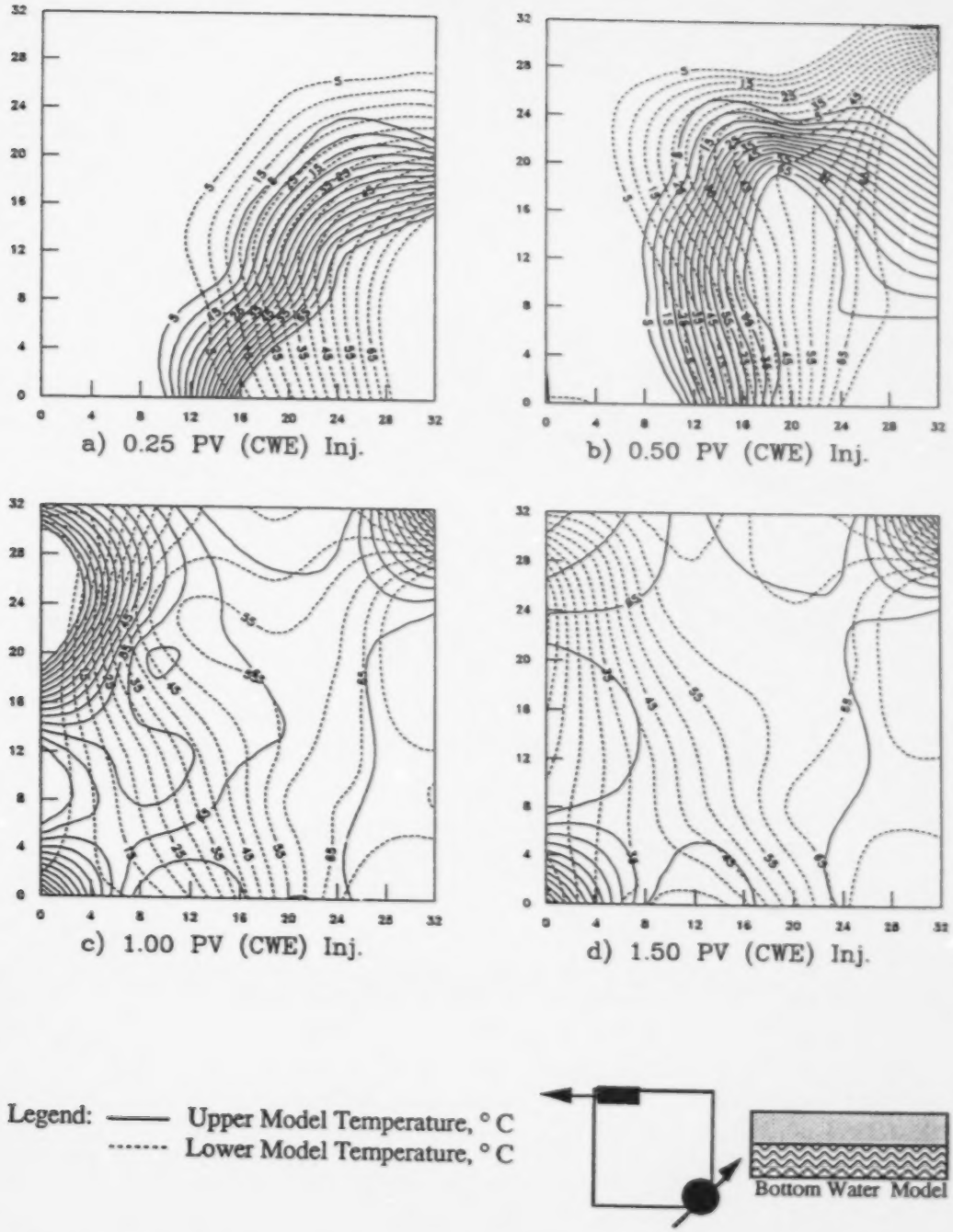
a) 0.25 PV (CWE) Inj.
b) 0.50 PV (CWE) Inj.
c) 1.00 PV (CWE) Inj.
d) 1.50 PV (CWE) Inj.
Legend: —— Upper Model Temperature, ° C
------- Lower Model Temperature, ° C
Bottom Water Model

Figure 6.28— Plan view, of the temperature distribution inside the model reservoir after the injection of: a) 0.25, b) 0.50, c) 1.00, and d) 1.50 PV CWE of steam. Run 161: 50% bottom water model, medium length horizontal producer, (30.5-cm) placed at the oil-water contact, and a vertical injection well.

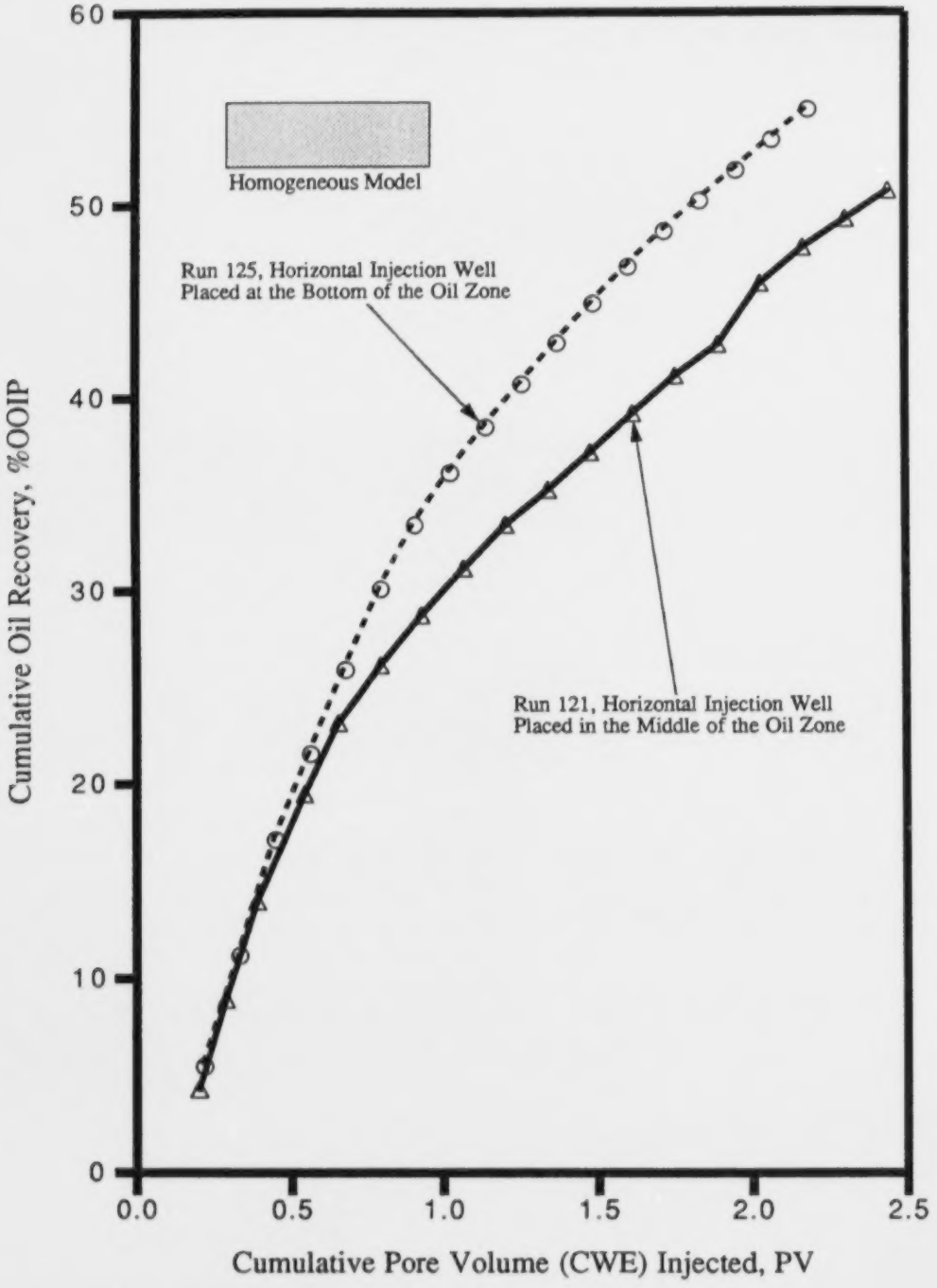

Figure 6.29 — Cumulative Oil Recovery vs. Cumulative PV Injected; Horizontal Injector on the Bottom of the Oil Zone (Run 125) vs. Horizontal Injector in the Middle of the Oil Zone (Run 121), Using a Vertical Production Well in a Homogeneous Model.

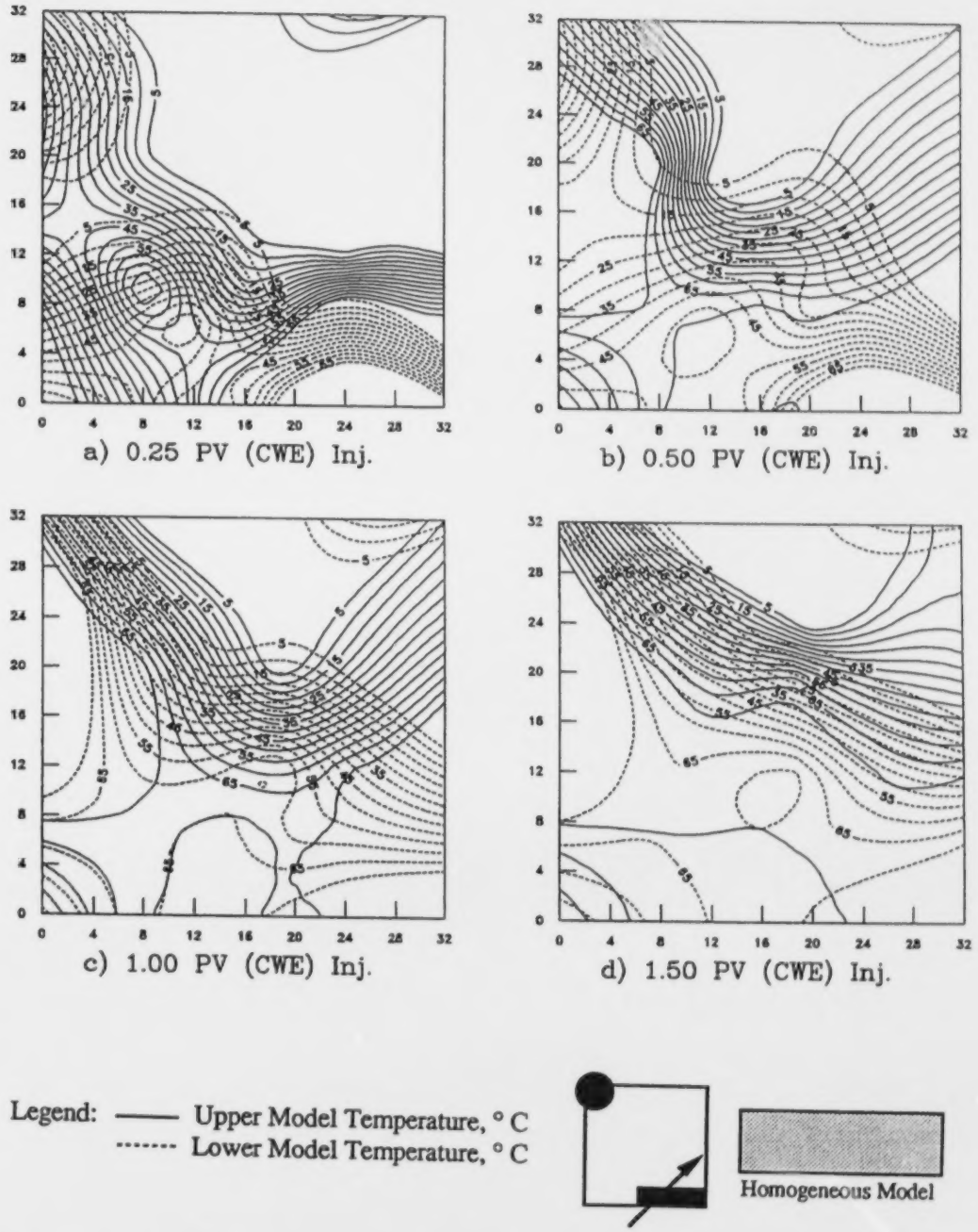
a) 0.25 PV (CWE) Inj.
b) 0.50 PV (CWE) Inj.
c) 1.00 PV (CWE) Inj.
d) 1.50 PV (CWE) Inj.
Legend: —— Upper Model Temperature, ° C
------- Lower Model Temperature, ° C
Homogeneous Model

Figure 6.30— Plan view, of the temperature distribution inside the model reservoir after the injection of: a) 0.25, b) 0.50, c) 1.00, and d) 1.50 PV CWE of steam, for Run 121: homogeneous model, long horizontal injector, (40.6-cm) placed in the middle of the oil zone, and a vertical production well.

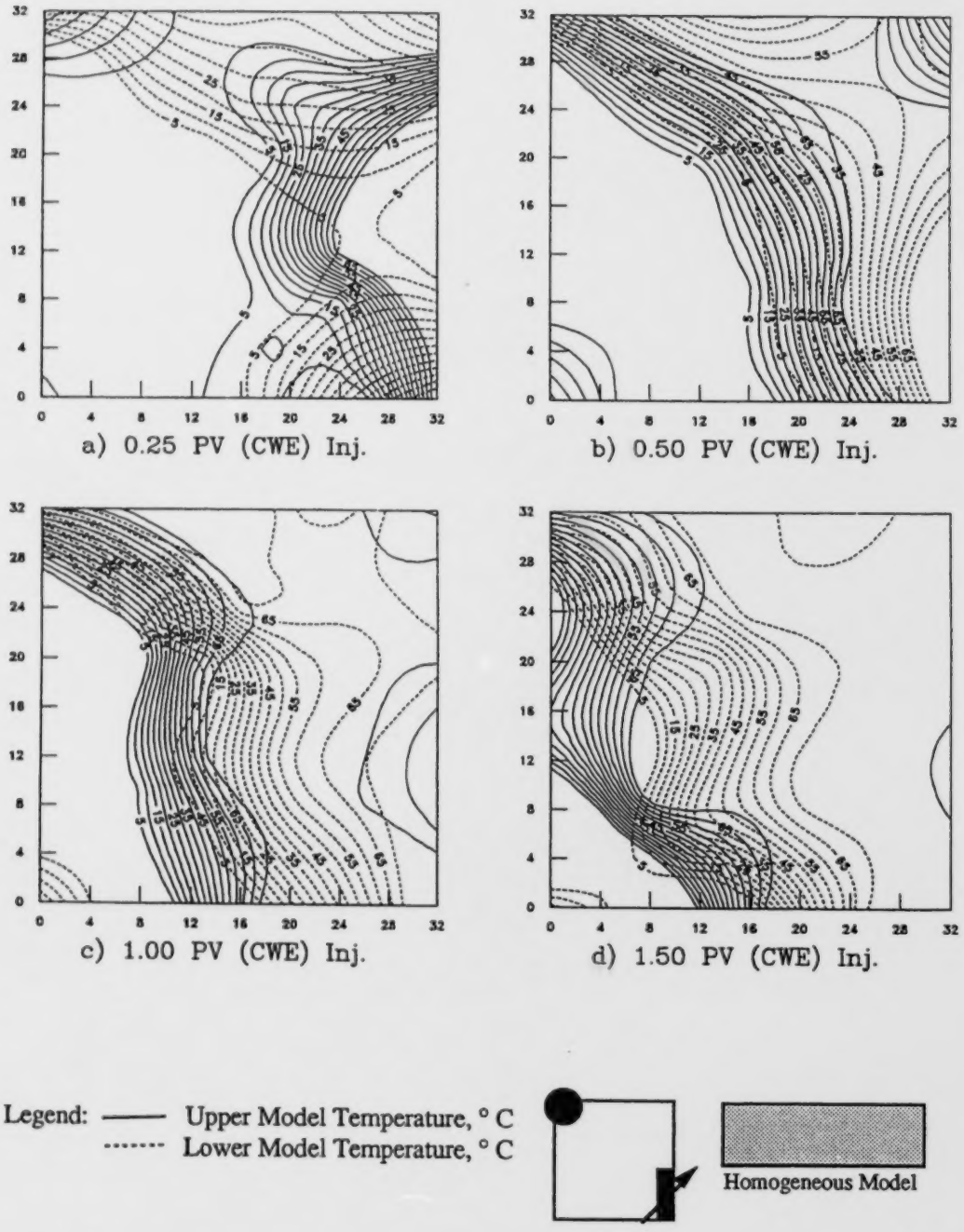
a) 0.25 PV (CWE) Inj.
b) 0.50 PV (CWE) Inj.
c) 1.00 PV (CWE) Inj.
d) 1.50 PV (CWE) Inj.
Legend: —— Upper Model Temperature, ° C
------- Lower Model Temperature, ° C
Homogeneous Model

Figure 6.31— Plan view, of the temperature distribution inside the model reservoir after the injection of: a) 0.25, b) 0.50, c) 1.00, and d) 1.50 PV CWE of steam, for Run 125: homogeneous model, long horizontal injector, (40.6-cm) placed at the bottom of the oil zone, and a vertical production well.

injected for both experiments, Run 125 (injection well at the bottom of the formation) has the isothermal contours in the bottom layer of the model reaching the production well, whereas the upper layer contours travel only to the middle of the model. On the other hand, the opposite observations can be made for Run 121: the upper contours reach the production well and the lower contours travel only about half-way into the model. The upper isothermal contours for Run 121, at 0.50 PV of steam injected, show steam breakthrough at the vertical producer while the bottom contours are just past the middle of the model. In contrast, at 0.50 PV of steam injected for Run 125, the steam zone in the upper portion of the model is close to the producer with the lower contours mirroring the upper contours at a slightly lower temperature. The results of this better sweep for Run 125 can be seen in Figure 6.29, where after 0.50 PV of steam injected the rate of oil production in Run 121 starts to decline slightly. At 1.00 PV of steam injected, Run 125 continues to have a more uniformed sweep than Run 121; over half of the top area of the model is heated. Comparing the sweeps of the two experiments it can be seen that Run 121 has the heat going all over the top of the model and the vertical conformance seems not to be as good as for Run 125.

In summary, for the same amount of energy invested in the model an optimum positioning of the horizontal producer in the vertical plane can contribute to a better distribution of energy before steam breakthrough. After steam breakthrough (1.00 PV of steam injected) the position of the well continues to influence oil recovery. The recovery performance of a horizontal injection well is dependent on its vertical placement. Placing a well too high in the model promotes early steam override.

6.6 Multi-layered Models

Steam injection experiments in multi-layered reservoirs constitute another aspect of this study. The objective of these experiments is to study the effects of reservoir heterogeneity on steam override. During the packing process, glass beads of two different sizes were separated by a permeable nylon membrane. This prevented any mixing of the glass beads. The multi-layered model had two stratifications: unfavourable, (a high permeability layer in the top half and a low permeability layer in the bottom half), or favourable (a low permeability layer in the top half and a high permeability layer in the bottom half of the model).

6.6.1 Effect of Reservoir Heterogeneity

Runs 115, 120, and 163 were performed to compare the recovery performances of the three permeability scenarios: homogeneous, unfavourable, and favourable, respectively.

In Figures 6.32 and 6.33 the production histories of these runs are compared. Initially, oil recovery is primarily due to the pressure drawdown, and the runs recover more or less the same amount of oil up to 0.50 PV injected. Run 163 (favourable stratification) has the highest oil recovery at 69.0 % of the OOIP after 2.00 PV of steam injected. Runs 115 and 120 have similar recovery curves up to 1.50 PV of steam injected, and then Run 120 (unfavourable stratification) starts to fall below Run 115 (homogeneous). Run 115 recovered 53.0 % of the OOIP after the injection of 2.00 PV; this is 3% more than Run 120 and 16% less than Run 163. The cumulative OSR curves of Figure 6.33 show, as expected, that the OSR for Run 163 exceeds that for the homogeneous and unfavourable permeability cases.

Figures 6.34, 6.35, and 6.36 display the plan view temperature contours for these three runs. At 0.50 PV of steam injected the steam zone is established in all three cases. Figure 6.36 (favourable permeability case) shows that at 0.25 PV of steam injected, the steam zone has advanced the furthest in the lower portion of the model while the upper portion is still at initial reservoir temperature. At 0.50 PV of steam injected, the top-layer steam zone reaches the same depth of penetration into the model as the bottom layer steam zone. At 1.00 PV of steam injected, there is steam breakthrough in the upper portion of the model from the injector to the producer. At 1.50 PV of steam injected, the heated channel extends to the bottom of the model. The plots for Runs 115 and 120 display similar trends. This similarity in the first 1.50 PV of steam injected could be caused by the sweep of the upper layer of both models. It is at 1.50 PV of steam injected that the differences can be seen between the two cases. The upper contours of Run 120 show steam breakthrough and most of the upper layer is at the saturation temperature. The lower contours have not advanced much from the 1.00 PV injected plot. Run 115 has a large area at the saturation temperature but there is no steam breakthrough, indicating that more of the heat injected is going into the lower portion of the model. After the injection of 1.50 PV of steam the unfavourable stratification case shows a decline in the oil recovery rate, as shown in Figure 6.32. It is postulated that the reason for this decline is that the low permeability layer has a lower fluid flow rate through it.

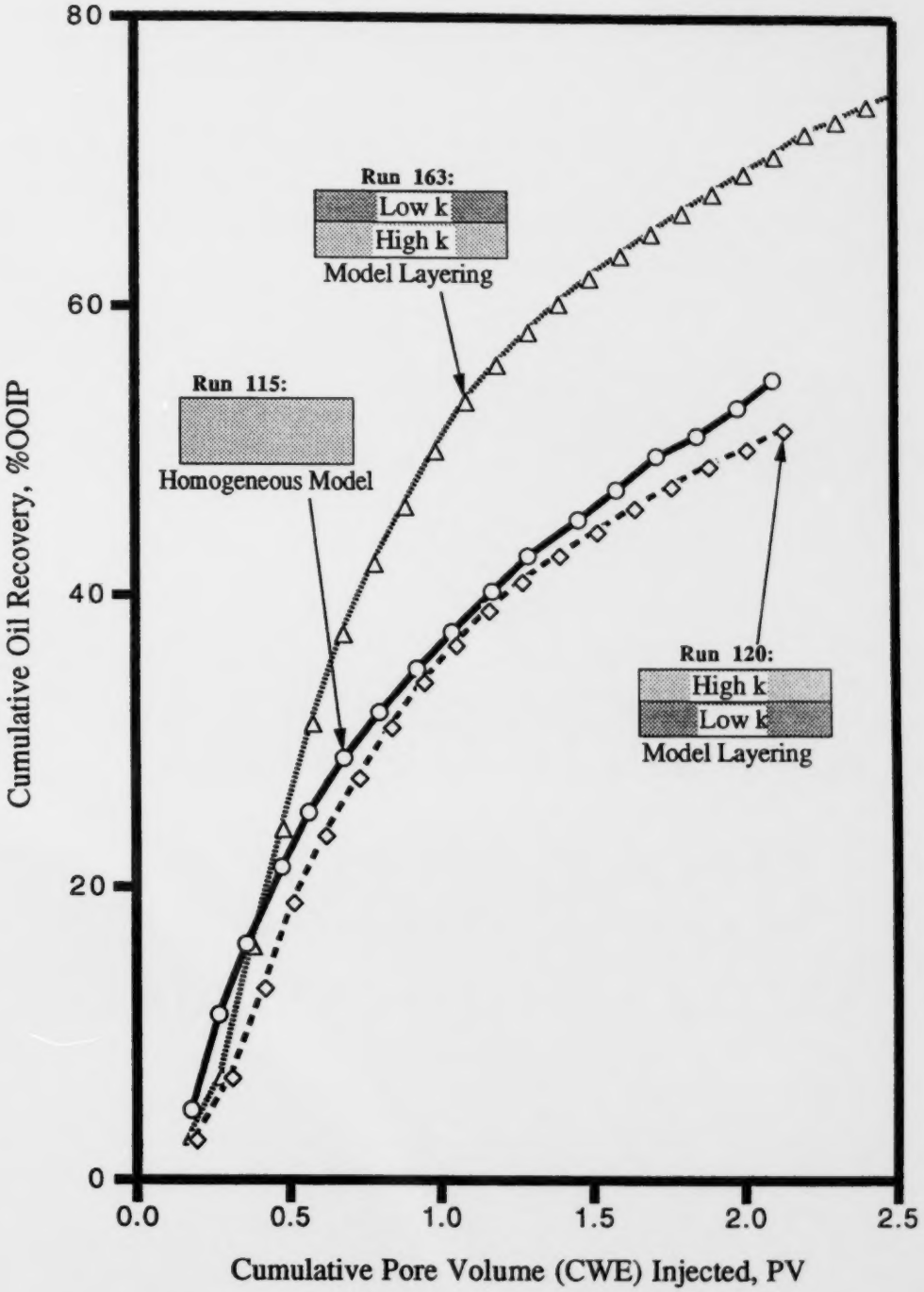

Figure 6.32 — Cumulative Oil Recovery vs. Cumulative PV Injected for a Homogeneous Model (Run 115), an Unfavourably Layered Model (Run 120), and a Favourably Layered Model (Run 163), Vertical Injection and Production Wells.

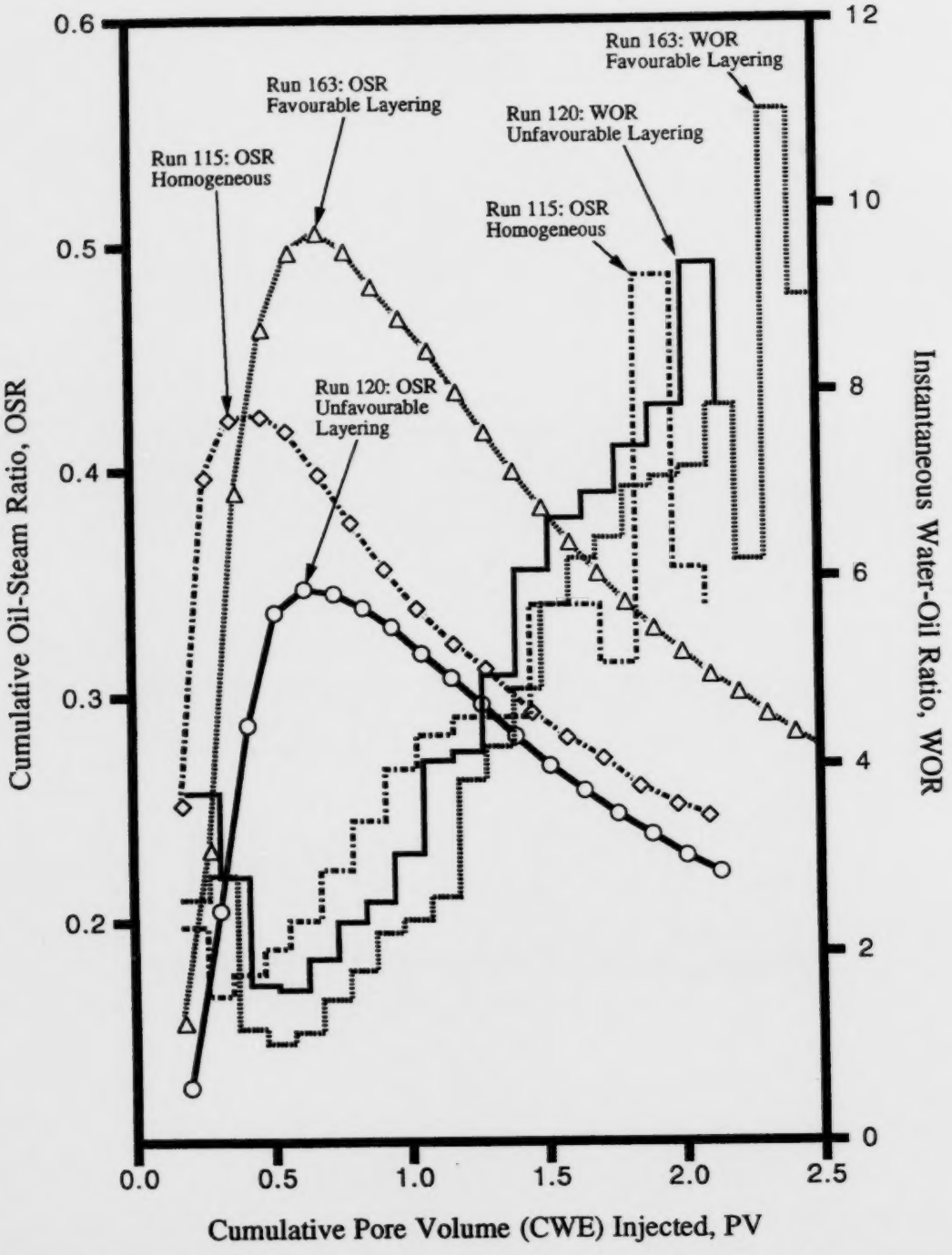

Figure 6.33 — Cumulative OSR and Instantaneous WOR vs. Cumulative PV Injected for: a Homogeneous Model (Run 115), an Unfavourably Layered Model (Run 120) and a Favourably Layered Model (Run 163), Vertical Injection and Production Wells.

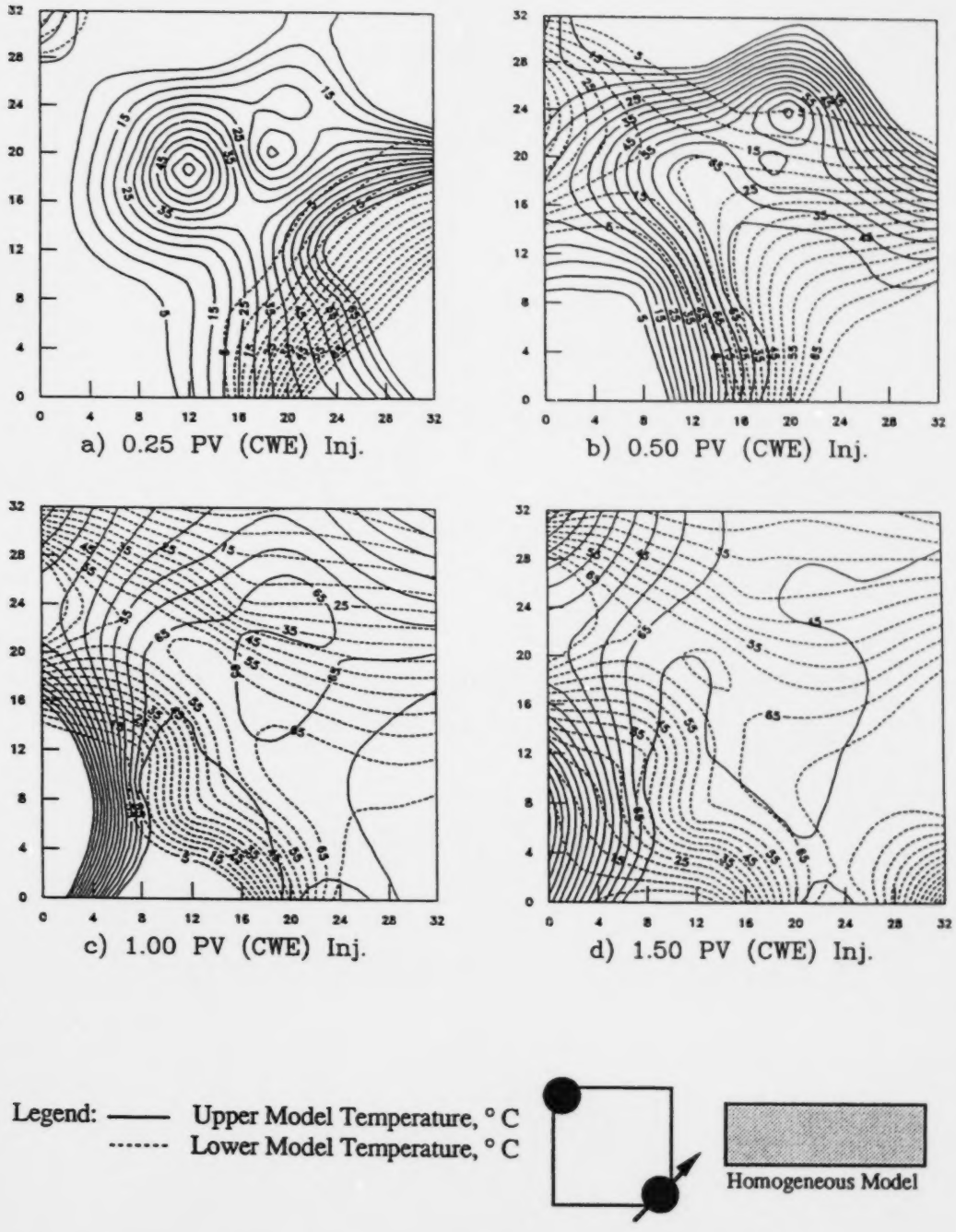
a) 0.25 PV (CWE) Inj.
b) 0.50 PV (CWE) Inj.
c) 1.00 PV (CWE) Inj.
d) 1.50 PV (CWE) Inj.
Legend: —— Upper Model Temperature, ° C
------- Lower Model Temperature, ° C
Homogeneous Model

Figure 6.34 — Plan view, of the temperature distribution inside the model reservoir after the injection of: a) 0.25, b) 0.50, c) 1.00, and d) 1.50 PV CWE of steam, for Run 115: homogeneous model, vertical injection and production wells.

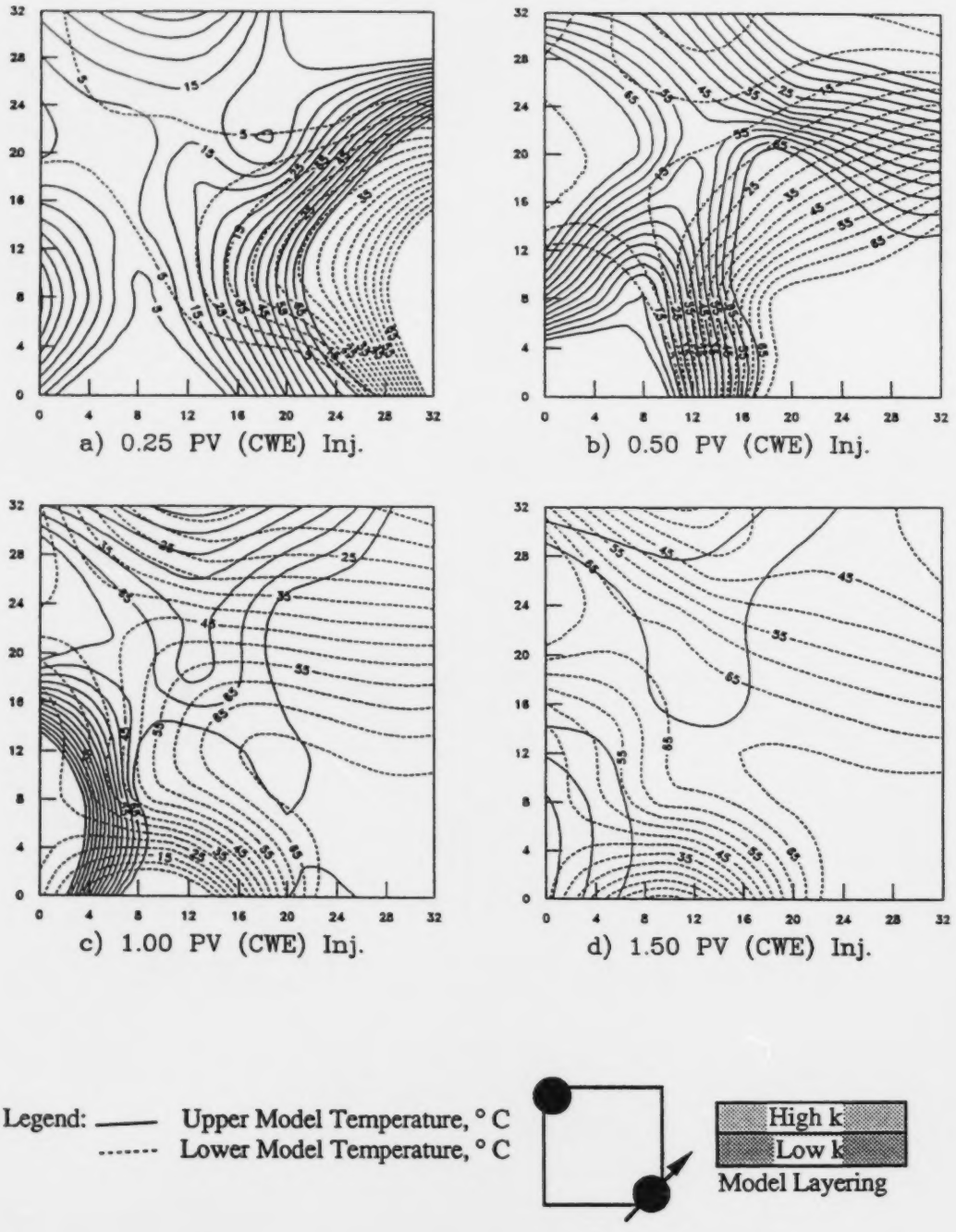
a) 0.25 PV (CWE) Inj.
b) 0.50 PV (CWE) Inj.
c) 1.00 PV (CWE) Inj.
d) 1.50 PV (CWE) Inj.
Legend: —— Upper Model Temperature, ° C
------- Lower Model Temperature, ° C
High k
Low k
Model Layering

Figure 6.35 — Plan view, of the temperature distribution inside the model reservoir after the injection of: a) 0.25, b) 0.50, c) 1.00, and d) 1.50 PV CWE of steam, for Run 120: unfavourably layered model, vertical injection and production wells.

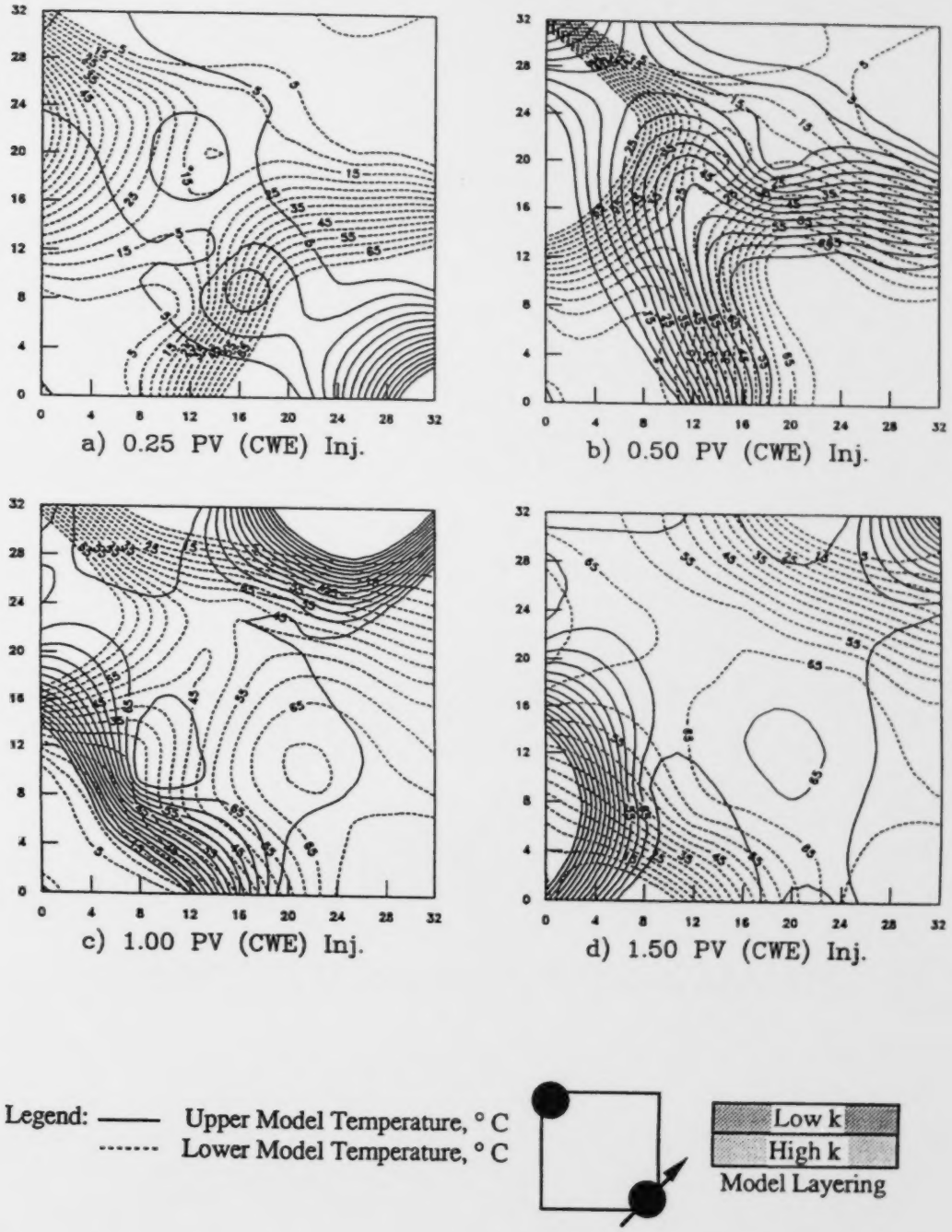
a) 0.25 PV (CWE) Inj.
b) 0.50 PV (CWE) Inj.
c) 1.00 PV (CWE) Inj.
d) 1.50 PV (CWE) Inj.
Legend: —— Upper Model Temperature, ° C
------- Lower Model Temperature, ° C
Low k
High k
Model Layering

Figure 6.36— Plan view, of the temperature distribution inside the model reservoir after the injection of: a) 0.25, b) 0.50, c) 1.00, and d) 1.50 PV CWE of steam, for Run 163: favourably layered model, vertical injection and production wells.

This lower rate slows the stripping-off of the oil at the steam-oil interface, reducing the downward growth of the steam zone.

Figures 6.37, 6.38, and 6.39 display the cross-section plots that correspond to Figures 6.34, 6.35, and 6.36. Figures 6.37 and 6.38 display similar trends with regards to the steam overriding in the early plots. From Figure 6.38 (1.00 and 1.50 PV injected plots) it can be seen that the heated area grows downward near the producer. It is believed that this is caused by the low permeability layer impeding the flow of hot fluids in the lower zone, thereby reducing the sweep and the rate of heating. In Figure 6.39 (0.25 PV injected) the steam zone is only in the lower portion of the model showing how the low permeability layer can suppress the upward growth of the steam zone. Through the subsequent plots the highest temperature area remains in the lower portion of the model for this experiment.

In summary, permeability contrast in the favourable stratification case causes the steam to initially underride the low permeability layer. This sweeps the reservoir in the most favourable way and results in the highest oil recovery. The unfavourable permeability slows the downward growth of the steam zone, thus lowering the recovery rate.

6.6.2 Unfavourable Stratification

Unfavourable stratification is detrimental to the steam injection process. The thrust of this part of the study is to examine possible methods to overcome the resultant poor oil recovery for these cases. The three strategies examined are: the use of a horizontal injection well, a solvent pre-flush in a horizontal injection well, and fracture orientation.

6.6.2.1 Fractured Multi-layered Model

Run 138 involves an unfavourably layered model. It was performed to investigate the effectiveness of a vertical fracture between the injection well and the production well. The fracture is simulated by placing a coarse screen in the low permeability layer at the bottom of the model during the packing process. Run 138 was compared with Run 142. Both of these runs have the same stratification, and the only difference between them is the presence of the fracture in Run 138.

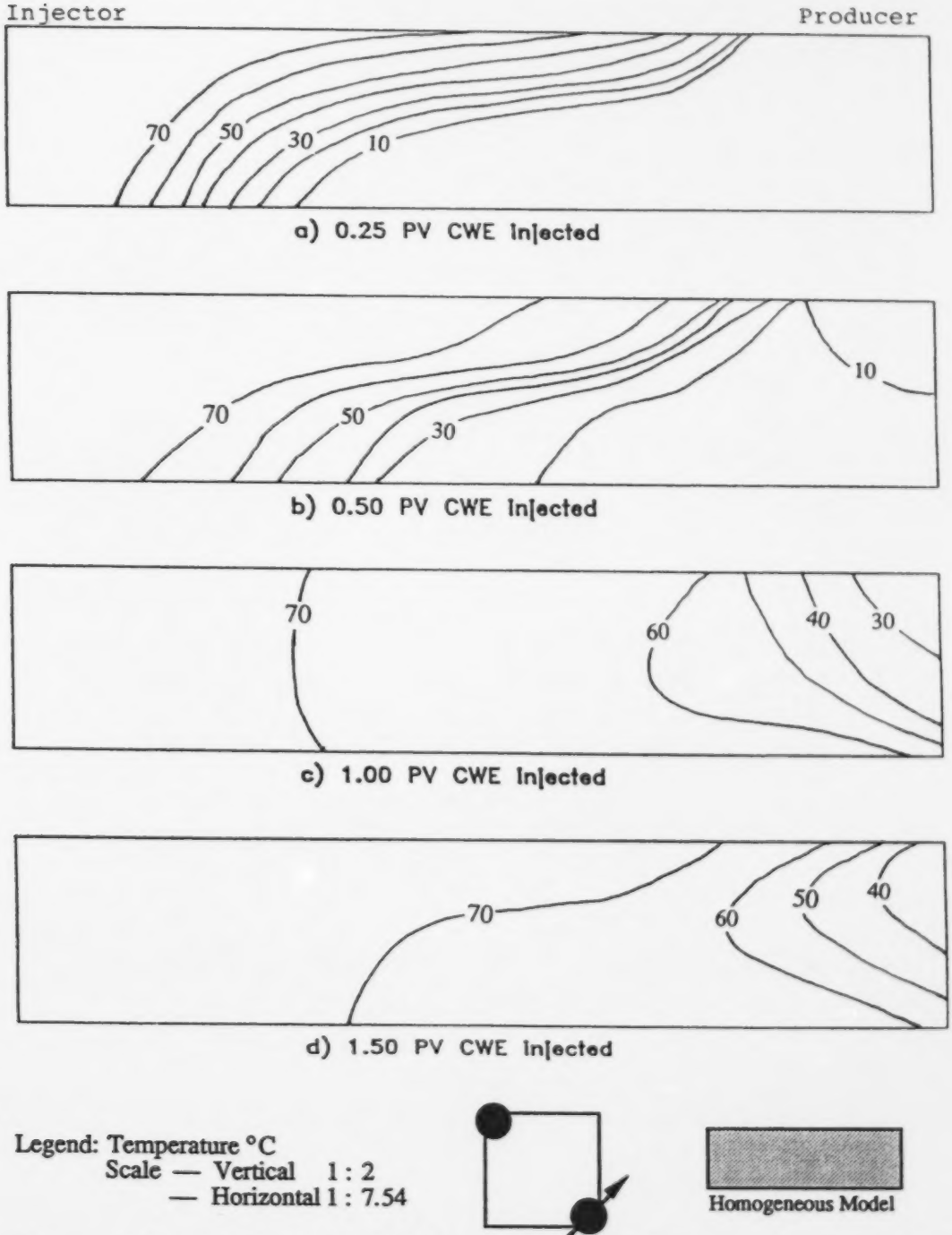

Figure 6.37 — Cross-section of the temperature distribution inside the model reservoir after the injection of: a) 0.25, b) 0.50, c) 1.00, and d) 1.50 PV CWE of steam, for Run 115: homogeneous model, vertical injection and production wells.

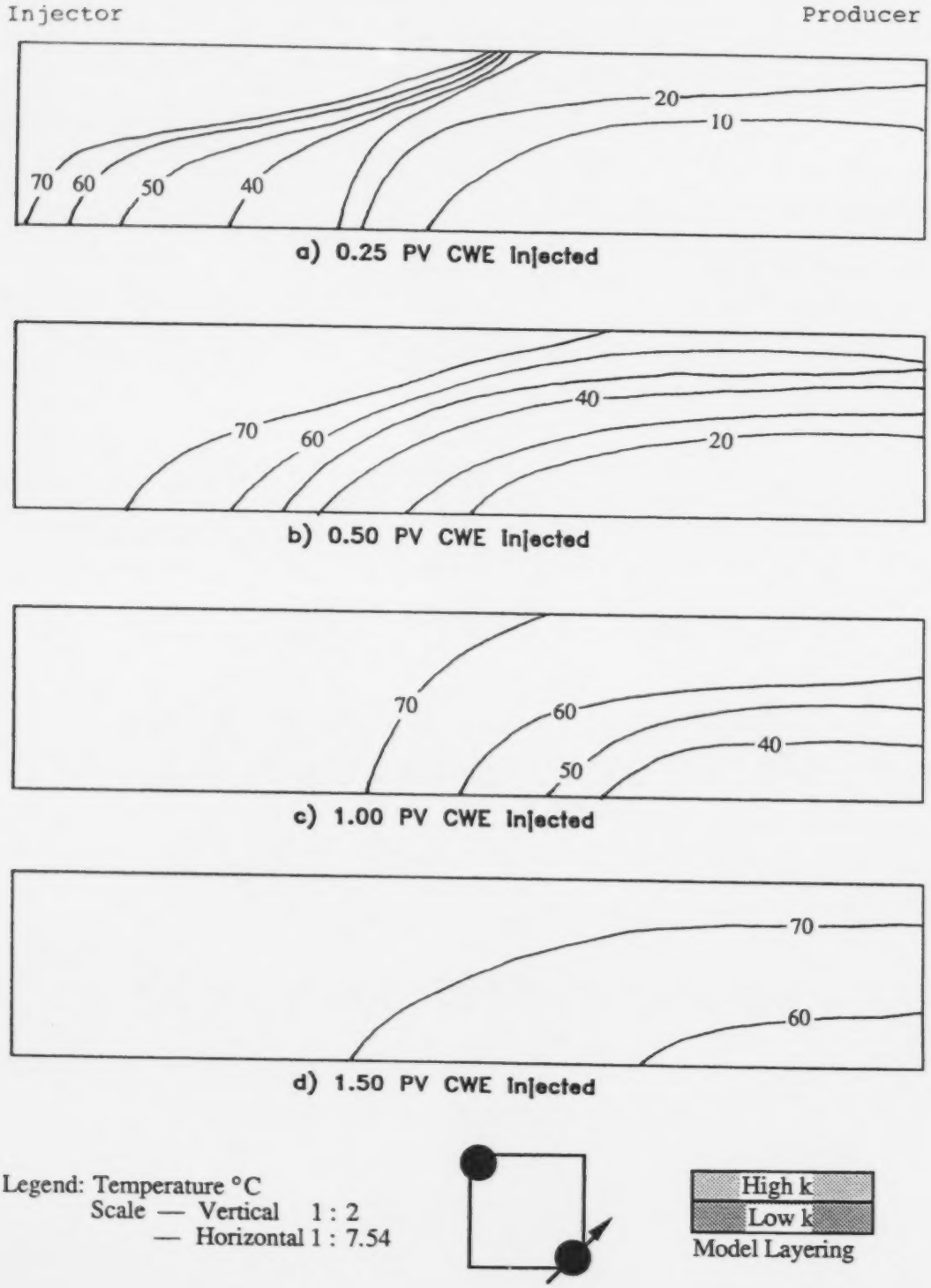

Figure **6.38** — Cross-section of the temperature distribution inside the model reservoir after the injection of: a) 0.25, b) 0.50, c) 1.00, and d) 1.50 PV CWE of steam, for Run 120: unfavourably layered model, vertical injection and production wells.

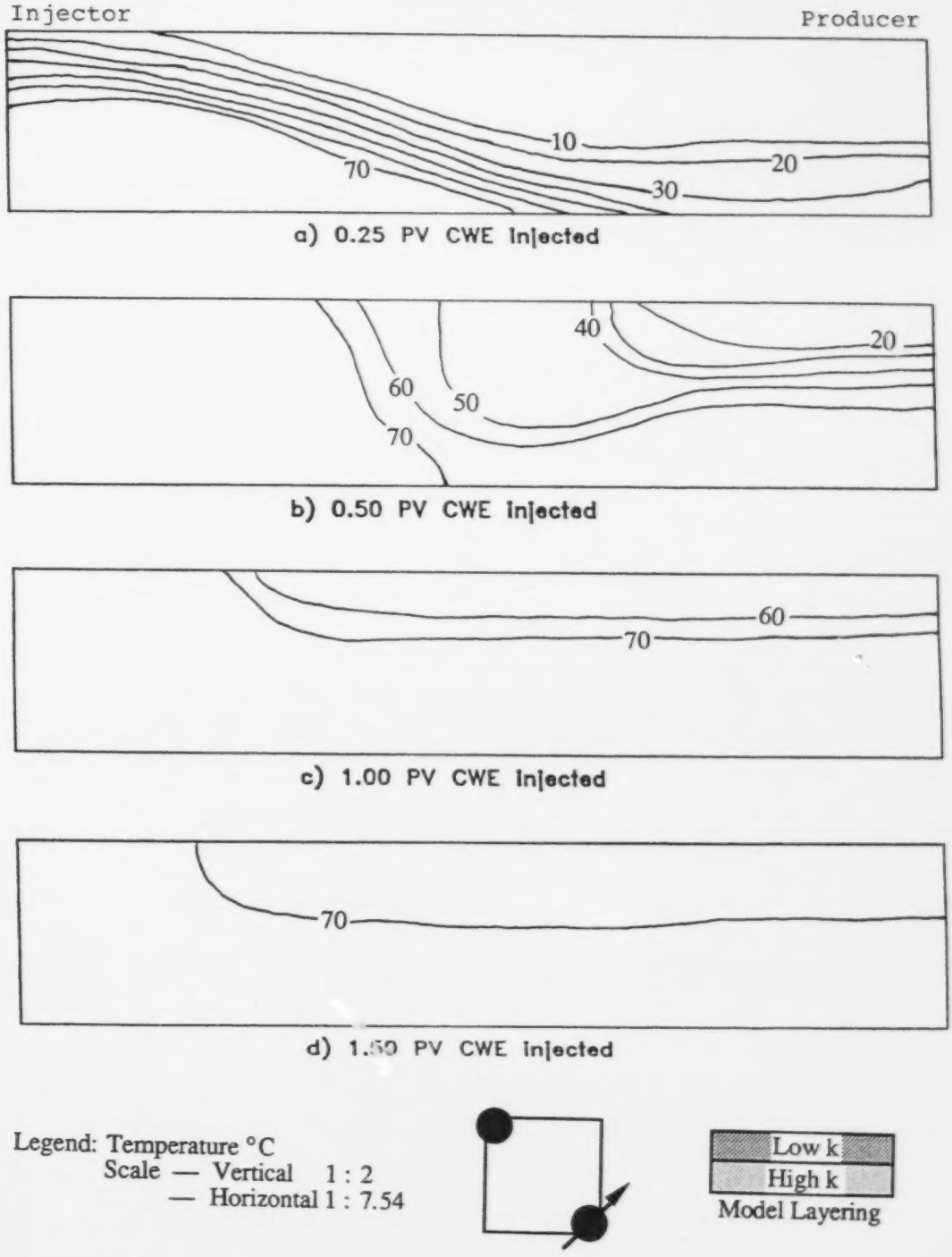

Figure **6.39** — Cross-section of the temperature distribution inside the model reservoir after the injection of: a) 0.25, b) 0.50, c) 1.00, and d) 1.50 PV CWE of steam, for Run 163: favourably layered model, vertical injection and production wells.

It can be seen from Tables D.16 and D.18 that the cumulative oil recoveries at 2.00 PV of steam injected are 48.8% and 48.1 % of the OOIP for Runs 138 and 142, respectively. Figure 6.40 is a comparative plot showing the cumulative recovery curves for Runs 138 and 142. There is very little difference in the recovery curves. Figure 6.41 displays no noticeable difference in the instantaneous OSR for the two experiments.

Figures 6.42 and 6.43 show the temperature contour plots for the two runs. In the case of Run 138 (fracture) there is little evidence of the fracture from the temperature contour plots.

In summary, a fracture in the low permeability lower portion of the model did not improve the cumulative oil recovery. Steam override dominates the recovery process and although the fracture provides a path of low resistance, the density difference still forces the steam up into the top of the model.

6.6.2.2 Horizontal Injection Well in a Multi-layered Model

Two runs were performed with a horizontal injector in an unfavourably layered model. Runs 124 and 126 use a long slotted horizontal injector and a vertical producer. In Run 124, a 0.10 PV solvent pre-flush is injected through the horizontal well to establish greater mobility in the lower layer of the model.

Figure 6.44 compares these two runs with Run 120, which uses a vertical injector and a vertical producer in an unfavourably layered model. From this plot, the solvent run has an almost linear recovery curve, indicating a steady oil production rate. Run 126 initially has a similar recovery curve, but after 1.00 PV of steam injected the oil recovery rate starts to fall below that of Run 124. Run 120 has the highest recovery up to 2.00 PV of steam injected. However, after 2.00 PV of steam injected, the oil recovery rate of Run 124 starts to exceed that of Run 120.

Figure 6.45 displays the cumulative OSR and the instantaneous WOR versus the cumulative PV of steam injected. Because of the solvent injection, the OSR curve for Run 124 does not start at the same point as those for the other two runs. The WOR for Run 124 starts in the range of the other two runs, and similarly continues to increase up to 1.50 PV of steam injected. At 1.50 PV of steam injected, the WOR for Runs 120 and 126 increase rapidly while Run 124 maintains a more gradual increase.

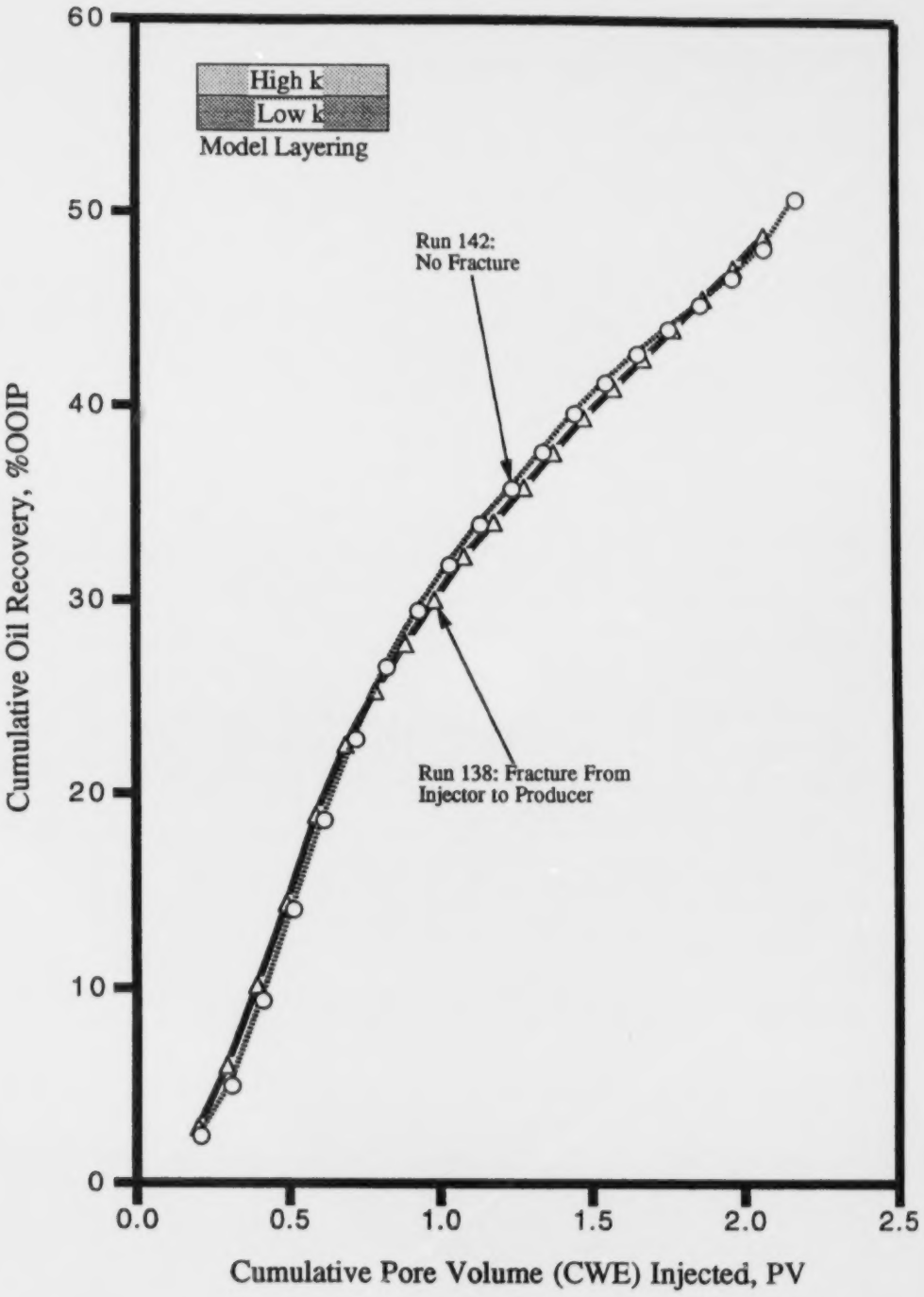

Figure 6.40— Cumulative Oil Recovery vs. Cumulative PV Injected for Unfavourably Layered Models, Fracture Running From Injector to Producer in the Lower Layer (Run 138) vs. No Fracture (Run 142), Vertical Injection and Production Wells.

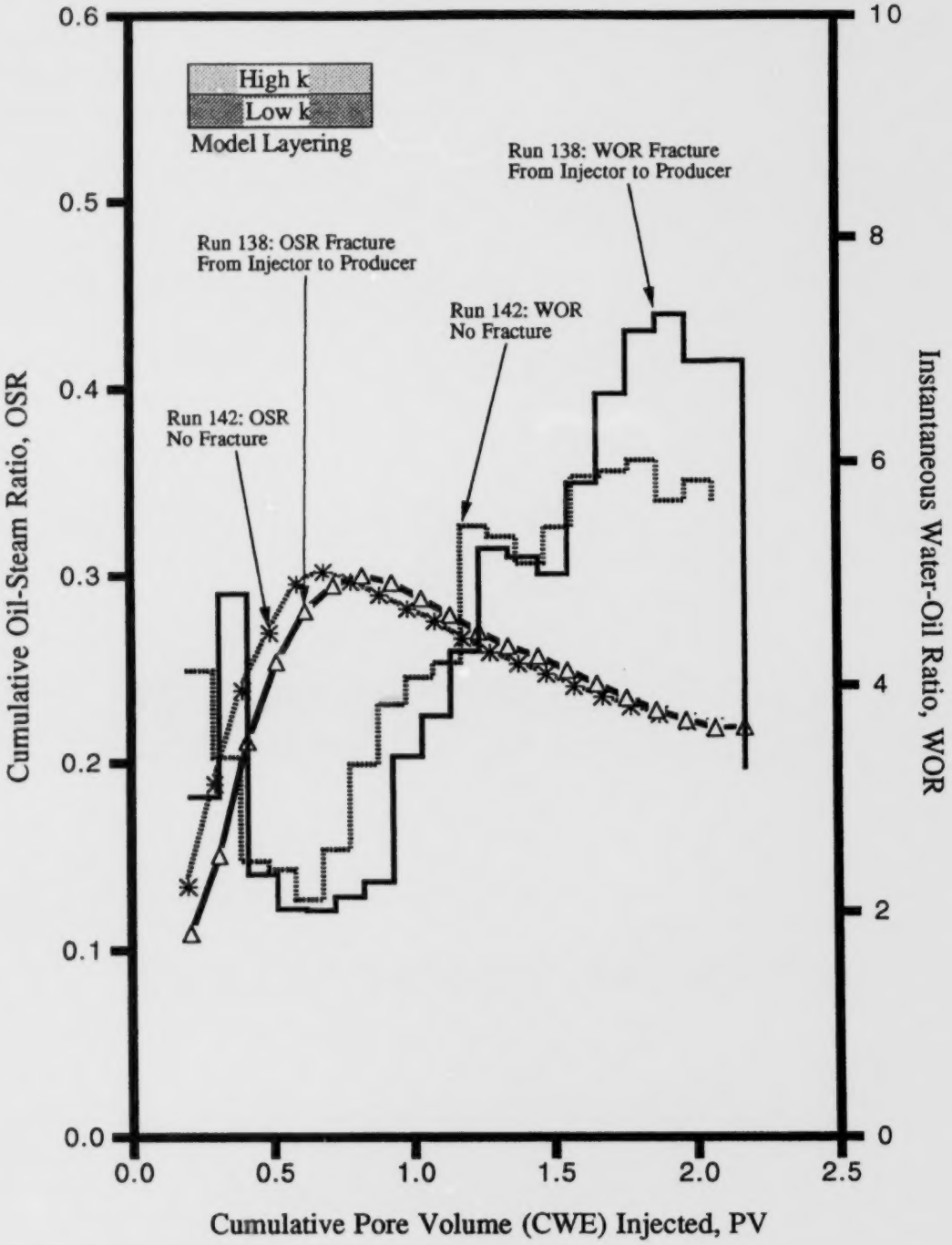

Figure 6.41 — Cumulative OSR and Instantaneous WOR vs. Cumulative PV Injected for Unfavourably Layered Models, Fracture Running From Injector to Producer in the Lower Layer (Run 138) vs. No Fracture (Run 142), Vertical Injection and Production Wells.

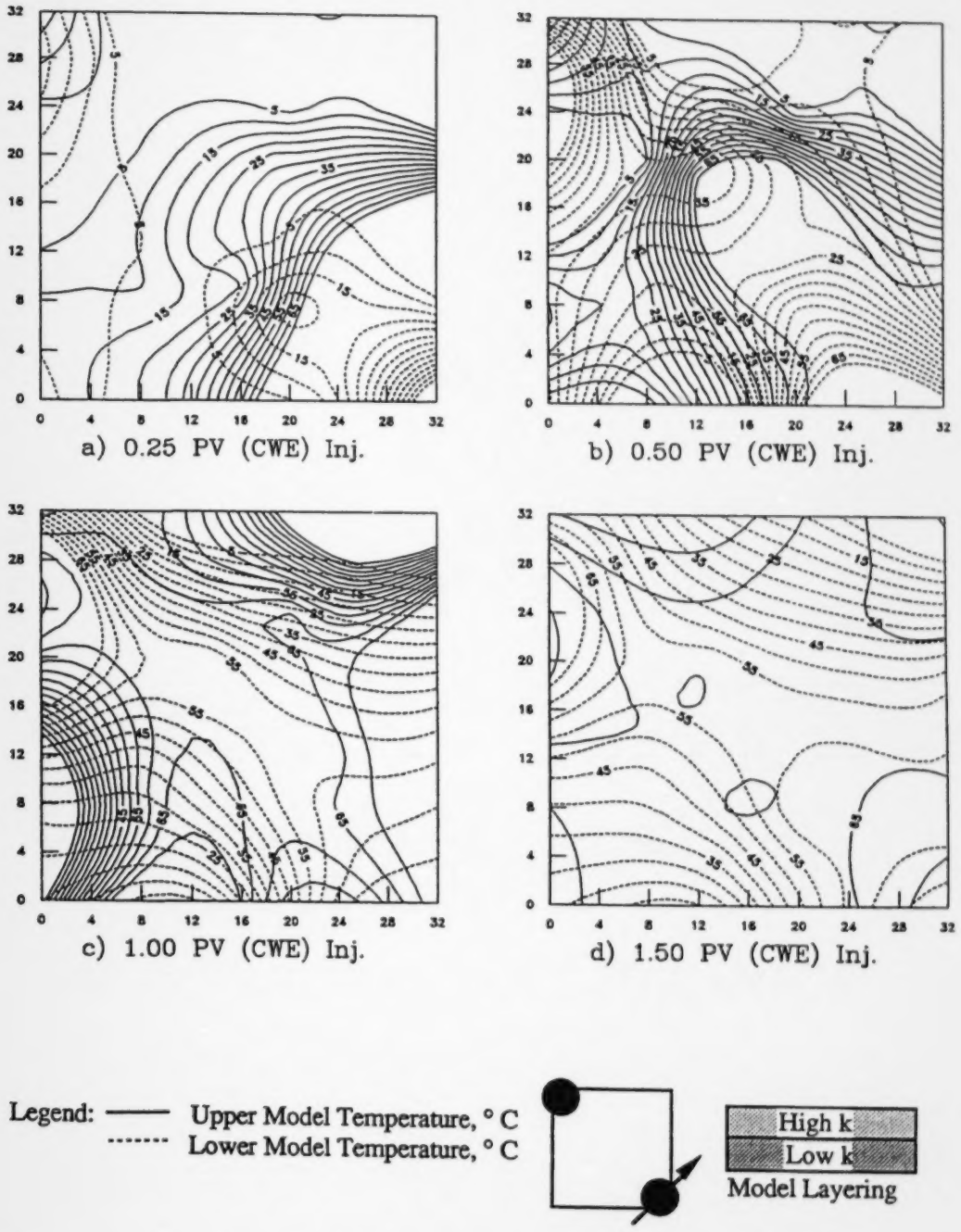

Figure 6.42— Plan view, of the temperature distribution inside the model reservoir after the injection of: a) 0.25, b) 0.50, c) 1.00, and d) 1.50 PV CWE of steam, for Run 138: unfavourably layered model with a fracture running from the injector to the producer in the bottom layer,vertical injection and production wells.

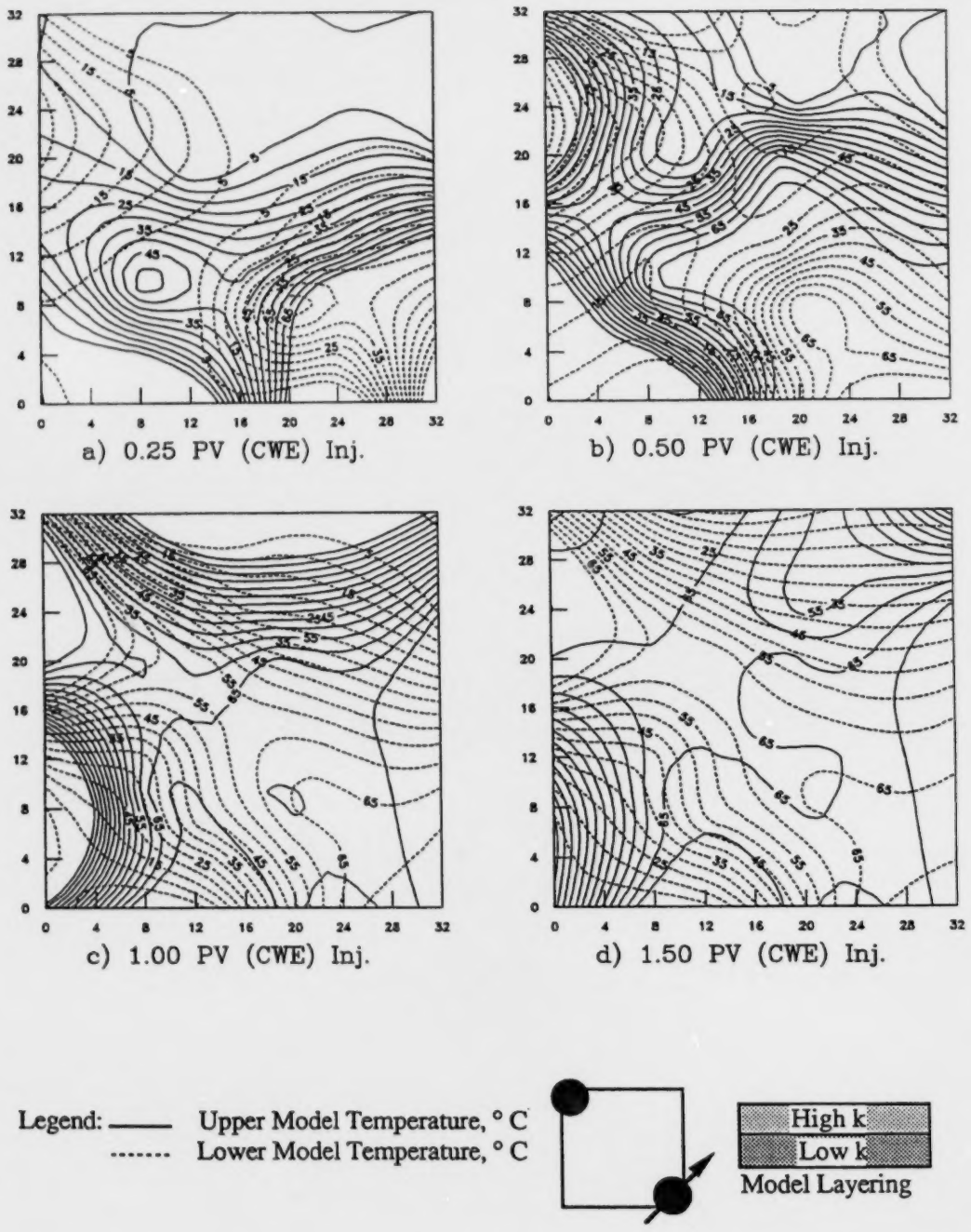
a) 0.25 PV (CWE) Inj.
b) 0.50 PV (CWE) Inj.
c) 1.00 PV (CWE) Inj.
d) 1.50 PV (CWE) Inj.
Legend: —— Upper Model Temperature, ° C
------- Lower Model Temperature, ° C
High k
Low k
Model Layering

Figure 6.43— Plan view, of the temperature distribution inside the model reservoir after the injection of: a) 0.25, b) 0.50, c) 1.00, and d) 1.50 PV CWE of steam, for Run 142: unfavourably layered model, vertical injection and production wells.

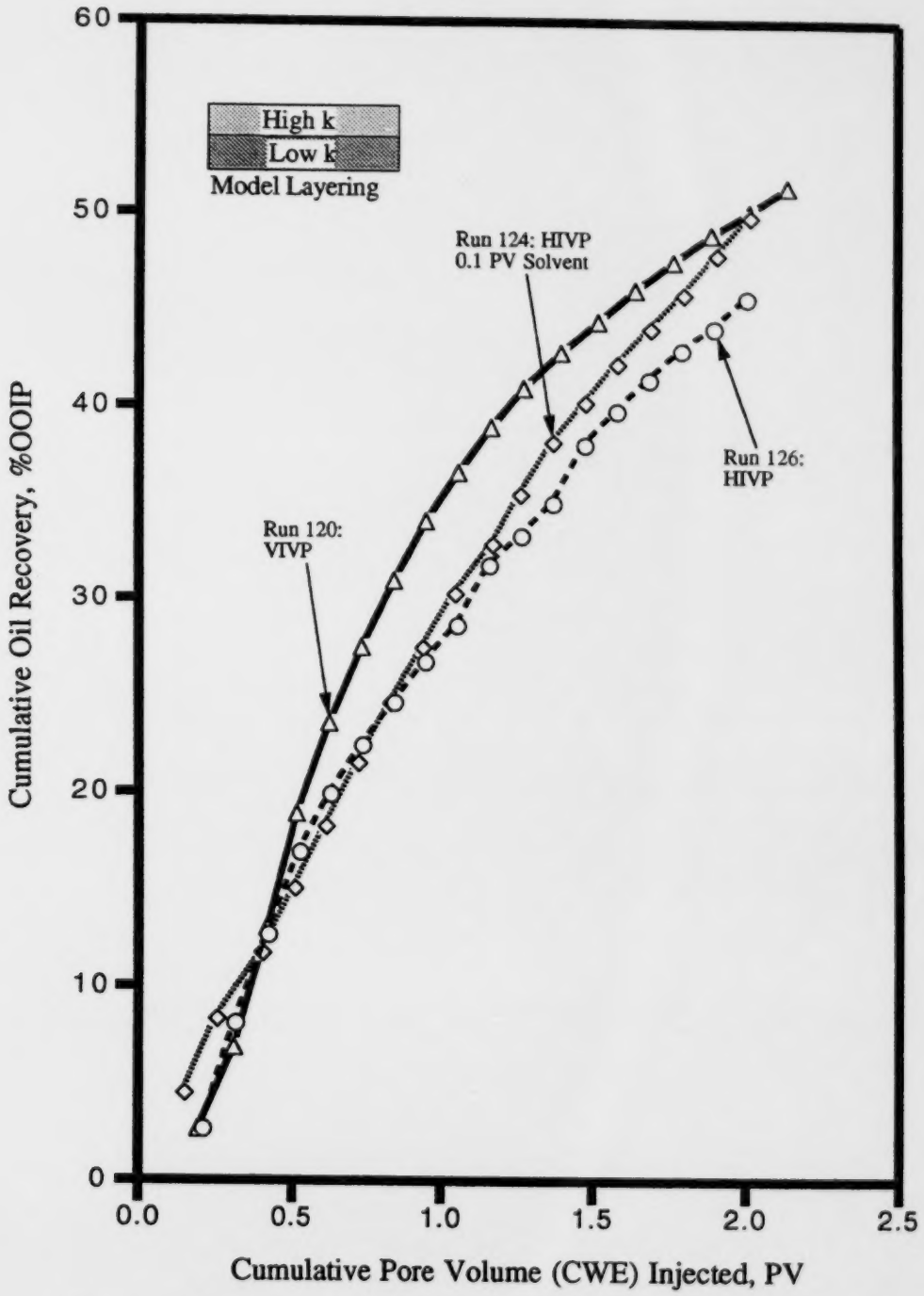

Figure 6.44 — Cumulative Oil Recovery vs. Cumulative PV Injected in Unfavourably Layered Models, Vertical Injector (Run 120), Horizontal Injector with a Solvent Preflush (Run 124) and a Horizontal Injector (Run 126), Vertical Production Wells.

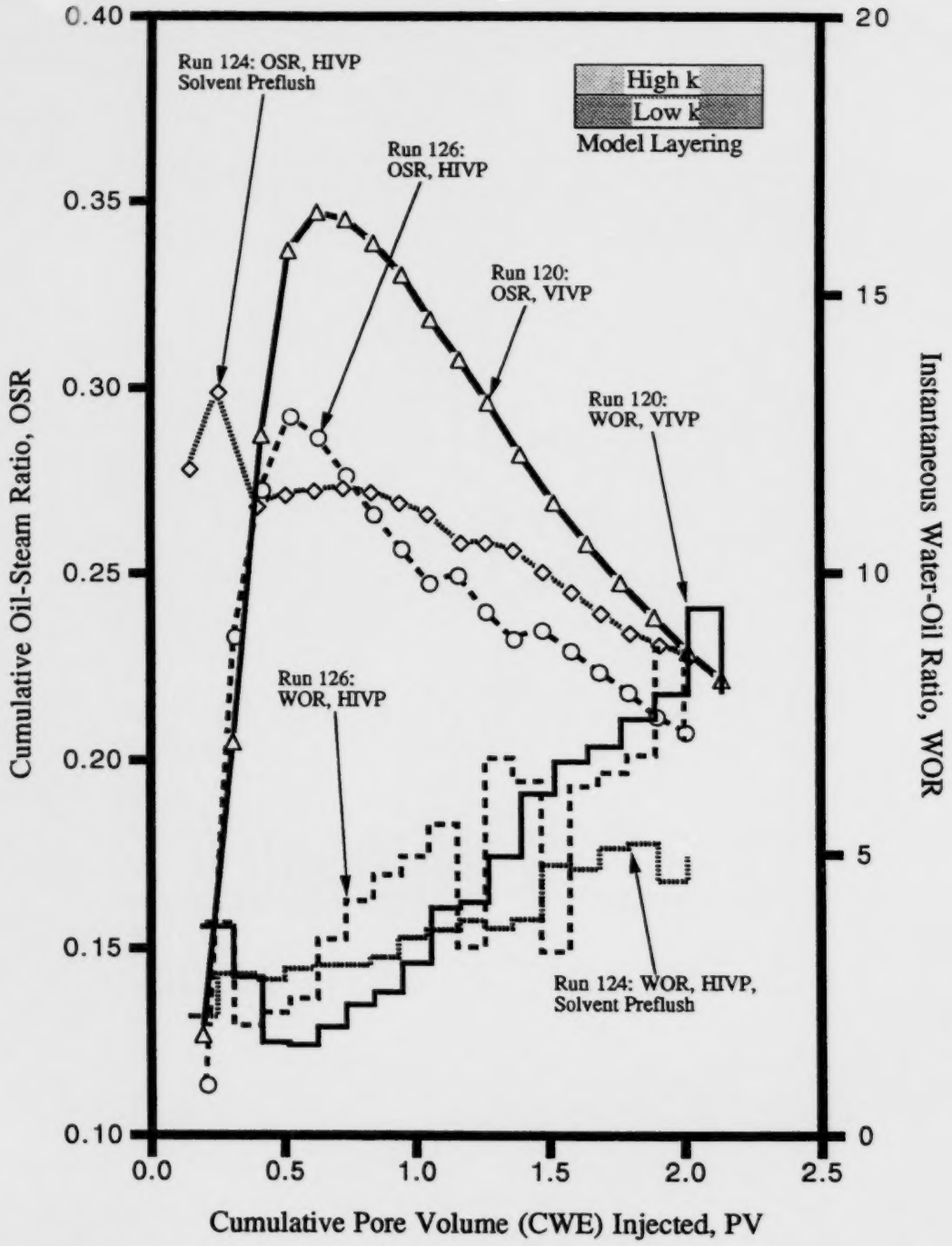

Figure 6.45 – Cumulative OSR and Instantaneous WOR vs. Cumulative PV Injected in Unfavourably Layered Models; Vertical Injector (Run 120), Horizontal Injector with a 0.1 PV Solvent Preflush (Run 124), and a Horizontal Injector (Run 126), Vertical Production Wells.

Figures 6.46, 6.47, and 6.48 display the top view temperature contour plots for the runs. Comparing the three runs at 0.25 PV of steam injected, Run 124 has a substantially smaller heated area. Due to the 0.10 PV solvent slug, Run 124 has less energy injected into the model with the same PV injected. A comparison of the three runs at 1.50 PV shows more of the upper layer is at the steam saturation temperature for Run 120, and steam breakthrough in all three cases. Run 124 has a different contour pattern in the lower portion of the model compared with Run 126. The bottom contours of Run 124 do go very far up the right side of the plot, and instead the contours channel through the middle.

In summary, horizontal wells changed the flow pattern in the model by focusing the sweep in the area representing the shortest distance between the injector and the producer, while leaving the other areas unswept. The horizontal steam injector did not promote earlier oil production, and the cumulative oil recovery was less using a horizontal injector.

6.7 Waterflooding, then Steamflooding Heavy Oil Reservoirs

Waterflooding, then steamflooding a heavy oil reservoir was also investigated in this study. This is of practical interest because of the very low oil recoveries achieved by primary production typically less than 5%, and between 5% and 10% by secondary (waterflood) recovery methods. Four experiments, Runs 114, 127, 128, and 129 are discussed. Run 114 involves a warm waterflood followed by a steamflood in a homogeneous model. The other three runs involve cold waterflooding for varying lengths of time prior to the steamflood.

6.7.1 Warm and Cold Waterfloods

Runs 114 and 127 were performed to examine waterflood recoveries using warm water and initial reservoir temperature water. In Run 114, 1.10 PV of water was injected at 23° C with an enthalpy of 92.23 kJ/kg. Using the scaling criteria in chapter 4 the scaled-up temperature is 93°C. In Run 127, 1.00 PV of water was injected at 3°C with an enthalpy of 21.01 kJ/kg and a scaled-up temperature of 23°C. After the waterflood portion of the run was completed, a steamflood was carried out. The injected enthalpy difference between the two runs, prior to the start of the steamflood, was 1100 kJ.

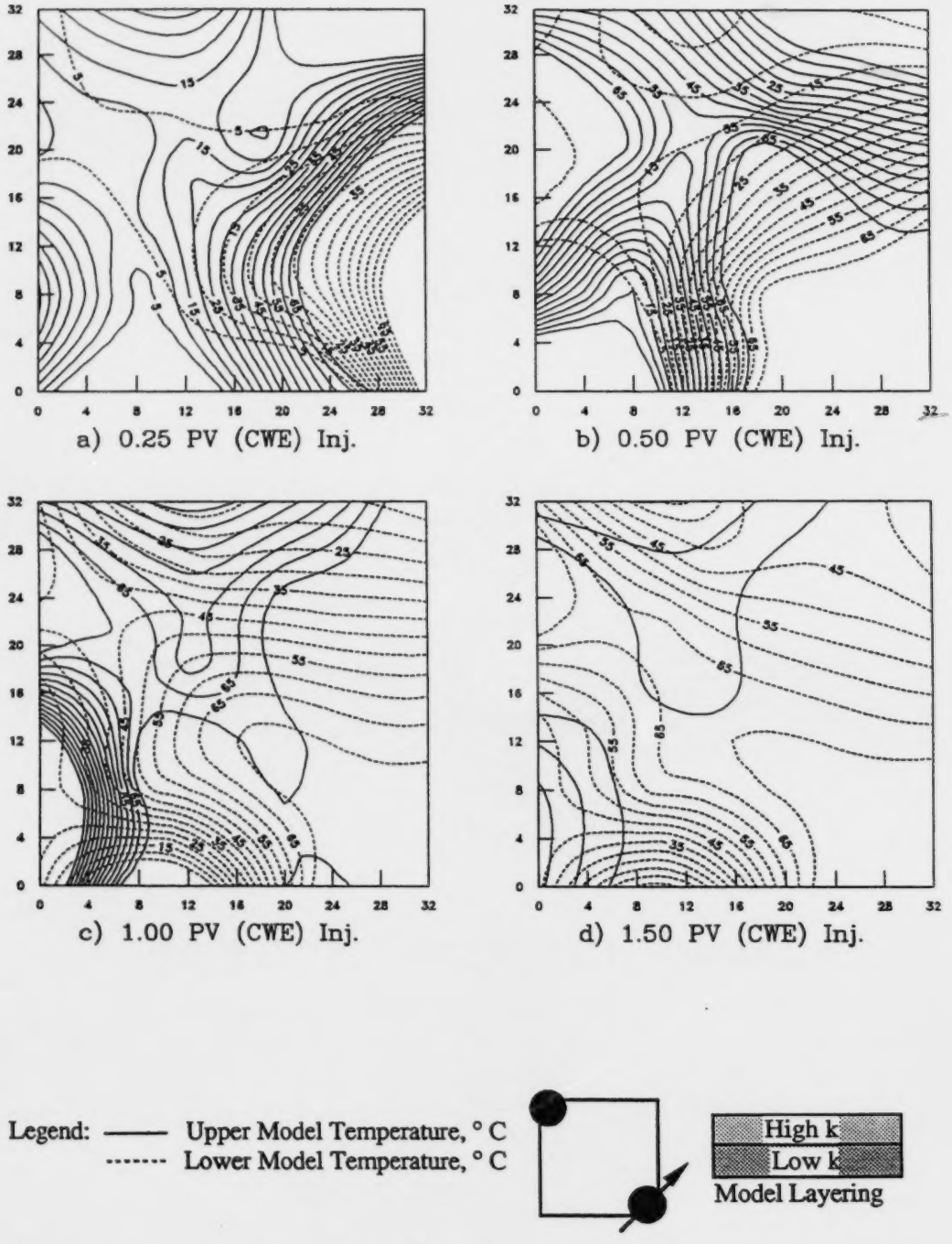
a) 0.25 PV (CWE) Inj.
b) 0.50 PV (CWE) Inj.
c) 1.00 PV (CWE) Inj.
d) 1.50 PV (CWE) Inj.
Legend: —— Upper Model Temperature, ° C
------- Lower Model Temperature, ° C
High k
Low k
Model Layering

Figure 6.46 – Plan view, of the temperature distribution inside the model reservoir after the injection of: a) 0.25, b) 0.50, c) 1.00, and d) 1.50 PV CWE of steam, for Run 120: unfavourably layered model, using vertical injection and production wells.

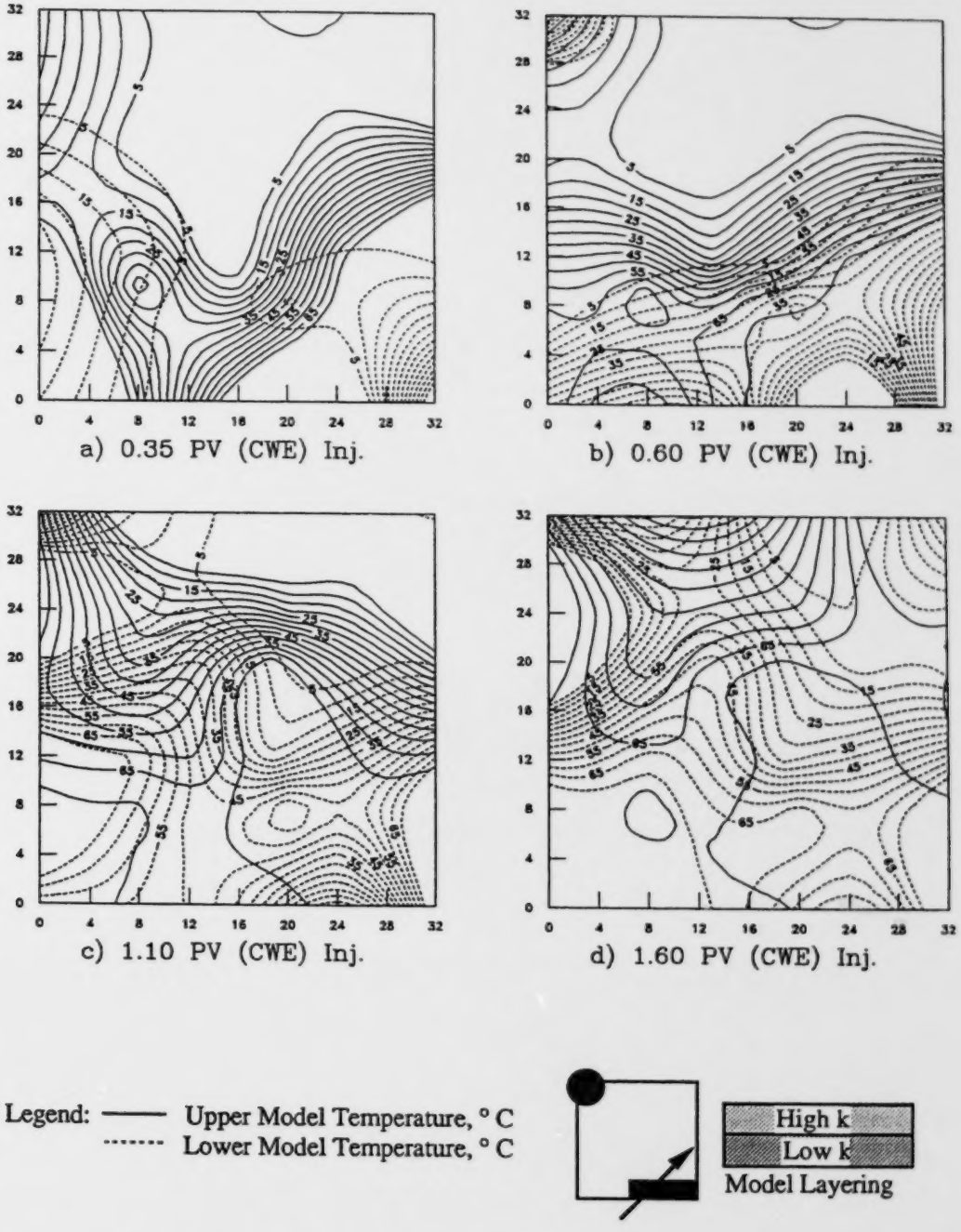
a) 0.35 PV (CWE) Inj.
b) 0.60 PV (CWE) Inj.
c) 1.10 PV (CWE) Inj.
d) 1.60 PV (CWE) Inj.
Legend: —— Upper Model Temperature, ° C
------- Lower Model Temperature, ° C
High k
Low k
Model Layering

Figure 6.47 – Plan view, of the temperature distribution inside the model reservoir after the injection of: a) 0.25, b) 0.50, c) 1.00, and d) 1.50 PV CWE of steam, for Run 124: unfavourably layered model, horizontal injector and a vertical producer, 0.10 PV solvent pre-flush prior to start of the steamflood.

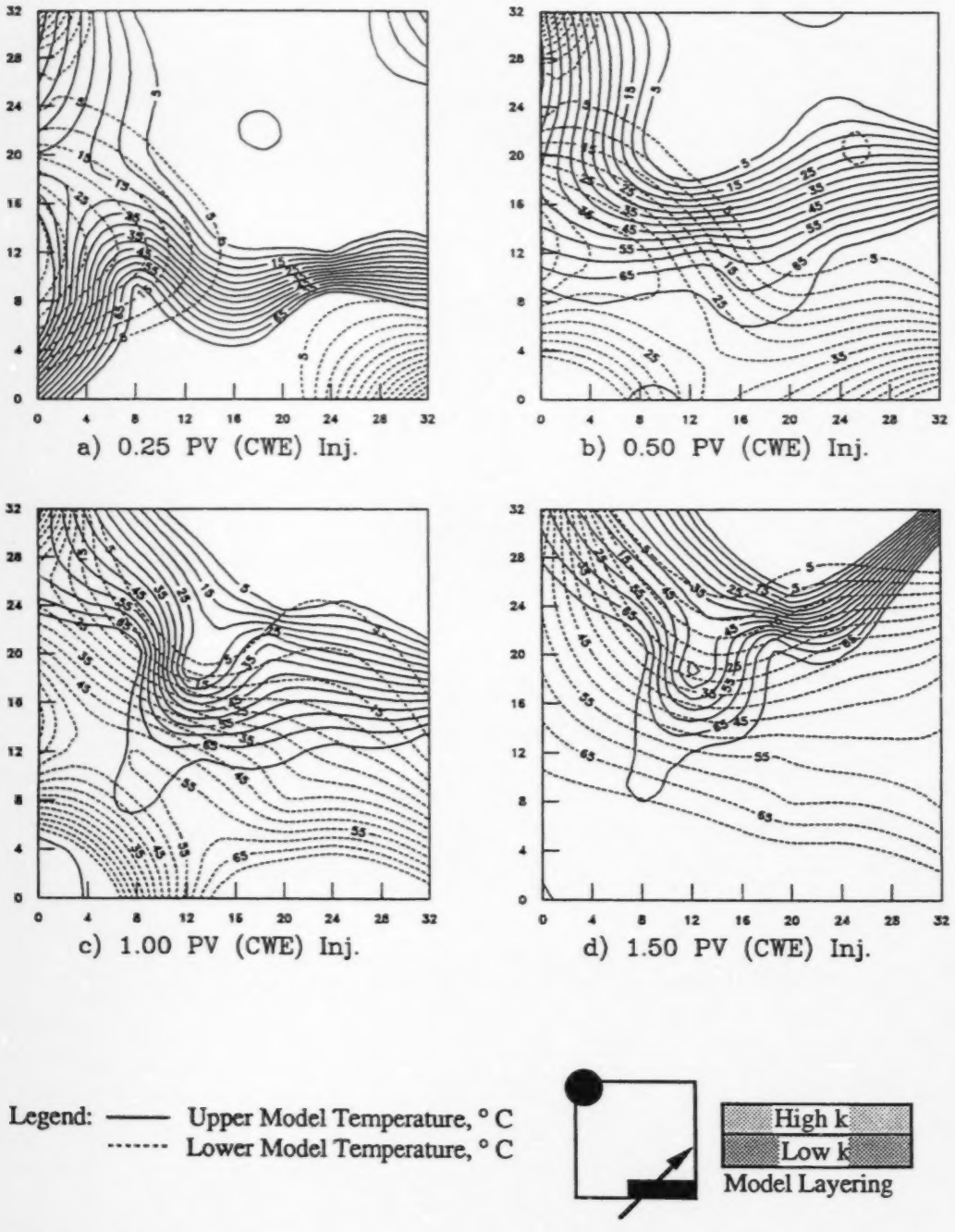
a) 0.25 PV (CWE) Inj.
b) 0.50 PV (CWE) Inj.
c) 1.00 PV (CWE) Inj.
d) 1.50 PV (CWE) Inj.
Legend: —— Upper Model Temperature, ° C
------- Lower Model Temperature, ° C
High k
Low k
Model Layering

Figure 6.48 – Plan view, of the temperature distribution inside the model reservoir after the injection of: a) 0.25, b) 0.50, c) 1.00, and d) 1.50 PV CWE of steam, for Run 126: unfavourably layered model, horizontal injector and a vertical producer.

Figure 6.49 shows the oil recovery curves for these two experiments. Both runs have similar recovery up to 1.35 PV of steam injected. Though the steamflood starts at 1.00 PV of water injected, the recovery rate does not increase until after 0.30 PV of steam injected. After 1.00 PV of water and 1.00 PV of steam injected, Run 114 has the higher oil recovery.

Figures 6.50 and 6.51 show the temperature contour plots for the two runs. At 1.00 PV of water injected, Run 114 has a 10°C channel from the injector to the producer, and Run 127 has the model uniformly at initial model temperature. At 1.50 PV of steam injected, Run 114 has a wider steam channel from the injector to the center of the model than does Run 127. At 2.00 PV CWE injected, Run 114 has most of the upper portion of the model at the steam saturation temperature, while Run 127 has only a wide saturation temperature channel going from the injector to the producer.

In summary, it appears that the effect of injecting water with four times the enthalpy content does not greatly affect the recovery performance.

6.7.2 Optimal Waterflood Duration Prior to Steamflooding

Runs 127, 128, and 129 involved the injection of reservoir temperature water for different periods (1.00 PV, 0.60 PV, and 1.60 PV of water injected, respectively). These runs were followed by a steamflood. The waterflood/steamflood recoveries were compared with the steamflood recovery of Run 115.

Figure 6.52 shows the oil recovery profiles for these four runs. During the waterflood portions of the experiments all the curves are very similar. Because of the delay in starting the steamflood after the waterflood the curves are offset, but their slopes are very similar. The rate of oil recovery in the steamflood portion of the runs is greater than that of the steamflood run. After the injection of 1.00 PV of steam the recoveries are: 37.4, 44, 46, and 52% for Runs 115, 127, 128, and 129, respectively. In Run 129, 1.00 PV more water is injected resulting in the incremental recovery of 4% more of the OOIP. After the injection of 2.00 PV, Run 128 has recovered more of the OOIP than the steamflood (Run 115), but at a significantly lower energy investment.

In summary, waterflooding prior to steamflooding can reduce the energy investment for similar oil recovery performance. The length of the waterflood has some effect on the ultimate oil recovery.

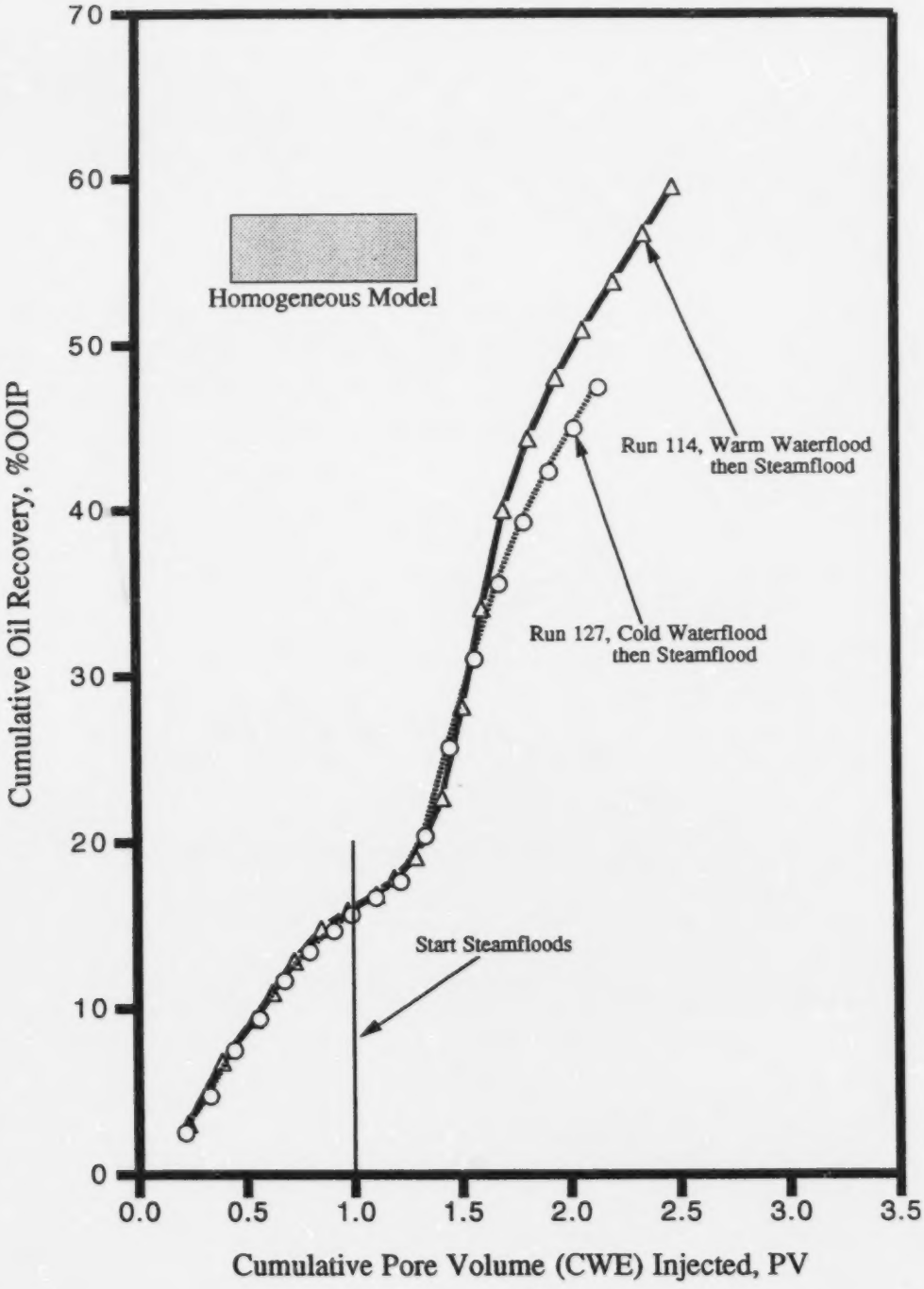

Figure 6.49 – Cumulative Oil Recovery vs. Cumulative PV Injected for Waterflooding Experiments in Homogeneous Models. Cold Waterflood (Run 127) vs. Warm Waterflood (Run 114) Prior to Steamflooding, Vertical Injection and Production Wells.

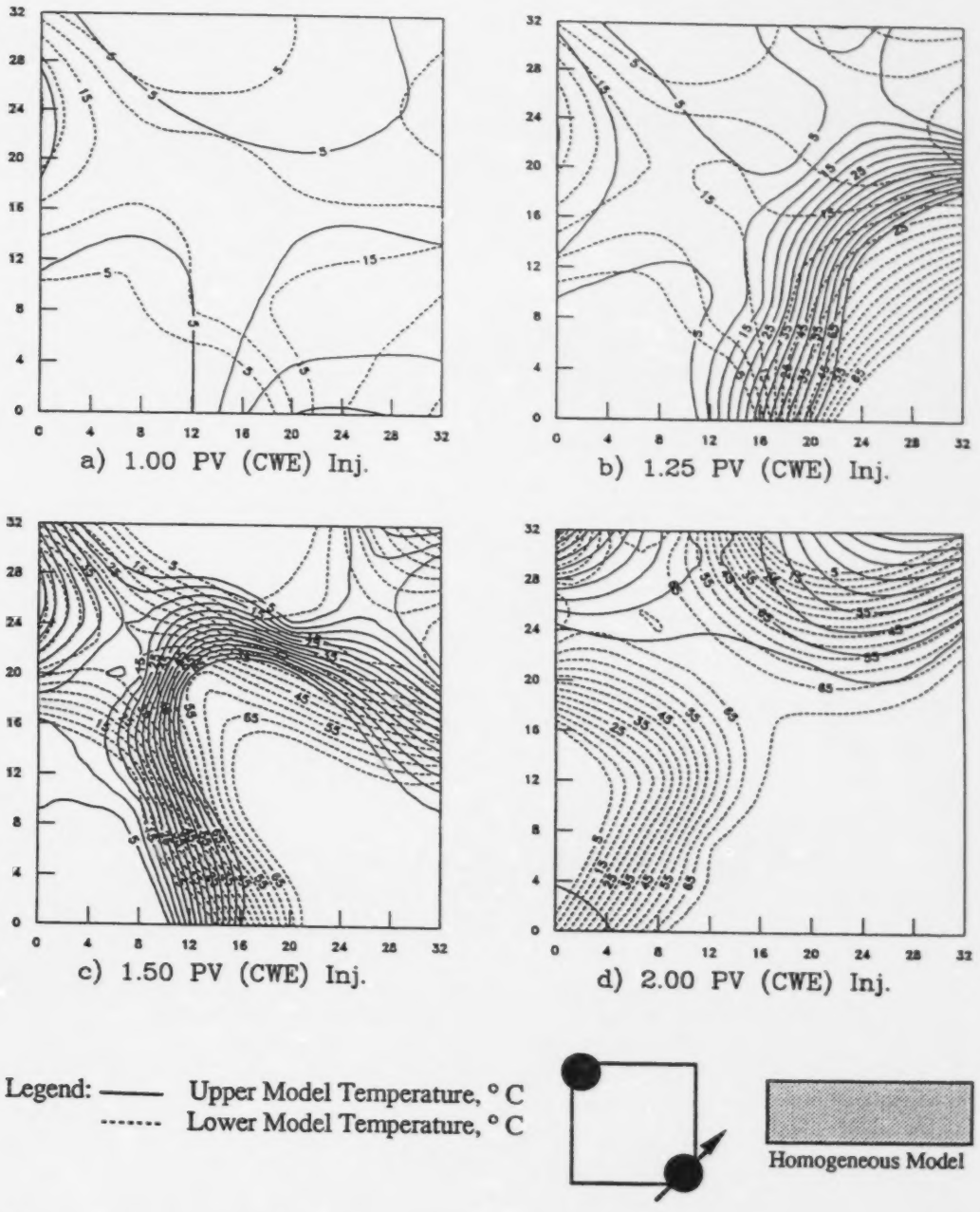
a) 1.00 PV (CWE) Inj.
b) 1.25 PV (CWE) Inj.
c) 1.50 PV (CWE) Inj.
d) 2.00 PV (CWE) Inj.
Legend: —— Upper Model Temperature, ° C
------- Lower Model Temperature, ° C
Homogeneous Model

Figure 6.50— Plan view, of the temperature distribution inside the model reservoir after the injection of: a) 1.00, b) 1.25, c) 1.50, and d) 2.00 PV CWE of steam, for Run 114: homogeneous model, warm waterflood prior to steamflooding, vertical injection and production wells

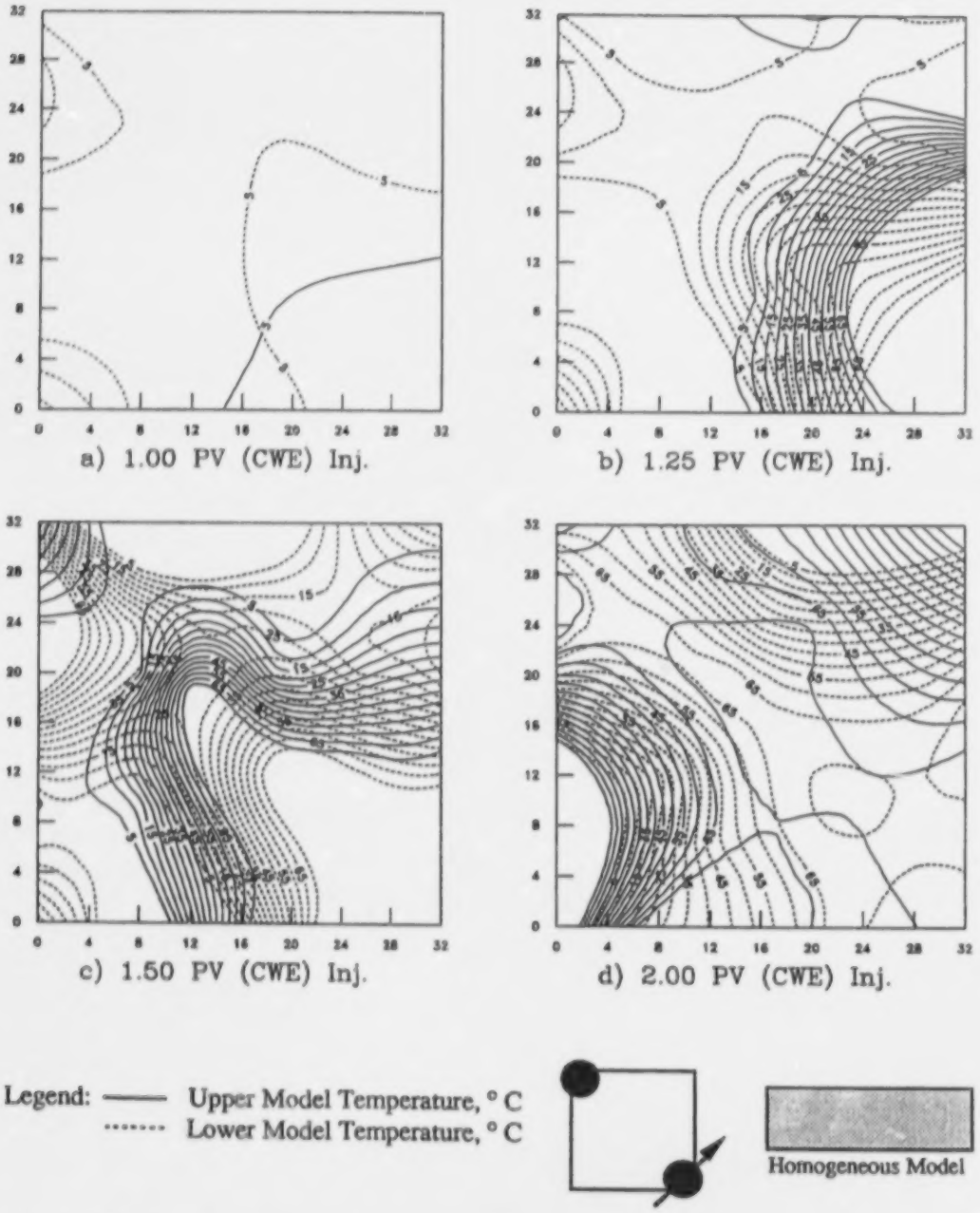
a) 1.00 PV (CWE) Inj.
b) 1.25 PV (CWE) Inj.
c) 1.50 PV (CWE) Inj.
d) 2.00 PV (CWE) Inj.
Legend: —— Upper Model Temperature, ° C
····· Lower Model Temperature, ° C
Homogeneous Model

Figure 6.51 — Plan view, of the temperature distribution inside the model reservoir after the injection of: a) 1.00, b) 1.25, c) 1.50, and d) 2.00 PV CWE of steam, for Run 127: homogeneous model, warm waterflood prior to steamflooding, vertical injection and production wells.

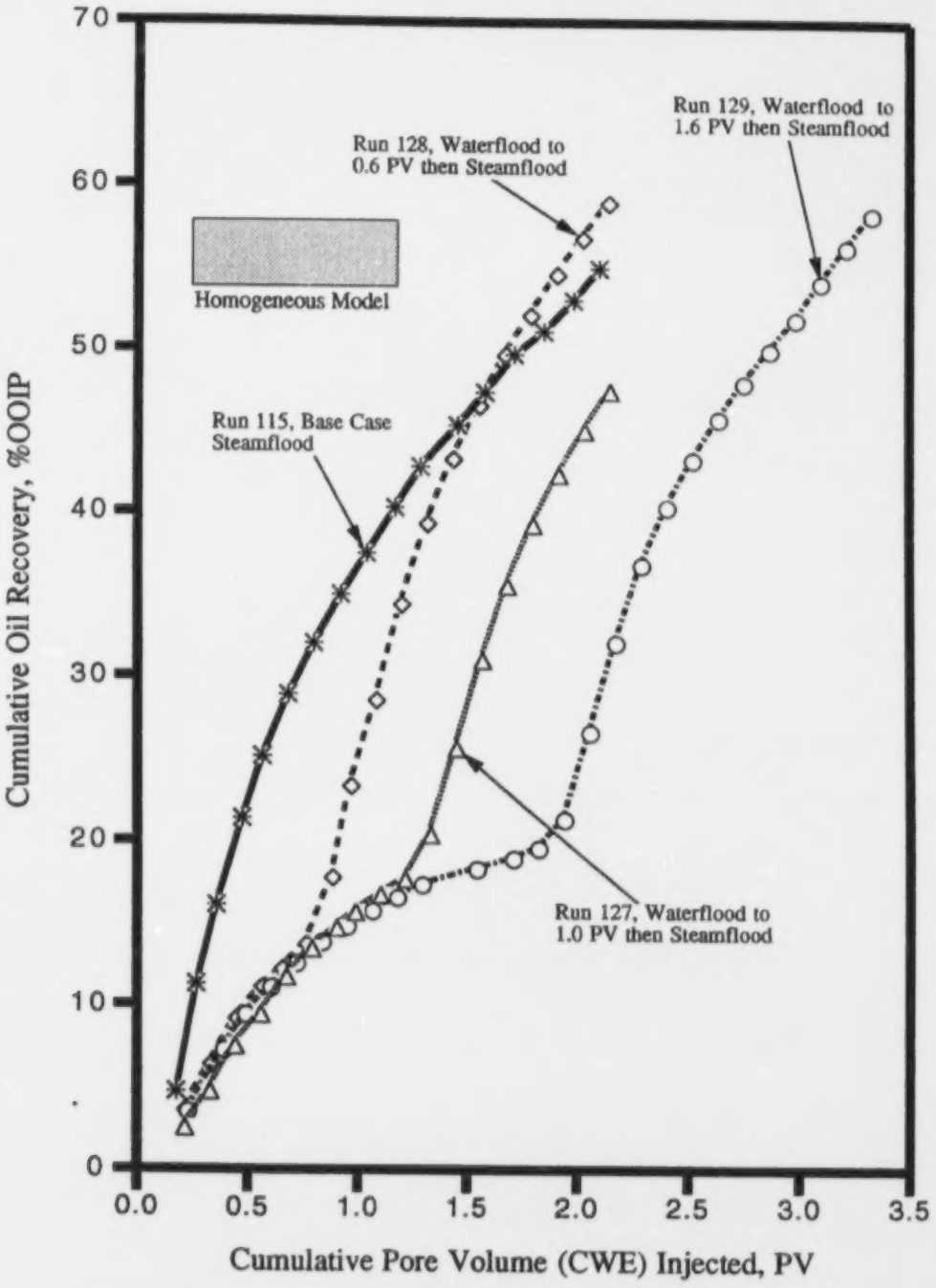

Figure **6.52** – Cumulative Oil Recovery vs. Cumulative PV Injected for Waterflooding Prior to Steamflooding Experiments and a Steamflood (Run 115), all in Homogeneous Models. Waterflood for 0.60 PV (Run 128), 1.00 PV (Run 128), and 1.6 PV (Run 128) Injected, Vertical Injection and Production Wells.

6.8 Heat Scavenging

Currently, some mature steamflood projects are at or near their economic limit. A large amount of the energy invested to recover the oil from the reservoir is accumulated in the heated overburden, underburden, and the reservoir matrix. This series of experiments examines the possibility of using the residual steamflood energy to recover some oil incremental oil. These experiments used vertical wells at the injection and production ends of the model. They consisted of gas injection after a steamflood, waterflooding after a steamflood, and injecting a water slug during a steamflood.

6.8.1 Gas Injection After a Steamflood

Run 140 involved the injection of 2.00 PV of steam. The steamflood was then stopped, and nitrogen gas was injected to scavenge the residual heat. It can be seen from Table D17 that the net oil recovery was 49.5% of the OOIP, while the recovery from the steamflood was 46.4% of the OOIP. The incremental oil recovery from the injection of approximately 20.0 PV of nitrogen gas was only 3.1% of the OOIP.

Figure 6.53 (2.00 PV of steam injected) indicates that prior to gas injection there was a heated channel extending from the injector to the producer which, along with the high mobility of the injected gas and the very high permeability of the glass bead pack, promoted almost instantaneous breakthrough of nitrogen gas to the producer. This immediate breakthrough of nitrogen gas resulted in poor sweep and very little incremental recovery. Figure 6.54 displays an inflection point at the start of the nitrogen gas injection (2.00 PV steam injected), which signifies a decrease in the slope of the cumulative oil recovery curve.

6.8.2 Waterflooding a Steamflooded Reservoir

Usually, after a steamflood there is substantial heat in the reservoir and there are steamed channels in the reservoir that form preferential flow paths. Injecting water into such a reservoir will collapse the steam zone and heat the injected water. This heated water will move to unswept high oil saturation areas in the reservoir. This group of experiments was undertaken to look at steamflooding a reservoir for a period of time and then injecting water so that the hot swept zone will heat the injected water and thereby re-use the heat to produce incremental oil. Three runs were performed with this strategy: Runs 109, 110, and 111.

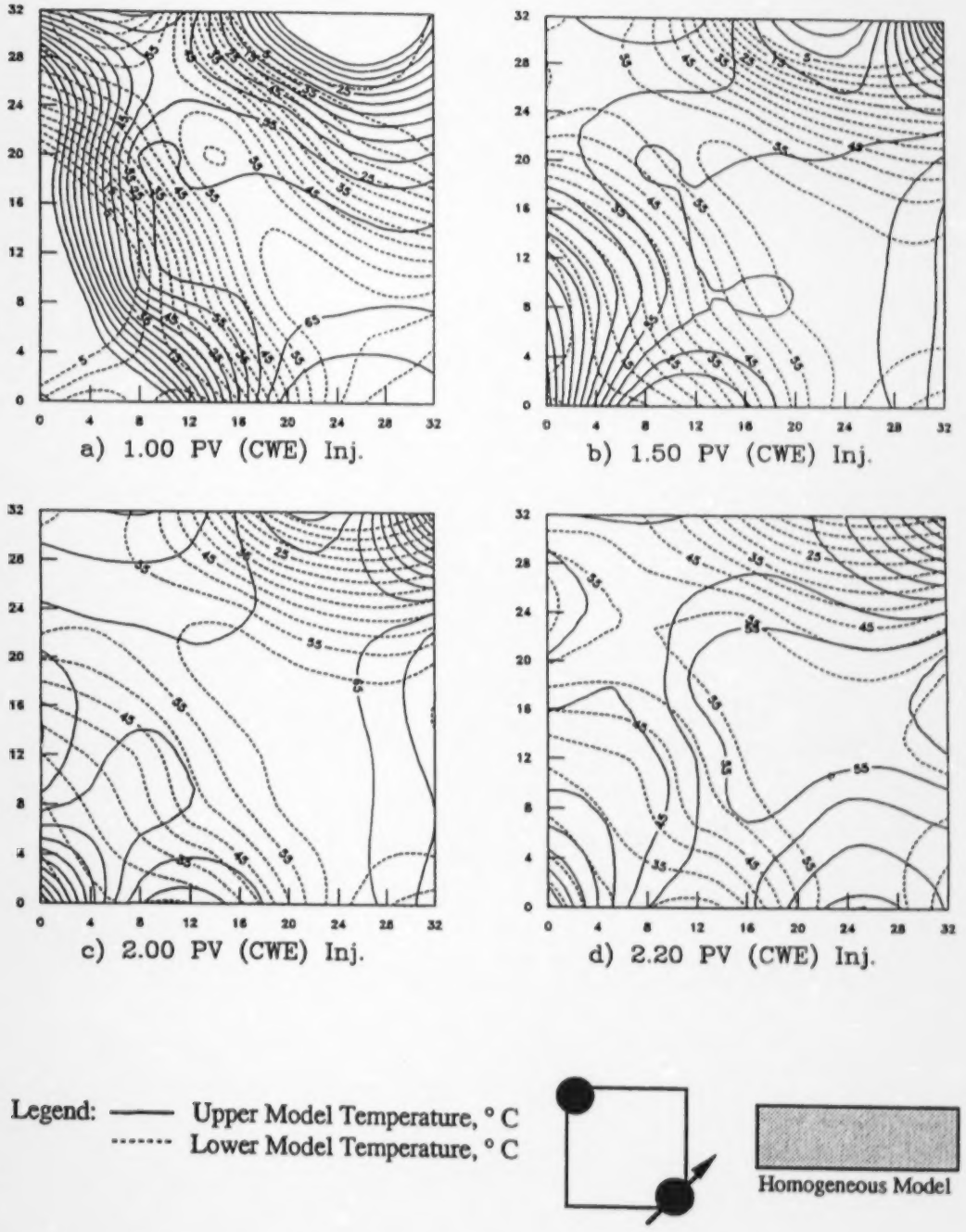
a) 1.00 PV (CWE) Inj.
b) 1.50 PV (CWE) Inj.
c) 2.00 PV (CWE) Inj.
d) 2.20 PV (CWE) Inj.
Legend: —— Upper Model Temperature, ° C
------- Lower Model Temperature, ° C
Homogeneous Model

Figure 6.53 – Plan view, of the temperature distribution inside the model reservoir after the injection of: a) 1.00, b) 1.50, c) 2.00, and d) 2.20 PV CWE of steam, for Run 140: homogeneous model, gasflood subsequent to 2.00 PV steamflood, vertical injection, and production wells.

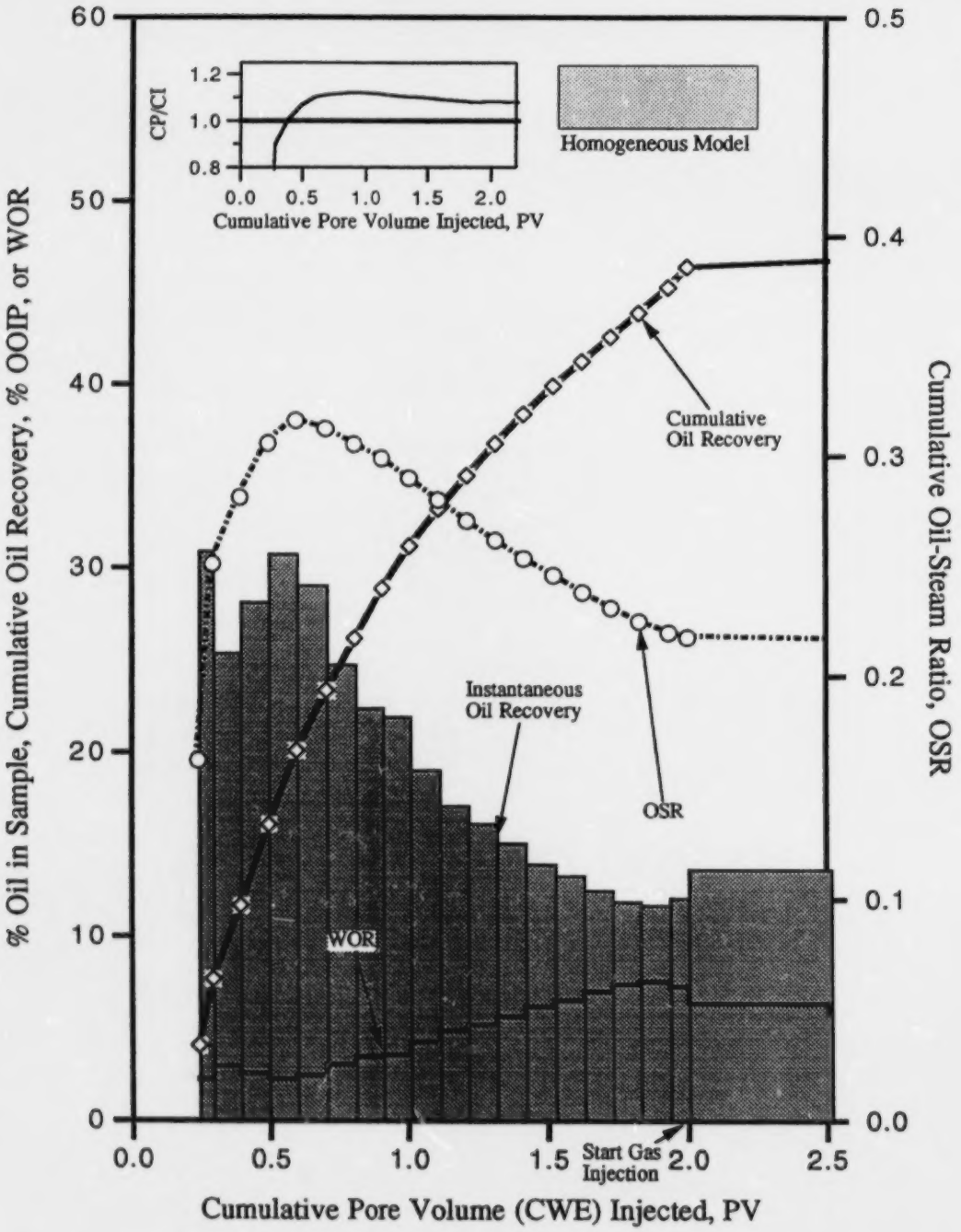

Figure 6.54 – Production History of a Heat Scavenging Experiment (Run 140); Instantaneous Percent Oil in Sample, Cumulative Oil Recovery, Instantaneous WOR, and Cumulative OSR vs. PV Injected (CWE). Inset Plot is CP/CI vs. PV Injected. Steamflood to 2.0 PV then Gasflood a Homogeneous Model, Vertical Injector and Producer.

Run 109 involved the injection of 0.60 PV of steam and then the injection of warm 23°C water. Run 110 was a repeat of Run 109, but a 0.10 PV gas slug was injected prior to the waterflood. This created a gas phase in the reservoir so that heated water could partially flash into steam. Run 111 was a steamflood for 1.00 PV prior to the waterflood.

Figure 6.55 shows that Runs 109 and 110 have similar production profiles. Run 110 has a slightly better recovery at 0.60 PV of steam injected, possibly due to the gas injection displacing more oil, while in Run 109 the waterflood collapsed the steam zone. Run 111 had 40% more steam injected, and this resulted in 15% more oil recovered by the steamflood portion of the run. The waterflood recovered 10% of the OOIP in Run 111. Runs 109 and 110 recovered incrementally 6% and 5%, respectively, from their waterflood portion.

Figures 6.56, 6.57, and 6.58 show the top view temperature contour plots prior to the waterflood portion of the runs (0.60 PV of steam injected for Runs 109 and 110, and 1.00 PV of steam injected for Run 111). The steam zone reached the middle of the model in Runs 109 and 110, and the production well in Run 111. In each case, the models cool once the waterflood begins.

In summary, the injection of water after a steamflood reduces the oil production rate. Furthermore, as the time allowed for steamflooding increases, the oil recovered by waterflooding also increases.

6.9 Reproducibility of the Results

An important aspect of any experimental investigation is the reproducibility of the results. In an effort to demonstrate the reproducibility of the experiments several base case experiment were repeated. Figure 6.59 displays three experiments that were performed with similar operating conditions. The runs have similar recovery profiles, and that at 2.00 PV injected the absolute difference between the three experiments is about 5% of the OOIP. These experiments represent the base cases with the greatest differences, and because of this it is felt that the error in these experiments is about 2% of the OOIP. This is in agreement with other observed errors as can be seen in Figure 6.49, there there is essentially no difference in the cumulative recovery curves until after 1.5 PV had been injected..

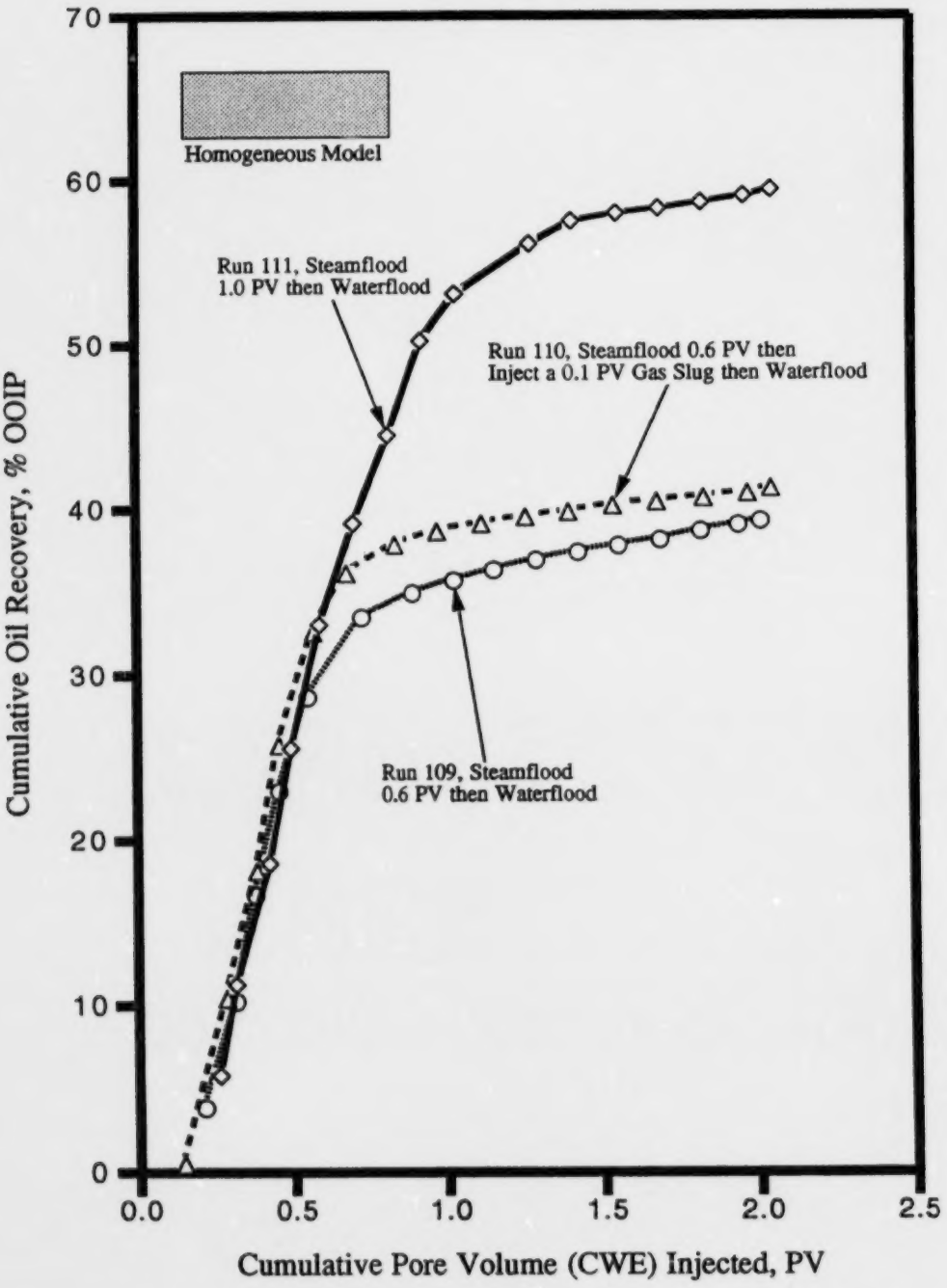

Figure **6.55**— Cumulative Oil Recovery vs. Cumulative PV Injected for Heat Scavenging Experiments in Homogeneous Models. Steamflood to 0.60 PV then Waterflood (Run 109), Steamflood to 0.60 PV then Inject a 0.10 PV Gas Slug, then Waterflood (Run 110), and Steamflood to 1.00 PV then Waterflood (Run 111), Vertical Injector and Producer Wells.

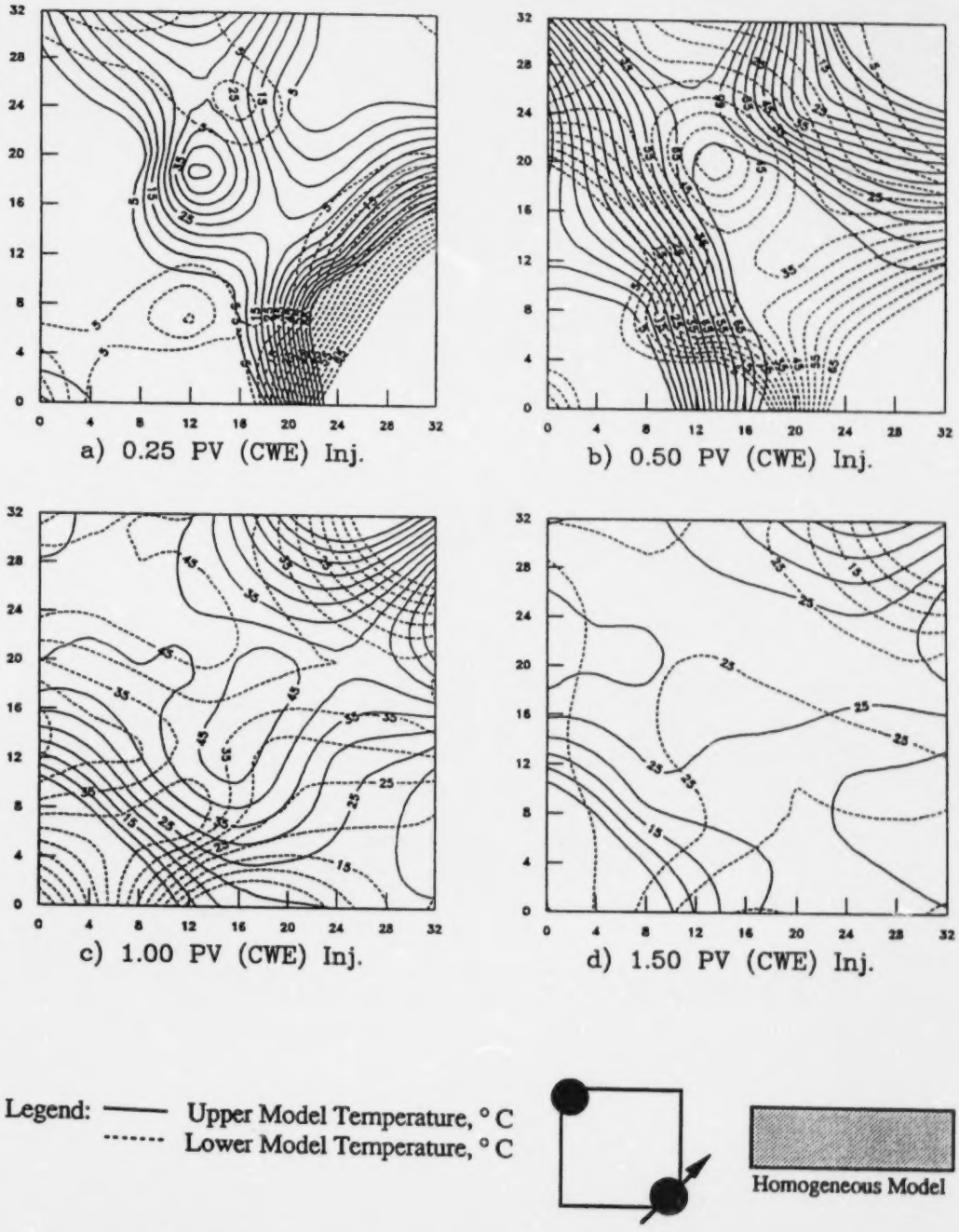
a) 0.25 PV (CWE) Inj.
b) 0.50 PV (CWE) Inj.
c) 1.00 PV (CWE) Inj.
d) 1.50 PV (CWE) Inj.
Legend:
Upper Model Temperature, ° C
Lower Model Temperature, ° C
Homogeneous Model

Figure 6.56 – Plan view, of the temperature distribution inside the model reservoir after the injection of: a) 0.25, b) 0.50, c) 1.00, and d) 1.50 PV CWE of steam, for Run 109: homogeneous model, steamflood to 0.60 PV then waterflood, vertical injection, and production wells.

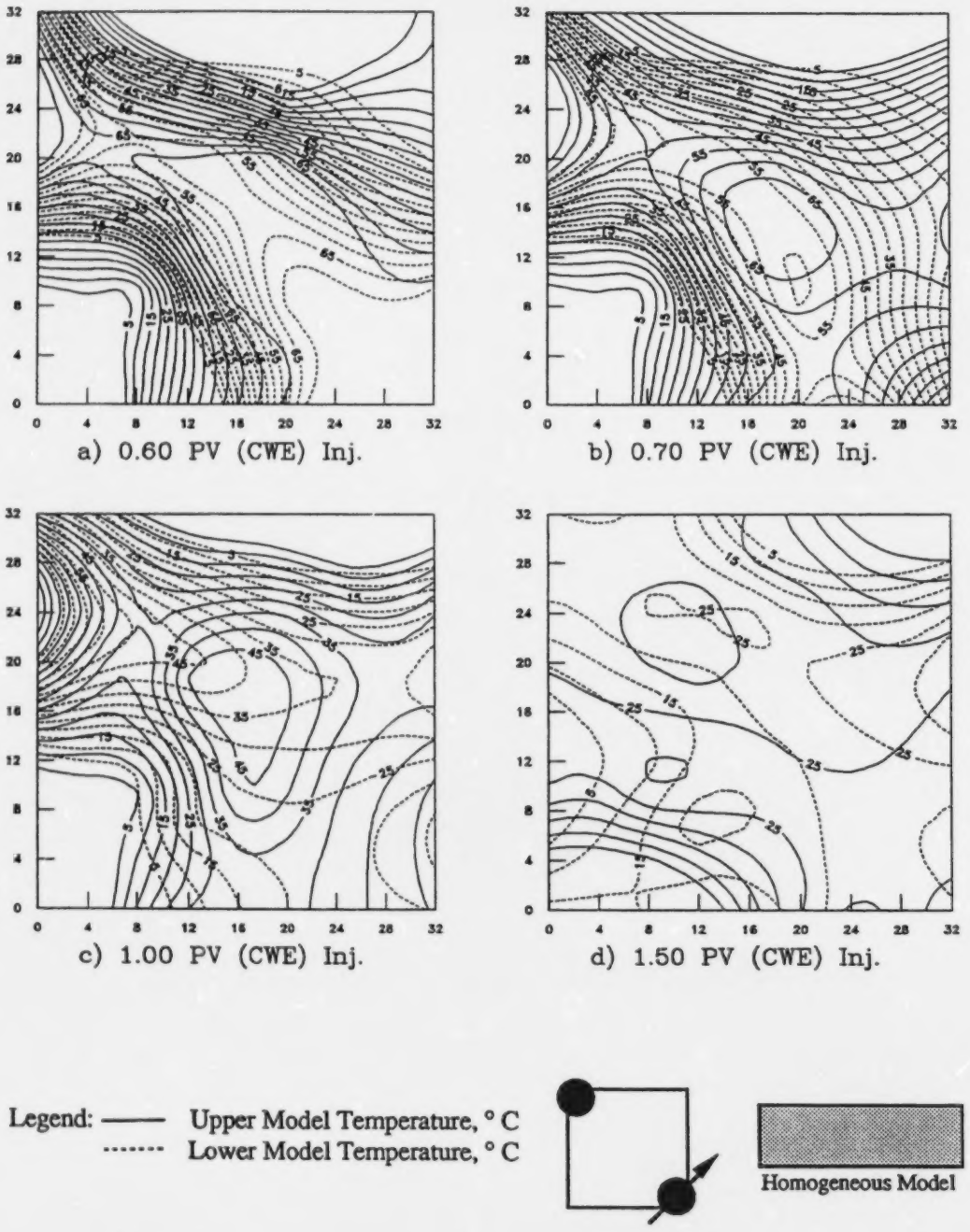
a) 0.60 PV (CWE) Inj.
b) 0.70 PV (CWE) Inj.
c) 1.00 PV (CWE) Inj.
d) 1.50 PV (CWE) Inj.
Legend: —— Upper Model Temperature, ° C
------- Lower Model Temperature, ° C
Homogeneous Model

Figure 6.57 – Plan view, of the temperature distribution inside the model reservoir after the injection of: a) 0.25, b) 0.50, c) 1.00, and d) 1.50 PV CWE of steam, for Run 110: homogeneous model, steamflood to 0.60 PV, inject a 0.10 PV gascap then waterflood, vertical injection and production wells.

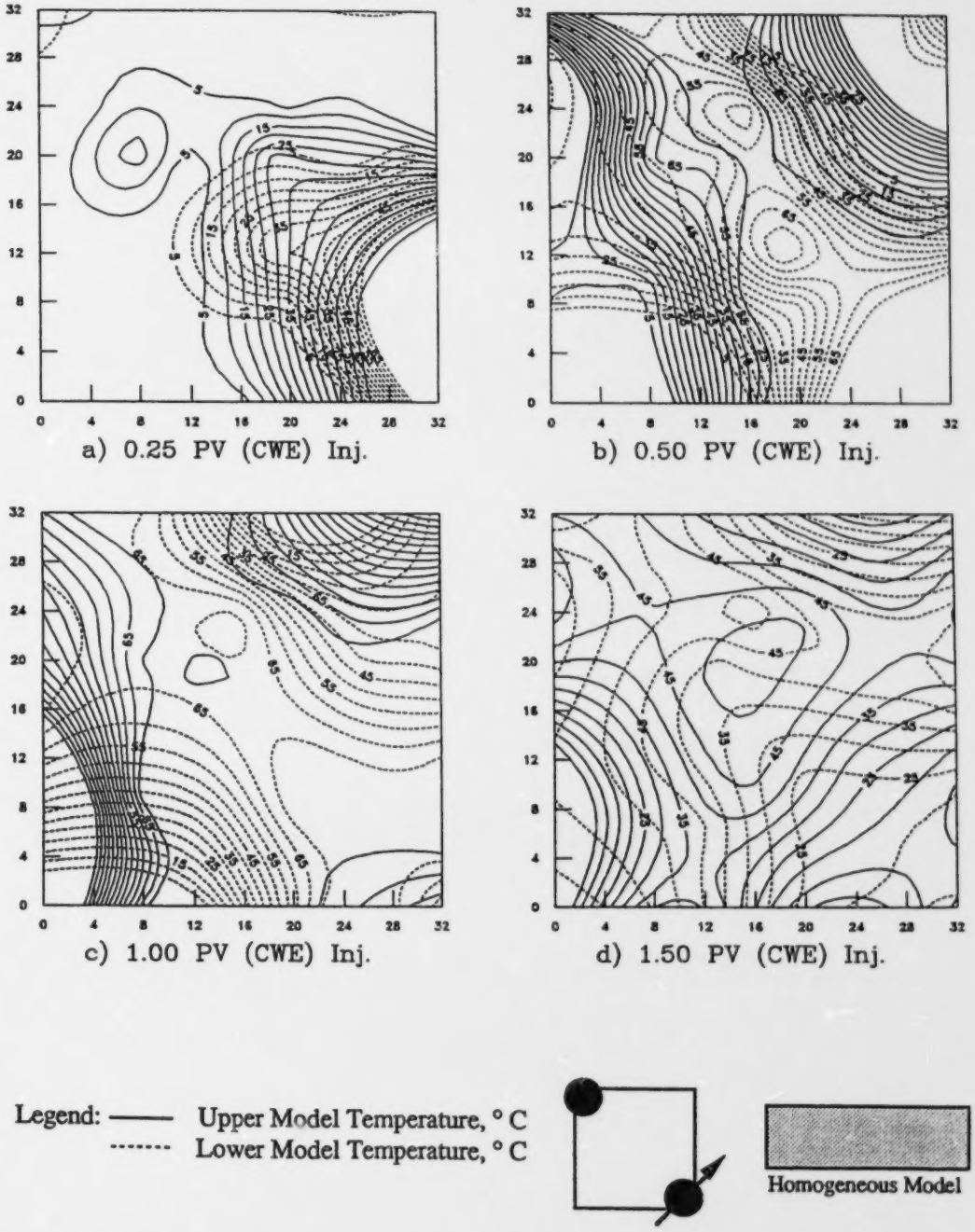
a) 0.25 PV (CWE) Inj.
b) 0.50 PV (CWE) Inj.
c) 1.00 PV (CWE) Inj.
d) 1.50 PV (CWE) Inj.
Legend: —— Upper Model Temperature, ° C
------- Lower Model Temperature, ° C
Homogeneous Model

Figure 6.58 – Plan view, of the temperature distribution inside the model reservoir after the injection of: a) 0.25, b) 0.50, c) 1.00, and d) 1.50 PV CWE of steam, for Run 111: homogeneous model, steamflood to 1.00 PV then waterflood, vertical injection, and production wells.

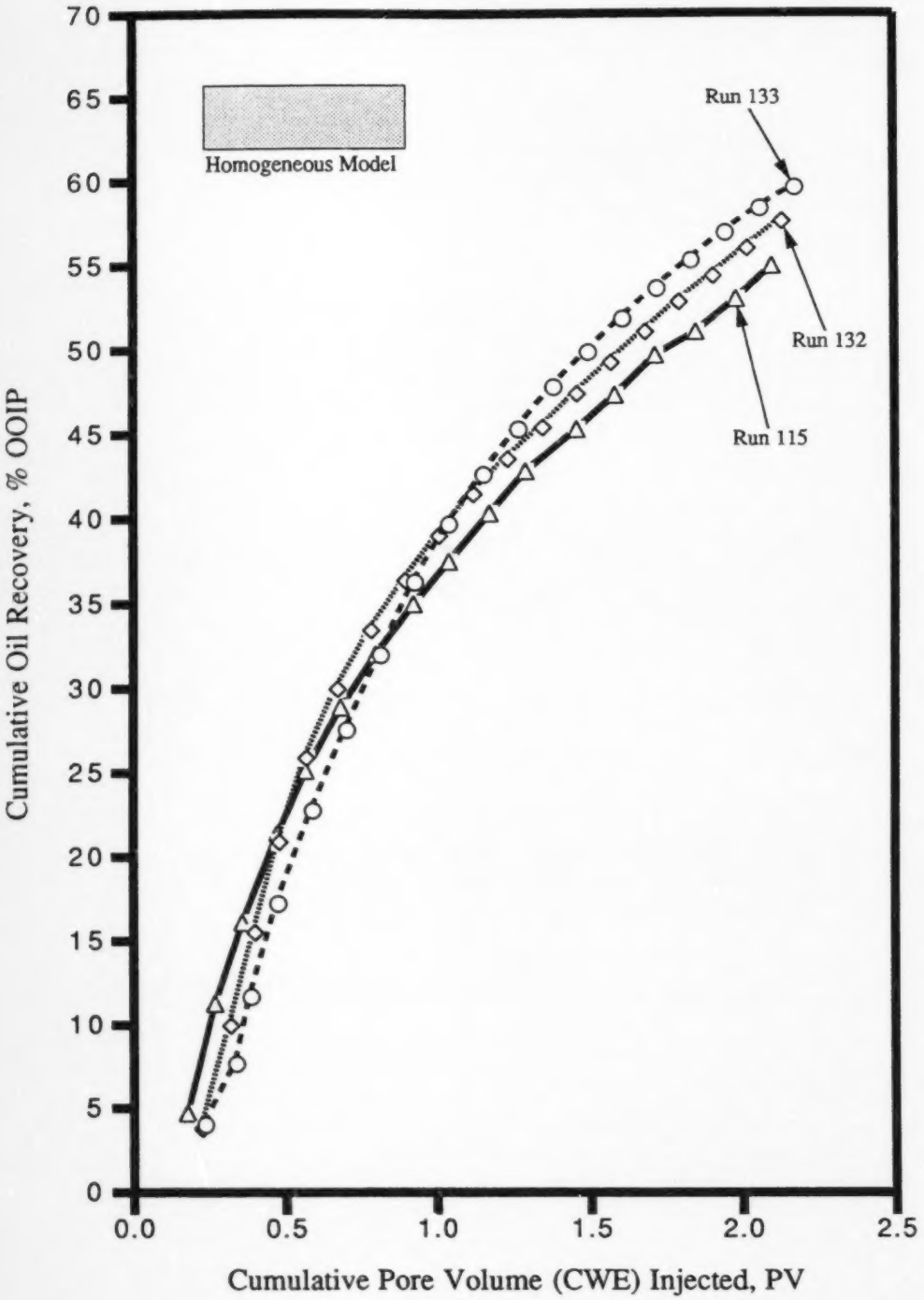

Figure 6.59 — Cumulative Oil Recovery vs. Cumulative PV Injected for Three Base Case Homogeneous Models, Using Vertical Injection and Production Wells; Run 115 ,Run 132, and Run 133.

Chapter 7

Conclusions

Steamfloods were performed in three types of model reservoirs; homogeneous, thick bottom water zone, and multi-layered. The steamflood strategies employed a variety of different recovery techniques including the use of horizontal wells and waterflooding at different times during an experiment. The following conclusions were reached based on the observations discussed previously:

1. Significant modifications were made to the experimental apparatus. In particular, steam quality measurements were made using two independent techniques, showing good agreement between the two.

2. The horizontal well experiments led to the following conclusions:

a) The horizontal well design based upon Doan's[41] scaling criteria is adequate for experimental purposes and it is of a reasonable size for the experiments. The effect of horizontal well length was more pronounced when a thick bottom water zone was present than in the homogeneous case.

b) Experiments in the multi-layered models demonstrated that mechanical efforts to overcome steam override, such as horizontal wells and the use of a fracture, were not effective. The permeability contrast was sufficient to cause the steam to flow preferentially in the high permeability zone.

c) A waterflood prior to a steamflood can reduce the energy investment for similar oil recovery performance.

d) In the heat scavenging experiments the water injected after a steamflood reduced the oil recovery rate as compared to that for steamflooding.

e) In the case of a thick bottom water zone a horizontal producer recovered oil earlier than the conventional vertical producer and generally yielded a higher cumulative oil-steam ratio than the vertical producer.

f) The completion interval of a horizontal well influenced the cumulative oil recovery in a steamflood, with the lower the well placement yielding higher oil recovery.

Chapter 8

Recommendations for Further Studies

During this study a large number of preliminary experiments were performed that investigated the following areas: anisotropic reservoirs (shale barriers), reservoir bottom topography effects, steam alternating water injection, impermeable barriers, and pattern inversion. This preliminary work proved to warrant a much more in-depth investigation, as proposed below.

1. The following areas could be investigated:

    a) Fracture orientation in the reservoirs with regards to horizontal wells intersecting them.

    b) Different reservoir top and bottom topographies to examine how this can change the flow paths of both the steam and the condensate in the reservoir.

    c) Dipping reservoirs.

    d) Shale barriers, continuous and discontinuous, impermeable streaks in the reservoir.

    e) Pressure up and blow down the reservoir.

    f) Pre-heating the injection and production points in the reservoir to reduce the high initial pressures.

2. The following areas should be looked into with regard to the physical model, and experimental design

    a) Saturating the model with oil from the updip end to maintain a density and gravity stabilized saturation front.

    b) Changing the injection system to a constant pressure injection system, this would eliminate the very high initial injection pressures, and give more control over the steam quality during an experiment.

c) Changing from a model tray to a model with only walls sealed directly to the granite blocks, for better heat loss modelling.

d) Changing the thermocouple pattern so that there are three layers of thermocouples: top, middle and bottom.

e) A very intensive sensor system around the horizontal wells will serve to better understand the productivity along the length of a horizontal well.

f) A thicker model should be used for bottom water experiments so that the bottom water does not reduce the net pay to less than marginal.

References

1. Leverett, M.C., Lewis, W.B., and True, M.E.:"Dimensional Model Studies of Oil Field Behavior", Petroleum Transactions, **AIME**,Vol. **146**, 1942, 175.

2. Rapoport, L.A. and Leas, W.J.:"Properties of Linear Waterfloods", Petroleum Transactions, **AIME**, Vol. **198**, 1953, 139.

3. Croes, G.A. and Schwarz, N.:"Dimensionally Scaled Experiments and the Theories in the Water Drive Process", Petroleum Transactions, **AIME**, Vol. **204**, 1955, 35.

4. Geertsma, J., Croes, G., and Schwarz, N.:"Theory of Dimensionally Scaled Models of Petroleum Reservoirs", Petroleum Transactions, **AIME**, Vol. **207**, 1956, pp. 118-127.

5. Pujol, L. and Boberg, T.C.:"Scaling Accuracy of Laboratory Steam Flooding Models", paper SPE 4191, presented at the California Regional Meeting of the Society of Petroleum Engineers, Bakersfield, November 8-10, 1972.

6. Willman, B.T., Valleroy, V.V., Runberg, G.W., Cornelius, A.J., Powers, L.W.:"Laboratory Studies of Oil Recovery by Steam Injection", presented at the 35th Annual Fall Meeting of the Society of Petroleum Engineers, Denver, October 2-5,1960.

7. Farouq Ali, S.M. and Redford, D.A.: "Physical Modeling of In Situ Recovery Methods For Oil Sands", presented at the 28th Annual Technical Meeting of the Petroleum Society of CIM, Canada-Venezuela Oil Sands Symposium of 1977, Edmonton (May 1977).

8. Kimber, K.D., Puttagunta, V.R. and Farouq Ali, S.M.: "New Scaling Criteria and Their Relative Merits for Steam Recovery Experiments," Paper 86-37-22 presented at the 37th Annual Technical Meeting of the Petroleum Society of CIM, Calgary, June 8-11 (1986) 303-318.

9. Kimber, K.D. and Farouq Ali, S.M.: "Application of New Scaling Approaches for Steam Injection Experiments", presented at the 25th National Heat Transfer Conference of AIChE, Houston (1988).

10. Kimber, K.D. and Farouq Ali, S.M.: "Verification of Scaling Approaches for Steam Injection Experiments", Paper 88-39-17 presented at the 39th Annual Technical Meeting of the Petroleum Society of CIM, Calgary, June 12-16 (1988).

11. Pursley, S.A.: "Experimental Studies of Thermal Recovery Processes", presented at the Symposium on Heavy Crude Oil, Maracaibo, Venezuela, July 1-3 (1974).

12. Huygen, H.H.A.: "Laboratory Steamfloods in Half of a Five-Spot", SPE 6171 presented at the 51st Annual Fall Technical Conference and Exhibition of the Society of Petroleum Engineers of AIME, New Orleans, October 3-6 (1976).

13. Stegemeier, G.L., Laumbach, D.D., and Volek, C.W.: "Representing Steam Processes with Vacuum Models", *SPEJ* (June 1980) 151-174.

14. B.J. Kristoff, Saskatchewan Research Council, Regina, Personal Communication (1991).

15. Proctor, M.L.: "Steam Injection Experiments in a Scaled Physical Model", M.Sc. Thesis, U of Alberta (Fall 1985).

16 Oracheski, D.: "Bottom Water Solvent Steam Injection Studies", M.Sc. Thesis, U of Alberta (Fall 1988).

17. Hall, A.L. and Bowman, R.W.: "Operation and Performance of the Slocum Thermal Recovery Project", *JPT* (April 1973) **25**, 402-408.

18. Prats, M.: "Peace River Steam Drive Scaled Model Experiments", presented at the 28th Annual Technical Meeting of the Petroleum Society of CIM, Canada-Venezuela Oil Sands Symposium of 1977, Edmonton (May 1977).

19. Ehrlich, R.: "Laboratory Investigation of Steam Displacement in the Wabasca Grand Rapids 'A' Sand", presented at the 28th Annual Technical Meeting of the Petroleum Society of CIM, Canada-Venezuela Oil Sands Symposium of 1977, Edmonton (May 1977).

20. Huygen, H.A. and Lowry, Jr., W.E.: "Steamflooding Wabasca Tar Sand Through the Bottom Water Zone - Scaled Lab Experiments", SPE 8398 presented at the 54th Annual Fall Technical Conference and Exhibition of the Society of Petroleum Engineers of AIME, Las Vegas, September 23-26 (1979).

21. Huygen, H.H.A. and Black, J.B.:Steaming Through Horizontal Wells and Fractures-Scaled Model Tests", Proceedings of 2nd European Symposium on Enhanced Oil Recovery, Paris, November 8-10, 1982, 507-517.

22 Ahner, P.F. and Sufi, A.H.: "Physical Model Steamflood Studies Using Horizontal Wells", SPE 20247 presented at the SPE/DOE Seventh Symposium on Enhanced Oil Recovery, Tulsa, April 22-25, 1990.

23 Chang, H.L., Farouq Ali, S.M., and George, A.E.:"Performance of Horizontal-Vertical Well Combination for Steamflooding Bottom Water Formations", *JCPT* (May 1992) 41-51.

24. Nasr, T.N. and Pierce, G.E.: "Steamflooding Cold Lake Oil Reservoirs Through a Bottom Water Zone: A scaled Physical Model Study", paper SPE 21772 presented at the Western Regional Meeting, Long Beach, California, March 20-22, 1991.

25. Gümrah, F., Palmgren, C.T.S., Bruining, J., and Godderij, R.R.G.G.:"Steamdrive in a Layered Reservoir: An Experimental and Mathematical Study", SPE 24171 presented at the SPE/DOE Eight Symposium on Enhanced Oil Recovery, Tulsa, April 22-24, 1992.

26. Yang, G. and Butler, R.M.: "Effects of Reservoir Heterogeneities on Heavy Oil Recovery by Steam-Assisted Gravity Drainage", *JCPT* (October 1992) 37-43.

27. Dietrich, J.K.: "The Kern River Horizontal-Well Steam Pilot", *SPE Reservoir Engineering* (August 1988) 935-944.

28. Buller, S.M.: "Evaluation of Horizontal, Radial , and Vertical Injection Wells in a Pilot Steamflood", SPE 24630 presented at the 67th Annual Technical Conference and Exhibition of the Society of Petroleum Engineers, Washington D.C., October 4-7, 1992.

29. Best, D.A., Lesage, R.P., and Arthur, J.E.: "Steam Circulation in Horizontal Wellbores", SPE 20203 presented at the Seventh Symposium on Enhanced Oil Recovery, Tulsa, April 22-25, 1990.

30. Joshi, S.D.: "Augmentation of Well Productivity Using Slant and Horizontal Wells", *JPT* (June 1988) 729-739.

31. Giger, F.M.: "Low-Permeability Reservoirs Development Using Horizontal Wells", SPE 18334 presented at the SPE/DOE Low Permeability Reservoirs Symposium, Denver, May 18-19 (1987).

32. Dikken, B.J.: "Pressure Drop in Horizontal Wells and Its Effect on Their Production Performance", JPT., November 1990, pp. 1426-1433.

33. Chaperon, I.: "Theoretical Study of Coning Toward Horizontal and Vertical Wells in Anisotropic Formations: Subcritical Rates", SPE 15377, presented at the 61st Annual Technical Conference and Exhibition of the Society of Petroleum Engineers, New Orleans, LA, October 5-8, 1986.

34. Joshi, S.D.; "Production Forecasting Methods for Horizontal Wells", paper SPE 17580, presented at the SPE International Meeting on Petroleum Engineering, Tianjin, China, November 1-4, 1988.

35. Butler, R.M., G.S. McNab, and H.Y. Lo: "Theoretical Studies on the Gravity Drainage of Heavy Oil During In-Situ Steam Heating", *The Canadian Journal of Chemical Engineering*, Vol. 59 (August 1981) 455-460.

36. Butler, R.M. and Stephens, D.J.: "The Gravity Drainage of Steam-Heated Heavy Oil to Parallel Horizontal Wells", *JCPT* (April-June 1981) 90-96.

37. Griffin, P.J. and Trofimenkoff, P.N.: "Laboratory Studies of the Steam-Assisted Gravity Drainage Process", presented at the AOSTRA 5th Annual 'Advances in Petroleum Recovery & Upgrading Technology' Conference, June 14-15 1984, Calgary, Alberta.

38. Butler, R.M.: "A New Approach to the Modelling of Steam-Assisted Gravity Drainage", JCPT, May-June 1985, pp. 42-51.

39. Joshi, S.D.: "A Laboratory Study of Thermal Oil Recovery Using Horizontal Wells", SPE/DOE Paper No. 14916, Proc. of the Fifth SPE/DOE EOR Conf., Tulsa, April 20-23 (1986) 457-468.

40. Edmunds, N.R., Haston, J.A., and Best, D.A.: "Analysis and Implementation of the Steam-Assisted Gravity Drainage Process at the AOSTRA UTF", paper no. 125, proceedings of the Fourth UNITAR/UNDP Conference on Heavy Crude and Tar Sands, Edmonton, August 7-12, 1988.

41. Doan, Q.T., Farouq Ali, S.M., and George, A.E.:"Scaling Criteria and Model Experiments of Horizontal Wells", *JCPT* (November, 1992), pp.57-65.

42 Wygal, R.J.: "Construction of Models that Simulate Oil Reservoirs", *SPEJ* (December 1963) 281-286.

43. Tortike, W.S. and Farouq Ali, S.M.: "Saturated-Steam-Property Functional Correlations for Fully Implicit Thermal Reservoir Simulation", paper SPE 17094, SPE Res. Eng., November 1989.

44. Van Wylen, G.L. and Sonntag, R.E.: Fundamentals of Classical Thermodynamics, 3rd Ed., SI Version, John Wiley & Sons, 1985.

45. Carslaw, H.S., Jaeger, J.C.: Conduction of Heat in Solids, Second Edition, Clarendon Press, Oxford, 1984.

46. Farouq Ali, S.M.: Heavy Oil Recovery, Chapter 5, (1989).

47. Marx, J.W. and Langenheim, R.H.: "Reservoir Heating by Hot Fluid Injection", *Trans.* **AIME** (1959) 312.

48. Mandl, G. and Volek, C.W.: "Heat and Mass Transport in Steam-Drive", *SPEJ* (March 1969) 59-79.

49. Prats, M.: Thermal Recovery, Monograph Volume 7, SPE Henry L. Doherty Series, Chapters 6 and 7, Society of Petroleum Engineers of AIME (1982).

Appendix A

Steam Quality

The crucial variable which governs the performance of steamfloods in the low pressure model is steam quality. Figures A1 and A2 display the production history for Runs 108 and 115. The two experiments were carried out with different steam qualities; Run 108 had 14% steam quality and Run 115 had 10% steam quality. From the production history curves, it can be seen that the two runs had the same initial point, but Run 108 (f_{st}=14%) out-performed Run 115. Figure A2 displays the Cumulative Produced Volume/ Cumulative Injected Volume (CP/CI) curves vs. cumulative PV CWE of steam injected. From these curves it can be seen that the higher steam quality causes substantially greater volumes of production. This is so because the greater enthalpy injected causes a steam zone to start sooner and grow more quickly. The steam quality scaling calls for the injection of 10% quality steam. Failure to meet the scaling requirement will result in significant changes to the recovery performance. It is for these reasons that steam quality tests were performed.

Experimental Apparatus and Procedure for Steam Quality Testing

During this study the steam injection system was rigorously studied. From the findings it was modified. The injection system was changed for three reasons: the first of these was that the original system had a surging problem causing the injection pressure at the sand face to pulse, the next problem was that prior to a run the injection system was run at atmospheric conditions which was the effective pressure in the steam generator. At the start of a run the injection line was connected to the low pressure model and the low pressure was transmitted into the boiler. The reduction of the internal boiler pressure caused a small additional volume of water to flash into steam, increasing the instantaneous injection rate. The last problem was that the low pressure in the boiler was transmitted through to the injection pumps leading to a slightly increased pump rate.

The original injection system consisted of a superheated steam line mixing with a warm water line to achieve the desired steam quality at the injection point. The steam quality was experimentally tested using a heat exchanger which was fundamental in performing an enthalpy balance. Problems with the injection system caused it to be re-evaluated, and a non-mixing system was tested. Unfortunately, the heat exchanger was

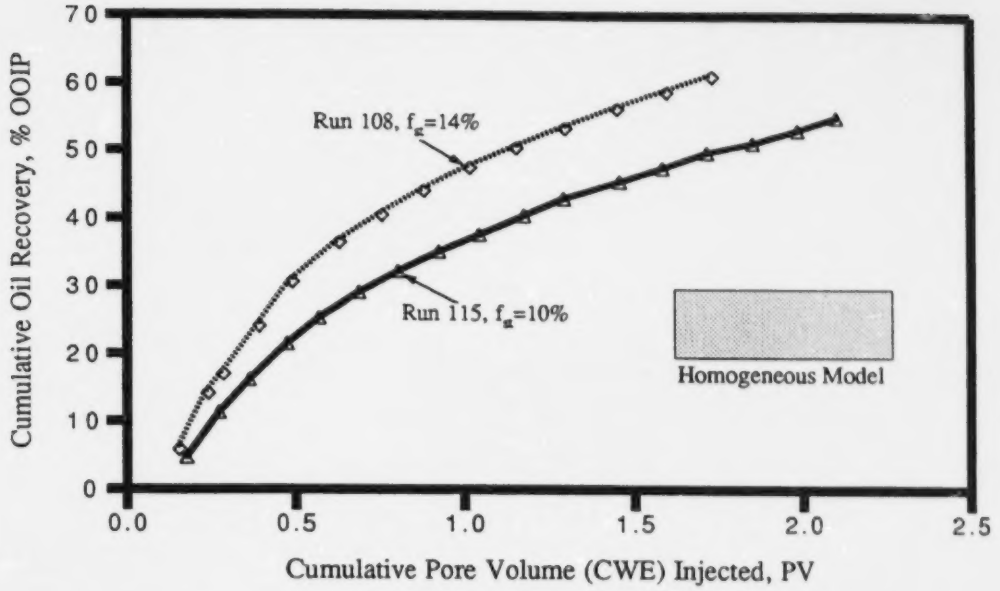

Figure A1 — Cumulative Oil Recovery vs. Cumulative PV Injected for Different Steam Qualities, f_{st}=0.14 vs. f_{st}=0.10, in Homogeneous Models Using Vertical Injection and Production Wells.

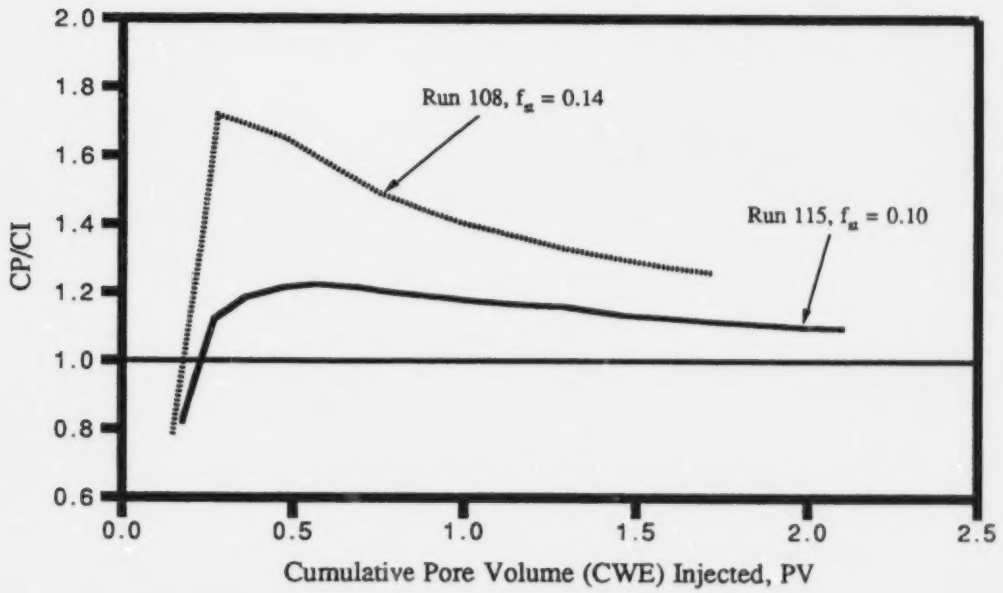

Figure A2 — Cumulative Volume Produced/Cumulative Volume Injected (CP/CI) for Different Steam Qualities, f_{st}=0.14 vs. f_{st}=0.10, in Homogeneous Models, Using Vertical Injection, and Production Wells.

no longer available so an alternate method of testing the steam quality had to be used. The new method used to test the steam quality from the non-mixing system was a two-trap system which allowed a mass balance to be performed. The two trap-system was tested on the mixing injection system first to calibrate it against the previous work. In the following discussion the two experimental methods will be explained.

Enthalpy Balance

The apparatus used to test the steam quality consisted of the steam injection equipment which included the two Milroyal control-volume pumps and a low pressure steam generator. The enthalpy balance testing equipment consisted of a counter-flow condenser (heat exchanger), a portable hybrid recorder, and the production system. Figure A3 displays a schematic of the experimental counter-flow condenser apparatus.

The experiments were carried out using constant steam flow rates, and by varying the boiler temperatures from 120 to 160 °C. The steam injection line from the steam generator was connected to the left side inlet of the counter-flow condenser, and the cooling water line was connected to the right side inlet. Thermocouple wires were taped to the inlet and outlet ends of the condenser cooling stream, the wires were connected to the hybrid chart recorder which monitored the temperature difference between the inlet and outlet flows of the cooling stream (Figure A3). This wiring method was used to avoid temperature fluctuations caused by inconsistent thermocouple readings. When the chart recorder indicated a constant voltage difference between the inlet and outlet ends the flow rate of the cooling water line was determined. The temperatures of the four streams were then measured with a thermometer. The temperatures and flow rates of the two streams were used to determine the enthalpy of the input steam stream. The flow rate for the cooling water stream was then changed and a new steady state was obtained and the process was repeated. This was done a minimum of three times for each steam generator temperature setting to get an average enthalpy output. An enthalpy balance was performed to determine the quality of the steam injection line. This cycle was repeated for five different boiler temperatures (120°C, 130°C, 140°C, 150°C, and 160 °C). It was found that there was a good correlation between boiler temperature and steam quality. One important point to note is that the flow rate of the cold water line must be large enough to ensure that there is a measurable temperature difference between the entering cooling water and exiting cooling water. One other consideration was the amount of heat loss to the surroundings from the counter-flow condenser,

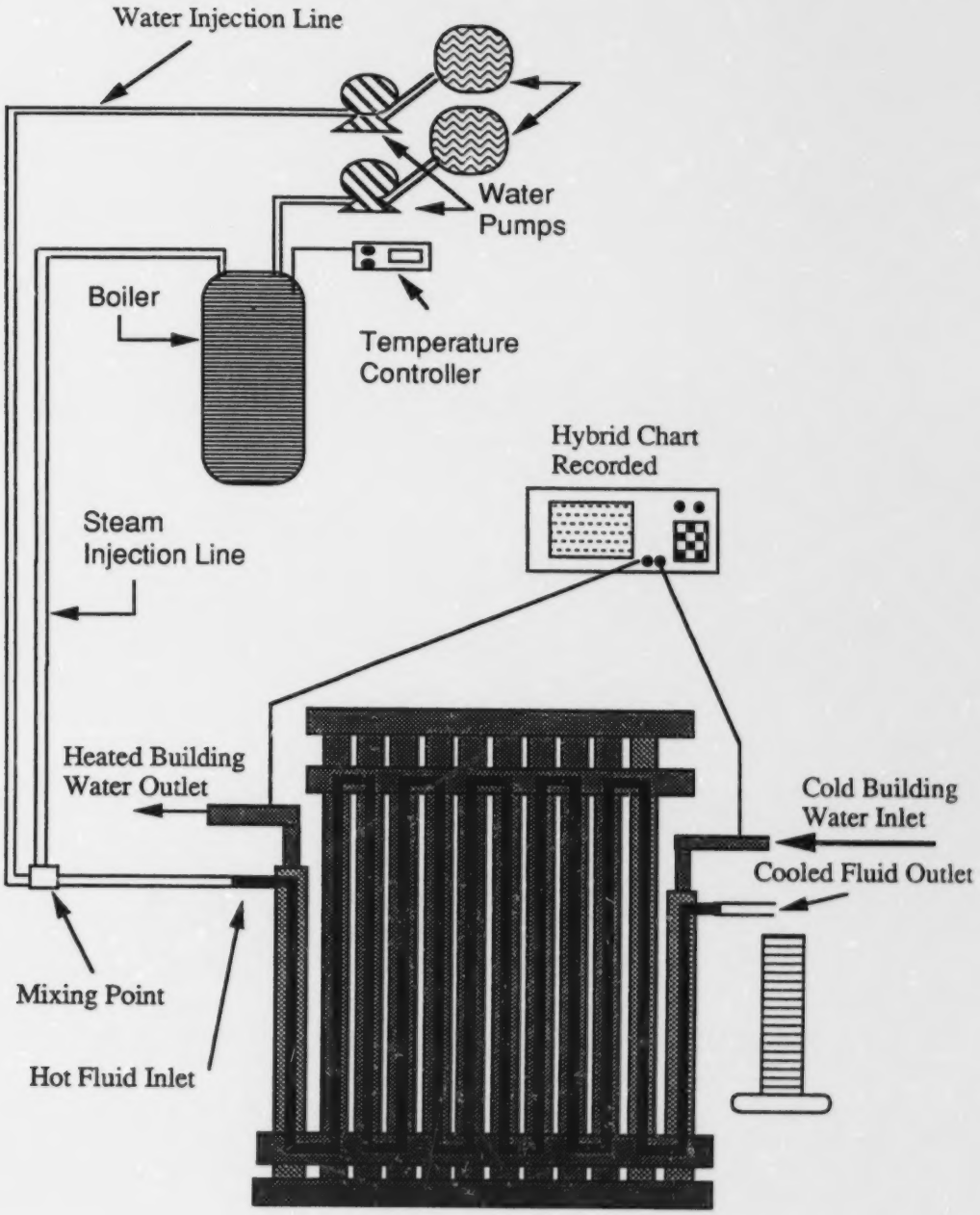

Figure A3 — Schematic of Overall Apparatus for Enthalpy-Balance Steam Quality Tests.

which can affect the accuracy of the heat transfer process. The heat loss was reduced by heavily insulating the counter flow condenser with fiberglass insulation, which in the interest of displaying the apparatus was not included in Figure A3. Figure A4 schematically displays the enthalpy balance.

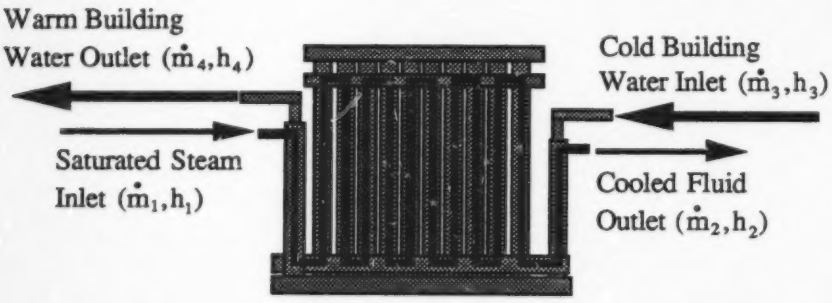

Figure A4

From the above diagram and assuming no heat losses the energy balance is as follows:

energy in = energy out

$$(\dot{m}_1 \times h_1) + (\dot{m}_3 \times h_3) = (\dot{m}_4 \times h_4) + (\dot{m}_2 \times h_2) \qquad \text{(A1)}$$

where: $$h_1 = f_{st} \times h_{vapour} + (1 - f_{st}) h_{liquid} \qquad \text{(A2)}$$

$\dot{m}_j$ = the mass of the fluid stream j, j=1,2,3,4

h_j = the enthalpy of the fluid in stream j, j=1,2,3,4

substituting Equation (A2) into Equation (A1) and solving for the steam quality yields:

$$\frac{(\dot{m}_4 \times h_4) + (\dot{m}_2 \times h_2) - (\dot{m}_3 \times h_3)}{\dot{m}_1 (h_{vapour} - h_{liquid})} - \frac{h_{vapour}}{h_{vapour} - h_{liquid}} = f_{st} \qquad \text{(A3)}$$

Mass Balance

The second method of measuring the steam quality was used when the injection system was modified to route all the water through the steam generator, and not mix the two fluid streams. The counter-flow condenser was not available so the mass balance method was tested against the results of the counter-flow condenser. The second method used a water trap and a vapour trap. The volume balance apparatus involved placing an insulated trap the same distance down the injection line as sand face. Figure A5 displays a schematic of the volume balance steam quality testing apparatus.

The procedure was to preheat the system so that there would be no excess condensation caught by a cold trap. Once the system was preheated the water trap bottom was installed and the injection system was run under, similar to experimental, vacuum conditions. Initially, both traps could be used, but after two tests the vapour trap cooling system could not condense all the vapour and some of the vapour would be lost out through the vacuum pump. When this happens, the vapour volume was determined by subtracting the total volume injected from the liquid volume caught in the water trap.

To calculate the steam quality the total injected mass was known. The liquid mass was measured and that was subtracted from the total mass and then divided by the total mass resulting in the steam quality. This method was tested on the existing mixing system and the results were adequate for experimental purposes.

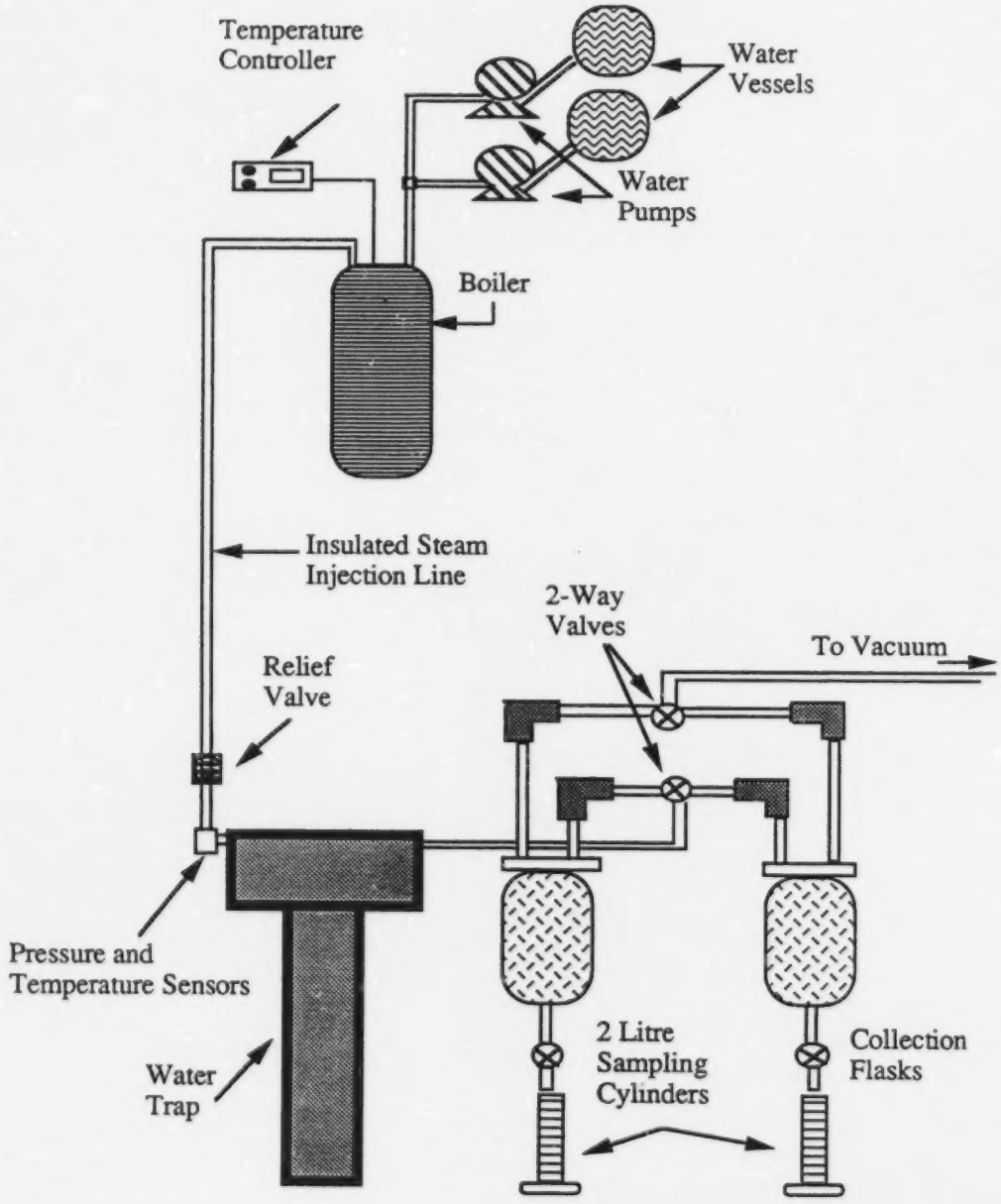

Figure A5 — Schematic of Overall Apparatus for Mass Balance Steam Quality Tests.

Appendix B

Heat Balance

One of the critical influences in thermal experiments is the amount of heat injected into the model reservoir and then knowing where this heat is going. In the following discussion, heat balance refers to cumulative heat balance and not instantaneous heat balance. The overall heat balance equation is:

$$Q_{inj} = Q_{production} + Q_{loss} + Q_{formation} \quad \text{(B1)}$$

Where:

Q_{inj} = Injected energy, (kJ)

$Q_{production}$ = Produced energy, (kJ)

Q_{loss} = Energy loss to the cap and base rock, (kJ)

$Q_{formation}$ = Heat accumulated in the formation, including the matrix (glass beads), oleic phase, aqueous phase, and the vapour phase (steam), (kJ).

Run 136 is a base case experiment. It was selected to determine how much heat is injected into the physical model, and where this heat went after it was injected. The heat balance considered the cumulative heat injected into the model at an instant during the experiment. The instant chosen was after the injection of 1.00 pore volume of 10% quality steam and this was just prior to steam breakthrough. After steam breakthrough the produced energy could not be easily accounted for. Consider the closed system to be the injection point, the outside faces of the granite blocks, and the production point. The areas into which the heat can go are into the reservoir matrix, the fluids initially in the reservoir, the granite blocks, and with the fluids out the production point. It was assumed that there were no heat losses out the sides of the model or granite blocks.

Assuming and that the energy contained in the produced samples and that the injected energy can be accurately calculated, the most difficult parts of the heat balance are determining the heat losses and the heat accumulated in the formation.

Schematically, the problem is as follows:

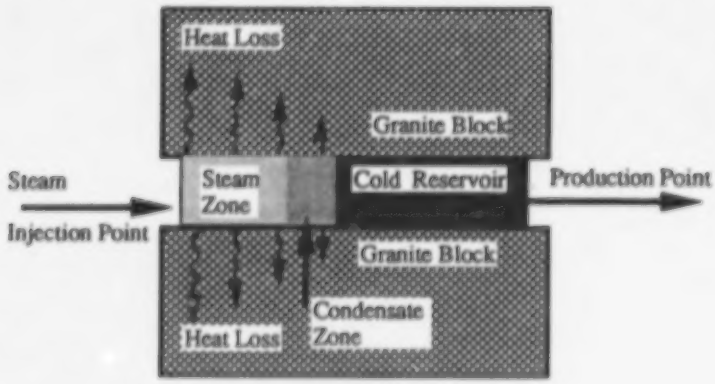

Figure B1

Heat is injected on one side and heat transfer occurs to the cap and base rocks near the injection point, and a steam zone is created. As the injection continues warmed fluids leave the model out the production point. In addition, the heat transfer to the cap and base rocks moves further away into the rock near the injection point, and starts to enter the cap and base rocks near the center of the model as is illustrated by the magnitude of the squiggly lines.

Cumulative Heat Injected

Assuming there is good control over the steam injection rate, pressure, temperature, and steam quality, then the heat injected into the model was constant. Equation B2 can be used to calculate the energy injected into the model.

$$Q_{inj.} = i_{st}\left\{h_{inj.} - h_{res.} + f_{st}L_v\right\}t \qquad (B2)$$

Where:

$Q_{inj.}$ = heat injected, (kJ)
i_{st} = steam injection rate, (kg/sec.)
h_W = saturated water enthalpy, (kJ/kg)
h_R = enthalpy of water at initial temperature, T_R (kJ/kg)
f_{st} = steam quality, (ratio)
L_V = latent heat of vapourization, (kJ/kg)
t = time, (seconds)

Sample calculation for t = 4080 seconds:

$Q_{inj.}$ =3.3703E-3 (kg/sec){273(kJ/kg)-12.6(kJ/kg)+0.1(2333.3(kJ/kg)}4080 sec

= 6789.2 kJ @ f_{st}=0.10

= 6468.3 kJ @ f_{st}=0.09

= 7110.0 kJ @ f_{st}=0.11

It can be seen that a change of 1% in the steam quality changes the injected enthalpy by 4.73%.

Calculation of Cumulative Heat Produced (Q_{prod})

The produced heat was calculated by matching the produced fluid volumes with the production temperatures during the production of that sample. This involved the averaging of the temperature over the time the sample was collected. In all but one sample the temperature increase during the collection of a sample was small. It was felt that this method gave a good estimate of the heat produced. The equation to determine the heat in the produced fluids is:

$$Q_{prod.} = \sum_{i=1}^{n} \{(V_{w,i} \times C_{w,i} \times \rho_{w,i} + V_{o,i} \times C_{o,i} \times \rho_{o,i}) \times \Delta T\} \qquad (B3)$$

where: i = any sample

n = number of samples

ΔT = the temperature difference between the initial reservoir temperature and the production temperature of sample i

C_W = the specific heat capacity of the water and oil, (kJ/kg K)

C_W = 4.3245 - 3.696 E-3 T + 2.482 E-5 T^2

C_O = 1.7915 T + 0.00361 T^2

ρ_W,ρ_O = the density of the water and oil, (kJ/kg)

ρ_W = 1 / (0.001 + 1.436 E-6 (-4.8872 + 0.134186 T + 0.00212868 T^2))

ρ_O = 1.7915(kJ/kg K)+0.00361 T

The relationships for the oil were obtained from Imperial Oil Resources Limited who supplied the oil.

Table B1 displays the produced heat data.

Table B1 — Total Heat Produced After the Injection of 1.00 PV of Steam, Run 136.

Sample No.	Oil Volume (ml)	Water Volume (ml)	Temp Increase From 3 °C	Heat Water (kJ)	Heat Oil (kJ)
1	440	1000	0	0.0	0.0
2	520	1680	22	154.9	18.8
3	460	1110	30	139.5	23.1
4	680	1260	37	195.3	42.6
5	580	1300	42	228.8	41.7
6	510	1370	44.2	253.7	38.7
7	390	1280	44.9	240.8	30.1
8	270	1440	46	277.5	21.4
9	400	1400	47.9	281.0	33.1
Totals =	4250	11840		1771.5	249.5

Total Liquid Produced = 16090 ml

Total Heat Produced Run 136 = 2021.03 kJ

Calculation of the Total Heat Accumulated in the Model

The heat accumulated in the reservoir was determined by mapping the isothermal areas using the SURFER contouring software. Once the area was mapped the phase saturations were estimated. This was done by first determining the volumes of the three phases in the model. The saturations in the unheated areas of the model were assumed to be at initial values. The saturations in the highest temperature areas were more difficult to determine.

The volume of the steam zone was an important factor in determining the saturations in the model. This volume was calculated using three different methods. The first method of determining the steam volume was to perform a volume balance. It was assumed that all thermal expansion was negligible and any production volume above the volume injected was due to the presence of steam. The volume produced minus the volume injected resulted in a steam volume of 1742 ml. The second method was based on the Marx-Langenheim model which resulted in a steam volume of 2116.6 ml. The Marx-Langenheim model does not account for the convective heat transport by the hot water or the cooling of the condensation to the reservoir temperature. The Mandl-Volek model describes more closely the processes in the model. Using the Mandl-Volek model it was determined that the time of steam injection was greater than the critical time and therefore the Mandl-Volek modification of the Marx-Langenheim model was used. The steam zone volume using the Mandl-Volek model was calculated to be 1334.3 ml.

Once the steam volume was established the heat accumulated in the model could be calculated. The known values were the volumes of each phase and the total volume of the system. A spreadsheet was set up to create an interdependence between the volumes. The saturations in each isothermal area were estimated using engineering judgement with steam existing only in the 70 and 65°C areas; these areas were also given the lowest oil saturations. Equation B4 was the equation used to determine the accumulated heat in the model. It was assumed that each volume was at thermal equilibrium.

$$Q_{form} = (\text{Vol. in contour at Temp. °C}) \times \{\phi S_o \rho_o C_o + \phi S_w \rho_w C_w + \phi S_s \rho_s C_s + (1-\phi)\rho_{glass} C_{glass}\} \quad \text{(B4)}$$

where: ϕ = porosity

S_o, S_w, S_s = Saturation of oleic, aqueous, and vapour, phases.

ρ_o, ρ_w, ρ_s, ρ_{glass}, = Density of the three phases and glass beads.

C_o, C_w, C_s, C_{glass} = Specific heat capacity of the three phases and glass beads.

Table B2 displays the spreadsheet data used to determine the accumulated heat in the model. An extensive sensitivity test of the results was performed varying the saturations, and the results did not change significantly. When the volumes of the fluids in the model were changed there were significant changes especially when the steam volume was changed. The reason for the sensitivity of the results to the steam volume was because of the small mass of steam.

Heat Loss to Overburden and Underburden (Q_{loss})

The calculation of the heat loss to the overburden and the underburden (i.e. cap and base rock) is probably the most difficult among all of the calculations. This is due primarily to the limited knowledge of the effects of the Neoprene layer used to seal the top of the model, and the effect of the fiberglass bottom of the model tray. There is also limited knowledge regarding the temperatures of the cap and base rocks (granite blocks in this case) as a function of time. The only temperature data is the temperature at the reservoir-Neoprene interface and the reservoir-fiberglass tray interface. One approach that can be used is to solve Equation (B1) for the unaccounted energy, Q_{loss}, knowing with a good degree of accuracy the other three terms in the equation. This method gives the answer of 735 kJ for Q_{loss} ,which is the remaining 10.8% of the total energy injected. Other more mathematically intensive methods are discussed below.

Two very important considerations in the calculation of the heat loss to the over/underburden are the effect of the Neoprene sheet on the top of the model and the thick fiberglass tray bottom. Using a geometric average, the effective thermal conductivity for the layered system is 2.958 W/m-K. This is only 0.042 W/m-K less than the 3.000 W/m-K for the granite block. This indicates that in theory the thermal conductivity of the cap rock is not greatly affected by the thin Neoprene layer. Figure B2 displays the temperature on either side of the Neoprene sheet for Run 125, considered to be a typical experiment. One thermocouple was placed between the Neoprene and the granite block; a second was placed in the porous medium and touching the Neoprene directly below the first thermocouple. Considering the temperature difference, it can be intuitively surmised that the effective thermal conductivity as calculated above does not adequately account the the thermal resistance of the Neoprene sheet.

Table B2 — Total Heat Accumulated in the Model After the Injection of 1.00 PV of Steam CWE, Run 136

Temp. (°C)	Top Volume m 3	Bottom Volume m 3	Oil Sat.	Oil Vol. m3	Water Sat.	Water Vol. m3	Steam Sat.	Steam Vol. m 3	Heat in Oil kJ	Heat in Water kJ	Heat in Glass kJ	Heat in Steam kJ
0	0.00174419	0.0026565	0.9259	0.001388216	0.0741	0.000111099	0.0000	0	0	0	0	0
5	0.00038122	0.00061675	0.9259	0.000314814	0.0741	2.51946E-05	0.0000	0	0.9966208	0.2113617	3.1655318	0
10	0.00042481	0.00065001	0.9259	0.000339056	0.0741	2.71348E-05	0.0000	0	3.7944831	0.7979537	11.932542	0
15	0.00047256	0.00068969	0.9000	0.000356381	0.1000	3.95979E-05	0.0000	0	6.9051256	1.9941424	22.119739	0
20	0.00055224	0.00073332	0.8500	0.000372292	0.1500	6.56985E-05	0.0000	0	10.319531	4.6793479	34.660951	0
25	0.00064667	0.00079743	0.8500	0.000418204	0.1500	7.38007E-05	0.0000	0	15.147777	6.7916996	50.387075	0
30	0.00079395	0.00087404	0.8047	0.000457298	0.1953	0.000110986	0.0000	0	20.524429	12.51329	71.426012	0
35	0.00113767	0.0009822	0.7600	0.000548902	0.2400	0.000173338	0.0000	0	29.476971	23.11742	107.58665	0
40	0.00093816	0.00111595	0.7100	0.000496883	0.2900	0.000202952	0.0000	0	31.144768	31.230088	120.53818	0
45	0.00078658	0.00132118	0.6600	0.000473955	0.3400	0.000244159	0.0000	0	34.038374	42.55953	140.40082	0
50	0.00076138	0.00182916	0.6100	0.000538384	0.3900	0.000344213	0.0000	0	43.670488	66.993276	193.10226	0
55	0.0008343	0.00242919	0.5600	0.000622648	0.4400	0.000489223	0.0000	0	56.392654	105.08811	269.14408	0
60	0.00119441	0.00263929	0.5100	0.000666132	0.4900	0.000640009	0.0000	0	66.735165	150.3165	346.57097	0
65	0.00646242	0.00269689	0.4600	0.001435465	0.3000	0.000936173	0.2400	0.0007489	157.83783	238.55772	900.64501	0.0028954
70	0.0038448	0.00094377	0.3500	0.000571013	0.0500	8.15733E-05	0.6000	0.0009789	68.457322	22.4005	508.83836	0.0024405

Total Oil Vol.= 0.009000 m 3
Total Water Vol.= 0.00356515 m 3
Total Steam Vol.= 0.00172782 m 3
Total Vol.= 0.01429261 m 3
Pore Volume = 0.01429237 m 3
Pore Volume= 14310 ml
Porosity= 0.3407
Hyc. PV: 13250 ml

% OOIP Recovered at 1.00 PV Inj. = 32%
Bulk Vol. = 0.04195 ml

Oil = 545.4 kJ
Water = 707.3 kJ
Glass = 2780.5 kJ
Steam = 0.005336 kJ
Total = 4033.2 kJ

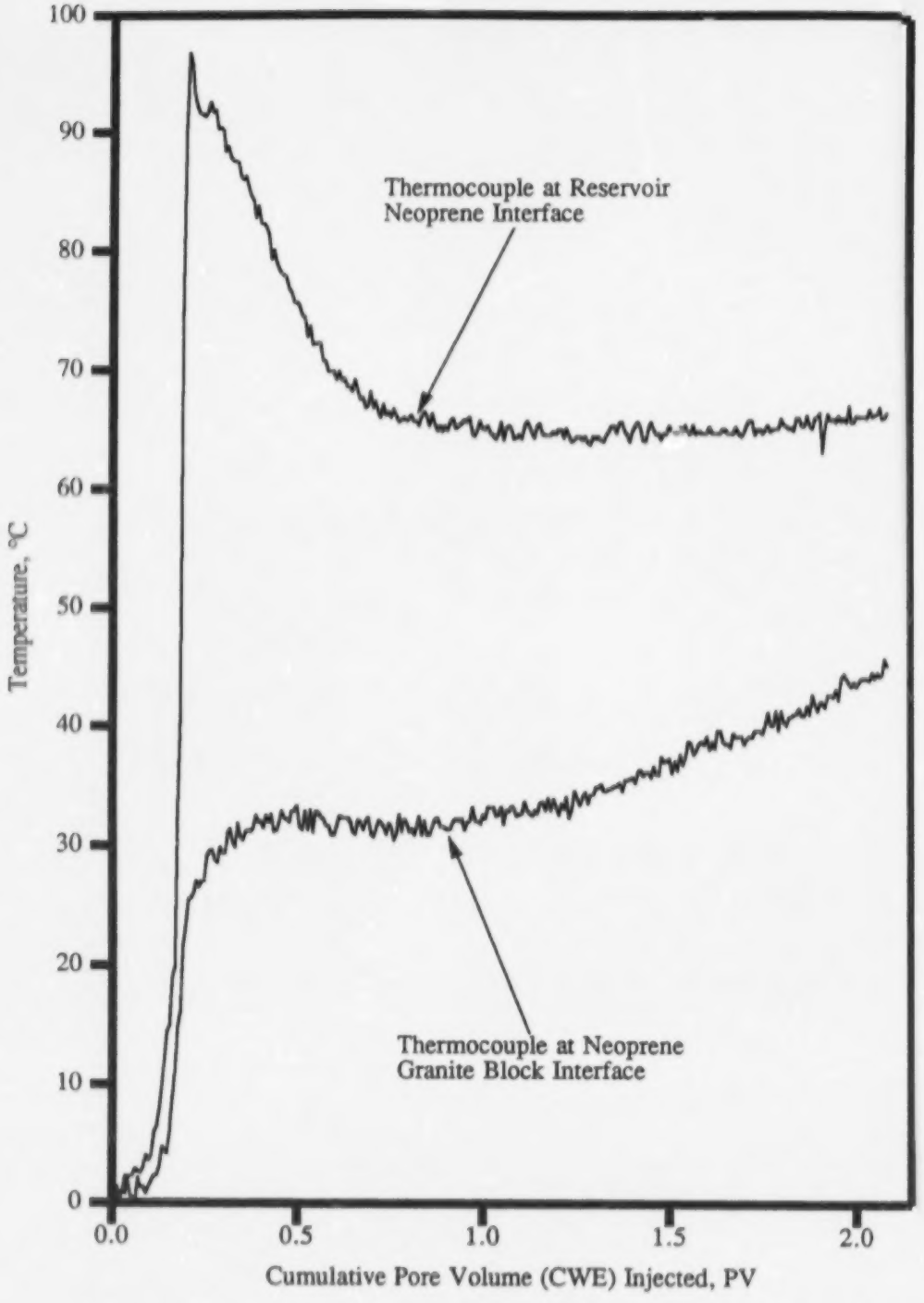

Figure B2 — Temperature on Either Side of the Sealing 1/8 inch Thick Neopreme Sheet. Thermocouples Placed 4 inches Diagonally out fron the Injection Point.

The following, Equation (B5) was used to calculate the heat loss to the cap/base rock. The results are listed in Table B3

$$Q = \frac{2k_h \Delta T \sqrt{t}}{\sqrt{\alpha \pi}} \qquad \text{(B5)}$$

Equation (B5) is for an infinite cap rock at uniform temperature that has had its lower boundary temperature raised an amount, ΔT. Equation (B5) is used to calculate the heat losses to the cap and base rocks. The thermal conductivities of the granite/Neoprene and the granite/fiberglass were used. Table (B3) displays the isothermal areas (calculated using SURFER software), the calculated heat losses for these areas, and the total heat losses. The heat lost to the overburden and underburden was calculated to be 10106 kJ. This is ten-fold more heat than was injected to start with. Sensitivity of the heat loss to different operating conditions is included in Table (B3) and even with the effect of the Neoprene and fiberglass considered the heat losses are too high. Thus, more accurate methods of determining the heat losses to the overburden and underburden were investigated.

Numerical and Analytical Methods of Determining Overburden and Underburden Heat Losses

The heat loss to the overburden and underburden is complex because, with the advance of the heat front in the porous media the adjacent formations are exposed to the temperature changes for varying lengths of time. The resulting temperature gradients give rise to flow of heat in two or three dimensions in the overburden and underburden. The volume in the model at the steam saturation temperature increases continuously, thus the problem is a three-dimensional moving boundary problem. To account for the heat loss to the overburden and underburden some simplifying assumptions were made. First, it was assumed that the heat loss from the reservoir was due to a one dimensional vertical conduction of heat from the reservoir to the overburden and underburden. Second, it was assumed that all of the areas inside the model were at the same temperature from the start of the experiment to the point where the heat balance was performed. This second assumption eliminates the moving boundary aspect of the problem, and should increase the calculated heat losses to the overburden and underburden due to its assumption that the high temperature is at each location for a longer period of time. The heat transfer is by conduction, since there is no fluid flow.

Table B3 — Heat Loss To the Over/Underburden Using Equation (B5) from Stegemier et al. (Ref. 13)

Thermal Conductivities

Granite:	3.0 W/mK
Neoprene:	0.030 W/mK
Fiberglass:	0.035 W/mK
Neoprene/Granite:	2.5 W/mK
Fiberglass /Granite	2.267 W/mK

Heat Loss

Using K granite:	10106 kJ
Using K eff:	9015 kJ
Considering the Effect of the Neoprene and Fiberglass:	4381 kJ

Temp. °C	Bottom Area m 2	Heat Loss (kJ) k eff. = 2.267	Heat Loss (kJ) K =3.0	Heat Loss (kJ) k eff. = 2.267 Temp. -30° C	Top Area m 2	Heat Loss (kJ) K eff =2.5	Heat Loss (kJ) K =3.0	Heat Loss (kJ) K eff =2.5 Temp. -30° C
3	0.0835	0.0	0.0	0.0	0.0549	0.0	0.0	0.0
8	0.0194	15.3	17.6	0.0	0.0120	9.9	10.9	0.0
13	0.0204	32.2	37.1	0.0	0.0134	22.2	24.3	0.0
18	0.0217	51.3	59.0	0.0	0.0149	37.0	40.5	0.0
23	0.0231	72.7	83.7	0.0	0.0174	57.6	63.1	0.0
28	0.0251	98.9	113.7	0.0	0.0204	84.3	92.4	0.0
33	0.0275	130.0	149.6	13.0	0.0250	124.2	136.1	12.4
38	0.0309	170.6	196.2	39.0	0.0358	207.7	227.5	47.5
43	0.0351	221.4	254.7	72.0	0.0295	195.7	214.4	63.6
48	0.0415	294.5	338.8	117.8	0.0248	184.6	202.3	73.9
53	0.0575	453.4	521.6	208.6	0.0240	198.6	217.5	91.3
58	0.0764	662.7	762.3	337.4	0.0263	239.4	262.2	121.9
63	0.0830	785.4	903.5	432.0	0.0376	373.8	409.5	205.6
68	0.0848	869.3	1000.0	508.2	0.2035	2191.1	2400.3	1281.0
73	0.0297	327.9	377.2	201.4	0.0779	903.5	989.7	555.0
Totals =	0.6596	4185.7	4815.0	1929.3	0.0341	4829.8	5290.7	2452.2

Schematically, the problem is as follows:

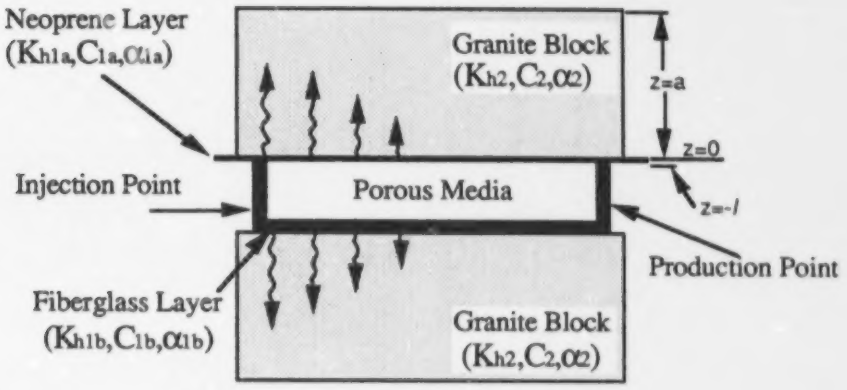

Figure B3

The cap and base rock are of thickness a and it is assumed that the thickness of the block is such that after a long experiment the boundary effects of the block are not felt. The overlapping of the granite block eliminates the heat losses out the sides of the block.

The differential equations describing the heat transfer problem are:

$$\frac{\partial^2 T_1}{\partial z^2} - \frac{1}{\alpha_1}\frac{\partial T_1}{\partial t} = 0 \qquad -l < z < 0, \quad t > 0 \qquad \text{(B6)}$$

$$\frac{\partial^2 T_2}{\partial z^2} - \frac{1}{\alpha_2}\frac{\partial T_2}{\partial t} = 0 \qquad z > 0, \; t > 0 \qquad \text{(B7)}$$

The above partial differential equations are for both regions (Neoprene or fiberglass, and granite). They are subject to the following initial and boundary conditions:

Initial Condition: $T(z,t=0) = 3.0°C$

Boundary Conditions: a) $T(z=-l,t) = 70.0°C$ Lower Boundary

b) $T(z=a,t) = 3.0°C$ Upper Boundary

Assuming no contact resistance at the surface of separation and to ensure continuity in the system at the interface between the Neoprene layer and the granite block the following additional conditions are:

$$c)\ T_1 = T_2\ ,\ \text{For } z = 0$$

$$d)\ K_{h1}\frac{\partial T_1}{\partial t} = K_{h2}\frac{\partial T_2}{\partial t},\ \text{for } z = 0$$

The solution of Equations (B6) and (B7) will give a temperature distribution in the vertical plane of the granite blocks. The temperature distribution and the specific heat capacity of the granite were then used to determine the energy stored in the granite blocks.

Analytical Solution

In terms of an analytical solution, Carslaw and Jaeger[45] provided the following solution to Equations (B6) and (B7). This is the closest approximation to the solution for the actual problem:

$$T_1 = \frac{T^*(K_{h1}a - K_{h2}x)}{K_{h1}a + K_{h2}l} \qquad \text{(B8)}$$

$$-2T^*\sum_{m=1}^{\infty}\frac{\{\cos(\beta_m z)\sin(ka\beta_m) - \sigma\sin(\beta_m z)\cos(ka\beta_m)\}}{\beta_m\{(l+\sigma ka)\sin(\beta_m l)\sin(ka) - (\sigma l + ka)\cos(\beta_m l)\cos(ka\beta_m)\}}$$

$$\bullet\exp-(K_{h1}\beta_m^2 t)$$

$$T_2 = \frac{T^*K_{h1}(a - z)}{K_{h1}a + K_{h2}l} \qquad \text{(B9)}$$

$$-2T^*\sum_{m=1}^{\infty}\frac{\sin[(k\beta_m(a-z)]}{\beta_m\{(l+\sigma ka)\sin(\beta_m l)\sin(ka) - (\sigma l + ka)\cos(\beta_m l)\cos(ka\beta_m)\}}$$

$$\bullet\exp-(K_{h2}\beta_m^2 t)$$

The above equations are Equations 30 and 31, Case 3, Section 8, Chapter 12 of (Ref. 45). In the above equations ,

$$\alpha = \frac{K_{hi}}{C_i}, \quad k = \left(\frac{\alpha_2}{\alpha_2}\right)^{1/2}, \quad \sigma = \frac{K_{h2}k}{k_{h1}}, \text{ and } \quad \alpha = \frac{\sigma - 1}{\sigma + 1}$$

and β_m, m=1,2,3,..., are the roots of:

$$\cos(\beta l)\sin(k\beta a) + \sigma \sin(\beta l)\cos(k\beta a) = 0$$

A simpler approach is to use the Stehfest algorithm to invert the solution in Laplace space to real space. The solution in Laplace space is:

$$\overline{T}_1 = \frac{T^*\{\cosh(q_1 z)\sinh(q_2 a) - \sigma \sinh(q_1 z)\cosh(q_2 a)\}}{P\{\cosh(q_1 l)\sinh(q_2 a) + \sigma \sinh(q_1 l)\cosh(q_2 a)\}} \tag{B10}$$

$$\overline{T}_2 = \frac{T^* \sinh[q_2(a - z)]}{P\{\cosh(q_1 l)\sinh(q_2 a) + \sigma \sinh(q_1 l)\cosh(q_2 a)\}} \tag{B11}$$

The above equations are Equations 27 and 28, Case 3 ,Section 8, Chapter 12 (Ref. 46). In the above equations,

$$q_1 = (P/\alpha_1)^{1/2}, \quad \text{and} \quad q_2 = (P/\alpha_2)^{1/2}$$

k, σ and α are defined previously.

A computer program written to solve Equations (B10) and (B11) is listed in Appendix C. The data generated by it are in Table B4. In Table B4 the results of a sensitivity analysis is also presented. The first variable tested was the Laplace parameter (P). It can be seen that increasing or decreasing the value of P by two units changes the magnitude of the temperature distribution by about 10°C. Next, the effect of the Neoprene layer was examined. This was done by changing the thermal properties of the Neoprene to that of granite. It can be seen that the resulting temperature distribution has temperatures that are inconsistent with what is possible. A further area investigated was contact resistance. This was done with the information given when the temperature difference between the Neoprene and the reservoir were measured. The difference was about 30°C and so $T_{res.}$ was given a reduced value of 40°C. From this smaller temperature gradient the temperatures near the outer boundary are lower, as expected. This would reduce the heat transfer to the over/underburden. The last area looked at was

Table B4 - Sensitivity of the Solution Presented by Carslaw and Jaeger

Distance From Res. (m)	Number of Slices per Layer: Neoprene 20, Granite 30 Reservoir Contact Temperature =70° C P=20 °C	P=18 °C	P=22 °C	Neoprene= Granite P=20 °C	Tres.=40 P=20 °C
0.0002	60.7	52.6	68.9	235.3	34.7
0.0003	51.6	44.3	59.0	234.5	29.5
0.0005	42.5	36.1	49.1	233.7	24.3
0.0006	33.3	27.8	39.1	232.9	19.1
0.0008	69.4	60.5	78.3	234.5	39.6
0.0010	69.3	60.5	78.2	234.2	39.6
0.0011	69.2	60.4	78.1	233.9	39.5
0.0013	69.1	60.3	78.0	233.6	39.5
0.0014	69.0	60.2	78.0	233.3	39.4
0.0016	68.9	60.1	77.9	233.0	39.4
0.0018	68.8	60.0	77.8	232.7	39.3
0.0019	68.7	60.0	77.7	232.4	39.3
0.0021	68.6	59.9	77.6	232.1	39.2
0.0022	68.5	59.8	77.5	231.8	39.2
0.0024	68.5	59.7	77.4	231.5	39.1
0.0025	68.4	59.6	77.3	231.2	39.1
0.0027	68.3	59.6	77.2	230.9	39.0
0.0029	68.2	59.5	77.1	230.6	39.0
0.0030	68.1	59.4	77.0	230.3	38.9
0.0032	68.0	59.3	76.9	230.0	38.9
0.0074	65.7	57.2	74.3	222.1	37.5
0.0148	61.7	53.6	70.0	208.8	35.3
0.0222	58.0	50.3	65.9	196.2	33.2
0.0296	54.5	47.1	62.0	184.2	31.1
0.0370	51.1	44.1	58.3	172.8	29.2
0.0445	47.9	41.2	54.8	162.0	27.4
0.0519	44.9	38.5	51.4	151.8	25.6
0.0593	42.0	36.0	48.2	142.0	24.0
0.0667	39.2	33.5	45.1	132.7	22.4
0.0741	36.6	31.2	42.2	123.8	20.9
0.0815	34.1	29.0	39.3	115.3	19.5
0.0889	31.7	26.9	36.6	107.2	18.1
0.0963	29.4	24.9	34.0	99.5	16.8
0.1037	27.2	23.0	31.5	92.0	15.6
0.1111	25.1	21.2	29.1	84.9	14.3
0.1185	23.1	19.5	26.8	78.1	13.2
0.1259	21.1	17.8	24.6	71.5	12.1
0.1333	19.3	16.2	22.4	65.1	11.0
0.1407	17.4	14.6	20.3	59.0	10.0
0.1482	15.7	13.2	18.3	53.0	9.0
0.1556	14.0	11.7	16.3	47.2	8.0
0.1630	12.3	10.3	14.4	41.6	7.0
0.1704	10.7	8.9	12.5	36.1	6.1
0.1778	9.1	7.6	10.6	30.7	5.2
0.1852	7.5	6.3	8.8	25.5	4.3
0.1926	6.0	5.0	7.0	20.3	3.4
0.2000	4.5	3.7	5.3	15.1	2.6
0.2074	3.0	2.5	3.5	10.1	1.7
0.2148	1.5	1.2	1.7	5.0	0.8
0.2222	0.0	0.0	0.0	0.0	0.0

Table B4 (continued)

Change Number of Slices in each layer

Distance From Res. (m)	20/20 P=20 °C	Distance From Res. (m)	Slices 10:30 °C
0.0002	60.7	0.0003	51.6
0.0003	51.6	0.0006	33.3
0.0005	42.5	0.0010	15.1
0.0006	33.3	0.0013	-3.1
0.0008	69.4	0.0016	68.9
0.0010	69.3	0.0019	68.7
0.0011	69.2	0.0022	68.5
0.0013	69.1	0.0025	68.4
0.0014	69.0	0.0029	68.2
0.0016	68.9	0.0032	68.0
0.0018	68.8	0.0074	65.7
0.0019	68.7	0.0148	61.7
0.0021	68.6	0.0222	58.0
0.0022	68.5	0.0296	54.5
0.0024	68.5	0.0370	51.1
0.0025	68.4	0.0445	47.9
0.0027	68.3	0.0519	44.9
0.0029	68.2	0.0593	42.0
0.0030	68.1	0.0667	39.2
0.0032	68.0	0.0741	36.6
0.0111	63.7	0.0815	34.1
0.0222	58.0	0.0889	31.7
0.0333	52.8	0.0963	29.4
0.0445	47.9	0.1037	27.2
0.0556	43.4	0.1111	25.1
0.0667	39.2	0.1185	23.1
0.0778	35.3	0.1259	21.1
0.0889	31.7	0.1333	19.3
0.1000	28.3	0.1407	17.4
0.1111	25.1	0.1482	15.7
0.1222	22.1	0.1556	14.0
0.1333	19.3	0.1630	12.3
0.1445	16.6	0.1704	10.7
0.1556	14.0	0.1778	9.1
0.1667	11.5	0.1852	7.5
0.1778	9.1	0.1926	6.0
0.1889	6.8	0.2000	4.5
0.2000	4.5	0.2074	3.0
0.2111	2.2	0.2148	1.5
0.2222	0.0	0.2222	0.0

the number of slices for each layer. Reducing the number of slices in the granite layer does not affect the magnitude of the temperatures at the corresponding nodes. In the case of the thin Neoprene layer, reducing the number of slices causes some instability in the temperature at the first four nodes. The temperatures after this unstable area corresponds to those of the base run. It can be concluded that the number of slices is very important in the thin Neoprene layer. The instability in the first few nodes is magnified when there are not enough slices.

Numerical Solution

The development of the numerical solution involved the use of Crank-Nicholson discretization of the equations B1 and B2, subject to the initial and boundary conditions as stated above. The general form of the discretization of the governing equation is:

$$\frac{1}{\alpha}\left[\frac{T_i^{n+1}-T_i^n}{\Delta t}\right]-\frac{1}{2}\left[\frac{T_{i-1}^n-2T_i^n+T_{i+1}^n}{\Delta z^2}+\frac{T_{i-1}^{n+1}-2T_i^{n+1}+T_{i+1}^{n+1}}{\Delta z^2}\right]=0 \qquad \text{(B12)}$$

Rearranging equation (B12) gives:

$$T_i^{n+1}-T_i^n-\frac{\alpha_1\Delta t}{2\Delta z_i^2}\left[T_{i-1}^n-2T_i^n+T_{i+1}^n-2T_i^{n+1}+T_{i+1}^{n+1}\right]=0 \qquad \text{(B13)}$$

Define $R = \alpha\Delta t / 2\Delta z^2$, for the Neoprene or

fiberglass layer $R_1 = \alpha_1\Delta t / 2\Delta z_1^2$

for the granite block $R_2 = \alpha_2\Delta t / 2\Delta z_2^2$

Substitute in the definition for R, for the Neoprene or fiberglass layer results in:

$$-R_1T_{l_{i-1}}^{n+1}+(1+2R_1)T_{l_i}^{n+1}-R_1T_{i+1}^{n+1} = R_1T_{l_{i-1}}^n+(1-2R_1)T_{l_i}^n+R_1T_{l_{i+1}}^n \qquad \text{(B14)}$$

This equation was written for every block i1, with i1 = 1, 2, 3, ..., N1, with N1 being the number of slices that the Neoprene or fiberglass layer is cut into.

For block i1 = 1 (z = 0): $T_{l_1} = 70.0°C$ for all times

For block i1 = 2: [$z = l/(N1 - 1)$]

$$-R_1 T_{l_1}^{n+1} + (1+2R_1) T_{l_2}^{n+1} - R_1 T_3^{n+1} = R_1 T_{l_1}^{n} + (1-2R_1) T_{l_2}^{n} + R_1 T_{l_3}^{n} \tag{B15}$$

For block i1 = N1:

$$\left.\frac{\partial T_1}{\partial z}\right|_{z_1} = \frac{T_{l_{N1+1}}^{n+1} - T_{l_{N1-1}}^{n+1}}{2\Delta z_1} = \frac{a}{K_{h1}} \tag{B16}$$

Rearranging the above equation gives:

$$T_{l_{N1+1}}^{n+1} = \frac{2a\Delta z_1}{K_{h1}} + T_{l_{N1-1}}^{n+1} \tag{B17}$$

Combining the above equations and equation (B14) results in:

$$-R_1 T_{l_{N1-1}}^{n+1} + (1+2R_1) T_{l_{N1}}^{n+1} - R_1\left[\frac{2a\Delta z_1}{K_{h1}} + T_{l_{N1+1}}^{n+1}\right] = R_1 T_{l_{N1-1}}^{n} + (1-2R_1) T_{l_{N1}}^{n} + R_1\left[\frac{2a\Delta z_1}{K_{h1}} + T_{l_{N1-1}}^{n}\right] \tag{B18}$$

Simplifying:

$$-2R_1 T_{l_{N1-1}}^{n+1} + (1+2R_1) T_{l_{N1}}^{n+1} = 2R_1 T_{l_{N1-1}}^{n} + (1-2R_1) T_{l_{N1}}^{n} + \frac{4a\Delta z_1 R_1}{K_{h1}} \tag{B19}$$

The resulting system of equations is tri-diagonal. As such, Thomas' algorithm can be used to solve the the temperature distribution in region 1 (T_1). When this is determined , T_1 (N1) = T_2 (1)

For region 2 (granite block) again using the same development as above results in:

$$-2R_2T_{2_{i-1}}^{n+1} + (1+2R_2)T_{2_i}^{n+1} = 2R_2T_{2_{i-1}}^{n} + (1-2R_2)T_{2_i}^{n} - \frac{4a\Delta z_2 R_2}{K_{h2}} \quad \text{(B20)}$$

Again the resulting system of equations is tri-diagonal. As before, Thomas' algorithm can be used to solve for the temperature distribution in the granite block (T_2). A sample output is presented in Table B5. The resulting temperature distribution is then used to calculate the energy stored in the granite block. In Table B6 a sensitivity test was performed on some of the parameters. The first parameter tested was A. It can be seen that the value of A does not greatly change the solution until it approaches unity. The effect of changing the properties of the Neoprene to those of the granite showed a negligible difference in the solution. The number of slices was examined and it can be seen that there is little effect on the solution when the number of slices was doubled.

The resulting heat loss to the overburden and underburden for these two cases was calculated to be about 665 kJ, which is a more realistic value than obtained from Equation (B5). Furthermore it is close to the 735 kJ that was accounted for in the heat loss in Equation (B1). Figure B4 shows the comparison of the temperature distribution as given by these two solution methods. It can be seen that their results agree with one another quite closely. It can also be seen that the analytical solution has some instability in the Neoprene layer which is closest to the heat source and should be at 70°C.

Table B5 — Sensitivity of the Crank-Nicholson Discrietization Method

Distance From Res. (m)	A=0.0001 °C	A=0.001 °C	A=0.010 °C	A=0.100 °C	A=1.000 °C	No Neo. °C	Δ Neo Considered °C	0° Initial °C	Double # of Slices (m)	°C
0.0000	70.00	70.00	70.00	70.00	70.00	70.00	40.00	70.00	0.0000	70.00
0.0032	69.99	70.06	71.40	80.37	173.66	69.97	40.00	70.01	0.0032	69.98
0.0254	58.93	58.99	59.80	67.00	147.38	58.94	33.89	58.43	0.0143	64.45
0.0476	48.33	48.37	49.02	55.49	120.10	48.36	28.03	47.34	0.0254	58.95
0.0698	38.60	38.64	39.14	44.23	95.08	38.64	22.66	37.17	0.0365	53.56
0.0921	30.05	30.08	30.45	34.33	73.06	30.10	17.94	28.24	0.0476	48.35
0.1143	22.83	22.85	23.12	25.96	54.43	22.88	13.95	20.69	0.0587	43.36
0.1365	16.94	16.96	17.14	19.15	39.23	16.99	10.70	14.54	0.0698	38.63
0.1587	12.27	12.28	12.40	13.74	27.14	12.31	8.12	9.67	0.0810	34.19
0.1810	8.60	8.60	8.68	9.49	17.59	8.63	6.09	5.84	0.0921	30.07
0.2032	5.62	5.62	5.66	6.04	9.84	5.63	4.45	2.73	0.0103	26.28
0.2254	3.00	3.00	3.00	3.00	3.00	3.00	3.00	0.00	0.0114	22.84
									0.1254	19.72
									0.1365	16.94
									0.1476	14.46
									0.1587	12.26
									0.1699	10.32
									0.1810	8.59
									0.1921	7.03
									0.2032	5.61
									0.2143	4.28
									0.2254	3.00

Thermal Conductivity of Neoprene:	0.00003 kW/mK
Specific Heat Capacity of Neoprene:	140.7 kJ/m3K
Thermal Conductivity of Granite:	0.0030 kW/mK
Specific Heat Capacity of Granite:	2112.1 kJ/m3K
Thickness of Neoprene Layer:	0.003175 m
Thickness of Granite Block:	0.222225 m

Table B6 — Heat Distribution in Overburden Using Two Different Solution Methods.

Carslaw & Jaegar Solution Ref. No. 45				Discretized Fouriers's Equation	
Distance From Heat Source	Temperature	Distance From Heat Source Con't	Temperature	Distance From Heat Source	Temperature
m	°C	m	°C	m	°C
0.00016	60.694	0.12593	21.137	0.00000	70.000
0.00032	51.575	0.13334	19.256	0.00300	66.140
0.00048	42.457	0.14074	17.438	0.01100	62.310
0.00064	33.339	0.14815	15.677	0.01900	58.810
0.00079	69.359	0.15556	13.967	0.02600	54.770
0.00095	69.268	0.16297	12.302	0.03400	51.110
0.00111	69.178	0.17037	10.678	0.04100	47.550
0.00127	69.087	0.17778	9.089	0.04900	44.090
0.00143	68.997	0.18519	7.529	0.05700	40.750
0.00159	68.907	0.19260	5.994	0.06400	37.550
0.00175	68.817	0.20000	4.479	0.08200	34.490
0.00191	68.727	0.20741	2.978	0.08000	31.590
0.00206	68.637	0.21482	1.486	0.08700	28.840
0.00222	68.547	0.22223	0.000	0.09500	26.260
0.00238	68.457			0.10300	23.830
0.00254	68.368			0.11000	21.570
0.00270	68.278			0.11800	19.480
0.00286	68.189			0.12600	17.530
0.00302	68.099			0.13300	15.740
0.00318	68.010			0.14100	14.090
0.00741	65.670			0.14900	12.580
0.01482	61.740			0.15600	11.190
0.02222	58.012			0.16400	9.910
0.02963	54.473			0.17200	8.730
0.03704	51.112			0.17900	7.640
0.04445	47.918			0.18700	6.620
0.05185	44.880			0.19500	5.660
0.05926	41.989			0.20200	4.750
0.06667	39.235			0.21000	3.870
0.07408	36.609			0.21800	3.000
0.08148	34.102				
0.08889	31.707				
0.09630	29.415				
0.10371	27.219				
0.11111	25.112				
0.11852	23.086				
0.12593	21.137				

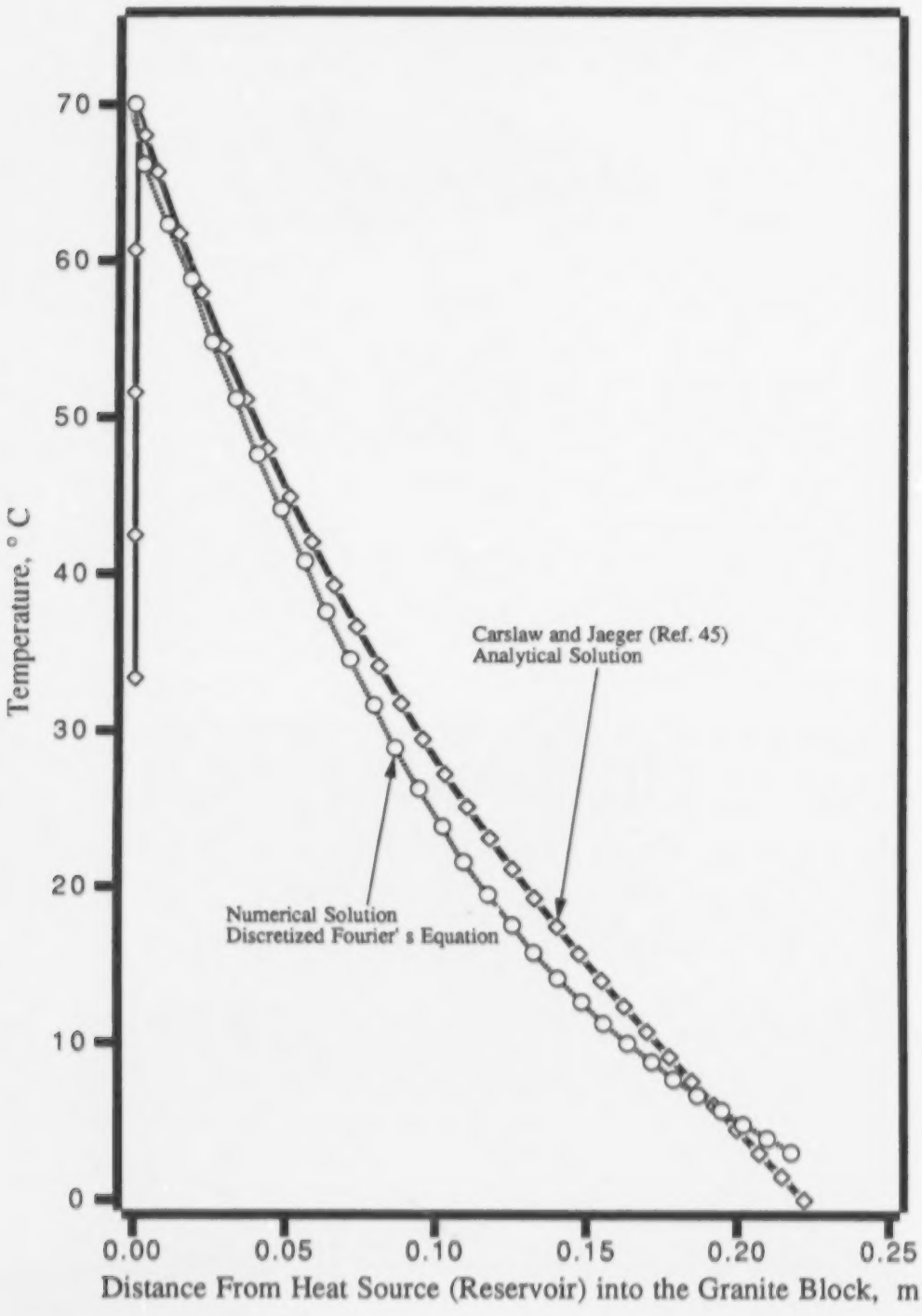

Figure B4 — Temperature Distribution in the Cap Rock vs. Distance From Heat Source. Two solutions: Numerical Discretization of Fourier' s Equation vs. Analytical Solution from Carslaw and Jaeger (Ref. 45).

Appendix C: Computer Programs

```
      PROGRAM CARSLAW
C   LAPLACE TRANSFORMATION:
C   PROBLEM IN LINEAR FLOW
C   COMPOSITE SOLID
C   INITIALIZE VARIABLES
      IMPLICIT REAL*8 (A - H,O - Z)
      INTEGER N1,N2,M,J
      REAL*8  KH1,KH2
      COMMON TRES,THETA,DX,J
C   ASSIGN INITIAL VALUES
      DATA THICK1,THICK2, KH1, KH2, CH1, CH2/0.003175,
     +     0.222225, 0.000030, 0.0030, 140.70, 2112.1/
      P = 18.00
      TRES = 70.0D0
      M = 50
      N1 = 20
      N2 = 30
      TZ1=THICK1/N1
      TZ2=THICK2/N2
C   CALCULATE A CONSTANT VALUE
      THETA = DSQRT(KH2*CH2/(KH1*CH1))
      DO 10 J=1,M
      IF (J.LE.N1) THEN
        DX= TZ1*J
      ELSE
        DX=TZ2*(J-N1)
      ENDIF
      CALL INVERT(P,TEMP)
      WRITE(6,104) DX,TEMP
 104  FORMAT('DISTANCE =',F8.5,'    ','TEMP = ',F7.3)
 10   CONTINUE
      STOP
      END
*****************************************************************
*                    THE STEHFEST ALGORITHEM
*****************************************************************
      SUBROUTINE INVERT(TD,TEMP)
*        THIS SUBRUINTINE COMPUTES NUMERICALLY
*        THE LAPLACE TRANSFROM INVERSE OF F(S)
      IMPLICIT REAL*8(A - H,O - Z)
      INTEGER N,M
      COMMON TRES,THETA,DX,J
      DIMENSION G(50), V(50), H(25)
*
*        NOW IF THE ARRAY V(I) WAS COMPUTED BEFORE THE PROGRAM
*        GOES DIRECTLY TO THE END OF THE SUBRUTINE TO CALCULATE
*        F(S)
*
      N=8
      IF (N .EQ. M) GO TO 130
      M = N
      DLOGTW = 0.6931471805599
      NH = N / 2
*
*        THE FACTORIALS OF 1 TO N ARE CALCULATED INTO ARRAY G.
*
      G(1) = 1
      DO 10 I = 2, N
```

```
      G(I) = G(I - 1) * I
   10 CONTINUE
*
*     TERMS WITH K ONLY ARE CALCULATED INTO ARRAYH.
*
      H(1) = 2. / G(NH - 1)
      DO 40 I = 2, NH
        FI = I
        IF (I - NH) 20, 30, 40
   20   H(I) = FI ** NH * G(2*I) / (G(NH - I)*G(I)*G(I - 1))
        GO TO 40
   30   H(I) = FI ** NH * G(2*I) / (G(I)*G(I - 1))
   40 CONTINUE
*
*       THE TERMS (-1)**NH+1 ARE CALCULATED.
*       FIRST THE TERM FOR I=1
      SN = 2 * (NH - NH/2*2) - 1
*
*       THE REST OF THE SN'S ARE CALCULATED IN THE MAIN ROUTINE.
*
*       THE ARRAY V(I) IS CALCULATED.
      DO 120 I = 1, N
*
*       FIRST SET V(I) =0
        V(I) = 0
*
*       THE LIMITS FOR K ARE ESTABLISHED.
*       THE LOWER LIMIT IS K1=INTEG((I+1/2))
        K1 = (I + 1) / 2
*
*       THE UPPER LIMIT IS K2=MIN(I,N/2)
        K2 = I
        IF (K2 - NH) 60, 60, 50
   50   K2 = NH
*       THE SUMATION TERM IN V(I) IS CALCULATED.
*
   60   DO 110 K = K1, K2
          IF (2*K - I) 70, 90, 70
   70     IF (I - K) 80, 100, 80
   80     V(I) = V(I) + H(K) / (G(I - K)*G(2*K - I))
          GO TO 110
   90     V(I) = V(I) + H(K) / G(I - K)
          GO TO 110
  100     V(I) = V(I) + H(K) / G(2*K - I)
  110   CONTINUE
*
*       THE V(I) ARRAY IS FINALLY CALCULATED BY WEIGHTING
*       ACCORING TO SN.
        V(I) = SN * V(I)
*
*       THE TERM SN CHANGES ITS SIGN EACH INTERATION.
        SN = -SN
  120 CONTINUE
*
*       THE NUMERICAL APPROXIMATION IS CALCULATED.
  130 PD = 0.0
      A = DLOGTW / TD
      DO 140 I = 1, N
```

```
        ARG = A * I
        CALL LAP(ARG,TEMP)
        PD = PD + V(I) * PWDL
  140 CONTINUE
      PD = PD * A
  150 RETURN
      END
*
*   SUBROUTINE LAP HAS THE FUNCTIONS OF INTEREST
*
      SUBROUTINE LAP(P,TEMP)
      IMPLICIT REAL*8(A-H,O-Z)
      REAL*8 KH1,KH2
      COMMON TRES,THETA,DX,J
      DATA THICK1,THICK2,KH1,KH2,CH1,CH2/0.003175,
     +     0.222225,0.000030,0.0030,140.7,2112.1/
      PI=DACOS(-1.0D0)
      Q1 = DSQRT(P*CH1/KH1)
      Q2 = DSQRT(P*CH2/KH2)
      Q1L = Q1*THICK1
      Q1X = Q1*DX
      Q2A = Q2*THICK2
      Q2AX = Q2*(THICK2-DX)
      CQ1X = DCOSH(Q1X*PI/180.0D0)
      SQ2A = DSINH(Q2A*PI/180.0D0)
      SQ1X = DSINH(Q1X*PI/180.0D0)
      CQ2A = DCOSH(Q2A*PI/180.0D0)
      CQ1L = DCOSH(Q1L*PI/180.0D0)
      SQ1L = DSINH(Q1L*PI/180.0D0)
      SQ2AX =DSINH(Q2AX*PI/180.0D0)
      DENOM = P*(CQ1L*SQ2A+THETA*SQ1L*CQ2A)
      IF (J.LE.4)THEN
        TEMP=(TRES*(CQ1X*SQ2A-THETA*SQ1X*CQ2A))/DENOM
      ELSE
        TEMP=TRES*SQ2AX/DENOM
      ENDIF
      RETURN
      END
```

This program solves the Crank-Nicholson discretization of Fouriers' s heat flow equation.

```
C    INITIALIZE VARIABLES
       INTEGER N1,N2,I,J,I1,I2,IF1,IF2,L1R1,L1R2,L2R2
       REAL A1(90),B1(90),C1(90),D1(90),V1(90),T1(90,55),T2(90,55),TZ1,
      +     TZ2,THICK1,THICK2,DT,TOTIME,TIME,KH1,KH2,CH1,CH2,ALPHA1,
      +     ALPHA2,A,R1,R2,EXRHS,Z(90),A2(90),B2(90),C2(90),D2(90),V2(90)
C    ASSIGN INITIAL VALUES
       DATA THICK1,THICK2,KH1,KH2,CH1,CH2,DT,TOTIME/0.003175,0.22225,
      +     0.000030,0.0030,140.70,2112.1,102.0,4080.0/
       N1 = 5
       N2 = 11
       TZ1 = THICK1/(N1-1)
       TZ2 = THICK2/(N2-1)
       A = 0.00010
C    CALCULATE SOME CONSTANT VALUES
       ALPHA1 = KH1/CH1
       ALPHA2 = KH2/CH2
       R1 = ALPHA1*DT/(2.0*(TZ1**2))
       R2 = ALPHA2*DT/(2.0*(TZ2**2))
       EXRHS = 4.0*A*TZ1*R1/KH1
       WRITE(6,100)
       WRITE(6,101)
       WRITE(6,102)
       WRITE(6,103)
C    SPECIFY INITIAL CONDITION IN BOTH REGIONS
       TIME = 0.0
       J = 1
       DO 10 I1=1,N1
        T1(I1,1) = 3.0
 10    CONTINUE
       DO 15 I2=1,N2
        T2(I2,1) = 3.0
 15    CONTINUE
C    SPECIFY LOWER AND UPPER BOUNDARY CONDITIONS
       DO 20 J=2,41
        T1(1,J) =  5.0
        T2(N2,J) = 3.0
 20    CONTINUE
       Z(1) = 3.0
       Z1 = (N1-1)*TZ1
       DO 25 I=2,N2+1
        Z(I) = (I-2)*TZ2 + Z1
 25    CONTINUE
       WRITE(6,104) (Z(I),I=1,N2+1)
       WRITE(6,105) TIME,T1(1,1),(T2(I2,1),I2=1,N2-1,1),T2(N2,1)
C    START CALCULATION LOOP TO DETERMINE FIRST THE DISTRIBUTION OF
C    TEMPERATURE IN THE LOWER REGION (NEOPRENE LAYER)
       J = 2
 1     TIME = (J-1)*DT
       IF1 = 2
       L1R1 = N1 - 1
       DO 30 I1=3,N1
        IF(I1.EQ.N1)THEN
         A1(I1) = -2.0*R1
        ELSE
         A1(I1) = -R1
```

```
      ENDIF
30    CONTINUE
      DO 35 I1=2,N1
       B1(I1) = 1.0 + 2.0*R1
35    CONTINUE
      DO 40 I1=2,L1R1
       C1(I1) = -R1
40    CONTINUE
      DO 45 I1=2,N1
       IF(I1.EQ.2)THEN
        D1(I1) = R1*(T1(I1-1,J)+T1(I1-1,J-1)) + (1.0-2*R1)*T1(I1,J-1)
     +           + R1*T1(I1+1,J-1)
       ELSEIF(I1.EQ.N1)THEN
        D1(I1) = 2*R1*T1(I1-1,J-1) + (1.0-2*R1)*T1(I1,J-1) + EXRHS
       ELSE
        D1(I1) = R1*T1(I1-1,J-1) + (1.0-2*R1)*T1(I1,J-1) +
     +           R1*T1(I1+1,J-1)
       ENDIF
45    CONTINUE
C     CALL SUBROUTINE TRIDAG TO SOLVE THE SYSTEM OF TRI-DIAGONAL EQUATIONS
C     USING THOM FOR TEMPERATURE DISTRIBUTION IN REGION IAS' S ALGORITHM
      CALL TRIDAG(IF1,N1,A1,B1,C1,D1,V1)
      DO 50 I1=2,N1
       T1(I1,J) = V1(I1)
50    CONTINUE
C     FIX THE BOUNDARY CONDITIONS AT THE INTERFACE BETWEEN THE TWO REGIONS
      T2(1,J) = T1(N1,J)
      IF2 = 2
      L1R2 = N2 - 1
      DO 55 I2=3,L1R2
       A2(I2) = -R2
55    CONTINUE
      DO 60 I2=2,L1R2
       B2(I2) = 1.0 + 2.0*R2
60    CONTINUE
      DO 65 I2=2,L1R2-1
       C2(I2) = -R2
65    CONTINUE
      DO 70 I2=2,L1R2
       IF(I2.EQ.2)THEN
        D2(I2) = R2*(T2(I2-1,J)+T2(I2-1,J-1)) + (1.0-2*R2)*T2(I2,J-1)
     +           + R2*T2(I2+1,J-1)
       ELSEIF(I2.EQ.L1R2)THEN
        D2(I2) = R2*T2(I2-1,J-1) + (1.0-2*R2)*T2(I2,J-1) +
     +           R2*(T2(I2+1,J)+T2(I2+1,J-1))
       ELSE
        D2(I2) = R2*T2(I2-1,J-1) + (1.0-2*R2)*T2(I2,J-1) +
     +           R2*T2(I2+1,J-1)
       ENDIF
70    CONTINUE
C     CALL SUBROUTINE TRIDAG TO SOLVE THE SYSTEM OF TRI-DIAGONAL EQUATIONS
C     USING THOMAS' S ALGORITHM FOR TEMPERATURE DISTRIBUTION IN REGION 2
      CALL TRIDAG(IF2,L1R2,A2,B2,C2,D2,V2)
      DO 75 I2=2,L1R2
       T2(I2,J) = V2(I2)
75    CONTINUE
      WRITE(6,105) TIME,T1(1,J),(T2(I2,J),I2=1,N2-1,1),T2(N2,J)
C     TEST FOR POSSIBLE TERMINATION OF CALCULATION LOOP
```

```
      IF(TIME.LT.TOTIME)THEN
        J = J + 1
        GO TO 1
      ELSE
        GO TO 2
      ENDIF
C   FORMAT STATEMENTS
 100  FORMAT('1','TEMPERATURE DISTRIBUTION IN CAP ROCK WITH TIME')
 101  FORMAT(' ',(LINEAR CONDUCTIVE HEAT TRANSFER PROCESS)')
 102  FORMAT(' ',T40,'****************************')
 103  FORMAT(' ','TIME(s)',3X,12('DIST.',4X))
 104  FORMAT(' ',T11,12(F6.4,'m',3X))
 105  FORMAT(' ',F7.2,2X,12(F6.2,3X))
C   END OF MAIN PROGRAM
 2    STOP
      END
C*******************************************************************************
**
      SUBROUTINE TRIDAG(IF,L,SA,SB,SC,D,V)
C   SUBROUTINE TO SOLVE A SYSTEM OF LINEAR SIMULTANEOUS EQUATIONS
C   HAVING A TRI-DIAGONAL COEFFICIENT MATRIX. THE EQUATIONS ARE
C   NUMBERED FROM IF TO L, AND THEIR SUB-DIAGONAL, MAIN-DIAGONAL, AND
C   SUPER-DIAGONAL COEFFICIENTS ARE STORED IN THE ARRAYS SA, SB, SC,
C   RESPECTIVELY. THE COMPUTED SOLUTION VECTOR IS STORED IN V(I)
C   DECLARE VARIABLES
      DIMENSION SA(91),SB(91),SC(91),D(91),V(91),BETA(91),GAMMA(91)
      BETA(IF) = SB(IF)
      GAMMA(IF) = D(IF)/BETA(IF)
      IFP = IF + 1
      DO 1 I=IFP,L
        BETA(I) = SB(I) - SA(I)*SC(I-1)/BETA(I-1)
 1      GAMMA(I) = (D(I) - SA(I)*GAMMA(I-1))/BETA(I)
      V(L) = GAMMA(L)
      LAST = L - IF
      DO 2 K=1,LAST
        I = L - K
 2      V(I) = GAMMA(I) - SC(I)*V(I+1)/BETA(I)
      RETURN
      END
```

Appendix D: Tables of Experimental Results

Table D1 — Run 108: Steamflood of a Homogeneous Model, Steam Quality = 14%.

HC Pore Volume:	12435 ml	Type of Oil Used:	Faxam-100
Pore Volume:	12510 ml	Initial Model Temperature:	3.0 °C
Bulk Volume:	42000 ml	Total Flow Rate of Steam:	227 ml/min.
Porosity:	33.8%	Steam Quality, fst:	0.14
Initial Oil Saturation:	92.0%	Total Steam Volume Injected:	21678 ml
Initial Water Saturation:	8.0%		
Net Oil Recovery:	**68.6%**	**Final Oil Saturation:**	**23.4%**

Cylinder No.	Total Vol. Produced (ml)	Instantaneous Oil Prod. (ml)	Cum. Oil Recovery (ml)	Cum. Oil Rec. %OOIP	Instantaneous Produced WOR	% Sample Vol. Oleic Phase	Cum. PV Injected
1	1500	720	720	5.8	1.1	48.0	0.34
2	2440	1025	1745	14.0	1.4	42.0	0.42
3	2080	350	2095	16.8	4.9	16.8	0.46
4	2160	870	2965	23.8	1.5	40.3	0.57
5	1880	820	3785	30.4	1.3	43.6	0.67
6	2140	720	4505	36.2	2.0	33.6	0.81
7	1790	500	5005	40.2	2.6	27.9	0.93
8	1840	450	5455	43.9	3.1	24.5	1.06
9	1880	420	5875	47.2	3.5	22.3	1.20
10	1880	365	6240	50.2	4.2	19.4	1.33
11	1890	370	6610	53.2	4.1	19.6	1.48
12	2000	360	6970	56.1	4.6	18.0	1.63
13	1870	310	7280	58.5	5.0	16.6	1.78
14	1780	290	7570	60.9	5.1	16.3	1.91
15	1420	405	7975	64.1	2.5	28.5	2.12
16	1260	560	8535	68.6	1.3	44.4	2.87

* Line indicates the start of the nitrogen injection

Table D2 — Run 109: Steamflood of a Homogeneous Model to 0.60 PV then Waterflood Using a Verical Injection Well and a Vertical Production Well.

HC Pore Volume:	13020 ml	Type of Oil Used:	Faxam-100
Pore Volume:	14190 ml	Initial Model Temperature:	1.5° C
Bulk Volume:	42005 ml	Total Flow Rate of Steam:	230 ml/min.
Porosity:	33.8%	Steam Quality, fst:	0.1
Initial Oil Saturation:	91.8%	Total Steam Volume Injected:	28980 ml (2.62 PV)
Initial Water Saturation	8.3%		
Net Oil Recovery:	**39.2%**	**Final Oil Saturation:**	**52.6%**

Cylinder No.	Total Vol. Produced (ml)	Instantaneous Oil Prod. (ml)	Cum. Oil Recovery (ml)	Cum. Oil Rec. %OOIP	Instantaneous Produced WOR	% Sample Vol. Oleic Phase	Cum. PV Injected
1	1395	495	495	3.8	1.8	35.5	0.21
2	2170	830	1325	10.2	1.6	38.2	0.32
3	1940	840	2165	16.6	1.3	43.3	0.38
4	1940	820	2985	22.9	1.4	42.3	0.46
5	1840	740	3725	28.6	1.5	40.2	0.56
6	1800	620	4345	33.4	1.9	34.4	0.74
7	1740	190	4535	34.8	8.2	10.9	0.91
8	1965	100	4635	35.6	18.7	5.1	1.05
9	1860	80	4715	36.2	22.3	4.3	1.18
10	1970	80	4795	36.8	23.6	4.1	1.31
11	1940	60	4855	37.3	31.3	3.1	1.45
12	1850	50	4905	37.7	36.0	2.7	1.58
13	1940	50	4955	38.1	37.8	2.6	1.72
14	1880	70	5025	38.6	25.9	3.7	1.85
15	1760	45	5070	38.9	38.1	2.6	1.97
16	1010	30	5100	39.2	32.7	3.0	2.04

* Line indicates the start of the waterflod

Table D3 — Run 110: Steamflood of a Homogeneous Model to 0.60 PV then Inject a 0.10 PV Nitrogen Gas Cap Prior to a Waterflood.

HC Pore Volume:	12690 ml	Type of Oil Used:	Faxam-100
Pore Volume:	13685 ml	Initial Model Temperature:	3.0 °C
Bulk Volume:	42000 ml	Total Flow Rate of Steam:	211 ml/min.
Porosity:	32.6%	Steam Quality, fst:	0.1
Initial Oil Saturation:	92.7%	Total Steam Volume Injected:	28034 ml
Initial Water Saturation:	7.3%		
Net Oil Recovery:	**41.2%**	**Final Oil Saturation:**	**51.6%**

Cylinder No.	Total Vol. Produced (ml)	Instantaneous Oil Prod. (ml)	Cum. Oil Recovery (ml)	Cum. Oil Rec. %OOIP	Instantaneous Produced WOR	% Sample Vol. Oleic Phase	Cum. PV Injected
1	100	60	60	0.5	0.7	60.0	0.13
2	2950	1260	1320	10.4	1.3	42.7	0.26
3	2400	980	2300	18.1	1.4	40.8	0.35
4	1880	965	3265	25.7	0.9	51.3	0.42
5	2100	860	4125	32.5	1.4	41.0	0.53
6	990	450	4575	36.1	1.2	45.5	0.63
7	1160	220	4795	37.8	4.3	19.0	0.78
8	1780	100	4895	38.6	16.8	5.6	0.91
9	1900	60	4955	39.0	30.7	3.2	1.04
10	1920	50	5005	39.4	37.4	2.6	1.17
11	1920	40	5045	39.8	47.0	2.1	1.30
12	1920	50	5095	40.1	37.4	2.6	1.43
13	1900	30	5125	40.4	62.3	1.6	1.56
14	2060	30	5155	40.6	67.7	1.5	1.70
15	1950	30	5185	40.9	64.0	1.5	1.83
16	1100	40	5225	41.2	26.5	3.6	1.90

* Line indicates the start of the nitrogen injection

Table D4 — Run 111: Steamflood of a Homogeneous Model to 1.00 PV Then Waterflood Using a Vertical Injection Well and a Vertical Production Well.

HC Pore Volume:	13185 ml	Type of Oil Used:	Faxam-100
Pore Volume:	14210 ml	Initial Model Temperature:	3.0 °C
Bulk Volume:	42000 ml	Total Flow Rate of Steam:	211 ml/min.
Porosity:	33.8%	Steam Quality, fst:	0.1
Initial Oil Saturation:	92.8%	Total Steam Volume Injected:	27113 ml
Initial Water Saturation:	7.2%		
Net Oil Recovery:	**59.4%**	**Final Oil Saturation:**	**33.4%**

Cylinder No.	Total Vol. Produced (ml)	Instantaneous Oil Prod. (ml)	Cum. Oil Recovery (ml)	Cum. Oil Rec. %OOIP	Instantaneous Produced WOR	% Sample Vol. Oleic Phase	Cum. PV Injected
1	1910	760	760	5.8	1.5	39.8	0.26
2	2080	720	1480	11.2	1.9	34.6	0.31
3	2530	970	2450	18.6	1.6	38.3	0.42
4	1820	920	3370	25.6	1.0	50.5	0.50
5	1920	980	4350	33.0	1.0	51.0	0.59
6	1865	805	5155	39.1	1.3	43.2	0.70
7	1870	710	5865	44.5	1.6	38.0	0.81
8	1995	755	6620	50.2	1.6	37.8	0.93
9	1355	375	6995	53.1	2.6	27.7	1.04
10	1780	400	7395	56.1	3.5	22.5	1.28
11	1795	185	7580	57.5	8.7	10.3	1.41
12	2050	60	7640	57.9	33.2	2.9	1.56
13	1880	40	7680	58.2	46.0	2.1	1.69
14	1930	50	7730	58.6	37.6	2.6	1.83
15	1970	50	7780	59.0	38.4	2.5	1.96
16	1290	50	7830	59.4	24.8	3.9	2.05

* Line indicates the start of the waterflood

Table D5 — Run 114: Waterflood to 1.00 PV then Steamflood a Homogeneous Model Using a Vertical Injection Well and a Vertical Production Well.

HC Pore Volume:	12470 ml	Type of Oil Used:	Faxam-100
Pore Volume:	13510 ml	Initial Model Temperature:	3.0 °C
Bulk Volume:	42000 ml	Total Flow Rate of Steam:	211 ml/min.
Porosity:	32.2%	Steam Quality,fst:	0.1
Initial Oil Saturation:	92.3%	Total Steam Volume Injected:	31780 ml
Net Oil Recovery:	**59.4%**	**Final Oil Saturation:**	**32.9%**

Cylinder No.	Total Vol. Produced (ml)	Instantaneous Oil Prod. (ml)	Cum. Oil Recovery (ml)	Cum. Oil Rec. %OOIP	Instantaneous Produced WOR	% Sample Vol. Oleic Phase	Cum. PV Injected
1	1620	380	380	3.0	3.3	23.5	0.21
2	2060	460	840	6.7	3.5	22.3	0.36
3	2280	320	1160	9.3	6.1	14.0	0.50
4	1720	200	1360	10.9	7.6	11.6	0.58
5	1600	240	1600	12.8	5.7	15.0	0.67
6	1860	240	1840	14.8	6.8	12.9	0.79
7	1720	140	1980	15.9	11.3	8.1	0.91
8	1860	120	2100	16.8	14.5	6.5	1.03
9	1780	120	2220	17.8	13.8	6.7	1.11
10	1820	160	2380	19.1	10.4	8.8	1.20
11	1780	440	2820	22.6	3.0	24.7	1.32
12	2040	680	3500	28.1	2.0	33.3	1.41
13	1860	740	4240	34.0	1.5	39.8	1.49
14	1930	740	4980	39.9	1.6	38.3	1.59
15	1830	540	5520	44.3	2.4	29.5	1.69
16	1940	460	5980	48.0	3.2	23.7	1.81
17	1820	360	6340	50.8	4.1	19.8	1.93
18	1920	360	6700	53.7	4.3	18.8	2.06
19	1920	360	7060	56.6	4.3	18.8	2.19
20	1970	350	7410	59.4	4.6	17.8	2.31
21	1380	240	7650	61.3	4.8	17.4	2.41

* Line indicates the start of the steamflood.

Table D6 — Run 115: Steamflood of a Homogeneous Model (Base Case).

HC Pore Volume:	12820 ml	Type of Oil Used:	Faxam-100
Pore Volume:	13620 ml	Initial Model Temperature:	3.0° C
Bulk Volume:	42000 ml	Total Flow Rate of Steam:	227 cc/min
Porosity:	32.1%	Steam Quality, fst:	0.10
Initial Oil Saturation:	94.1%	Total Steam Volume Injected:	29010 ml (2.13 PV)
Initial Water Saturation:	5.9%		
Net Oil Recovery:	**54.9%**	**Final Oil Saturation:**	**39.2%**

Cylinder No.	Total Vol. Produced (cc)	Instantaneous Oil Prod. (cc)	Cumulative Oil Recovery (cc)	Cum. Oil Rec. %OOIP	Instantaneous Produced WOR	% Sample Vol. Oleic Phase	Cum. PV Injected
1	1960	600	600	4.7	2.3	30.6	0.18
2	2120	840	1440	11.2	1.5	39.6	0.27
3	1710	620	2060	16.1	1.8	36.3	0.36
4	2060	680	2740	21.4	2.0	33.0	0.48
5	1600	480	3220	25.1	2.3	30.0	0.57
6	1860	480	3700	28.9	2.9	25.8	0.69
7	1760	400	4100	32.0	3.4	22.7	0.81
8	1880	380	4480	34.9	3.9	20.2	0.94
9	1700	320	4800	37.4	4.3	18.8	1.06
10	1980	360	5160	40.2	4.5	18.2	1.19
11	1760	320	5480	42.7	4.5	18.2	1.31
12	2140	320	5800	45.2	5.7	15.0	1.48
13	1740	260	6060	47.3	5.7	14.9	1.60
14	1820	300	6360	49.6	5.1	16.5	1.74
15	1840	180	6540	51.0	9.2	9.8	1.87
16	1770	250	6790	53.0	6.1	14.1	2.01
17	1670	250	7040	54.9	5.7	15.0	2.13

Table D7 — Run 120: Steamflood of a Multilayered Model Low Permeability Bottom Layer Using a Vertical Injection Well and a Vertical Production Well.

HC Pore Volume:	13550 ml	Type of Oil Used:	Faxam-100
Pore Volume:	14700 ml	Initial Model Temperature:	1.5° C
Bulk Volume:	42005 ml	Total Flow Rate of Steam:	230 ml/min.
Porosity:	35.0%	Steam Quality, fst:	0.1
Initial Oil Saturation:	92.2%	Total Steam Volume Injected:	31855 ml

Net Oil Recovery: 51.4% **Final Oil Saturation: 40.8%**

Cylinder No.	Total Vol. Produced (ml)	Instantaneous Oil Prod. (ml)	Cum. Oil Recovery (ml)	Cum. Oil Rec. %OOIP	Instantaneous Produced WOR	% Sample Vol. Oleic Phase	Cum. PV Injected
1	1700	360	360	2.7	3.7	21.2	0.20
2	2180	570	930	6.9	2.8	26.1	0.31
3	2210	830	1760	13.0	1.7	37.6	0.42
4	2090	800	2560	18.9	1.6	38.3	0.52
5	1850	630	3190	23.5	1.9	34.1	0.63
6	1770	530	3720	27.5	2.3	29.9	0.74
7	1670	470	4190	30.9	2.6	28.1	0.85
8	1710	420	4610	34.0	3.1	24.6	0.96
9	1720	340	4950	36.5	4.1	19.8	1.07
10	1650	320	5270	38.9	4.2	19.4	1.18
11	1610	270	5540	40.9	5.0	16.8	1.29
12	1770	250	5790	42.7	6.1	14.1	1.42
13	1680	220	6010	44.4	6.6	13.1	1.54
14	1740	220	6230	46.0	6.9	12.6	1.67
15	1680	200	6430	47.5	7.4	11.9	1.79
16	1680	190	6620	48.9	7.8	11.3	1.92
17	1660	160	6780	50.0	9.4	9.6	2.04
18	1600	180	6960	51.4	7.9	11.3	2.17

Table D8 — Run 121: Steamflood of a Homogeneous Model Using a Horizontal Injection Well Placed in the Middel of the Oil Zone and a Vertical Production Well.

HC Pore Volume:	12330 ml	Type of Oil Used:	Faxam-100
Pore Volume:	13180 ml	Initial Model Temperature:	1.5° C
Bulk Volume:	42005 ml	Total Flow Rate of Steam:	230 ml/min.
Porosity:	31.4%	Steam Quality, fst:	0.1
Initial Oil Saturation:	93.6%	Total Steam Volume Injected:	32660 ml

Net Oil Recovery: **50.7%** **Final Oil Saturation:** **42.9%**

Cylinder No.	Total Vol. Produced (ml)	Instantaneous Oil Prod. (ml)	Cum. Oil Recovery (ml)	Cum. Oil Rec. %OOIP	Instantaneous Produced WOR	% Sample Vol. Oleic Phase	Cum. PV Injected
1	2160	530	530	4.3	3.1	24.5	0.20
2	1760	570	1100	8.9	2.1	32.4	0.29
3	1820	620	1720	13.9	1.9	34.1	0.39
4	2520	680	2400	19.5	2.7	27.0	0.55
5	1780	450	2850	23.1	3.0	25.3	0.66
6	1990	370	3220	26.1	4.4	18.6	0.80
7	1960	320	3540	28.7	5.1	16.3	0.94
8	1950	300	3840	31.1	5.5	15.4	1.08
9	1950	280	4120	33.4	6.0	14.4	1.22
10	1820	220	4340	35.2	7.3	12.1	1.36
11	1930	240	4580	37.1	7.0	12.4	1.50
12	1910	250	4830	39.2	6.6	13.1	1.64
13	1920	240	5070	41.1	7.0	12.5	1.78
14	1980	200	5270	42.7	8.9	10.1	1.92
15	1870	390	5660	45.9	3.8	20.9	2.06
16	1850	230	5890	47.8	7.0	12.4	2.20
17	1790	180	6070	49.2	8.9	10.1	2.34
18	1810	180	6250	50.7	9.1	9.9	2.48

Table D9 — Run 124: Steamflood of a Multi-layered Model, Low Permeability Bottom Layer 0.10 PV Solvent Pre-flush, Using a Horizontal Injector and a Vertical Producer.

HC Pore Volume:	13600 ml	Type of Oil Used:	Faxam-100
Pore Volume:	14750 ml	Initial Model Temperature:	3.0 °C
Bulk Volume:	42000 ml	Total Flow Rate of Steam:	230 ml/min.
Porosity:	35.1%	Steam Quality, fst:	0.1
Initial Oil Saturation:	92.2%	Total Steam Volume Injected:	30360 ml

Net Oil Recovery: **49.8%** **Final Oil Saturation:** **42.4%**

Cylinder No.	Total Vol. Produced (ml)	Instantaneous Oil Prod. (ml)	Cum. Oil Recovery (ml)	Cum. Oil Rec. %OOIP	Instantaneous Produced WOR	% Sample Vol. Oleic Phase	Cum. PV Injected
1	1880	610	610	4.5	2.1	32.4	0.24
2	2000	520	1130	8.3	2.8	26.0	0.37
3	1720	460	1590	11.7	2.7	26.7	0.47
4	1770	450	2040	15.0	2.9	25.4	0.58
5	1760	440	2480	18.2	3.0	25.0	0.69
6	1760	440	2920	21.5	3.0	25.0	0.80
7	1740	420	3340	24.6	3.1	24.1	0.90
8	1750	390	3730	27.4	3.5	22.3	1.01
9	1760	380	4110	30.2	3.6	21.6	1.12
10	1680	350	4460	32.8	3.8	20.8	1.23
11	1630	350	4810	35.4	3.7	21.5	1.34
12	1780	370	5180	38.1	3.8	20.8	1.45
13	1620	280	5460	40.1	4.8	17.3	1.56
14	1540	270	5730	42.1	4.7	17.5	1.67
15	1520	250	5980	44.0	5.1	16.4	1.78
16	1480	240	6220	45.7	5.2	16.2	1.89
17	1540	280	6500	47.8	4.5	18.2	2.00
18	1600	270	6770	49.8	4.9	16.9	2.11

Table D10 — Run 125: Steamflood of a Homogeneous Model Using a Horizontal Injection Well Placed at the Bottom of the Oil Zone and a Vertical Production Well.

HC Pore Volume:	12640 ml	Type of Oil Used:	Faxam-100
Pore Volume:	13700 ml	Initial Model Temperature:	3.0 °C
Bulk Volume:	42000 ml	Total Flow Rate of Steam:	230 ml/min.
Porosity:	32.6%	Steam Quality, fst:	0.1
Initial Oil Saturation:	92.3%	Total Steam Volume Injected:	30360 ml
Initial Water Saturation:	7.7%		
Net Oil Recovery:	**54.9%**	**Final Oil Saturation:**	**37.4%**

Cylinder No.	Total Vol. Produced (ml)	Instantaneous Oil Prod. (ml)	Cum. Oil Recovery (ml)	Cum. Oil Rec. %OOIP	Instantaneous Produced WOR	% Sample Vol. Oleic Phase	Cum. PV Injected
1	2760	690	690	5.5	3.0	25.0	0.22
2	2060	720	1410	11.2	1.9	35.0	0.34
3	2160	750	2160	17.1	1.9	34.7	0.45
4	1760	560	2720	21.5	2.1	31.8	0.57
5	1880	550	3270	25.9	2.4	29.3	0.69
6	1820	530	3800	30.1	2.4	29.1	0.81
7	1720	420	4220	33.4	3.1	24.4	0.92
8	1660	340	4560	36.1	3.9	20.5	1.04
9	1620	300	4860	38.4	4.4	18.5	1.16
10	1520	280	5140	40.7	4.4	18.4	1.28
11	1600	270	5410	42.8	4.9	16.9	1.39
12	1560	260	5670	44.9	5.0	16.7	1.51
13	1550	240	5910	46.8	5.5	15.5	1.63
14	1600	230	6140	48.6	6.0	14.4	1.75
15	1540	200	6340	50.2	6.7	13.0	1.86
16	1500	200	6540	51.7	6.5	13.3	1.98
17	1540	200	6740	53.3	6.7	13.0	2.10
18	1520	200	6940	54.9	6.6	13.2	2.22

Table D11 — Run126: Steamflood of a Multi-layered Model, Low Permeability Bottom Layer Using a Horizontal Injection Well and a Vertical Production Well.

HC Pore Volume:	13740 ml	Type of Oil Used:	Faxam-100
Pore Volume:	15040 ml	Initial Model Temperature:	3.0 °C
Bulk Volume:	42000 ml	Total Flow Rate of Steam:	230 ml/min.
Porosity:	35.8%	Steam Quality, fst:	0.1
Initial Oil Saturation:	91.4%	Total Steam Volume Injected:	30590 ml
Initial Water Saturation:	8.6%		
Net Oil Recovery:	**45.5%**	**Final Oil Saturation:**	**45.8%**

Cylinder No.	Total Vol. Produced (ml)	Instantaneous Oil Prod. (ml)	Cum. Oil Recovery (ml)	Cum. Oil Rec. %OOIP	Instantaneous Produced WOR	% Sample Vol. Oleic Phase	Cum. PV Injected
1	1710	360	360	2.6	3.8	21.1	0.21
2	2200	750	1110	8.1	1.9	34.1	0.32
3	1960	620	1730	12.6	2.2	31.6	0.43
4	2010	590	2320	16.9	2.4	29.4	0.54
5	1830	410	2730	19.9	3.5	22.4	0.64
6	1750	340	3070	22.3	4.1	19.4	0.75
7	1710	305	3375	24.6	4.6	17.8	0.86
8	1720	290	3665	26.7	4.9	16.9	0.96
9	1690	260	3925	28.6	5.5	15.4	1.07
10	1860	430	4355	31.7	3.3	23.1	1.18
11	1610	210	4565	33.2	6.7	13.0	1.28
12	1670	230	4795	34.9	6.3	13.8	1.39
13	1780	420	5215	38.0	3.2	23.6	1.50
14	1720	240	5455	39.7	6.2	14.0	1.61
15	1630	220	5675	41.3	6.4	13.5	1.71
16	1620	210	5885	42.8	6.7	13.0	1.82
17	1540	160	6045	44.0	8.6	10.4	1.93
18	1680	210	6255	45.5	7.0	12.5	2.03

Table D12 — Run 127: Waterflood a Homogeneous Model to 1PV then Steamflood Using a Vertical Injection Well and a Vertical Production Well.

HC Pore Volume:	12370 ml	Type of Oil Used:	Faxam-100
Pore Volume:	13720 ml	Initial Model Temperature:	3.0 °C
Bulk Volume:	42000 ml	Total Flow Rate of Steam:	230 ml/min.
Porosity:	32.7%	Steam Quality, fst:	0.1
Initial Oil Saturation:	90.2%	Total Steam Volume Injected:	29900 ml
Initial Water Saturation:	9.8%		
Net Oil Recovery:	**47.3%**	**Final Oil Saturation:**	**42.8%**

Cylinder No.	Total Vol. Produced (ml)	Instantaneous Oil Prod. (ml)	Cum. Oil Recovery (ml)	Cum. Oil Rec. %OOIP	Instantaneous Produced WOR	% Sample Vol. Oleic Phase	Cum. PV Injected
1	1490	310	310	0.03	3.81	0.21	0.22
2	1450	270	580	0.05	4.37	0.19	0.34
3	1790	340	920	0.07	4.26	0.19	0.45
4	1920	235	1155	0.09	7.17	0.12	0.57
5	1955	285	1440	0.12	5.86	0.15	0.69
6	1895	215	1655	0.13	7.81	0.11	0.80
7	1755	155	1810	0.15	10.32	0.09	0.92
8	1290	120	1930	0.16	9.75	0.09	1.01
9	2120	130	2060	0.17	15.31	0.06	1.12
10	2050	120	2180	0.18	16.08	0.06	1.24
11	1890	335	2515	0.20	4.64	0.18	1.36
12	2400	650	3165	0.26	2.69	0.27	1.48
13	2150	660	3825	0.31	2.26	0.31	1.59
14	2000	560	4385	0.35	2.57	0.28	1.71
15	1860	460	4845	0.39	3.04	0.25	1.83
16	1790	380	5225	0.42	3.71	0.21	1.94
17	1710	330	5555	0.45	4.18	0.19	2.06
18	1720	300	5855	0.47	4.73	0.17	2.18

* Line indicates the start of the steamflood.

Table D13 — Run 132: Steamflood of a Homogeneous Model No Thermocouples Using a Vertical Injection Well and a Vertical Production Well.

HC Pore Volume:	12995 ml	Type of Oil Used:	Faxam-100
Pore Volume:	14150 ml	Initial Model Temperature:	3.0 °C
Bulk Volume:	42000 ml	Total Flow Rate of Steam:	230 ml/min.
Porosity:	33.7%	Steam Quality, fst:	0.1
Initial Oil Saturation:	91.8%	Total Steam Volume Injected:	30590 ml
Initial Water Saturation:	8.2%		
Net Oil Recovery:	**57.6%**	**Final Oil Saturation:**	**34.3%**

Cylinder No.	Total Vol. Produced (ml)	Instantaneous Oil Prod. (ml)	Cum. Oil Recovery (ml)	Cum. Oil Rec. %OOIP	Instantaneous Produced WOR	% Sample Vol. Oleic Phase	Cum. PV Injected
1	1790	490	490	3.8	2.7	27.4	0.23
2	2540	800	1290	9.9	2.2	31.5	0.33
3	1880	720	2010	15.5	1.6	38.3	0.41
4	1740	700	2710	20.9	1.5	40.2	0.49
5	1770	650	3360	25.9	1.7	36.7	0.58
6	1790	530	3890	29.9	2.4	29.6	0.68
7	1830	450	4340	33.4	3.1	24.6	0.80
8	1760	380	4720	36.3	3.6	21.6	0.91
9	1680	340	5060	38.9	3.9	20.2	1.02
10	1720	320	5380	41.4	4.4	18.6	1.14
11	1590	270	5650	43.5	4.9	17.0	1.25
12	1560	240	5890	45.3	5.5	15.4	1.37
13	1700	260	6150	47.3	5.5	15.3	1.48
14	1610	240	6390	49.2	5.7	14.9	1.59
15	1630	240	6630	51.0	5.8	14.7	1.71
16	1690	230	6860	52.8	6.3	13.6	1.82
17	1590	200	7060	54.3	7.0	12.6	1.93
18	1610	210	7270	55.9	6.7	13.0	2.05
19	1600	210	7480	57.6	6.6	13.1	2.16

Table D14 — Run 133: Steamflood of a Homogeneous Model Following the Re-plaining of the Model Tray Using A vertical Injection Well and a Vertical Production Well.

HC Pore Volume:	12980 ml	Type of Oil Used:	Faxam-100
Pore Volume:	14030 ml	Initial Model Temperature:	3.0 °C
Bulk Volume:	42000 ml	Total Flow Rate of Steam:	230 ml/min.
Porosity:	33.4%	Steam Quality, fst:	0.1
Initial Oil Saturation:	92.5%	Total Steam Volume Injected:	30935 ml
Initial Water Saturation:	7.5%		
Net Oil Recovery:	**59.6%**	**Final Oil Saturation:**	**33.0%**

Cylinder No.	Total Vol. Produced (ml)	Instantaneous Oil Prod. (ml)	Cum. Oil Recovery (ml)	Cum. Oil Rec. %OOIP	Instantaneous Produced WOR	% Sample Vol. Oleic Phase	Cum. PV Injected
1	1700	520	520	4.0	2.3	30.6	0.24
2	2000	470	990	7.6	3.3	23.5	0.34
3	1780	520	1510	11.6	2.4	29.2	0.39
4	1860	720	2230	17.2	1.6	38.7	0.48
5	2110	720	2950	22.7	1.9	34.1	0.60
6	1980	620	3570	27.5	2.2	31.3	0.71
7	1980	570	4140	31.9	2.5	28.8	0.83
8	1910	560	4700	36.2	2.4	29.3	0.94
9	1800	440	5140	39.6	3.1	24.4	1.06
10	1740	380	5520	42.5	3.6	21.8	1.17
11	1690	350	5870	45.2	3.8	20.7	1.29
12	1700	320	6190	47.7	4.3	18.8	1.40
13	1630	270	6460	49.8	5.0	16.6	1.52
14	1620	260	6720	51.8	5.2	16.0	1.63
15	1610	230	6950	53.5	6.0	14.3	1.75
16	1590	220	7170	55.2	6.2	13.8	1.86
17	1600	210	7380	56.9	6.6	13.1	1.98
18	1600	190	7570	58.3	7.4	11.9	2.09
19	1560	160	7730	59.6	8.8	10.3	2.20

Table D15 — Run 136: Steamflood of a Homogenous Model (Base Case), Using a Vertical Injection Well and a Vertical Production Well.

HC Pore Volume:	13250 ml	Type of Oil Used:	Faxam-100
Pore Volume:	14310 ml	Initial Model Temperature:	3.0° C
Bulk Volume:	42000 ml	Total Flow Rate of Steam:	211 ml/min.
Porosity:	34.1%	Steam Quality, fst:	0.1
Initial Oil Saturation:	92.6%	Total Steam Volume Injected:	24687 ml
Initial Water Saturation	7.4%		
Net Oil Recovery:	**47.7%**	**Final Oil Saturation:**	**44.9%**

Cylinder No.	Total Vol. Produced (ml)	Instantaneous Oil Prod. (ml)	Cum. Oil Recovery (ml)	Cum. Oil Rec. %OOIP	Instantaneous Produced WOR	% Sample Vol. Oleic Phase	Cum. PV Injected
1	1440	440	440	0.03	2.27	0.31	0.24
2	2200	520	960	0.07	3.23	0.24	0.32
3	1570	460	1420	0.11	2.41	0.29	0.40
4	1940	680	2100	0.16	1.85	0.35	0.49
5	1880	580	2680	0.20	2.24	0.31	0.59
6	1880	510	3190	0.24	2.69	0.27	0.69
7	1670	390	3580	0.27	3.28	0.23	0.80
8	1710	270	3850	0.29	5.33	0.16	0.90
9	1800	400	4250	0.32	3.50	0.22	1.00
10	1660	330	4580	0.35	4.03	0.20	1.11
11	1600	270	4850	0.37	4.93	0.17	1.21
12	1570	236	5086	0.38	5.65	0.15	1.31
13	1510	210	5296	0.40	6.19	0.14	1.42
14	1600	220	5516	0.42	6.27	0.14	1.52
15	1560	220	5736	0.43	6.09	0.14	1.62
16	1560	220	5956	0.45	6.09	0.14	1.73
17	1540	190	6146	0.46	7.11	0.12	1.83
18	1500	170	6316	0.48	7.82	0.11	1.93

Table D16 — Run 138: Steamflood of a Multi-layered Model Low Permeability Bottom Layer with a Fracture from the Vertical Injector to the Vertical Producer in Lower layer.

HC Pore Volume:	13845 ml	Type of Oil Used:	Faxam-100
Pore Volume:	14980 ml	Initial Model Temperature:	3.0 °C
Bulk Volume:	42000 ml	Total Flow Rate of Steam:	211 ml/min.
Porosity:	35.7%	Steam Quality, fst:	0.1
Initial Oil Saturation:	92.4%	Total Steam Volume Injected:	29540 ml
Initial Water Saturation:	7.6%		
Net Oil Recovery:	**48.8%**	**Final Oil Saturation:**	**43.6%**

Cylinder No.	Total Vol. Produced (ml)	Instantaneous Oil Prod. (ml)	Cum. Oil Recovery (ml)	Cum. Oil Rec. %OOIP	Instantaneous Produced WOR	% Sample Vol. Oleic Phase	Cum. PV Injected
1	2025	395	395	2.9	4.1	19.5	0.20
2	1920	440	835	6.0	3.4	22.9	0.30
3	1960	570	1405	10.1	2.4	29.1	0.39
4	1950	580	1985	14.3	2.4	29.7	0.49
5	1950	630	2615	18.9	2.1	32.3	0.59
6	1770	500	3115	22.5	2.5	28.2	0.69
7	1655	385	3500	25.3	3.3	23.3	0.79
8	1640	340	3840	27.7	3.8	20.7	0.89
9	1595	315	4155	30.0	4.1	19.7	0.99
10	1610	310	4465	32.2	4.2	19.3	1.08
11	1540	240	4705	34.0	5.4	15.6	1.18
12	1580	250	4955	35.8	5.3	15.8	1.28
13	1520	250	5205	37.6	5.1	16.4	1.38
14	1600	250	5455	39.4	5.4	15.6	1.48
15	1440	210	5665	40.9	5.9	14.6	1.58
16	1450	210	5875	42.4	5.9	14.5	1.68
17	1470	210	6085	44.0	6.0	14.3	1.77
18	1460	220	6305	45.5	5.6	15.1	1.87
19	1500	220	6525	47.1	5.8	14.7	1.97
20	1555	235	6760	48.8	5.6	15.1	2.07

Table D17 — Run 140: Steamflood of a Homogeneous Model to 2.00 PV then Gasflood Using Vertical Injection Well and a Vertical Production Well.

HC Pore Volume:	13470 ml	Type of Oil Used:	Faxam-100
Pore Volume:	14330 ml	Initial Model Temperature:	3.0 °C
Bulk Volume:	42000 ml	Total Flow Rate of Steam:	211 ml/min.
Porosity:	34.1%	Steam Quality, fst:	0.1
Initial Oil Saturation:	94.0%	Total Steam Volume Injected:	28692 ml (2.0 PV)
Initial Water Saturation:	6.0%	Total Nitrogen Injected:	20 PV
Net Oil Recovery:	**49.5%**	**Final Oil Saturation:**	**44.5%**

Cylinder No.	Total Vol. Produced (ml)	Instantaneous Oil Prod. (ml)	Cum. Oil Recovery (ml)	Cum. Oil Rec. %OOIP	Instantaneous Produced WOR	% Sample Vol. Oleic Phase	Cum. PV Injected
1	1780	550	550	4.1	2.2	30.9	0.24
2	1915	485	1035	7.7	2.9	25.3	0.29
3	1920	540	1575	11.7	2.6	28.1	0.39
4	1920	590	2165	16.1	2.3	30.7	0.49
5	1860	540	2705	20.1	2.4	29.0	0.60
6	1740	430	3135	23.3	3.0	24.7	0.70
7	1700	380	3515	26.1	3.5	22.4	0.80
8	1690	370	3885	28.8	3.6	21.9	0.91
9	1630	310	4195	31.1	4.3	19.0	1.01
10	1580	270	4465	33.1	4.9	17.1	1.11
11	1520	245	4710	35.0	5.2	16.1	1.21
12	1560	235	4945	36.7	5.6	15.1	1.32
13	1580	220	5165	38.3	6.2	13.9	1.42
14	1540	205	5370	39.9	6.5	13.3	1.52
15	1440	180	5550	41.2	7.0	12.5	1.63
16	1510	180	5730	42.5	7.4	11.9	1.73
17	1495	175	5905	43.8	7.5	11.7	1.83
18	1570	190	6095	45.2	7.3	12.1	1.94
19	1100	150	6245	46.4	6.3	13.6	2.00
20	1080	420	6665	49.5	1.6	38.9	22.00

Table D18 — Run 142: Steamflood of a Multi-layered Model Low Permeability Bottom Layer Using a Vertical Injection Well and a Vertical Production Well.

HC Pore Volume:	13915 ml	Type of Oil Used:	Faxam-100
Pore Volume:	14865 ml	Initial Model Temperature:	3.0 °C
Bulk Volume:	42000 ml	Total Flow Rate of Steam:	211 ml/min.
Porosity:	35.4%	Steam Quality, fst:	0.1
Initial Oil Saturation:	93.6%	Total Steam Volume Injected:	31017 ml (2.09 PV)
Initial Water Saturation:	6.4%		
Net Oil Recovery:	**50.7%**	**Final Oil Saturation:**	**42.9%**

Cylinder No.	Total Vol. Produced (ml)	Instantaneous Oil Prod. (ml)	Cum. Oil Recovery (ml)	Cum. Oil Rec. %OOIP	Instantaneous Produced WOR	% Sample Vol. Oleic Phase	Cum. PV Injected
1	1350	335	335	2.4	3.0	24.8	0.21
2	2100	360	695	5.0	4.8	17.1	0.32
3	2020	605	1300	9.3	2.3	30.0	0.43
4	1970	650	1950	14.0	2.0	33.0	0.53
5	1930	640	2590	18.6	2.0	33.2	0.64
6	1820	580	3170	22.8	2.1	31.9	0.75
7	1700	520	3690	26.5	2.3	30.6	0.86
8	1775	405	4095	29.4	3.4	22.8	0.96
9	1540	325	4420	31.8	3.7	21.1	1.07
10	1540	290	4710	33.8	4.3	18.8	1.18
11	1620	260	4970	35.7	5.2	16.0	1.28
12	1600	260	5230	37.6	5.2	16.3	1.39
13	1680	280	5510	39.6	5.0	16.7	1.50
14	1500	220	5730	41.2	5.8	14.7	1.60
15	1560	205	5935	42.7	6.6	13.1	1.71
16	1470	180	6115	43.9	7.2	12.2	1.82
17	1455	175	6290	45.2	7.3	12.0	1.92
18	1540	195	6485	46.6	6.9	12.7	2.03
19	1660	210	6695	48.1	6.9	12.7	2.14
20	1540	360	7055	50.7	3.3	23.4	2.24

Table D19 — Run 149: Steamflood of a 50% Bottom Water Model Using a Vertical Injection Well and a Vertical Production Well.

HC Pore Volume:	6955 ml	Type of Oil Used:	Faxam-100
Pore Volume:	12042.5 ml	Initial Model Temperature:	3.0 °C
Bulk Volume:	42000 ml	Total Flow Rate of Steam:	211 ml/min.
Porosity:	28.7%	Steam Quality, fst:	0.1
Initial Oil Saturation:	57.8%	Total Steam Volume Injected:	27641 ml
Initial Water Saturation:	42.3%	Bottom Water Thickness:	48.2% (% Gross Thickness)
Net Oil Recovery:	**31.2%**	**Final Oil Saturation:**	**26.5%**

Cylinder No.	Total Vol. Produced (ml)	Instantaneous Oil Prod. (ml)	Cum. Oil Recovery (ml)	Cum. Oil Rec. %OOIP	Instantaneous Produced WOR	% Sample Vol. Oleic Phase	Cum. PV Injected
1	1850	0	0	0.0	0.0	0.0	0.09
2	2140	0	0	0.0	0.0	0.0	0.21
3	2020	0	0	0.0	0.0	0.0	0.33
4	1920	0	0	0.0	0.0	0.0	0.46
5	1970	0	0	0.0	0.0	0.0	0.58
6	1850	0	0	0.0	0.0	0.0	0.70
7	1790	30	30	0.4	58.7	1.7	0.82
8	1440	40	70	1.0	35.0	2.8	0.95
9	1010	185	255	3.7	4.5	18.3	1.07
10	1485	165	420	6.0	8.0	11.1	1.19
11	1680	205	625	9.0	7.2	12.2	1.31
12	1690	230	855	12.3	6.3	13.6	1.44
13	1600	200	1055	15.2	7.0	12.5	1.56
14	1525	165	1220	17.5	8.2	10.8	1.68
15	1540	180	1400	20.1	7.6	11.7	1.80
16	1540	190	1590	22.9	7.1	12.3	1.93
17	1500	145	1735	24.9	9.3	9.7	2.05
18	1490	155	1890	27.2	8.6	10.4	2.17
19	1510	150	2040	29.3	9.1	9.9	2.30
20	1470	130	2170	31.2	10.3	8.8	2.42

Table D20 — Run 151: Steamflood of a 50% Bottom Water Model Using a Vertical Injection Well and a 8 in. Horizontal Production Well.

HC Pore Volume:	7075 ml	Type of Oil Used:	Faxam-100
Pore Volume:	12980 ml	Initial Model Temperature:	3.0 °C
Bulk Volume:	42000 ml	Total Flow Rate of Steam:	211 ml/min.
Porosity:	30.9%	Steam Quality, fst:	0.1
Initial Oil Saturation:	54.5%	Total Steam Volume Injected:	28063 ml
Initial Water Saturation:	45.5%		
Net Oil Recovery:	**29.3%**	**Final Oil Saturation:**	**25.2%**

Cylinder No.	Total Vol. Produced (ml)	Instantaneous Oil Prod. (ml)	Cum. Oil Recovery (ml)	Cum. Oil Rec. %OOIP	Instantaneous Produced WOR	% Sample Vol. Oleic Phase	Cum. PV Injected
1	1620	0	0	0.0	0.0	0.0	0.11
2	2050	0	0	0.0	0.0	0.0	0.23
3	1970	0	0	0.0	0.0	0.0	0.34
4	1910	0	0	0.0	0.0	0.0	0.46
5	1980	20	20	0.3	98.0	1.0	0.57
6	1940	20	40	0.6	96.0	1.0	0.68
7	1740	40	80	1.1	42.5	2.3	0.80
8	1370	70	150	2.1	18.6	5.1	0.91
9	1490	135	285	4.0	10.0	9.1	1.02
10	1760	200	485	6.9	7.8	11.4	1.14
11	1790	220	705	10.0	7.1	12.3	1.25
12	1595	195	900	12.7	7.2	12.2	1.37
13	1500	170	1070	15.1	7.8	11.3	1.48
14	1480	180	1250	17.7	7.2	12.2	1.59
15	1480	160	1410	19.9	8.3	10.8	1.71
16	1440	140	1550	21.9	9.3	9.7	1.82
17	1460	140	1690	23.9	9.4	9.6	1.93
18	1480	140	1830	25.9	9.6	9.5	2.05
19	1390	125	1955	27.6	10.1	9.0	2.16
20	1440	120	2075	29.3	11.0	8.3	2.28

Table D21 — Run 152: Steamflood of a 50% Bottom Water Model Using a 16 in. Horizontal Injection Well and a Vertical Production Well.

HC Pore Volume:	6850 ml	Type of Oil Used:	Faxam-100
Pore Volume:	12529 ml	Initial Model Temperature:	3.0 °C
Bulk Volume:	42000 ml	Total Flow Rate of Steam:	211 ml/min.
Porosity:	29.8%	Steam Quality, fst:	0.1
Initial Oil Saturation:	54.7%	Total Steam Volume Injected:	29540 ml
Initial Water Saturation:	45.3%		
Net Oil Recovery:	**30.3%**	**Final Oil Saturation:**	**24.4%**

Cylinder No.	Total Vol. Produced (ml)	Instantaneous Oil Prod. (ml)	Cum. Oil Recovery (ml)	Cum. Oil Rec. %OOIP	Instantaneous Produced WOR	% Sample Vol. Oleic Phase	Cum. PV Injected
1	1700	0	0	0.0	0.0	0.0	0.12
2	2010	0	0	0.0	0.0	0.0	0.24
3	1710	0	0	0.0	0.0	0.0	0.35
4	2180	20	20	0.3	108.0	0.9	0.47
5	1925	30	50	0.7	63.2	1.6	0.59
6	2060	20	70	1.0	102.0	1.0	0.71
7	1720	80	150	2.2	20.5	4.7	0.83
8	1450	170	320	4.7	7.5	11.7	0.94
9	1710	230	550	8.0	6.4	13.5	1.06
10	1600	200	750	10.9	7.0	12.5	1.18
11	1470	175	925	13.5	7.4	11.9	1.30
12	1420	155	1080	15.8	8.2	10.9	1.41
13	1425	145	1225	17.9	8.8	10.2	1.53
14	1440	140	1365	19.9	9.3	9.7	1.65
15	1420	120	1485	21.7	10.8	8.5	1.77
16	1420	120	1605	23.4	10.8	8.5	1.89
17	1430	130	1735	25.3	10.0	9.1	2.00
18	1430	130	1865	27.2	10.0	9.1	2.12
19	1420	110	1975	28.8	11.9	7.7	2.24
20	1380	100	2075	30.3	12.8	7.2	2.36

Table D22 — Run 156: Steamflood of a Homogeneous Model Using a Vertical Injection Well and a 8 in. Horizontal Production Well.

HC Pore Volume:	13310 ml	Type of Oil Used:	Faxam-100
Pore Volume:	14400 ml	Initial Model Temperature:	3.0 °C
Bulk Volume:	42000 ml	Total Flow Rate of Steam:	211 ml/min.
Porosity:	34.3%	Steam Quality, fst:	0.1
Initial Oil Saturation:	92.4%	Total Steam Volume Injected:	62034 ml
Initial Water Saturation:	7.6%		
Net Oil Recovery:	**71.1%**	**Final Oil Saturation:**	**21.3%**

Cylinder No.	Total Vol. Produced (ml)	Instantaneous Oil Prod. (ml)	Cum. Oil Recovery (ml)	Cum. Oil Rec. %OOIP	Instantaneous Produced WOR	% Sample Vol. Oleic Phase	Cum. PV Injected
1	1520	605	605	4.55	1.51	39.80	0.21
2	2520	750	1355	10.18	2.36	29.76	0.31
3	2090	675	2030	15.25	2.10	32.30	0.41
4	2090	690	2720	20.44	2.03	33.01	0.51
5	1870	620	3340	25.09	2.02	33.16	0.62
6	1830	540	3880	29.15	2.39	29.51	0.72
7	1705	455	4335	32.57	2.75	26.69	0.82
8	1620	380	4715	35.42	3.26	23.46	0.92
9	1580	325	5040	37.87	3.86	20.57	1.03
10	1555	300	5340	40.12	4.18	19.29	1.13
11	1540	270	5610	42.15	4.70	17.53	1.23
12	1480	220	5830	43.80	5.73	14.86	1.33
13	1510	230	6060	45.53	5.57	15.23	1.44
14	1495	210	6270	47.11	6.12	14.05	1.54
15	1460	200	6470	48.61	6.30	13.70	1.64
16	1490	205	6675	50.15	6.27	13.76	1.74
17	1470	170	6845	51.43	7.65	11.56	1.85
18	1460	165	7010	52.67	7.85	11.30	1.95

Table D22 (con't) — Run 156: Steamflood of a Homogeneous Model Using a Vertical Injection Well and a 8 in. Horizontal Production Well.

Cylinder No.	Total Vol. Produced (ml)	Instantaneous Oil Prod. (ml)	Cum. Oil Recovery (ml)	Cum. Oil Rec. %OOIP	Instantaneous Produced WOR	% Sample Vol. Oleic Phase	Cum. PV Injected
19	1460	170	7180	53.94	7.59	11.64	2.05
20	1460	160	7340	55.15	8.13	10.96	2.15
20	1450	165	7505	56.39	7.79	11.38	2.26
20	1445	150	7655	57.51	8.63	10.38	2.36
20	1440	150	7805	58.64	8.60	10.42	2.46
20	1445	135	7940	59.65	9.70	9.34	2.56
20	1420	120	8060	60.56	10.83	8.45	2.67
20	1445	125	8185	61.50	10.56	8.65	2.77
20	1440	120	8305	62.40	11.00	8.33	2.87
20	1445	125	8430	63.34	10.56	8.65	2.97
20	1440	110	8540	64.16	12.09	7.64	3.08
20	1435	95	8635	64.88	14.11	6.62	3.18
20	1410	90	8725	65.55	14.67	6.38	3.28
20	1400	100	8825	66.30	13.00	7.14	3.38
20	1380	80	8905	66.90	16.25	5.80	3.49
20	1400	80	8985	67.51	16.50	5.71	3.59
20	1370	75	9060	68.07	17.27	5.47	3.69
20	1390	75	9135	68.63	17.53	5.40	3.80
20	1380	80	9215	69.23	16.25	5.80	3.90
20	1560	75	9290	69.80	19.80	4.81	4.01
20	1175	55	9345	70.21	20.36	4.68	4.10
20	1360	60	9405	70.66	21.67	4.41	4.21
20	1380	60	9465	71.11	22.00	4.35	4.31

Table D23 — Run 157: Steamflood of a Homogenous Model Using a Vertical Injection Well and a 16 in. Horizontal Production Well.

HC Pore Volume:	13180 ml	Type of Oil Used:	Faxam-100
Pore Volume:	14020 ml	Initial Model Temperature:	3.0 °C
Bulk Volume:	42000 ml	Total Flow Rate of Steam:	211 ml/min.
Porosity:	33.4%	Steam Quality, fst:	0.1
Initial Oil Saturation:	94.0%	Total Steam Volume Injected:	59080 ml
Initial Water Saturation:	6.0%		
Net Oil Recovery:	**76.6%**	**Final Oil Saturation:**	**17.4%**

Cylinder No.	Total Vol. Produced (ml)	Instantaneous Oil Prod. (ml)	Cum. Oil Recovery (ml)	Cum. Oil Rec. %OOIP	Instantaneous Produced WOR	% Sample Vol. Oleic Phase	Cum. PV Injected
1	50	38	38	0.3	0.3	76.0	0.11
2	1200	470	508	3.9	1.6	39.2	0.21
3	2770	1010	1518	11.5	1.7	36.5	0.32
4	2205	695	2213	16.8	2.2	31.5	0.42
5	1920	660	2873	21.8	1.9	34.4	0.53
6	1900	580	3453	26.2	2.3	30.5	0.63
7	1800	520	3973	30.1	2.5	28.9	0.74
8	1840	630	4603	34.9	1.9	34.2	0.84
9	1610	355	4958	37.6	3.5	22.0	0.95
10	1540	290	5248	39.8	4.3	18.8	1.05
11	1550	275	5523	41.9	4.6	17.7	1.16
12	1535	255	5778	43.8	5.0	16.6	1.26
13	1510	230	6008	45.6	5.6	15.2	1.37
14	1515	225	6233	47.3	5.7	14.9	1.47
15	1535	215	6448	48.9	6.1	14.0	1.58
16	1520	225	6673	50.6	5.8	14.8	1.69
17	1560	220	6893	52.3	6.1	14.1	1.79
18	1530	210	7103	53.9	6.3	13.7	1.90

Table D23 (con't) — Run 157: Steamflood of a Homogenous Model Using a Vertical Injection Well and a 16 in. Horizontal Production Well.

Cylinder No.	Total Vol. Produced (ml)	Instantaneous Oil Prod. (ml)	Cum. Oil Recovery (ml)	Cum. Oil Rec. %OOIP	Instantaneous Produced WOR	% Sample Vol. Oleic Phase	Cum. PV Injected
19	1520	210	7313	55.5	6.2	13.8	2.00
20	1535	210	7523	57.1	6.3	13.7	2.11
21	1520	200	7723	58.6	6.6	13.2	2.21
22	1515	190	7913	60.0	7.0	12.5	2.32
23	1500	170	8083	61.3	7.8	11.3	2.42
24	1520	165	8248	62.6	8.2	10.9	2.53
25	1520	170	8418	63.9	7.9	11.2	2.63
26	1520	170	8588	65.2	7.9	11.2	2.74
27	1500	150	8738	66.3	9.0	10.0	2.84
28	1510	150	8888	67.4	9.1	9.9	2.95
29	1420	120	9008	68.3	10.8	8.5	3.06
30	1500	130	9138	69.3	10.5	8.7	3.16
31	1410	120	9258	70.2	10.8	8.5	3.27
32	1440	95	9353	71.0	14.2	6.6	3.37
33	1430	80	9433	71 6	16.9	5.6	3.48
34	1455	115	9548	72.4	11.7	7.9	3.58
35	1455	110	9658	73.3	12.2	7.6	3.69
36	1440	90	9748	74.0	15.0	6.3	3.79
37	1405	85	9833	74.6	15.5	6.0	3.90
38	1425	95	9928	75.3	14.0	6.7	4.00
39	1415	65	9993	75.8	20.8	4.6	4.11
40	1440	100	10093	76.6	13.4	6.9	4.21

Table D24 — Run 158: Steamflood of a Homogenous Model Using a Vertical Injection Well and a 12 in. Horizontal Production Well.

HC Pore Volume:	13060 ml	Type of Oil Used:	Faxam-100
Pore Volume:	14180 ml	Initial Model Temperature:	3.0 °C
Bulk Volume:	42000 ml	Total Flow Rate of Steam:	211 ml/min.
Porosity:	33.8%	Steam Quality, fst:	0.1
Initial Oil Saturation:	92.1%	Total Steam Volume Injected:	29751
Initial Water Saturation:	7.9%		
Net Oil Recovery:	**66.9%**	**Final Oil Saturation:**	**25.2%**

Cylinder No.	Total Vol. Produced (ml)	Instantaneous Oil Prod. (ml)	Cum. Oil Recovery (ml)	Cum. Oil Rec. %OOIP	Instantaneous Produced WOR	% Sample Vol. Oleic Phase	Cum. PV Injected
1	1260	530	530	4.1	1.4	42.1	0.22
2	2570	800	1330	10.2	2.2	31.1	0.33
3	2140	730	2060	15.8	1.9	34.1	0.43
4	1950	680	2740	21.0	1.9	34.9	0.54
5	1810	570	3310	25.3	2.2	31.5	0.64
6	1705	445	3755	28.8	2.8	26.1	0.74
7	1660	425	4180	32.0	2.9	25.6	0.85
8	1600	360	4540	34.8	3.4	22.5	0.95
9	1580	340	4880	37.4	3.6	21.5	1.06
10	1635	325	5205	39.9	4.0	19.9	1.16
11	1705	335	5540	42.4	4.1	19.6	1.26
12	1435	265	5805	44.4	4.4	18.5	1.37
13	1540	265	6070	46.5	4.8	17.2	1.47
14	1555	260	6330	48.5	5.0	16.7	1.58
15	1535	235	6565	50.3	5.5	15.3	1.68
16	1525	230	6795	52.0	5.6	15.1	1.79
17	1540	220	7015	53.7	6.0	14.3	1.89
18	1500	200	7215	55.2	6.5	13.3	1.99

Table D24 (con't) — Run 158: Steamflood of a Homogenous Model Using a Vertical Injection Well and a 12 in. Horizontal Production Well.

Cylinder No.	Total Vol. Produced (ml)	Instantaneous Oil Prod. (ml)	Cum. Oil Recovery (ml)	Cum. Oil Rec. %OOIP	Instantaneous Produced WOR	% Sample Vol. Oleic Phase	Cum. PV Injected
19	1495	200	7415	56.8	6.5	13.4	2.10
20	1535	215	7630	58.4	6.1	14.0	2.20
21	1460	185	7815	59.8	6.9	12.7	2.31
22	1520	195	8010	61.3	6.8	12.8	2.41
23	1500	185	8195	62.7	7.1	12.3	2.51
24	1500	180	8375	64.1	7.3	12.0	2.62
25	1515	185	8560	65.5	7.2	12.2	2.72
26	1520	180	8740	66.9	7.4	11.8	2.83
27	1445	155	8895	68.1	8.3	10.7	2.93
28	1480	150	9045	69.3	8.9	10.1	3.04
29	1445	140	9185	70.3	9.3	9.7	3.14
30	1460	140	9325	71.4	9.4	9.6	3.24
31	1415	135	9460	72.4	9.5	9.5	3.35
32	1515	170	9630	73.7	7.9	11.2	3.45
33	1415	115	9745	74.6	11.3	8.1	3.56
34	1410	110	9855	75.5	11.8	7.8	3.66
35	1390	90	9945	76.1	14.4	6.5	3.76
36	1390	95	10040	76.9	13.6	6.8	3.87
37	1340	80	10120	77.5	15.8	6.0	3.97
38	1360	80	10200	78.1	16.0	5.9	4.08
39	1415	80	10280	78.7	16.7	5.7	4.18
40	1430	85	10365	79.4	15.8	5.9	4.29

Table D25 — Run 159: Steamflood of a 50% Bottom Water Model Using a Vertical Injection Well and a 12 in. Horizontal Production Well Placed at the Top of the Oil Zone.

HC Pore Volume:	6230 ml	Type of Oil Used:	Faxam-100
Pore Volume:	12410 ml	Initial Model Temperature:	3.0 °C
Bulk Volume:	42000 ml	Total Flow Rate of Steam:	211 ml/min.
Porosity:	29.6%	Steam Quality,fst:	0.1
Initial Oil Saturation:	50.2%	Total Steam Volume Injected:	27957.5
Initial Water Saturation:	49.8%		
Net Oil Recovery:	**2439.8%**	**Final Oil Saturation:**	**-2389.6%**

Cylinder No.	Total Vol. Produced (ml)	Instantaneous Oil Prod. (ml)	Cum. Oil Recovery (ml)	Cum. Oil Rec. %OOIP	Instantaneous Produced WOR	% Sample Vol. Oleic Phase	Cum. PV Injected
1	1960	0	0	0.0	0.0	0.0	0.11
2	1940	0	0	0.0	0.0	0.0	0.23
3	1910	15	15	0.2	0.0	0.8	0.35
4	1920	0	15	0.2	75.8	0.0	0.47
5	1940	25	40	0.6	76.6	1.3	0.59
6	2000	10	50	0.8	199.0	0.5	0.71
7	1775	50	100	1.6	34.5	2.8	0.82
8	1440	145	245	3.9	8.9	10.1	0.94
9	1730	170	415	6.7	9.2	9.8	1.06
10	1640	145	560	9.0	10.3	8.8	1.18
11	1515	140	700	11.2	9.8	9.2	1.30
12	1425	125	825	13.2	10.4	8.8	1.42
13	1415	115	940	15.1	11.3	8.1	1.54
14	1435	105	1045	16.8	12.7	7.3	1.66
15	1420	100	1145	18.4	13.2	7.0	1.78
16	1400	100	1245	20.0	13.0	7.1	1.90
17	1400	95	1340	21.5	13.7	6.8	2.01
18	1395	95	1435	23.0	13.7	6.8	2.13
19	1420	85	1520	24.4	15.7	6.0	2.25
20	1400	90	1610	25.8	14.6	6.4	2.37

Table D25 (con't) — Run 159: Steamflood of a 50% Bottom Water Model Using a Vertical Injection Well and a 12 in. Horizontal Production Well Placed at the Top of the Oil Zone.

Cylinder No.	Total Vol. Produced (ml)	Instantaneous Oil Prod. (ml)	Cum. Oil Recovery (ml)	Cum. Oil Rec. %OOIP	Instantaneous Produced WOR	% Sample Vol. Oleic Phase	Cum. PV Injected
21	1380	90	1700	27.3	14.3	6.5	2.49
22	1360	70	1770	28.4	18.4	5.1	2.61
23	1400	80	1850	29.7	16.5	5.7	2.73
24	1325	25	1875	30.1	52.0	1.9	2.85
25	1340	40	1915	30.7	32.5	3.0	2.97
26	1375	75	1990	31.9	17.3	5.5	3.09
27	1360	60	2050	32.9	21.7	4.4	3.21
28	1370	50	2100	33.7	26.4	3.6	3.32

Table D26 — Run 160: Steamflood of a 50% Bottom Water Model Using a Vertical Injection Well and a 12 in. Horizontal Production Well Placed in the Middle of the Oil Zone.

HC Pore Volume:	6815 ml	Type of Oil Used:	Faxam-100
Pore Volume:	12440 ml	Initial Model Temperature:	3.0 °C
Bulk Volume:	42000 ml	Total Flow Rate of Steam:	211 ml/min.
Porosity:	29.6%	Steam Quality, fst:	0.1
Initial Oil Saturation:	54.8%	Total Steam Volume Injected:	27957 ml
Initial Water Saturation:	45.2%		
Net Oil Recovery:	**21.9%**	**Final Oil Saturation:**	**32.9%**

Cylinder No.	Total Vol. Produced (ml)	Instantaneous Oil Prod. (ml)	Cum. Oil Recovery (ml)	Cum. Oil Rec. %OOIP	Instantaneous Produced WOR	% Sample Vol. Oleic Phase	Cum. PV Injected
1	1440	0	0	0.0	0.0	0.0	0.11
2	1820	0	0	0.0	0.0	0.0	0.23
3	1860	20	20	0.3	92.0	1.1	0.35
4	1900	20	40	0.6	94.0	1.1	0.47
5	2020	20	60	0.9	100.0	1.0	0.59
6	2025	25	85	1.2	80.0	1.2	0.70
7	1480	60	145	2.1	23.7	4.1	0.82
8	1415	80	225	3.3	16.7	5.7	0.94
9	1460	85	310	4.5	16.2	5.8	1.06
10	1495	115	425	6.2	12.0	7.7	1.18
11	1485	125	550	8.1	10.9	8.4	1.30
12	1450	115	665	9.8	11.6	7.9	1.42
13	1430	110	775	11.4	12.0	7.7	1.54
14	1440	100	875	12.8	13.4	6.9	1.65
15	1445	105	980	14.4	12.8	7.3	1.77
16	1410	95	1075	15.8	13.8	6.7	1.89
17	1405	90	1165	17.1	14.6	6.4	2.01
18	1420	110	1275	18.7	11.9	7.7	2.13
19	1400	105	1380	20.2	12.3	7.5	2.25
20	1400	110	1490	21.9	11.7	7.9	2.37

Table D26 — Run 160: Steamflood of a 50% Bottom Water Model Using a Vertical Injection Well and a 12 in. Horizontal Production Well Placed in the Middel of the Oil Zone.

Cylinder No.	Total Vol. Produced (ml)	Instantaneous Oil Prod. (ml)	Cum. Oil Recovery (ml)	Cum. Oil Rec. %OOIP	Instantaneous Produced WOR	% Sample Vol. Oleic Phase	Cum. PV Injected
21	1380	100	1590	23.3	12.8	7.2	2.48
22	1385	95	1685	24.7	13.6	6.9	2.60
23	1370	90	1775	26.0	14.2	6.6	2.72
24	1380	100	1875	27.5	12.8	7.2	2.84
25	1380	110	1985	29.1	11.5	8.0	2.96
26	1365	105	2090	30.7	12.0	7.7	3.08
27	1350	80	2170	31.8	15.9	5.9	3.20
28	1345	85	2255	33.1	14.8	6.3	3.32
29	1365	85	2340	34.3	15.1	6.2	3.43
30	1360	85	2425	35.6	15.0	6.3	3.55

Table D27 — Run 161: Steamflood of a 50% Bottom Water Model Using a Vertical Injection Well and a 12 in. Horizontal Production Well Placed at the Oil-Water Contact.

HC Pore Volume:	6560 ml	Type of Oil Used:	Faxam-100
Pore Volume:	12368 ml	Initial Model Temperature:	3.0 °C
Bulk Volume:	42000 ml	Total Flow Rate of Steam:	211 ml/min.
Porosity:	29.5%	Steam Quality, fst:	0.1
Initial Oil Saturation:	53.0%	Total Steam Volume Injected:	27957 ml
Initial Water Saturation:	47.0%		
Net Oil Recovery:	**29.6%**	**Final Oil Saturation:**	**23.4%**

Cylinder No.	Total Vol. Produced (ml)	Instantaneous Oil Prod. (ml)	Cum. Oil Recovery (ml)	Cum. Oil Rec. %OOIP	Instantaneous Produced WOR	% Sample Vol. Oleic Phase	Cum. PV Injected
1	2255	0	0	0.0	0.0	0.0	0.11
2	1850	0	0	0.0	0.0	0.0	0.23
3	1780	0	0	0.0	0.0	0.0	0.35
4	1970	20	20	0.3	97.5	1.0	0.47
5	2115	15	35	0.5	140.0	0.7	0.59
6	2020	35	70	1.1	56.7	1.7	0.71
7	1675	35	105	1.6	46.9	2.1	0.83
8	1170	70	175	2.7	15.7	6.0	0.95
9	1500	160	335	5.1	8.4	10.7	1.07
10	1830	210	545	8.3	7.7	11.5	1.19
11	1740	225	770	11.7	6.7	12.9	1.31
12	1550	185	955	14.6	7.4	11.9	1.42
13	1460	160	1115	17.0	8.1	11.0	1.54
14	1430	150	1265	19.3	8.5	10.5	1.66
15	1440	140	1405	21.4	9.3	9.7	1.78
16	1415	125	1530	23.3	10.3	8.8	1.90
17	1420	120	1650	25.2	10.8	8.5	2.02
18	1425	120	1770	27.0	10.9	8.4	2.14
19	1400	90	1860	28.4	14.6	6.4	2.26
20	1380	85	1945	29.6	15.2	6.2	2.38

Table D27 — Run 161: Steamflood of a 50% Bottom Water Model Using a Vertical Injection Well and a 12 in. Horizontal Production Well Placed at the Oil-Water Contact.

Cylinder No.	Total Vol. Produced (ml)	Instantaneous Oil Prod. (ml)	Cum. Oil Recovery (ml)	Cum. Oil Rec. %OOIP	Instantaneous Produced WOR	% Sample Vol. Oleic Phase	Cum. PV Injected
21	1380	80	2025	30.9	16.3	5.8	2.50
22	1390	90	2115	32.2	14.4	6.5	2.62
23	1355	95	2210	33.7	13.3	7.0	2.74
24	1410	90	2300	35.1	14.7	6.4	2.86
25	1400	70	2370	36.1	19.0	5.0	2.98
26	1400	70	2440	37.2	19.0	5.0	3.10
27	1320	60	2500	38.1	21.0	4.5	3.22
28	1340	60	2560	39.0	21.3	4.5	3.34
29	1360	65	2625	40.0	19.9	4.8	3.45
30	1340	55	2680	40.9	23.4	4.1	3.57

Table D28 — Run 163: Steamflood of a Muliti-Layered Model with the High Permeability Zone at the Bottom of the Resevoir, Using Vertical Injection and Production Wells.

HC Pore Volume:	14000 ml	Type of Oil Used:	Faxam-100
Pore Volume:	15120 ml	Initial Model Temperature:	3.0° C
Bulk Volume:	42005 ml	Total Flow Rate of Steam:	220 ml/min.
Porosity:	35.16%	Steam Quality, fst:	0.1
Initial Oil Saturation:	93.36%	Total Steam Volume Injected:	42680 ml
Initial Water Saturation:	7.4%		
Net Oil Recovery:	**77.8%**	**Final Oil Saturation:**	**15.5%**

Cylinder No.	Total Vol. Produced (ml)	Instantaneous Oil Prod. (ml)	Cum. Oil Recovery (ml)	Cum. Oil Rec. %OOIP	Instantaneous Produced WOR	% Sample Vol. Oleic Phase	Cum. PV Injected
1	1460	410	410	2.93	2.56	28.08	0.17
2	2140	560	970	6.93	2.82	26.17	0.28
3	2740	1260	2230	15.93	1.17	45.99	0.38
4	2280	1130	3360	24.00	1.02	49.56	0.48
5	2160	1010	4370	31.21	1.14	46.76	0.58
6	2125	855	5225	37.32	1.49	40.24	0.68
7	1900	680	5905	42.18	1.79	35.79	0.79
8	1775	555	6460	46.14	2.20	31.27	0.89
9	1770	530	6990	49.93	2.34	29.94	0.99
10	1720	480	7470	53.36	2.58	27.91	1.09
11	1740	360	7830	55.93	3.83	20.69	1.19
12	1635	315	8145	58.18	4.19	19.27	1.29
13	1595	275	8420	60.14	4.80	17.24	1.40
14	1640	245	8665	61.89	5.69	14.94	1.50
15	1580	220	8885	63.46	6.18	13.92	1.60
16	1555	210	9095	64.96	6.40	13.50	1.70
17	1550	195	9290	66.36	6.95	12.58	1.80
18	1530	190	9480	67.71	7.05	12.42	1.91

Table D28 con't — Run 163: Steamflood of a Muliti-Layered Model with the High Permeability Zone at the Bottom of the Resevoir, Using Vertical Injection and Production Wells.

Cylinder No.	Total Vol. Produced (ml)	Instantaneous Oil Prod. (ml)	Cum. Oil Recovery (ml)	Cum. Oil Rec. %OOIP	Instantaneous Produced WOR	% Sample Vol. Oleic Phase	Cum. PV Injected
19	1550	190	9670	69.07	7.16	12.26	2.01
20	1500	170	9840	70.29	7.82	11.33	2.11
21	1540	215	10055	71.82	6.16	13.96	2.21
22	1500	125	10180	72.71	11.00	8.33	2.31
23	1500	150	10330	73.79	9.00	10.00	2.42
24	1480	130	10460	74.71	10.38	8.78	2.52
25	1500	150	10610	75.79	9.00	10.00	2.62
26	1535	155	10765	76.89	8.90	10.10	2.72
27	1510	130	10895	77.82	10.62	8.61	2.82